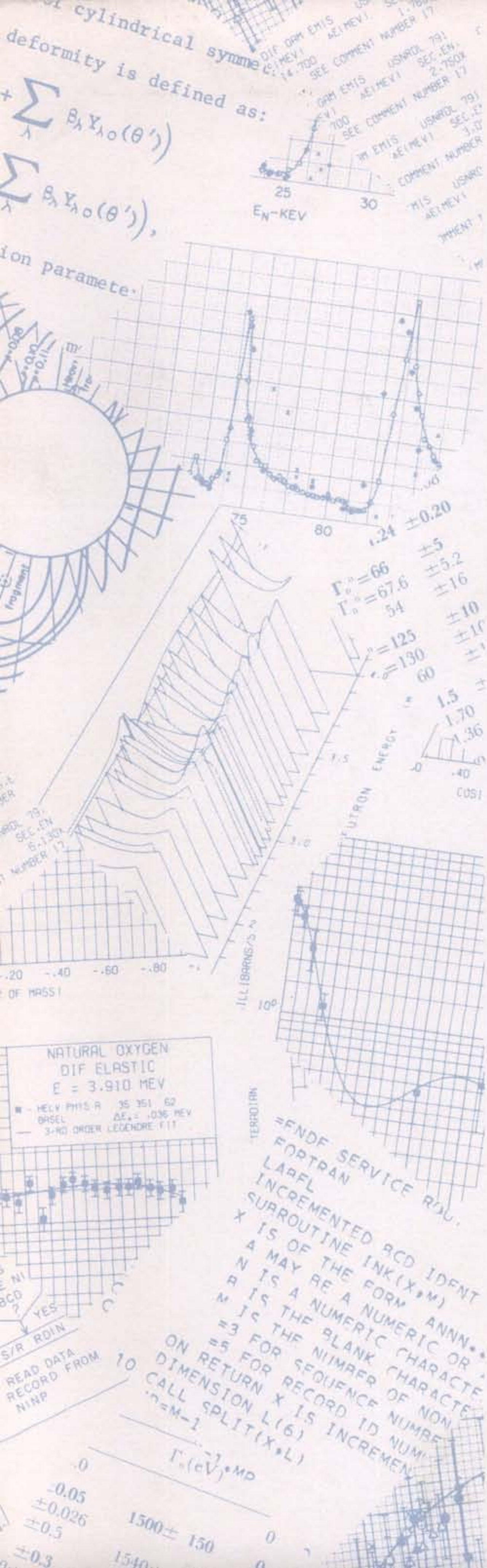

BNL-NCS-31052
DOE/NDC-27/U
NEANDC(US)-212/U
INDC(USA)-88/L
Informal Report
Limited Distribution

REPORTS TO THE DOE NUCLEAR DATA COMMITTEE

Compiled by
NATIONAL NUCLEAR DATA CENTER
for the
U.S. Department of Energy
Nuclear Data Committee

May 1982

BROOKHAVEN NATIONAL LABORATORY
ASSOCIATED UNIVERSITIES, INC.
UPTON, LONG ISLAND, NEW YORK 11973

national nuclear data Center

BNL-NCS-31052
DOE/NDC-27/U

REPORTS TO THE DOE NUCLEAR DATA COMMITTEE

May 1982

Compiled by
NATIONAL NUCLEAR DATA CENTER
for the
U.S. Department of Energy
Nuclear Data Committee

NATIONAL NUCLEAR DATA CENTER

BROOKHAVEN NATIONAL LABORATORY
ASSOCIATED UNIVERSITIES, INC.

UNDER CONTRACT NO. DE-AC02-76CH00016 WITH THE

UNITED STATES DEPARTMENT OF ENERGY

Printed in the United States of America
Available from
National Technical Information Service
U.S. Department of Commerce
5285 Port Royal Road
Springfield, VA 22161

NTIS price codes:
Printed Copy: A09; Microfiche Copy: A01

PREFACE

The reports in this document were submitted to the Department of Energy, Nuclear Data Committee (DOE-NDC) in April, 1982. The reporting laboratories are those with a substantial program for the measurement of neutron and nuclear cross sections of relevance to the U.S. applied nuclear energy program.

The authors of the Status Report contributions are responsible for collecting and editing individual contributions from their laboratory and are not necessarily the sole authors of the contributions. The scientists responsible for the work described in each individual contribution are listed at the beginning of the contribution.

The material contained in these reports is to be regarded as comprised of informal statements of recent developments and preliminary data. Persons wishing to make use of these data should contact the individual experimenter for further details. The data which appear in this document should be quoted only by permission of the contributor and should be referenced as private communication, and not by this document number. Appropriate subjects are listed as follows:

1. Microscopic neutron cross sections relevant to the nuclear energy program, including shielding. Inverse reactions where pertinent are included.

2. Charged-particle cross sections, where they are relevant to (1.) above, and where relevant to developing and testing nuclear models.

3. Gamma ray production, radioactive decay, and theoretical developments in nuclear structure which are applicable to nuclear energy programs.

4. Proton and alpha-particle cross sections, at energies of up to 1 GeV, which are of interest to the space program.

These reports cannot be regarded as a complete summary of the nuclear research efforts in the U.S. A number of laboratories whose research is less programmatically oriented do not submit reports; neither do the submitted reports reflect all the work related to nuclear data in progress at the submitting laboratory.

This compilation has been produced almost completely from master copies prepared by the individual contributors listed in the Table of Contents.

The CINDA-type index which follows the Table of Contents was prepared by Norman E. Holden of the National Nuclear Data Center, Brookhaven National Laboratory, Upton, Long Island, New York.

TABLE OF CONTENTS

NEUTRON DATA REFERENCES

Element	Quantity	Energy (eV) Min	Max	Type	Documentation Ref	Page	Date	Lab	Comments
Li	$\sigma_{n,\alpha}$	1.5+7		Expt	DOE-NDC-27	144	Apr82	AI	Kneff+NDG.TBC
^{6}Li	σ_{tot}	7.0+4	5.0+5	Expt	DOE-NDC-27		Apr82	ANL	Poenitz. PAGE A-7. NDG. TBC.
^{6}Li	σ_{el}	7.0+4	5.0+5	Expt	DOE-NDC-27		Apr82	ANL	Poenitz. PAGE A-7. NDG. TBC.
^{6}Li	$\sigma_{n,t}$	7.0+4	5.0+5	Expt	DOE-NDC-27		Apr82	ANL	Poenitz. PAGE A-7. NDG. TBC.
^{6}Li	$\sigma_{n,t}$	2.4+5	5.4+6	Expt	DOE-NDC-27	67	Apr82	LAS	Drosg+GRPH.INV.REACT.CFD R-MATRIX
^{6}Li	$\sigma_{n,t}$	2.0+6	2.5+6	Expt	DOE-NDC-27	133	Apr82	OHO	Knox+NDG.ANAL.TBD.
^{6}Li	$\sigma_{n,\alpha}$	1.5+7		Expt	DOE-NDC-27	144	Apr82	AI	Kneff+NDG.TBC
^{7}Li	$\sigma_{el}(\theta)$	NDG		Eval	DOE-NDC-27	134	Apr82	OHO	Knox+NDG.ANAL.TBD.
^{7}Li	$\sigma_{dif.inl}$	NDG		Eval	DOE-NDC-27	134	Apr82	OHO	Knox+NDG.ANAL.TBD.
^{7}Li	$\sigma_{n,t}$	NDG		Eval	DOE-NDC-27	134	Apr82	OHO	Knox+NDG.ANAL.TBD.
^{7}Li	$\sigma_{n,nt}$	1.0+5	2.0+7	Eval	DOE-NDC-27	75	Apr82	LAS	Young. GRPH CFD EXPT,ENDF
^{7}Li	$\sigma_{n,\alpha}$	1.5+7		Expt	DOE-NDC-27	144	Apr82	AI	Kneff+NDG.TBC
^{9}Be	$\sigma_{el}(\theta)$	1.4+7		Expt	DOE-NDC-27	51	Apr82	LRL	Hansen+SIG CFD EXPT.NDG
^{9}Be	$\sigma_{dif.inl}$	1.4+7		Expt	DOE-NDC-27	51	Apr82	LRL	Hansen+SIG CFD EXPT.NDG
^{9}Be	$\sigma_{n,\alpha}$	1.5+7		Expt	DOE-NDC-27	144	Apr82	AI	Kneff+NDG.TBC
B	$\sigma_{n,\alpha}$	1.5+7		Expt	DOE-NDC-27	144	Apr82	AI	Kneff+NDG.TBC
^{10}B	$\sigma_{el}(\theta)$	8.0+6	1.4+7	Expt	DOE-NDC-27	147	Apr82	TNL	Gould.TBP NSE
^{10}B	$\sigma_{dif.inl}$	8.0+6	1.4+7	Expt	DOE-NDC-27	147	Apr82	TNL	Gould.TBP NSE
^{10}B	$\sigma_{n,\alpha}$	1.5+7		Expt	DOE-NDC-27	144	Apr82	AI	Kneff+NDG.TBC
^{11}B	$\sigma_{el}(\theta)$	2.0+6	8.0+6	Eval	DOE-NDC-27	135	Apr82	OHO	Koehler+R-MATRIX ANAL.CFD EXPT.
^{11}B	$\sigma_{el}(\theta)$	8.0+6	1.4+7	Expt	DOE-NDC-27	147	Apr82	TNL	Gould.TBP NSE
^{11}B	$\sigma_{dif.inl}$	2.0+6	8.0+6	Eval	DOE-NDC-27	135	Apr82	OHO	Koehler+R-MATRIX ANAL.CFD EXPT.
^{11}B	$\sigma_{dif.inl}$	8.0+6	1.4+7	Expt	DOE-NDC-27	147	Apr82	TNL	Gould.TBP NSE
^{11}B	$\sigma_{n,\alpha}$	1.5+7		Expt	DOE-NDC-27	144	Apr82	AI	Kneff+NDG.TBC
^{12}C	σ_{tot}	NDG		Expt	DOE-NDC-27	129	Apr82	OHO	Knox+NDG.TBP NP/A
^{12}C	$\sigma_{el}(\theta)$	1.4+7		Expt	DOE-NDC-27	51	Apr82	LRL	Hansen+SIG CFD EXPT.NDG
^{12}C	$\sigma_{el}(\theta)$	NDG		Expt	DOE-NDC-27	129	Apr82	OHO	Knox+NDG.TBP NP/A
^{12}C	$\sigma_{el}(\theta)$	2.1+7	2.6+7	Expt	DOE-NDC-27	129	Apr82	OHO	Meigooni+ NDG.
^{12}C	$\sigma_{dif.inl}$	1.4+7		Expt	DOE-NDC-27	51	Apr82	LRL	Hansen+SIG CFD EXPT.NDG
^{12}C	$\sigma_{dif.inl}$	NDG		Expt	DOE-NDC-27	129	Apr82	OHO	Knox+NDG.TBP NP/A
^{12}C	$\sigma_{dif.inl}$	2.1+7	2.6+7	Expt	DOE-NDC-27	129	Apr82	OHO	Meigooni+ NDG.
^{12}C	$\sigma_{n,\alpha}$	NDG		Expt	DOE-NDC-27	129	Apr82	OHO	Knox+NDG.TBP NP/A
^{13}C	σ_{el}	1.0+7	1.8+7	Expt	DOE-NDC-27	147	Apr82	TNL	Gould.TBP NSE

NEUTRON DATA REFERENCES

Element	Quantity	Energy (eV) Min	Max	Type	Documentation Ref	Page	Date	Lab	Comments
^{13}C	$\sigma_{el}(\theta)$	7.6+6	1.1+7	Expt	DOE-NDC-27	130	Apr82	OHO	Resler+11 ANGLES.TBC
^{13}C	$\sigma_{el}(\theta)$	1.0+7	1.8+7	Expt	DOE-NDC-27	147	Apr82	TNL	Gould.TBP NSE
^{13}C	$\sigma_{dif.inl}$	1.0+7		Expt	DOE-NDC-27	147	Apr82	TNL	Gould.TBP NSE
N	$\sigma_{n,\alpha}$	1.5+7		Expt	DOE-NDC-27	144	Apr82	AI	Kneff+NDG.TBC
^{16}O	$\sigma_{n,\alpha}$	1.5+7		Expt	DOE-NDC-27	144	Apr82	AI	Kneff+NDG.TBC
^{18}O	$\sigma_{el}(\theta)$	5.0+6	7.0+6	Expt	DOE-NDC-27	130	Apr82	OHO	Koehler+ TBD.
^{18}O	$\sigma_{dif.inl}$	5.0+6	7.0+6	Expt	DOE-NDC-27	130	Apr82	OHO	Koehler+ TBD.
^{19}F	$\sigma_{n,\alpha}$	1.5+7		Expt	DOE-NDC-27	144	Apr82	AI	Kneff+NDG.TBC
^{26}Mg	$\sigma_{el}(\theta)$	2.4+7		Expt	DOE-NDC-27	131	Apr82	OHO	Tailor+NDG.C-C ANALYSIS.
^{26}Mg	$\sigma_{dif.inl}$	2.4+7		Expt	DOE-NDC-27	131	Apr82	OHO	Tailor+NDG.C-C ANALYSIS.
^{27}Al	$\sigma_{el}(\theta)$	1.4+7		Expt	DOE-NDC-27	51	Apr82	LRL	Hansen+SIG CFD EXPT.NDG
^{27}Al	$\sigma_{dif.inl}$	1.4+7		Expt	DOE-NDC-27	51	Apr82	LRL	Hansen+SIG CFD EXPT.NDG
Si	$\sigma_{n,\alpha}$	1.5+7		Expt	DOE-NDC-27	144	Apr82	AI	Kneff+TBL.
^{28}Si	Lvl Density	NDG		Theo	DOE-NDC-27	59	Apr82	LRL	Bloom+EXCIT.E=8-15MEV,CFD EXPT.NDG
S	σ_{abs}	2.5-2		Expt	DOE-NDC-27	110	Apr82	ORL	Jurney+CS=513+-15 MB.
^{34}S	$\sigma_{n,\gamma}$	2.5-2		Expt	DOE-NDC-27	109	Apr82	ORL	Carlton+AGREES WITH LANE+LYNN
^{36}S	$\sigma_{n,\gamma}$	2.5-2		Expt	DOE-NDC-27	111	Apr82	ORL	Raman+CS=230+-20 MB.
^{35}Cl	Res.Params.	4.0+2		Expt	DOE-NDC-27	109	Apr82	ORL	Hussein+P-WAVE RES.AT 398 EV.
Ca	Evaluation	2.0+7	4.0+7	Eval	DOE-NDC-27	126	Apr82	ORL	Hetrick+ NDG.
Ca	σ_{el}	1.5+6	4.0+6	Expt	DOE-NDC-27		Apr82	ANL	Smith+ PAGE A-4,ANG.INTEGRATION,NDG.
Ca	$\sigma_{el}(\theta)$	1.5+6	4.0+6	Expt	DOE-NDC-27		Apr82	ANL	Smith+ PAGE A-4, GRPH.
^{40}Ca	$\sigma_{el}(\theta)$	1.0+7	1.4+7	Expt	DOE-NDC-27	150	Apr82	TNL	Walter.TBP.NP/A
^{40}Ca	$\sigma_{n,xn}$	NDG		Expt	DOE-NDC-27	13	Apr82	DAV	Ford+NDG,TBD
Ti	σ_{tot}	1.0+4	3.0+7	Expt	DOE-NDC-27	113	Apr82	ORL	Larsen+ TBC.
^{46}Ti	$\sigma_{n,\alpha}$	1.5+7		Expt	DOE-NDC-27	144	Apr82	AI	Kneff+NDG.TBC
^{47}Ti	$\sigma_{n,\alpha}$	1.5+7		Expt	DOE-NDC-27	144	Apr82	AI	Kneff+NDG.TBC
^{48}Ti	$\sigma_{n,\alpha}$	1.5+7		Expt	DOE-NDC-27	144	Apr82	AI	Kneff+NDG.TBC
^{49}Ti	$\sigma_{n,\alpha}$	1.5+7		Expt	DOE-NDC-27	144	Apr82	AI	Kneff+NDG.TBC
^{50}Ti	$\sigma_{n,\alpha}$	1.5+7		Expt	DOE-NDC-27	144	Apr82	AI	Kneff+NDG.TBC
^{51}V	$\sigma_{dif.inl}$	2.6+7		Expt	DOE-NDC-27	132	Apr82	OHO	Marcinkowski+7 ANGS.ANAL.TBC.
^{51}V	$\sigma_{n,\alpha}$	1.5+7		Expt	DOE-NDC-27	144	Apr82	AI	Kneff+TBL.
Cr	σ_{tot}	1.0+4	3.0+7	Expt	DOE-NDC-27	113	Apr82	ORL	Larsen+ TBC.
Cr	$\sigma_{n,\alpha}$	1.5+7		Expt	DOE-NDC-27	144	Apr82	AI	Kneff+NDG.TBC

NEUTRON DATA REFERENCES

Element	Quantity	Energy (eV) Min	Max	Type	Documentation Ref	Page	Date	Lab	Comments
^{50}Cr	$\sigma_{n,\alpha}$	1.5+7		Expt	DOE-NDC-27	144	Apr82	AI	Kneff+NDG.TBC
^{52}Cr	$\sigma_{n,\alpha}$	1.5+7		Expt	DOE-NDC-27	144	Apr82	AI	Kneff+NDG.TBC
^{53}Cr	$\sigma_{n,\alpha}$	1.5+7		Expt	DOE-NDC-27	144	Apr82	AI	Kneff+NDG.TBC
^{54}Cr	$\sigma_{n,\alpha}$	1.5+7		Expt	DOE-NDC-27	144	Apr82	AI	Kneff+NDG.TBC
^{55}Mn	$\sigma_{n,\alpha}$	1.5+7		Expt	DOE-NDC-27	144	Apr82	AI	Kneff+NDG.TBC
Fe	$\sigma_{el}(\theta)$	1.4+7		Expt	DOE-NDC-27	51	Apr82	LRL	Hansen+SIG CFD EXPT.NDG
Fe	$\sigma_{dif.inl}$	1.4+7		Expt	DOE-NDC-27	51	Apr82	LRL	Hansen+SIG CFD EXPT.NDG
Fe	$\sigma_{n,\alpha}$	1.5+7		Expt	DOE-NDC-27	144	Apr82	AI	Kneff+TBL.
^{54}Fe	σ_{tot}	5.0+5	4.0+6	Expt	DOE-NDC-27		Apr82	ANL	Guenther+ PAGE A-3, NDG. TBC.
^{54}Fe	$\sigma_{el}(\theta)$	5.0+5	4.0+6	Expt	DOE-NDC-27		Apr82	ANL	Guenther+ PAGE A-3, NDG. TBC.
^{54}Fe	$\sigma_{el}(\theta)$	8.0+6	1.4+7	Expt	DOE-NDC-27	151	Apr82	TNL	Walter.NDG
^{54}Fe	$\sigma_{dif.inl}$	5.0+5	4.0+6	Expt	DOE-NDC-27		Apr82	ANL	Guenther+ PAGE A-3, NDG. TBC.
^{54}Fe	$\sigma_{dif.inl}$	8.0+6	1.4+7	Expt	DOE-NDC-27	151	Apr82	TNL	Walter.NDG
^{54}Fe	$\sigma_{n,n'\gamma}$	5.0+5	4.0+6	Expt	DOE-NDC-27		Apr82	ANL	Guenther+ PAGE A-3, NDG. TBC.
^{54}Fe	$\sigma_{n,\alpha}$	1.5+7		Expt	DOE-NDC-27	144	Apr82	AI	Kneff+TBL.
^{56}Fe	$\sigma_{el}(\theta)$	8.0+6	1.4+7	Expt	DOE-NDC-27	151	Apr82	TNL	Walter.NDG
^{56}Fe	$\sigma_{dif.inl}$	2.6+7		Expt	DOE-NDC-27	132	Apr82	OHO	Marcinkowski+7 ANGS.ANAL.TBC.
^{56}Fe	$\sigma_{dif.inl}$	8.0+6	1.4+7	Expt	DOE-NDC-27	151	Apr82	TNL	Walter.NDG
^{56}Fe	$\sigma_{n,n'\gamma}$	8.5+5	3.0+7	Expt	DOE-NDC-27	114	Apr82	ORL	Bell+846 KEV GAMMA,NDG.
^{56}Fe	$\sigma_{n,\alpha}$	1.5+7		Expt	DOE-NDC-27	144	Apr82	AI	Kneff+TBL.
^{57}Fe	$\sigma_{n,n'\gamma}$	2.0+5	2.0+6	Expt	DOE-NDC-27	114	Apr82	ORL	Bell+ NDG.
^{57}Fe	$\sigma_{n,\alpha}$	1.5+7		Expt	DOE-NDC-27	144	Apr82	AI	Kneff+TBL.
^{58}Fe	$\sigma_{n,\alpha}$	1.5+7		Expt	DOE-NDC-27	144	Apr82	AI	Kneff+TBL.
^{59}Co	$\sigma_{el}(\theta)$	1.4+7		Expt	DOE-NDC-27	51	Apr82	LRL	Hansen+SIG CFD EXPT.NDG
^{59}Co	$\sigma_{dif.inl}$	1.4+7		Expt	DOE-NDC-27	51	Apr82	LRL	Hansen+SIG CFD EXPT.NDG
^{59}Co	$\sigma_{n,\alpha}$	1.5+7		Expt	DOE-NDC-27	144	Apr82	AI	Kneff+TBL.
Ni	σ_{tot}	2.4+4	2.0+7	Expt	DOE-NDC-27	112	Apr82	ORL	Larsen+ NDG
Ni	$\sigma_{n,\alpha}$	1.5+7		Expt	DOE-NDC-27	144	Apr82	AI	Kneff+TBL.
^{58}Ni	σ_{tot}	9.0+5	4.5+6	Expt	DOE-NDC-27		Apr82	ANL	Budtz-Jorgensen+PAGE A-2,NDG
^{58}Ni	$\sigma_{el}(\theta)$	1.4+6	4.0+6	Expt	DOE-NDC-27		Apr82	ANL	Budtz-Jorgensen+PAGE A-2,GRPH
^{58}Ni	$\sigma_{el}(\theta)$	8.0+6	1.4+7	Expt	DOE-NDC-27	152	Apr82	TNL	Walter.GRPH
^{58}Ni	$\sigma_{dif.inl}$	1.4+6	4.0+6	Expt	DOE-NDC-27		Apr82	ANL	Budtz-Jorgensen+PAGE A-2,NDG
^{58}Ni	$\sigma_{dif.inl}$	8.0+6	1.4+7	Expt	DOE-NDC-27	152	Apr82	TNL	Walter.GRPH

NEUTRON DATA REFERENCES

Element	Quantity	Energy (eV) Min	Max	Type	Documentation Ref	Page	Date	Lab	Comments
^{58}Ni	$\sigma_{n,p}$	8.0+6		Expt	DOE-NDC-27	133	Apr82	OHO	Graham+NDG.TBC
^{58}Ni	$\sigma_{n,\alpha}$	1.5+7		Expt	DOE-NDC-27	144	Apr82	AI	Kneff+TBL.
^{58}Ni	$\sigma_{n,\alpha}$	8.0+6		Expt	DOE-NDC-27	133	Apr82	OHO	Graham+NDG.TBC
^{60}Ni	$\sigma_{el}(\theta)$	8.0+6	1.4+7	Expt	DOE-NDC-27	152	Apr82	TNL	Walter.NDG
^{60}Ni	$\sigma_{dif.inl}$	8.0+6	1.4+7	Expt	DOE-NDC-27	152	Apr82	TNL	Walter.NDG
^{60}Ni	$\sigma_{n,\alpha}$	1.5+7		Expt	DOE-NDC-27	144	Apr82	AI	Kneff+TBL.
^{61}Ni	$\sigma_{n,\alpha}$	1.5+7		Expt	DOE-NDC-27	144	Apr82	AI	Kneff+TBL.
^{62}Ni	$\sigma_{n,\alpha}$	1.5+7		Expt	DOE-NDC-27	144	Apr82	AI	Kneff+TBL.
^{64}Ni	$\sigma_{n,\alpha}$	1.5+7		Expt	DOE-NDC-27	144	Apr82	AI	Kneff+TBL.
Cu	$\sigma_{n,\alpha}$	1.5+7		Expt	DOE-NDC-27	144	Apr82	AI	Kneff+TBL.
^{63}Cu	$\sigma_{el}(\theta)$	8.0+6	1.4+7	Expt	DOE-NDC-27	151	Apr82	TNL	Walter.NDG
^{63}Cu	$\sigma_{dif.inl}$	8.0+6	1.4+7	Expt	DOE-NDC-27	151	Apr82	TNL	Walter.NDG
^{63}Cu	γ Spectra	2.0+3	2.4+4	Expt	DOE-NDC-27	2	Apr82	BNL	Chrien.2E.STUDY E1,M1 STRENGTHS
^{63}Cu	$\sigma_{n,\alpha}$	1.5+7		Expt	DOE-NDC-27	144	Apr82	AI	Kneff+TBL.
^{65}Cu	$\sigma_{el}(\theta)$	8.0+6	1.4+7	Expt	DOE-NDC-27	151	Apr82	TNL	Walter.NDG
^{65}Cu	$\sigma_{dif.inl}$	2.6+7		Expt	DOE-NDC-27	132	Apr82	OHO	Marcinkowski+7 ANGS.ANAL.TBC.
^{65}Cu	$\sigma_{dif.inl}$	8.0+6	1.4+7	Expt	DOE-NDC-27	151	Apr82	TNL	Walter.NDG
^{65}Cu	γ Spectra	2.0+3	2.4+4	Expt	DOE-NDC-27	2	Apr82	BNL	Chrien.2E.STUDY E1,M1 STRENGTHS
^{65}Cu	$\sigma_{n,\alpha}$	1.5+7		Expt	DOE-NDC-27	144	Apr82	AI	Kneff+TBL.
^{68}Zn	$\sigma_{n,\gamma}$	3.0+4		Expt	DOE-NDC-27	113	Apr82	ORL	Garg+ CS = 19.2 MB.
^{68}Zn	Res.Params.	+3	3.8+5	Expt	DOE-NDC-27	113	Apr82	ORL	Garg+ NDG.
^{68}Zn	$<\Gamma>/D$	+3	3.8+5	Expt	DOE-NDC-27	113	Apr82	ORL	Garg+S0,S1,S2,D0,D1 GIVEN.
^{76}Se	$\sigma_{el}(\theta)$	8.0+6		Theo	DOE-NDC-27	53	Apr82	LRL	Brown+NDG.CC CALC.2 PHONON STATES
^{76}Se	$\sigma_{dif.inl}$	8.0+6		Theo	DOE-NDC-27	53	Apr82	LRL	Brown+NDG.CC CALC.2 PHONON STATES
^{80}Se	$\sigma_{el}(\theta)$	8.0+6		Theo	DOE-NDC-27	53	Apr82	LRL	Brown+NDG.CC CALC.2 PHONON STATES
^{80}Se	$\sigma_{dif.inl}$	8.0+6		Theo	DOE-NDC-27	53	Apr82	LRL	Brown+NDG.CC CALC.2 PHONON STATES
^{80}Se	$\sigma_{dif.inl}$	8.0+6		Expt	DOE-NDC-27	131	Apr82	OHO	Kurup+ NDG. TBC.
^{82}Se	$\sigma_{el}(\theta)$	8.0+6		Theo	DOE-NDC-27	53	Apr82	LRL	Brown+NDG.CC CALC.2 PHONON STATES
^{82}Se	$\sigma_{dif.inl}$	8.0+6		Theo	DOE-NDC-27	53	Apr82	LRL	Brown+NDG.CC CALC.2 PHONON STATES
^{82}Se	Res.Params.	5.8+2	1.7+4	Expt	DOE-NDC-27	55	Apr82	LRL	Browne+NDG.EO
^{86}Kr	$\sigma_{n,\gamma}$	NDG		Expt	DOE-NDC-27	109	Apr82	ORL	Fogelberg+ NDG
^{86}Sr	$\sigma_{n,\gamma}$	3.0+3	+5	Expt	DOE-NDC-27	109	Apr82	ORL	Hicks+ NDG.
^{86}Sr	Res.Params.		3.7+4	Expt	DOE-NDC-27	109	Apr82	ORL	Hicks+AVG.PAR,AVG.WG,NDG

NEUTRON DATA REFERENCES

Element	Quantity	Energy (eV) Min	Max	Type	Documentation Ref	Page	Date	Lab	Comments
^{87}Sr	$\sigma_{n,\gamma}$	3.0+3	+5	Expt	DOE-NDC-27	109	Apr82	ORL	Hicks+ NDG.
^{87}Sr	Res.Params.		1.4+4	Expt	DOE-NDC-27	109	Apr82	ORL	Hicks+AVG.PAR,AVG.WG,NDG
^{88}Y	$\sigma_{n,2n}$	1.4+7	1.5+7	Expt	DOE-NDC-27	55	Apr82	LRL	Nethaway+TBL.SIG(M+G),M/(M+G).
^{89}Y	σ_{tot}	1.0+6	4.0+6	Expt	DOE-NDC-27		Apr82	ANL	Budtz-Jorgensen+ PAGE A-3, NDG.
^{89}Y	$\sigma_{el}(\theta)$	1.0+6	4.0+6	Expt	DOE-NDC-27		Apr82	ANL	Budtz-Jorgensen+ PAGE A-3, NDG.
^{89}Y	$\sigma_{el}(\theta)$	1.1+7		Expt	DOE-NDC-27	131	Apr82	OHO	Yan+ NDG
^{89}Y	$\sigma_{dif.inl}$	1.0+6	4.0+6	Expt	DOE-NDC-27		Apr82	ANL	Budtz-Jorgensen+ PAGE A-3, NDG.
^{89}Y	$\sigma_{dif.inl}$	1.1+7		Expt	DOE-NDC-27	131	Apr82	OHO	Yan+ NDG
Zr	$\sigma_{n,\alpha}$	1.5+7		Expt	DOE-NDC-27	144	Apr82	AI	Kneff+TBL.
^{88}Zr	$\sigma_{n,2n}$	1.5+7		Expt	DOE-NDC-27	55	Apr82	LRL	Nethaway+TBL.EN=14.8,CS=467+-24 MB
^{88}Zr	$\sigma_{n,np}$	1.5+7		Expt	DOE-NDC-27	55	Apr82	LRL	Nethaway+TBL.EN=14.8,CS=257+-26 MB
^{94}Zr	$\sigma_{n,\gamma}$	2.5-2	3.0+4	Expt	DOE-NDC-27		Apr82	ANL	Poenitz+PAGE A-5.TBL 2 E,SIG.GIVEN
^{96}Zr	$\sigma_{n,\gamma}$	2.5-2	3.0+4	Expt	DOE-NDC-27		Apr82	ANL	Poenitz+PAGE A-5.TBL 2 E,SIG.GIVEN
^{93}Nb	$\sigma_{dif.inl}$	2.6+7		Expt	DOE-NDC-27	132	Apr82	OHO	Marcinkowski+7 ANGS.ANAL.TBC.
^{93}Nb	$\sigma_{n,\alpha}$	1.5+7		Expt	DOE-NDC-27	144	Apr82	AI	Kneff+TBL.
Mo	σ_{tot}	1.0+4	3.0+7	Expt	DOE-NDC-27	113	Apr82	ORL	Larsen+ TBC.
Mo	$\sigma_{n,\alpha}$	1.5+7		Expt	DOE-NDC-27	144	Apr82	AI	Kneff+TBL.
^{92}Mo	$\sigma_{n,\alpha}$	1.5+7		Expt	DOE-NDC-27	144	Apr82	AI	Kneff+TBL.
^{94}Mo	$\sigma_{n,\alpha}$	1.5+7		Expt	DOE-NDC-27	144	Apr82	AI	Kneff+TBL.
^{95}Mo	$\sigma_{n,\alpha}$	1.5+7		Expt	DOE-NDC-27	144	Apr82	AI	Kneff+TBL.
^{96}Mo	$\sigma_{n,\alpha}$	1.5+7		Expt	DOE-NDC-27	144	Apr82	AI	Kneff+TBL.
^{97}Mo	$\sigma_{n,\alpha}$	1.5+7		Expt	DOE-NDC-27	144	Apr82	AI	Kneff+TBL.
^{98}Mo	$\sigma_{n,\gamma}$	2.5-2	3.0+4	Expt	DOE-NDC-27		Apr82	ANL	Poenitz+PAGE A-5.TBL 2 E,SIG.GIVEN
^{98}Mo	$\sigma_{n,\alpha}$	1.5+7		Expt	DOE-NDC-27	144	Apr82	AI	Kneff+TBL.
^{100}Mo	$\sigma_{n,\gamma}$	2.5-2	3.0+4	Expt	DOE-NDC-27		Apr82	ANL	Poenitz+PAGE A-5.TBL 2 E,SIG.GIVEN
^{100}Mo	$\sigma_{n,\alpha}$	1.5+7		Expt	DOE-NDC-27	144	Apr82	AI	Kneff+TBL.
^{99}Tc	$\sigma_{n,\gamma}$	2.7+3	2.0+6	Expt	DOE-NDC-27	110	Apr82	ORL	Macklin.AGREES ENDF ABOVE 900 KEV.
^{99}Tc	Res.Params.	2.7+3	5.1+3	Expt	DOE-NDC-27	110	Apr82	ORL	Macklin.LEAST SQS.ADJUSTMENT.NDG
Pd	σ_{tot}	5.0+5	4.5+6	Expt	DOE-NDC-27		Apr82	ANL	Smith+ PAGE A-3, ANALYSIS TBD.
Pd	$\sigma_{el}(\theta)$	1.5+6	3.8+6	Expt	DOE-NDC-27		Apr82	ANL	Smith+ PAGE A-3, ANALYSIS TBD.
Pd	$\sigma_{dif.inl}$	1.5+6	3.8+6	Expt	DOE-NDC-27		Apr82	ANL	Smith+ PAGE A-3, ANALYSIS TBD.
Cd	$\sigma_{n,\gamma}$	1.4+5	1.0+7	Expt	DOE-NDC-27		Apr82	ANL	Smith+PAGE A-5.CD-111M PROD.SIG.
^{110}Cd	$\sigma_{n,\gamma}$	1.4+5	1.6+6	Expt	DOE-NDC-27		Apr82	ANL	Smith+G.A-5,GRPH.M,G SIG.GIVEN.

NEUTRON DATA REFERENCES

Element	Quantity	Energy (eV) Min	Max	Type	Documentation Ref	Page	Date	Lab	Comments
^{111}Cd	$\sigma_{dif.inl}$	5.0+5	1.6+6	Expt	DOE-NDC-27		Apr82	ANL	Smith+PG.A-5,GRPH. CD-111M ST.PROD.
^{115}In	$\sigma_{el}(\theta)$	1.5+6	3.8+6	Expt	DOE-NDC-27		Apr82	ANL	Smith+ PAGE A-3, GRPH
^{115}In	$\sigma_{dif.inl}$	1.5+6	3.8+6	Expt	DOE-NDC-27		Apr82	ANL	Smith+ PAGE A-3, NDG.
^{115}In	$\sigma_{n,\gamma}$	2.3+4	9.6+5	Expt	DOE-NDC-27	93	Apr82	MHG	Grady+CS AT 3E.265KEV ALSO.
Sn	$\sigma_{n,\alpha}$	1.5+7		Expt	DOE-NDC-27	144	Apr82	AI	Kneff+TBL.
^{112}Sn	$\sigma_{n,\alpha}$	1.5+7		Expt	DOE-NDC-27	144	Apr82	AI	Kneff+NDG.TBC
^{114}Sn	$\sigma_{n,\alpha}$	1.5+7		Expt	DOE-NDC-27	144	Apr82	AI	Kneff+NDG.TBC
^{115}Sn	$\sigma_{n,\alpha}$	1.5+7		Expt	DOE-NDC-27	144	Apr82	AI	Kneff+NDG.TBC
^{116}Sn	σ_{tot}	3.0+5	5.0+6	Expt	DOE-NDC-27	31	Apr82	KTY	Harper+FIT SPHERICAL OPT.MDL.
^{116}Sn	$\sigma_{el}(\theta)$	1.0+6	4.0+6	Expt	DOE-NDC-27	31	Apr82	KTY	Harper+FIT SPHERICAL OPT.MDL.
^{116}Sn	$\sigma_{el}(\theta)$	1.0+7	1.4+7	Expt	DOE-NDC-27	154	Apr82	TNL	Walter.ANAL.TBC
^{116}Sn	$\sigma_{dif.inl}$	1.0+6	4.0+6	Expt	DOE-NDC-27	31	Apr82	KTY	Harper+FIT SPHERICAL OPT.MDL.
^{116}Sn	$\sigma_{dif.inl}$	1.0+7	1.4+7	Expt	DOE-NDC-27	154	Apr82	TNL	Walter.ANAL.TBC
^{116}Sn	$\sigma_{n,\alpha}$	1.5+7		Expt	DOE-NDC-27	144	Apr82	AI	Kneff+NDG.TBC
^{117}Sn	$\sigma_{n,\alpha}$	1.5+7		Expt	DOE-NDC-27	144	Apr82	AI	Kneff+NDG.TBC
^{118}Sn	σ_{tot}	3.0+5	5.0+6	Expt	DOE-NDC-27	31	Apr82	KTY	Harper+FIT SPHERICAL OPT.MDL.
^{118}Sn	$\sigma_{el}(\theta)$	1.0+6	4.0+6	Expt	DOE-NDC-27	31	Apr82	KTY	Harper+FIT SPHERICAL OPT.MDL.
^{118}Sn	$\sigma_{dif.inl}$	1.0+6	4.0+6	Expt	DOE-NDC-27	31	Apr82	KTY	Harper+FIT SPHERICAL OPT.MDL.
^{118}Sn	$\sigma_{n,\alpha}$	1.5+7		Expt	DOE-NDC-27	144	Apr82	AI	Kneff+NDG.TBC
^{119}Sn	$\sigma_{n,\alpha}$	1.5+7		Expt	DOE-NDC-27	144	Apr82	AI	Kneff+NDG.TBC
^{120}Sn	σ_{tot}	3.0+5	5.0+6	Expt	DOE-NDC-27	31	Apr82	KTY	Harper+FIT SPHERICAL OPT.MDL.
^{120}Sn	$\sigma_{el}(\theta)$	1.0+6	4.0+6	Expt	DOE-NDC-27	31	Apr82	KTY	Harper+FIT SPHERICAL OPT.MDL.
^{120}Sn	$\sigma_{el}(\theta)$	1.7+7		Expt	DOE-NDC-27	154	Apr82	TNL	Walter.ANAL.TBC
^{120}Sn	$\sigma_{dif.inl}$	1.0+6	4.0+6	Expt	DOE-NDC-27	31	Apr82	KTY	Harper+FIT SPHERICAL OPT.MDL.
^{120}Sn	$\sigma_{dif.inl}$	1.7+7		Expt	DOE-NDC-27	154	Apr82	TNL	Walter.ANAL.TBC
^{120}Sn	$\sigma_{n,\alpha}$	1.5+7		Expt	DOE-NDC-27	144	Apr82	AI	Kneff+NDG.TBC
^{122}Sn	σ_{tot}	3.0+5	5.0+6	Expt	DOE-NDC-27	31	Apr82	KTY	Harper+FIT SPHERICAL OPT.MDL.
^{122}Sn	$\sigma_{el}(\theta)$	1.0+6	4.0+6	Expt	DOE-NDC-27	31	Apr82	KTY	Harper+FIT SPHERICAL OPT.MDL.
^{122}Sn	$\sigma_{dif.inl}$	1.0+6	4.0+6	Expt	DOE-NDC-27	31	Apr82	KTY	Harper+FIT SPHERICAL OPT.MDL.
^{122}Sn	$\sigma_{n,\alpha}$	1.5+7		Expt	DOE-NDC-27	144	Apr82	AI	Kneff+NDG.TBC
^{124}Sn	σ_{tot}	3.0+5	5.0+6	Expt	DOE-NDC-27	31	Apr82	KTY	Harper+FIT SPHERICAL OPT.MDL.
^{124}Sn	$\sigma_{el}(\theta)$	1.0+6	4.0+6	Expt	DOE-NDC-27	31	Apr82	KTY	Harper+FIT SPHERICAL OPT.MDL.
^{124}Sn	$\sigma_{dif.inl}$	1.0+6	4.0+6	Expt	DOE-NDC-27	31	Apr82	KTY	Harper+FIT SPHERICAL OPT.MDL.

NEUTRON DATA REFERENCES

Element	Quantity	Energy (eV) Min	Energy (eV) Max	Type	Documentation Ref	Page	Date	Lab	Comments
^{124}Sn	$\sigma_{n,\alpha}$	1.5+7		Expt	DOE-NDC-27	144	Apr82	AI	Kneff+NDG.TBC
^{133}Cs	$\sigma_{n,\gamma}$	2.7+3	6.0+5	Expt	DOE-NDC-27	111	Apr82	ORL	Macklin.NDG.
^{133}Cs	Res.Params.	2.7+3	6.0+3	Expt	DOE-NDC-27	111	Apr82	ORL	Macklin.NDG.
^{144}Nd	$\sigma_{n,\gamma}$	2.0+3		Expt	DOE-NDC-27	112	Apr82	ORL	Raman+ NDG.
^{146}Nd	$\sigma_{n,\gamma}$	2.0+3		Expt	DOE-NDC-27	112	Apr82	ORL	Raman+ NDG.
^{167}Er	$\sigma_{n,\gamma}$	NDG		Expt	DOE-NDC-27	110	Apr82	ORL	Kahane+AVG.WG NDG
^{168}Tm	$\sigma_{n,2n}$	1.5+7		Expt	DOE-NDC-27	55	Apr82	LRL	Nethaway+TBL.EN=14.5,CS=2100+-110 MB
^{169}Tm	$\sigma_{n,\gamma}$	NDG		Theo	DOE-NDC-27	76	Apr82	LAS	Young+NDG.
^{169}Tm	$\sigma_{n,\gamma}$	2.6+3	2.0+6	Expt	DOE-NDC-27	68	Apr82	ORL	Macklin+GRPH.CFD EXPT.AVG.RES.PAR.
^{169}Tm	$\sigma_{n,2n}$	8.0+6	2.3+7	Theo	DOE-NDC-27	76	Apr82	LAS	Young+GRPH CFD EXPT.
^{169}Tm	$\sigma_{n,xn}$	NDG		Theo	DOE-NDC-27	76	Apr82	LAS	Young+NDG.
^{169}Tm	Res.Params.	2.6+3	2.0+6	Expt	DOE-NDC-27	68	Apr82	ORL	Macklin+AVG. WG/D GIVEN
^{169}Tm	$<\Gamma>/D$	2.6+3	2.0+6	Expt	DOE-NDC-27	68	Apr82	ORL	Macklin+S0,S1,S2 GIVEN
^{173}Yb	Res.Params.	1.0+1	5.3+2	Expt	DOE-NDC-27	110	Apr82	ORL	Shahal+J ASSIGNMENTS,PARTIAL WG.NDG
^{181}Ta	$\sigma_{el}(\theta)$	1.4+7		Expt	DOE-NDC-27	51	Apr82	LRL	Hansen+SIG CFD EXPT.NDG
^{181}Ta	$\sigma_{dif.inl}$	1.4+7		Expt	DOE-NDC-27	51	Apr82	LRL	Hansen+SIG CFD EXPT.NDG
W	$\sigma_{n,\alpha}$	1.5+7		Expt	DOE-NDC-27	144	Apr82	AI	Kneff+NDG.TBC
^{182}W	$\sigma_{n,\gamma}$	2.6+3	2.0+6	Expt	DOE-NDC-27	68	Apr82	ORL	Macklin+GRPH
^{182}W	$\sigma_{n,\alpha}$	1.5+7		Expt	DOE-NDC-27	144	Apr82	AI	Kneff+NDG.TBC
^{182}W	Res.Params.	2.6+3	7.0+3	Expt	DOE-NDC-27	68	Apr82	ORL	Macklin+AVG. WG/D GIVEN
^{182}W	$<\Gamma>/D$	2.6+3	7.0+3	Expt	DOE-NDC-27	68	Apr82	ORL	Macklin+S0,S1,S2 GIVEN
^{183}W	$\sigma_{n,\gamma}$	2.6+3	2.0+6	Expt	DOE-NDC-27	68	Apr82	ORL	Macklin+NDG.
^{183}W	$\sigma_{n,\alpha}$	1.5+7		Expt	DOE-NDC-27	144	Apr82	AI	Kneff+NDG.TBC
^{184}W	$\sigma_{n,\gamma}$	2.6+3	2.0+6	Expt	DOE-NDC-27	68	Apr82	ORL	Macklin+NDG.
^{184}W	$\sigma_{n,\alpha}$	1.5+7		Expt	DOE-NDC-27	144	Apr82	AI	Kneff+NDG.TBC
^{186}W	$\sigma_{n,\gamma}$	2.6+3	2.0+6	Expt	DOE-NDC-27	68	Apr82	ORL	Macklin+NDG.
^{186}W	$\sigma_{n,n'\gamma}$		2.0+6	Expt	DOE-NDC-27		Apr82	ANL	Guenther+ PAGE A-7. ANALYSIS TBD.
^{186}W	$\sigma_{n,\alpha}$	1.5+7		Expt	DOE-NDC-27	144	Apr82	AI	Kneff+NDG.TBC
^{187}Os	σ_{el}	6.1+4		Expt	DOE-NDC-27	30	Apr82	KTY	Hershberger+GRPH NEUT.SPECTRA
^{187}Os	$\sigma_{dif.inl}$	6.1+4		Expt	DOE-NDC-27	30	Apr82	KTY	Hershberger+CS(9.76KEV LVL)=1.8B
^{188}Os	σ_{el}	6.1+4		Expt	DOE-NDC-27	30	Apr82	KTY	Hershberger+GRPH NEUT.SPECTRA
^{190}Os	$\sigma_{dif.inl}$	1.6+6	3.9+6	Expt	DOE-NDC-27	33	Apr82	KTY	McEllistrem+RESOLV.LVLS,CC ANALY.TBD
^{192}Os	$\sigma_{dif.inl}$	1.6+6	3.9+6	Expt	DOE-NDC-27	33	Apr82	KTY	McEllistrem+RESOLV.LVLS,CC ANALY.TBD

NEUTRON DATA REFERENCES

Element	Quantity	Energy (eV) Min	Max	Type	Documentation Ref	Page	Date	Lab	Comments
^{192}Os	$\sigma_{n,n'\gamma}$	2.5+6		Expt	DOE-NDC-27	35	Apr82	KTY	Kleppinger+SIG CFD 56FE.NDG
Pt	$\sigma_{n,\alpha}$	1.5+7		Expt	DOE-NDC-27	144	Apr82	AI	Kneff+TBL.
^{197}Au	$\sigma_{n,\alpha}$	1.5+7		Expt	DOE-NDC-27	144	Apr82	AI	Kneff+TBL.
Pb	$\sigma_{el}(\theta)$	5.0+2	2.5+5	Expt	DOE-NDC-27	160	Apr82	YAL	Kruk+NDG
Pb	$\sigma_{n,\alpha}$	1.5+7		Expt	DOE-NDC-27	144	Apr82	AI	Kneff+TBL.
^{204}Pb	$\sigma_{n,\alpha}$	1.5+7		Expt	DOE-NDC-27	144	Apr82	AI	Kneff+NDG.TBC
^{206}Pb	$\sigma_{dif.inl}$	7.0+6	8.5+6	Expt	DOE-NDC-27	33	Apr82	KTY	Hanly+GRPHS,ISOT.ENRICHED SAMPLES
^{206}Pb	$\sigma_{n,\alpha}$	1.5+7		Expt	DOE-NDC-27	144	Apr82	AI	Kneff+NDG.TBC
^{207}Pb	$\sigma_{n,\alpha}$	1.5+7		Expt	DOE-NDC-27	144	Apr82	AI	Kneff+NDG.TBC
^{208}Pb	$\sigma_{el}(\theta)$	2.6+7		Theo	DOE-NDC-27	59	Apr82	LRL	Dietrich+GRPH.ANG.DIST.
^{208}Pb	$\sigma_{el}(\theta)$	7.2+6	2.4+7	Expt	DOE-NDC-27	132	Apr82	OHO	Dietrich+2 E'S, NDG.
^{208}Pb	$\sigma_{el}(\theta)$	1.0+7	1.7+7	Expt	DOE-NDC-27	154	Apr82	TNL	Walter.GRPH
^{208}Pb	$\sigma_{dif.inl}$	7.0+6	8.5+6	Expt	DOE-NDC-27	33	Apr82	KTY	Hanly+GRPHS,ISOT.ENRICHED SAMPLES
^{208}Pb	$\sigma_{dif.inl}$	1.0+7	1.7+7	Expt	DOE-NDC-27	154	Apr82	TNL	Walter.NDG
^{208}Pb	$\sigma_{n,\alpha}$	1.5+7		Expt	DOE-NDC-27	144	Apr82	AI	Kneff+NDG.TBC
^{209}Bi	$\sigma_{el}(\theta)$	1.4+7		Expt	DOE-NDC-27	51	Apr82	LRL	Hansen+SIG CFD EXPT.NDG
^{209}Bi	$\sigma_{el}(\theta)$	2.0+6	4.0+6	Expt	DOE-NDC-27	160	Apr82	YAL	Ahmed+20 ANGS.OM ANAL.NDG
^{209}Bi	$\sigma_{el}(\theta)$	5.0+2	2.5+5	Expt	DOE-NDC-27	160	Apr82	YAL	Kruk+NDG
^{209}Bi	σ_{pol}	2.0+6	4.0+6	Expt	DOE-NDC-27	160	Apr82	YAL	Ahmed+20 ANGS.OM ANAL.NDG
^{209}Bi	$\sigma_{dif.inl}$	1.4+7		Expt	DOE-NDC-27	51	Apr82	LRL	Hansen+SIG CFD EXPT.NDG
^{209}Bi	$\sigma_{dif.inl}$	2.6+7		Expt	DOE-NDC-27	132	Apr82	OHO	Marcinkowski+7 ANGS.ANAL.TBC.
^{229}Th	Fiss.Yield	2.5-2		Expt	DOE-NDC-27	116	Apr82	ORL	Dickens+37 FP CFD EXPT.NDG.
^{229}Th	Fiss.Yield	2.5-2		Expt	DOE-NDC-27	115	Apr82	ORL	Dickens+NDG.ABS.YLDS.CFD EXP,ENDF
^{229}Th	Frag.Chg.	2.5-2		Expt	DOE-NDC-27	116	Apr82	ORL	Dickens+NDG.CHARGE DISP.MOST PROB.CH
^{232}Th	σ_{tot}	4.4+2	2.0+3	Expt	DOE-NDC-27	117	Apr82	ORL	Olsen+ NDG.
^{232}Th	σ_{tot}	8.0-3	4.0+3	Expt	DOE-NDC-27	118	Apr82	ORL	Olsen+ NDG.
^{232}Th	σ_{inl}	1.0+6	3.5+6	Expt	DOE-NDC-27		Apr82	ANL	Smith+PAGE A-1,GRPH.
^{232}Th	$\sigma_{dif.inl}$	1.0+6	3.5+6	Expt	DOE-NDC-27		Apr82	ANL	Smith+PAGE A-1,GRPH.
^{232}Th	$\sigma_{dif.inl}$	9.0+5	2.1+6	Expt	DOE-NDC-27	82	Apr82	LTI	Beghian+NDC.125 DEGS.E0 STRENGTH
^{232}Th	$\sigma_{dif.inl}$	8.0+5	2.5+6	Theo	DOE-NDC-27	83	Apr82	LTI	Sheldon+GRPHS CFD EXPT.
^{232}Th	$\sigma_{n,\gamma}$	2.3+4		Expt	DOE-NDC-27	94	Apr82	MHG	Baldwin+CS=604MB+-4 PCT.SB-BE.
^{232}Th	Res.Int.Capt	5.0-1		Eval	DOE-NDC-27	125	Apr82	ORL	Olsen. SEE ORNL/TM-8056
^{232}Th	$\sigma_{n,f}$	1.2+6	8.5+6	Expt	DOE-NDC-27	55	Apr82	LRL	Becker.TBL.A2,A4.ANG.DIST.COEFF.

Element	Quantity	Energy (eV) Min	Max	Type	Documentation Ref	Page	Date	Lab	Comments
^{232}Th	$\sigma_{n,f}$	2.0+4	3.0+7	Expt	DOE-NDC-27	100	Apr82	LRL	Behrens+CS RATIO,NSE 80 393.
^{232}Th	$\sigma_{n,f}$	7.0+5	3.0+7	Expt	DOE-NDC-27	100	Apr82	LRL	Behrens+CS RATIO. NSE TBP.
^{232}Th	Frag Spectra	1.5+6	1.8+6	Expt	DOE-NDC-27		Apr82	ANL	Budtz-Jorgensen+PG.A9,NDG.ANGDIST.FF
^{232}Th	Res.Params.	4.4+2	2.0+3	Expt	DOE-NDC-27	117	Apr82	ORL	Olsen+ NDG.
^{232}Th	Res.Params.	5.0+0	4.0+3	Eval	DOE-NDC-27	125	Apr82	ORL	Olsen. SEE ORNL/TM-8056
^{232}Th	$<\Gamma>/D$	4.4+2	2.0+3	Expt	DOE-NDC-27	117	Apr82	ORL	Olsen+ NDG.
^{232}Th	$<\Gamma>/D$	5.0+0	4.0+3	Eval	DOE-NDC-27	125	Apr82	ORL	Olsen. SEE ORNL/TM-8056
^{233}U	σ_{inl}	1.0+6	3.5+6	Expt	DOE-NDC-27		Apr82	ANL	Smith+PAGE A-1,GRPH.
^{233}U	$\sigma_{dif.inl}$	1.0+6	3.5+6	Expt	DOE-NDC-27		Apr82	ANL	Smith+PAGE A-1,GRPH.
^{233}U	$\sigma_{dif.inl}$	8.0+5	2.5+6	Theo	DOE-NDC-27	83	Apr82	LTI	Sheldon+ NDG. TBD.
^{233}U	$\sigma_{n,f}$	1.4+7		Expt	DOE-NDC-27	95	Apr82	MHG	Mahdavi+NDG. TBD.
^{233}U	ν_p	5.0+2	1.0+7	Expt	DOE-NDC-27	118	Apr82	ORL	Gwin+233U/252CF CFD EXPT.NDG
^{233}U	ν_p		3.0-1	Expt	DOE-NDC-27	118	Apr82	ORL	Gwin+233U/252CF CFD EXPT.NDG
^{235}U	σ_{tot}	3.0-1	1.0+1	Expt	DOE-NDC-27	1	Apr82	BNL	Chrien.NDG
^{235}U	σ_{inl}	1.0+6	3.5+6	Expt	DOE-NDC-27		Apr82	ANL	Smith+PAGE A-1,GRPH.
^{235}U	$\sigma_{dif.inl}$	1.0+6	3.5+6	Expt	DOE-NDC-27		Apr82	ANL	Smith+PAGE A-1,GRPH.
^{235}U	$\sigma_{dif.inl}$	1.0+4	5.0+6	Theo	DOE-NDC-27	78	Apr82	LAS	Arthur.NDG
^{235}U	$\sigma_{dif.inl}$	8.0+5	2.5+6	Theo	DOE-NDC-27	83	Apr82	LTI	Sheldon+ NDG. TBD.
^{235}U	$\sigma_{n,f}$	1.0+0	1.0+2	Eval	DOE-NDC-27	80	Apr82	LAS	Moore+NDG.MULTI-LVL FIT
^{235}U	$\sigma_{n,f}$	1.0+4	5.0+6	Theo	DOE-NDC-27	78	Apr82	LAS	Arthur.NDG
^{235}U	$\sigma_{n,f}$	2.0+4	3.0+7	Expt	DOE-NDC-27	100	Apr82	LRL	Behrens+CS RATIO,NSE 80 393.
^{235}U	$\sigma_{n,f}$	7.0+5	3.0+7	Expt	DOE-NDC-27	100	Apr82	LRL	Behrens+CS RATIO. NSE TBP.
^{235}U	$\sigma_{n,f}$	1.4+7		Expt	DOE-NDC-27	95	Apr82	MHG	Mahdavi+NDG. TBC
^{235}U	$\sigma_{n,f}$	2.6+6		Expt	DOE-NDC-27	99	Apr82	NBS	Duvall+ASSOC.PART.TECHN.NDG.TBC.
^{235}U	$\sigma_{n,f}$	1.4+7		Expt	DOE-NDC-27	100	Apr82	NBS	Wasson.SEE NSE 80. 282
^{235}U	$\sigma_{n,f}$	3.0+5	3.0+6	Expt	DOE-NDC-27	99	Apr82	NBS	Carlson+BLACK DET. NDG.TBC.
^{235}U	$\sigma_{n,f}$	5.0+3	2.0+7	Expt	DOE-NDC-27	118	Apr82	ORL	Weston+239,240PU RATIOS CFD ENDF
^{235}U	$\sigma_{n,f}$	1.0-2	3.0+4	Expt	DOE-NDC-27	119	Apr82	ORL	Gwin+ CFD EXPT.NDG.
^{235}U	ν_d		3.5+6	Expt	DOE-NDC-27	87	Apr82	LTI	Couchell+E-SPECTRA.NDG.TBC.
^{235}U	Spect.fiss n		1.5+7	Theo	DOE-NDC-27	79	Apr82	LAS	Madland+GRPH FISS.NEUT.SPECT.MATRIX
^{235}U	Fiss.Yield	NDG		Expt	DOE-NDC-27	64	Apr82	LRL	Meyer+TBL.85SE-88SE YLDS.
^{235}U	Fiss.Yield	1.7+5	8.1+6	Expt	DOE-NDC-27		Apr82	ANL	Glendenin+ PAGE A-9. PR/C 24 2600
^{235}U	Fiss.Yield	2.5-2		Expt	DOE-NDC-27	140	Apr82	BNW	Reeder+ISOMER YLD.RATIO.NDG.TBC.

NEUTRON DATA REFERENCES

Element	Quantity	Energy (eV) Min	Max	Type	Documentation Ref	Page	Date	Lab	Comments
^{235}U	Frag Spectra	1.8+5	8.8+6	Expt	DOE-NDC-27		Apr82	ANL	Meadows+PG.A-7.GRPH ANGDIST.FIS.FRAG
^{235}U	Frag Spectra	1.4+7		Expt	DOE-NDC-27	98	Apr82	MHG	Mahdavi+ANG.DIST.NDG.TBC.
^{238}U	σ_{inl}	1.0+6	3.5+6	Expt	DOE-NDC-27		Apr82	ANL	Smith+PAGE A-1,GRPH.
^{238}U	$\sigma_{dif.inl}$	1.0+6	3.5+6	Expt	DOE-NDC-27		Apr82	ANL	Smith+PAGE A-1,GRPH.
^{238}U	$\sigma_{dif.inl}$	1.0+4	5.0+6	Theo	DOE-NDC-27	78	Apr82	LAS	Arthur.NDG
^{238}U	$\sigma_{dif.inl}$	9.0+5	2.1+6	Expt	DOE-NDC-27	82	Apr82	LTI	Beghian+NDC.125 DEGS.E0 STRENGTH
^{238}U	$\sigma_{dif.inl}$	8.0+5	2.5+6	Expt	DOE-NDC-27	83	Apr82	LTI	Sheldon+GRPHS
^{238}U	$\sigma_{n,f}$	1.0+4	5.0+6	Theo	DOE-NDC-27	78	Apr82	LAS	Arthur.NDG
^{238}U	$\sigma_{n,f}$	1.4+7		Expt	DOE-NDC-27	95	Apr82	MHG	Mahdavi+NDG. TBD.
^{238}U	Res.Params.	NDG		Expt	DOE-NDC-27	117	Apr82	ORL	Meszaros+ NDG.
^{238}U	$<\Gamma>/D$	4.0+3	6.0+3	Expt	DOE-NDC-27	117	Apr82	ORL	Meszaros+ NDG.
^{237}Np	σ_{tot}	4.0+1	1.2+2	Expt	DOE-NDC-27	70	Apr82	LAS	Auchampaugh+NDG
^{237}Np	$\sigma_{n,f}$	4.0+1	1.2+2	Expt	DOE-NDC-27	70	Apr82	LAS	Auchampaugh+SIG.NORMALIZATION TOO LO
^{237}Np	$\sigma_{n,f}$	7.0+5	3.0+7	Expt	DOE-NDC-27	100	Apr82	LRL	Behrens+CS RATIO. NSE TBP.
^{237}Np	$\sigma_{n,f}$	2.0+4	3.0+7	Expt	DOE-NDC-27	100	Apr82	LRL	Behrens+CS RATIO,NSE 80 393.
^{237}Np	$\sigma_{n,f}$	1.4+7		Expt	DOE-NDC-27	95	Apr82	MHG	Mahdavi+NDG. TBD.
^{238}Pu	$\sigma_{n,f}$	+6		Theo	DOE-NDC-27	100	Apr82	NBS	Behrens.TBL.EST.CS FROM SYSTEMATICS.
^{239}Pu	σ_{inl}	1.0+6	3.5+6	Expt	DOE-NDC-27		Apr82	ANL	Smith+PAGE A-1,GRPH.
^{239}Pu	$\sigma_{dif.inl}$	1.0+6	3.5+6	Expt	DOE-NDC-27		Apr82	ANL	Smith+PAGE A-1,GRPH.
^{239}Pu	$\sigma_{dif.inl}$	1.0+4	5.0+6	Theo	DOE-NDC-27	78	Apr82	LAS	Arthur.GRPH,CS(.057MEV LVL) CFD ENDF
^{239}Pu	$\sigma_{dif.inl}$	8.0+5	2.5+6	Theo	DOE-NDC-27	83	Apr82	LTI	Sheldon+ NDG. TBD.
^{239}Pu	γ Spectra	2.0+3		Expt	DOE-NDC-27	2	Apr82	BNL	Chrien.FISS.COMPETITION VS STAT.CAPT
^{239}Pu	$\sigma_{n,f}$	1.0+4	5.0+6	Theo	DOE-NDC-27	78	Apr82	LAS	Arthur.NDG
^{239}Pu	$\sigma_{n,f}$	1.4+7		Expt	DOE-NDC-27	95	Apr82	MHG	Mahdavi+NDG. TBC
^{239}Pu	$\sigma_{n,f}$	5.0+3	2.0+7	Expt	DOE-NDC-27	118	Apr82	ORL	Weston+239PU/235U CFD ENDF.
^{239}Pu	$\sigma_{n,f}$	1.0-2	6.0+4	Expt	DOE-NDC-27	119	Apr82	ORL	Gwin+ CFD EXPT.NDG.
^{239}Pu	Fiss.Yield	1.0+5	8.0+6	Expt	DOE-NDC-27		Apr82	ANL	Glendenin+ PAGE A-9, TBD.
^{239}Pu	Frag Spectra	1.4+7		Expt	DOE-NDC-27	98	Apr82	MHG	Mahdavi+ANG.DIST.NDG.TBC.
^{240}Pu	σ_{tot}	2.5+0	6.0+6	Expt	DOE-NDC-27	119	Apr82	ORL	Gwin. NDG.
^{240}Pu	σ_{inl}	1.0+6	3.5+6	Expt	DOE-NDC-27		Apr82	ANL	Smith+PAGE A-1,GRPH.
^{240}Pu	$\sigma_{dif.inl}$	1.0+6	3.5+6	Expt	DOE-NDC-27		Apr82	ANL	Smith+PAGE A-1,GRPH.
^{240}Pu	$\sigma_{n,f}$	5.0+3	2.0+7	Expt	DOE-NDC-27	118	Apr82	ORL	Weston+240PU/235U CFD ENDF.
^{240}Pu	Res.Params.	1.1+0		Expt	DOE-NDC-27	1	Apr82	BNL	Chrien.WN,WG OF 1.056 EV RES.

NEUTRON DATA REFERENCES

Element	Quantity	Energy (eV) Min	Max	Type	Documentation Ref	Page	Date	Lab	Comments
^{242}Pu	$\sigma_{dif.inl}$	1.0+4	5.0+6	Theo	DOE-NDC-27	78	Apr82	LAS	Arthur.NDG
^{242}Pu	$\sigma_{n,f}$	1.0+4	5.0+6	Theo	DOE-NDC-27	78	Apr82	LAS	Arthur.NDG
^{242}Pu	$\sigma_{n,f}$	NDG		Expt	DOE-NDC-27	71	Apr82	GEL	Moore+NDG
^{244}Pu	$\sigma_{n,f}$	NDG		Expt	DOE-NDC-27	71	Apr82	GEL	Moore+NDG
^{243}Cm	Fiss.Yield	2.5-2		Expt	DOE-NDC-27	115	Apr82	ORL	Breederland.NDG.23 CUMUL.YLDS.
^{244}Cm	$\sigma_{n,f}$	1.0-1	1.0+5	Expt	DOE-NDC-27	142	Apr82	RPI	Stopa+NDG
^{244}Cm	Res.Params.	7.7+0	3.5+1	Expt	DOE-NDC-27	142	Apr82	RPI	Stopa+NDG
^{246}Cm	$\sigma_{n,f}$	1.0-1	1.0+5	Expt	DOE-NDC-27	142	Apr82	RPI	Stopa+NDG
^{246}Cm	Res.Params.	4.3+0	1.5+1	Expt	DOE-NDC-27	142	Apr82	RPI	Stopa+NDG
^{248}Cm	$\sigma_{n,f}$	1.0-1	1.0+5	Expt	DOE-NDC-27	142	Apr82	RPI	Stopa+NDG
^{248}Cm	Res.Params.	7.3+0	7.6+1	Expt	DOE-NDC-27	142	Apr82	RPI	Stopa+NDG
^{252}Cf	ν_p	Spon		Expt	DOE-NDC-27	26	Apr82	INL	Smith.HALF-LIFE DERIV.FROM NUBAR EXP
^{252}Cf	ν_p	Spon		Expt	DOE-NDC-27	118	Apr82	ORL	Gwin+233U/252CF CFD EXPT.NDG
^{252}Cf	Spect.fiss n	Spon		Expt	DOE-NDC-27		Apr82	ANL	Poenitz+PAGE A-10.NDG.ANALY TBD

1. BROOKHAVEN NATIONAL LABORATORY

The Neutron Nuclear Physics Group at the HFBR is engaged in three areas of research: a) neutron cross sections, b) spectroscopy of fission product nuclei, and c) nuclear structure investigations with the (n,γ) reaction. A large and active user program is carried out in these areas, which are all relevant to nuclear energy applications. A summary of the principal experiments of the period March 1981 through March 1982 is contained in this report, with descriptive material presented on the work most closely related to applications.

A. NEUTRON CROSS SECTIONS

1. ^{240}Pu

^{240}Pu possesses a value for the resonance capture integral that is mostly due to the resonance at 1.056 eV. It is important to the neutron economy of a reactor to accurately know the parameters of the resonance, i.e., Γ_n and Γ_γ. The HFBR fast chopper facility has been used to make a determination of these resonance parameters. In this low energy region, the intensity and resolution of the instrument are adequate for precise measurements. Transmission measurements for ^{240}Pu oxide at room temperature, and capture measurements for both ^{240}Pu metal and oxide at room, liquid N_2 and He temperatures were made. The resolution of the experiment at 1 eV is nearly an order of magnitude smaller than the resonance intrinsic width and Doppler width. Thus the level parameters, Γ_n and Γ_γ, can be properly determined by a systematic study through shape analysis. By considering systematic uncertainties, including those due to transmission data normalization, sample uniformity and the assumed value of R', the level parameters and their total uncertainties for the 1.056 eV resonance were determined as $\Gamma_n = 2.32 \pm 0.06$ meV and $\Gamma_\gamma = 32.4 \pm 1.0$ meV. Compared to previously recommended values (BNL 325) the present results of neutron and capture widths are 0.9% and 4.5% higher, respectively. From these measurements and the variation of Doppler width with temperature, it is possible to infer the Debye temperature, θ_D, for plutonium. Within statistical uncertainties all measured θ_D are consistently found to be 175°K, except the case of metallic ^{240}Pu at liquid N_2 temperature, where the θ_D value is a little higher. We are unaware of any other θ_D measurement for ^{240}Pu.

2. ^{235}U

In the low energy region, extensive scattering, capture, and fission cross section measurements have been performed on ^{235}U in recent years. Such cross sections are of importance in reactor technology. The value of the total cross section places an important constraint on the evaluation of these cross sections, since the various partial cross sections must add up to the total. The currently accepted total cross sections are now quite old, and are characterized by fairly large errors. In view of this situation, a series of precise transmission measurements from 0.3 to 10.0 eV were undertaken with the

BNL fast chopper. Special care was taken to reduce systematic errors contributed by the backgrounds, dead time, and sample non-uniformity. The data have been reduced to cross section form and all known errors have been analyzed. It is intended to do a multi-channel R matrix fit to these data since the ratio of typical level widths to level spacings is too large to permit a single level fit. (BNL)

3. Resonance-Averaged Capture in ^{240}Pu

Last year a study of resonance-averaged neutron capture γ-ray spectra at E_n = 2 keV was carried out for the I = $1/2^+$ target nucleus ^{239}Pu. At that time, it was reported that the intensities of transitions to known states of both positive and negative parities in the spin range of $0^{\pm}$ to $2^{\pm}$ did not follow the intensity patterns predicted by statistical capture. It is now understood that this apparent discrepancy is due entirely to competition with the fission channel. For ^{239}Pu $\langle\Gamma_F\rangle(J=0)/\langle\Gamma_F\rangle(J=1)$ is about a factor of 70. Thus the J=0 radiative capture is strongly suppressed. When the competition effect is accounted for, the resulting spectrum is fully consistent with a purely statistical capture process. (BNL)

4. Capture in Copper at 2 and 24 keV

As part of a collaborative program with the ECN, Petten, Netherlands, capture spectra for ^{63}Cu and ^{65}Cu in a normal copper target have been recorded at 2 and 24 keV. At the same time, precise spectra for thermal capture in separated isotopes are being obtained at the Dutch High Flux Reactor at Petten. The analysis of these results will be combined. The object of the research is to study the systematics of the capture process for light and medium weight nuclei, and particularly the relative strengths of E1 and M1 radiation. (BNL/Petten)

B. SPECTROSCOPY OF FISSION PRODUCT NUCLEI

1. Research and Development in Support of Facilities

There were two significant advances which greatly improved the capability of the TRISTAN facility. The first is the implementation of a 4-detector, fixed angle, angular correlation apparatus. By the simultaneous data taking among the six pairs possible from 4 detectors, the measurement of angular correlations in γ-γ coincidences is improved with respect to both statistical and systematic errors. The device has been successfully employed in measurements on the first excited 0^+ states in the transitional nuclides $^{142-148}$Ce. The second breakthrough occurred by the substitution of a solid graphite cylindrical target in place of the graphite cloth target in the TRISTAN ion source. The solid target shows superior yield at lower source power levels, and therefore results in an ion source which shows little deterioration in output with time. The improved source reliability allows running of long experiments with little or no attention to the ion source. A comparison of the yields with those available at OSTIS (Grenoble) shows a factor of ten in favor of TRISTAN.

2. Beta-delayed Neutron Emission

a. Beta-delayed Two-neutron Emission

By using a time interval analyzer and a neutron counter consisting of 40 tubes of ^{3}He embedded in polyethylene, two-neutron emission from the decay of ^{96}Rb, ^{97}Rb, ^{98}Rb and ^{99}Rb could be investigated. The initial experiments indicated that ^{98}Rb was a 2-neutron emitter. However, the discovery of time correlated background events and major improvements in ion source output made it reasonable to repeat the experiment. Two-neutron emission was observed for ^{98}Rb with an emission probability of $P_{2n}=(0.060\pm0.009)\%$. For the other isotopes upper limits for P_{2n} were measured as 0.004, 0.008 and 0.024% for ^{96}Rb, ^{97}Rb and ^{99}Rb, respectively. The data for ^{98}Rb represent the first observation of two-neutron emission from a fission fragment, and a considerable improvement over data previously collected at TRISTAN. (PNW/BNL)

b. Half-lives, Average Energies, and P_n Values of Sr, Y, Ba, and La Precursors

The TRISTAN on-line isotope separator facility at the HFBR at Brookhaven National Laboratory has been used to provide sources of mass separated fission products for delayed neutron studies. Half-lives are measured by multiscaling the pulses from a high-efficiency neutron counter which surrounds the ion beam deposition point. Neutron decay curves are obtained from each of three rings of counter tubes embedded in polyethylene moderator. For mass chains containing more than one precursor, the neutron decay curves are analyzed by a least squares fitting program to give the half-lives and initial values of each component. The ratio of initial values from one ring to another is proportional to the average energy of the delayed neutron spectrum for a given component. Beta decay curves are simultaneously measured from a Si beta detector mounted inside the neutron counter. The delayed neutron emission probability (P_n) is obtained from the ratio of neutron initial value to beta initial value for a given component. The calibration of the neutron counter efficiency and ring ratio versus neutron energy was performed by a separate experiment using monoenergetic neutrons from $^{51}V(p,n)^{51}Cr$ and $^{57}Fe(p,n)^{57}Co$ reactions. Results for Sr, Y, Ba, and La precursors have been obtained. (PNW/Cornell/BNL)

c. Gamma Spectra Following Delayed Neutron Emission

Gamma spectra in coincidence with delayed neutrons are being measured for a number of Rb and Cs precursors produced at the TRISTAN facility. In this $\beta n \gamma$ process, beta-delayed neutrons populate excited states in the final nuclide which then decay by gamma emission. From the energies and intensities of gamma rays, we deduce the partial neutron emission probabilities ($P_n^{\,i}$) to the excited states. The $P_n^{\,i}$ provide a sensitive test of various models for delayed neutron emission. The gamma spectra are measured with a large GeLi detector which is gated by signals from a high-efficiency, long-resolving time, polyethylene array of ^{3}He filled proportional counters (SNC). The gamma spectra can be routed according to which ring of neutron from different rings is related to the average energy of the neutrons feeding the particular gamma transition. Initial experiments on ^{97}Rb and ^{145}Cs have demonstrated the feasibility of the technique. (PNW/LANL/Cornell/BNL)

d. Recoil Spectrometer Measurements of Beta-delayed Neutron Spectra

Hydrogen-filled proportional counters have been calibrated for neutron response at the HFBR tailored beam facility. Two-parameter measurements of the pulse rise time and height allow optimum application of pulse shape discrimination techniques. The detectors were used to collect delayed neutron spectral distributions from ^{94}Rb, ^{95}Rb, and ^{96}Rb. Initial results have been promising; for example, the 13 keV resonance from ^{95}Rb has been observed. Further experiments, at higher intensity, are planned. (INEL/BNL)

e. High Resolution Measurements of Delayed Neutron Emission Spectra from Fission Products

Considerable interest has developed in the details of the neutron emission spectra following beta decay of the fission products of ^{235}U. These delayed neutron spectra are of importance in reactor control applications, and also in the understanding of the variation of beta decay strength with nuclear excitation energy. Using the TRISTAN on-line mass separator at the BNL High Flux Reactor, an extensive survey has been undertaken of delayed neutron spectra in the light mass regions (Rb isotopes) and the heavy mass region (Cs isotopes) accessible with a surface ionization in-beam ion source. Particular emphasis has been placed on the low energy end of these spectra, with $E_n <$ 300 keV. The detection methods used are the Cutler-Shalev ^{3}He spectrometer and a time-of-flight spectrometer. Energy resolutions of about 15 keV have been obtained with the former, and with the latter, resolutions of from 5 to 10% in $\Delta E/E$ have been obtained. For the t-o-f measurement a high pressure ($\approx$1900 psi) ^{3}He-Xe gas scintillation detector has been employed. The survey includes data from ^{93}Rb, ^{94}Rb, ^{95}Rb, ^{96}Rb, and ^{97}Rb ; and ^{143}Cs, ^{144}Cs, ^{145}Cs, and ^{146}Cs. Calibration of the detector response function and efficiency for the Cutler-Shalev detector in the range 24-360 keV has been performed using the Fe and Sc-filtered beams from the HFBR. These filters provide discrete neutron groups of known energy and intensity. Both techniques have revealed considerable structure at low energy for some isotopes, attributable to compound nuclear states populated in the beta decay. Of particular interest are peaks near 13 keV for ^{95}Rb; at 40 keV for ^{96}Rb, and 20 keV for ^{143}Cs. For several of these peaks the resolution is adequate to obtain neutron widths by shape analysis. The study of such spectra represents the only way to obtain parameters for neutron resonances in nuclides far off the line of stability, and hence is of interest in the extrapolation of strength functions and level densities necessary to predict neutron capture cross sections for fission products. (Cornell/McGill/LANL/BNL)

3. Precise Mass Measurements from Beta-decay Spectra

a. Precise Q-values for Neutron-rich Rb, Ba and La Isotopes

Beta-ray end-point energies for Rb, Ba and La fission products were measured at TRISTAN using an intrinsic-Ge β spectrometer. Coincidence measurements were used to establish feeding relationships and to verify level schemes in daughter nuclides. Q_β values were measured for ^{88,94,96,98}Rb, ^{146,147,148}La and ^{145}Ba. The data for ^{148}La represents the first Q_β measurement on that nucleus and gives a value of 1-2 MeV higher than predicted by most mass equations. Similar discrepancies may be found for the other isotopes (experimental Q-value higher than predicted) as well. Further experiments appear necessary to get better statistics on ^{147}La and ^{145}Ba. Of particular interest are the Ba isotopes, as there have been few experimental Q-values reported for these isotopes and their yield at TRISTAN is very high. These nuclei may provide a good test of mass formulas in transition regions, since the Ba isotopes are known to be in transition from spherical (at N=82) to deformed. (Clark/Iowa State/Swarthmore/BNL)

4. Gamma-ray Spectroscopy of Fission Product Nuclei

a. Gamma-gamma Angular Correlation Studies for Cascades in ^{142}Ce

In a recent publication, Michelakakis et al. reported a 2^+ assignment for the spin of the 1219 keV level in ^{142}Ce, thus leading to a $0^+,2^+,2^+$ sequence for the lowest lying levels of ^{142}Ce, unlike the neighboring Ce isotopes. In view of the importance of this assignment, a γ-γ angular correlation experiment was undertaken at the TRISTAN isotope separator, at BNL to study the decay of $^{142}\text{La}\rightarrow{}^{142}\text{Ce}$. An experimental system consisting of four Ge spectrometers has been used. The angular correlation of the 578-641 keV cascade, which depopulates the 1219 keV level, was found to be consistent with a 4^+ assignment for this level in disagreement with ref. 1. Our results for several other cascades support this assignment. The 4^+ assignment agrees with earlier work of Basinger et al. in which one Ge(Li) and six NaI detectors were used. (BNL/Iowa State/Maryland/Stony Brook)

b. Confirmation of a First Excited 0^+ State in ^{148}Ce

The decay of ^{148}La to ^{148}Ce had been studied using the TRISTAN isotope separator installed at Brookhaven National Lab. A 0^+ assignment was previously proposed for the spin of the 770 keV level in ^{148}Ce, based on the decay scheme and on the systematics of N=90 isotones. In order to confirm this assignment, the γ-γ angular correlation of the 612-158 keV cascade depopulating this level was measured. A system composed of four Ge spectrometers at about 5 cm from the source was used, enabling measurement of six angles simultaneously. The correlation coefficients obtained are: $A_{22}=0.22\pm0.09$, $A_{44}=1.02\pm0.17$. These values are consistent with the theoretical values for a $0\rightarrow2\rightarrow0$ cascade. The A_{44} coefficient is more than three standard deviations larger than the maximum possible A_{44} for any $I\rightarrow2\rightarrow0$ cascade with $I>0$. Thus the proposed 0^+ assignment is unambiguously confirmed for the 770 keV level. (BNL/Iowa State/Maryland/Clark/Stony Brook)

c. Decay of ^{99}Sr to Levels in ^{99}Y

The level structure of ^{99}Y has been studied by γ multiscale and γ-γ coincidence measurements on the decay of ^{99}Sr. Approximately 90 γ lines have been associated with the decay of ^{99}Sr, and 90% of these have been placed in a level scheme for ^{99}Y. The halflife of ^{99}Sr has been measured to be 0.26 ± 0.02 s by the γ multiscale technique. (Oklahoma/Iowa State/BNL)

d. The Decay of ^{146}La to Levels of ^{146}Ce

Preliminary data on the levels of the transitional nuclide ^{146}Ce have been reported by groups at KFA, Julich and from ILL. ^{146}La is reported to decay with half-lives of 4.5 min and 8.5 sec. Recent studies at the isotope separator OSTIS at Grenoble, however, have shown that the 8.5 sec component actually consists of two components of 6 and 10 sec. An extensive study of the decay of ^{146}La was undertaken at the BNL TRISTAN mass separator to establish more firmly the level scheme of ^{146}Ce. These data include singles, γ-γ coincidence and angular correlations, and time-dependent spectral data (gamma-ray multiscale or GMS data). A greatly-extended knowledge of the ^{146}Ce level scheme has resulted, due to the superior beam intensities and low backgrounds available from TRISTAN. Experiments scheduled for FY 1982 include a detailed half-life search to identify the two isomers and an extended angular correlation experiment which will improve the statistics available for weak intraband transitions. (Iowa State/Maryland/Clark/Oklahoma/BNL)

e. Other Experiments

In addition to those described above, a number of other experiments have been pursued at TRISTAN. These include the following: a) Identification of the $7/2^-$ State in ^{141}Ba, b) The Decay of Mass Separated ^{146,148}Ba to Levels of ^{146,148}La, c) The Decay of Low Spin ^{148,150}Pr to Levels of ^{148,150}Nd, and d) Studies of the Decay of ^{145,147}Cs to ^{145,147}Ba.

C. NUCLEAR STRUCTURE WITH THE (n,γ) REACTION

1. ^{168}Er: Level Scheme and IBA Calculations

The level scheme for ^{168}Er, discussed in previous reports, was rechecked and extended with the new placement of a number of additional γ rays, the modification of a few spins and the finalization of the various band assignments. Searches were also made for upper limits on intensities of certain important low energy γ rays not observed. The upshot is a complete level scheme that was published. The interpretation of the scheme centers on the positive parity states for which extensive IBA calculations were done. In general these showed remarkable agreement with the data, correctly predicting the full series of $K=0^+$ and 2^+ bands below the pairing gap and providing a remarkable representation of the principal decay patterns. Specifically, the three most significant features of the level scheme, that is, the correct ratios of inter and intra band transition strengths, the totally unexpected preference for the β band to decay to the γ band and the weak $\beta \to$ground band decay, are all reproduced by the calculations. Moreover, this feature of the IBA is not the result of parameter tuning but an essential and virtually unavoidable characteristic of the IBA in deformed nuclei. In contrast, the traditional geometrical models, in the forms usually applied, either predict behavior contrary to experiment or require a microscopic extension to provide comparable predictions. These results in turn suggest a re-examination of the historical understanding of the nature of collective excitations in deformed nuclei, in particular, of the β band, which appears to be related in a collective way to the γ vibration. Subsequent efforts (see paragraphs below) to understand the structure and origin of the IBA predictions in deformed nuclei is beginning to lead to a new understanding of the basic excitations and interactions in deformed nuclei. (BNL/Nat. Research Council of Canada)

2. Bandmixing and the IBA

In order to elucidate the nature of the $\beta \to \gamma$ transitions that characterize both the data and the IBA in deformed nuclei, it is useful to consider whether they can arise in the geometrical model. In the limit of purely harmonic β and γ vibrations $\beta \to \gamma$ transitions are specifically forbidden. They violate the selection rule that limits changes in vibrational quanta by ± 1. However, if mixing of β and γ bands is introduced, albeit ad hoc, such transitions will occur. There is historic precedent for doing this: it has been common to introduce $\beta \to g$ and $\gamma \to g$ mixing to fine-tune theoretical predictions of $\beta \to g$ and $\gamma \to g$ transitions. We have, therefore, studied, in the geometrical model, the effects of $\beta \to \gamma$ mixing. Indeed, with it one can generate $\beta \to \gamma$ transitions with, on average, the correct (empirical) strength, and for reasonable values of the mixing parameter. However, the $\beta \to \gamma$ transition amplitudes arising from the mixing are, then, not a correction to an existing matrix element, but the entire source of the $\beta \to \gamma$ transition. Thus, their relative size one to another is independent of the strength of the mixing and turns out to disagree with the data. In the IBA, however, the $\beta \to \gamma$ transitions arise from both a direct matrix element and a mixing term, and the former, direct route dominates. Analysis of the ^{168}Er data in a Mikhailov formalism shows that, empirically, the $\beta \to \gamma$ transitions also arise predominantly from a direct matrix element. Thus on this key point, in which the IBA and geometrical models differ, the data support the IBA interpretation. (BNL)

3. A Study of the IBA E2 Operator in Deformed Nuclei

The detailed IBA calculations for ^{168}Er mentioned previously indicated the need to employ a parameterization of the IBA E2 operator which is considerably different from that corresponding to the SU(3) limit of the model. A more general study was, therefore, undertaken to investigate the structure of the E2 operator appropriate to deformed nuclei across the entire rare earth region. It was possible to show that, in the SU(3) limit of the Hamiltonian, the relative B(E2) values of transitions between different SU(3) representations are independent of the parameterization chosen for the operator. This feature in turn enables a correspondence to be established between the IBA

SU(3) states, and their geometrical analogues. In particular, it was shown that the third and fourth $K^{\pi}=0^{+}$ bands in the IBA do not correspond directly to $\beta\beta$ and $\gamma\gamma$ excitations built on the appropriate single phonon bands but rather to a mixture of these two modes. More generally, a study of empirical B(E2) values across the deformed region indicated the need for an almost constant form for the E2 operator which is very different from that of the SU(3) limit. Use of this parameterization then enables certain universal predictions to be made concerning the application of the IBA to deformed nuclei. The most significant of these is the dominance of $\beta\to g$ and $\gamma\to\beta$ transitions over $\beta\to g$ transitions, which implies that the "β" band in the IBA has a radically different structure from that expected from the geometrical model. Nevertheless, the properties of the IBA band seem to correspond well with those found empirically. (BNL)

4. A Revised Form for the IBA-1 Hamiltonian

The preceding study reveals a seeming inconsistency in the existing IBA-1 formalism. While the quadrupole operator in the Hamiltonian is always taken to have the SU(3) form, it is necessary to use a very different form to describe E2 transitions. Work is currently under way, therefore, to investigate the effect of using identical forms of the quadrupole operator in both cases. Preliminary results indicate that such an approach results in an improved description of deformed nuclei (e.g., ^{168}Er) with one less parameter than in the earlier formalism. In addition, by allowing the quadrupole operator to adopt the structure appropriate to the O(6) limit, a description of ^{196}Pt can be obtained which again is equivalent to the earlier description. In all these cases, the revised structure of the quadrupole operator obviates the need for any additional terms in the Hamiltonian other than those proportional to $Q\cdot Q$ and $L\cdot L$. Thus the revised formulation of the IBA-1 Hamiltonian becomes much closer to that of IBA-2, and it is hoped that this approach will aid in linking the two formalisms, and thus lead to an eventual effective microscopic description for the IBA-1 parameters. This study is still underway. (BNL)

5. Empirical Determination of IBA Solutions for Deformed Nuclei

The IBA Hamiltonian in deformed nuclei contains three parameterized terms. However, an analysis of its structure was undertaken to determine if the behavior of the IBA solutions (wave functions, energies, transition strengths) could be understood and predicted in a simple way. As a result, it was shown that, in fact, most observable properties depend on a single parameter which reflects the relative amount of SU(3) symmetry breaking. Moreover, this parameter can be uniquely fixed by a specific ratio of empirical energy levels involving the β and γ band energies. Given this, it is then possible to predict (indeed to read off from universal curves by inspection) all results of an IBA calculation, including energies, wave functions, E2 transition rates and their detailed composition, etc. simply by knowing this empirical ratio of energy levels. (BNL)

6. Re-expansion of IBA Wave Functions and Transition Rates in an SU(3) Basis

Given the above simple prescription for the IBA for deformed nuclei one might now hope to better understand the structure and behavior of the wave functions and transition rates. Unfortunately this is difficult since the IBA is normally expressed in an SU(5) basis which is terribly inconvenient for deformed nuclei. Therefore, the IBA wave functions were re-expanded in the SU(3) basis with the result that typical deformed nucleus wave functions now have at most 3-5 large amplitudes, each physically simple to understand, instead of the previous 30-60 amplitudes, none of which could be easily interpreted in a deformed context. Moreover, it is trivial now to inspect the behavior of these few amplitudes vs the simple empirical symmetry breaking parameter. When this is done, it is discovered that the IBA, in those deformed nuclei where the β band is above the γ band, is extraordinarily simple: it consists of the rotational bands and wave functions of the SU(3) limit broken (admixed) by only a $\Delta K=0$ interaction between certain pairs of bands. This immediately provides a simple rationale for the empirically observed constancy of γ vibration properties in deformed nuclei and the variability of the β band which has many more possible $\Delta K=0$ mixing partners lying nearby. It provides, moreover, hints toward a new understanding of the nature of deformed nuclei in terms of a new set of basic excitations and interactions. (BNL)

7. M1 Transitions in Deformed Nuclei and the IBA

Recent experimental and theoretical studies of M1 transitions in deformed even-even nuclei have pointed to a collective origin. Such a conclusion suggests that the IBA formalism should also be able to describe such transitions. The application of the IBA M1 operator to deformed nuclei has therefore been studied. It was possible to show that the spin dependence predicted for E2/M1 mixing ratios in the IBA is essentially identical to that which results from a geometrical approach, and, hence, that the IBA is capable of giving at least an equally good description of the data. More specifically, the IBA predicts that the reduced mixing ratios of transitions within the γ bands of deformed nuclei should be identical to those between γ and ground bands, if the initial and final spins involved are the same in the two cases. The available data seem to indicate that this prediction is at least approximately valid. It was also possible to show that the empirical signs of $\gamma \rightarrow g$ and $\beta \rightarrow g$ δ(E2/M1) values could be produced correctly. Finally, the form of the IBA M1 operator leads to certain predictions for M1 transitions in O(6) nuclei, which may be tested in the near future. (BNL)

8. Resonance-averaged Capture γ-ray Spectroscopy

a. Calculations of Fluctuations for Filtered Beam Experiments

The technique of resonance averaging has been utilized extensively in recent years as a means of identifying, in appropriate cases, sets of nuclear levels which are claimed to be complete over certain spin-parity and excitation energy ranges. The basis of these claims has largely rested on a semi-quantitative understanding of the averaging and capture process and on empirical evidence for good averaging for states of previously known spin and parity. However, a firm analytical basis has not yet been provided which quantitatively determines the capabilities and limitations of the technique. In view of this, an analysis of the resonance-averaged cross section was carried out with the use of Monte Carlo techniques, using the algorithm of Knuth. Test calculations were carried out for nuclei such as ^{168}Er and ^{164}Dy in which the relative probabilities for populating final states of different spin and parity were obtained as a function of the primary γ-ray intensity. The results substantiate the reliability of the technique for a nucleus such as ^{168}Er. For example, for the fifteen transitions previously classified as proceeding to $3^-,4^-$ final states, the probability of each being correct was $\geq$96.7%. For many of these transitions the probabilities were substantially closer to 100%. On the other hand, for the nucleus ^{164}Dy, where the level density near the neutron separation energy is less, the averaging process is less efficient. Here, similar calculations show overlapping distributions, and, therefore, suggest extreme caution in the use of the technique here. The utility of the averaging technique will be substantially enhanced in the future with the use of these analytic techniques to "calculate" the averaging process for each specific nucleus studied. (BNL)

b. Consequences of Completeness in Nuclear Spectroscopy: Search for 0^+ Bands in ^{164}Dy

The unique feature of the (n,γ) reaction is its inherent non-selectivity. This non-selectivity can be exploited to assure the observation of all states in certain spin and excitation energy ranges. Earlier, the development of these consequences has been pursued with studies of ^{193}Os, ^{109}Pd and ^{168}Er. The implications of completeness for the elucidation of rotational band structures was most extensively developed in the Er study. It was shown that a knowledge of the full set of negative parity states below 2200 keV with spins 2^-, 3^-, 4^-, and 5^- resulted in the correct deduction of the exact and complete number of rotational bands with each K value, and, in addition, that this set was complete, without going through the process of making specific band assignments for individual levels. The powers of this technique appears to be remarkable and has hardly been exploited. As an application of these ideas and as a followup to the study and interpretation of ^{168}Er, it was decided to investigate the structure of ^{164}Dy. Specifically, and surprising in the context of ^{168}Er, no 0^+ bands were known in ^{164}Dy. However, since the spin of ^{163}Dy is $5/2^-$ s wave neutron capture only feeds final states in ^{164}Dy with J=1, 2, 3 or 4. Therefore the search technique for 0^+ bands relied, not on their direct observation, but on the fact that such bands do not have 3^+ states, whereas K=2 bands do. Thus, studies at 2 and 24 keV were carried out, along with the measurement of γ rays from the 2^- resonance at 1.7 eV to help rule out 4^+ spins. Given a complete set of 2^+ and 3^+ states, then, an excess number of the former compared to the latter can only be ascribed to K=0 bands. In this way, it was possible to establish, from these data alone, that no excited 0^+ bands exist in ^{164}Dy below 1600 keV. Further collaborative experiments with the GAMS and BILL spectrometers at the ILL are planned to obtain a full level scheme. (BNL)

c. Other Experiments

A number of nuclides have been investigated using the 2- and 24-keV HFBR beam filters, the BNL monochrometer, and the facilities at Grenoble, including bent crystal data from the GAMS spectrometer and the conversion electron data from BILL. These include the following:

1) The $^{161}Dy(n,\gamma)^{162}Dy$ reaction, 2) $^{177}Hf(n,\gamma)^{178}Hf$; 3) $^{147}Sm(n,\gamma)^{148}Sm$, 4) Level Structure of ^{184}W, 5) Nuclear Structure of ^{136}Ba, 3) E0 Transitions in ^{188}Os and ^{196}Pt, 7) Study of ^{192}Os by Double Neutron Capture, 8) Study of ^{112}Cd and ^{114}Cd, 9) Odd Mass Pt Isotopes $^{193,195,197,199}Pt$, 10) ^{13}Ba, 11) ^{103}Ru, 12) ^{131}Ba and ^{133}Ba, 13) $^{176}La(n,\gamma)^{177}La$, and 14) Study of ^{108}Ag.

D. NATIONAL NUCLEAR DATA CENTER

1. Cross Section Evaluation Working Group (CSEWG) Activities

Two meetings of CSEWG were held in 1981. Revision 2 to ENDF/B-V will be released in the spring of 1982. Included will be revisions to Ca, Fe, ^{232}Th and ^{233}U, new evaluations for ^{7}Li, W isotopes, Ag isotopes and Rb isotopes. Natural element evalautions for B, Kr, Ag, Eu, Xe, Gd and Zr will be generated from existing isotopic evaluations.

The planning for ENDF/B-VI continues. The ENDF/B formats should be fixed in spring 1982 and the "standards" evaluations completed in spring of 1983.

Updates for the report "Standard Reference and Other Important Nuclear Data" (BNL-NCS-51123, ENDF-300) are in press. These discuss fast fission ratios of ^{232}Th, $^{233,238}U$, $^{239,241}Pu$ relative to ^{235}U and the half-lives of $^{232,233,234,235,236}U$ and ^{238}U.

2. BNL-325 Vol. 1 Part A

The fourth edition of BNL-325 Vol. 1 Part A, "Neutron Cross Sections" for Z = 1-60 was published by the Academic Press Inc. Work is in progress on Part B for Z = 61-100, and it will include a consistent fit to the thermal data of fissile elements. It is expected that work on Part B will be finished by September 1982 and that it will appear in print during 1982.

3. Nuclear Data Sheets

The transfer of responsibility for the publication of the Nuclear Data Sheets from the Nuclear Data Project at ORNL to NNDC is complete. NNDC has produced the Nuclear Data Sheets starting from the June 1981 issue (NDS 33 No. 2) and the subsequent issues (NDS 33 No. 3, 4, 34, No. 1, 2 in press) to date and will continue to do so in the future.

The U.S. is part of an international network of evaluators contributing recommended values of nuclear structure information to the Evaluated Nuclear Structure Data File (ENSDF). Publication of the Nuclear Data Sheets proceeds directly from this computerized file. In addition to the U.S., evaluations have been received or are anticipated from Germany, United Kingdom, USSR, France, Belgium, Kuwait, Sweden and Canada. International meetings of the network evaluators are sponsored by the IAEA.

It is planned to bring out a new edition of the Nuclear Wallet Cards (last published in January 1979) in June 1982 and a microfiche computerized chart of nuclides called Computope Chart in March 1982. Both these publications represent a subset of data extracted from the computerized ENSDF file and are therefore consistent and current with the Nuclear Data Sheets. An article on the Nuclear Physics Section of the Physics Vade Mecum published on the 50th anniversary of the American Institute of Physics was contributed by NNDC.

4. Seminar on Thermal Reactor Data

The National Nuclear Data Center will host a two-day Seminar/Workshop entitled "Thermal Reactor Benchmark Calculations, Techniques, Results and Applications." The meeting is scheduled for May 17 and 18, 1982. The Electric Power Research Institute (EPRI) will sponsor the meeting and publish the proceedings. The topics will include reactor physics and nuclear data, analysis of thermal reactor benchmarks, and utility and vendor needs.

A. NEUTRON DETECTION

1. A New Type of Neutron Detector Using MWC's* (T.D. Ford**, F.P. Brady, J.L. Romero, C.M. Castaneda, and M.L. Johnson)

The development of a new type of neutron detector, which uses multiwire chambers and large area ΔE and E detectors as a recoil proton spectrometer, is being carried out and a preliminary test of the system was very promising. The aim is to be able to measure neutron elastic and inelastic scattering (for example to giant resonances), and (n,xn) neutron continuum spectra.

Neutron time-of-flight (TOF) is the conventional way of measuring neutron spectra. With neutron beam experiments one does not always have a target trigger, and this complicates the problem of selecting by TOF the neutron beam peak from the tail, and of measuring the TOF of the scattered or outgoing neutron. Another problem with TOF is that there are large backgrounds of neutrons (and gamma rays) associated with the production of a neutron beam via (intense) proton or deuteron beams. Elastic cross sections away from forward angles as well as inelastic and continuum cross sections are relatively small and difficult (and very time consuming) to measure against the backgrounds present.

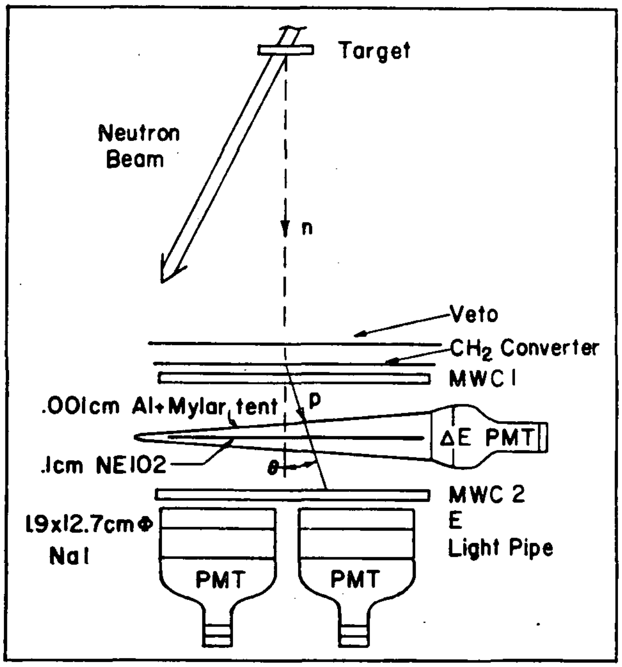

Figure A-1. Neutron detection system using multiwire chambers.

* Supported by National Science Foundation (Grant PHY79-26282)

** Supported by Associated Western Universities Fellowship

The system we have tested uses the arrangement shown in figure A-1. The CH_2 acts as a converter so that a recoil proton produced by a neutron is tracked in the multiwire chambers (MWC) and registered in the ΔE and E detectors. For neutrons coming from the target, the measurement of the n-p scattering angle and the proton energy determines the neutron energy. The closeness of the detector system to the target compensates for the low efficiency (compared to a large plastic scintillator many meters away) and renders small the target associated backgrounds, such as those due to second scatterings from the ground.

This new technique looks particularly useful when one wants to measure a neutron spectrum over a wide energy range as in (n,xn) reactions when searching for giant resonance continuum structures. TOF is difficult because of wrap-around from other beam bursts; or requires using a high-intensity beam sweep to reduce the number of beam bursts, which in turn reduces the average neutron beam intensity nearly an order of magnitude.

We have completed a test using the (p,n) reaction at low intensity beam with the detector at zero degrees. Some of the data for ^{7}Li is shown below in figure A-2. The energy resolution is approximately 3.6%, or about 2.2 MeV at 60 MeV. The effect of the carbon in CH_2 was small, $\lesssim 5\%$ at the highest neutron energies (50-60 MeV) and smaller at lower energies.

We are planning to make further tests using the (n,xn) reaction at high beam intensity and at forward angles for a ^{40}Ca target.

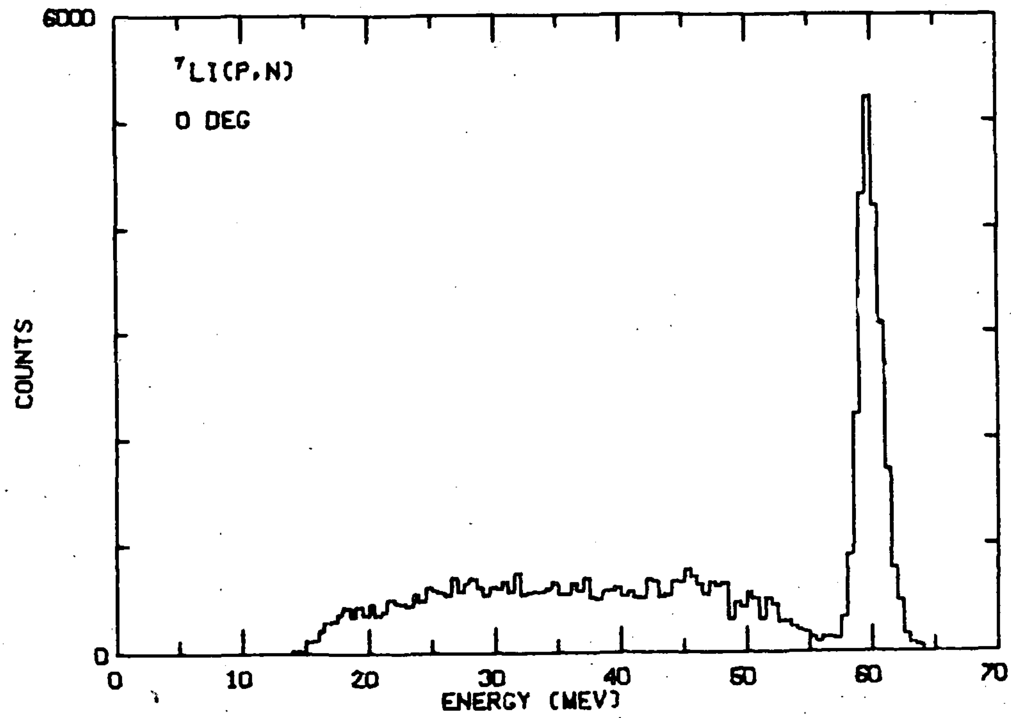

Figure A-2. Neutron Spectrum for ^{7}Li(p,n) at 61.8 MeV incident energy.

A. NUCLEAR-STRUCTURE AND DECAY-DATA EVALUATION ACTIVITIES

1. The Use of Data from Beta-Strength-Function Experiments to Obtain Average Decay-Energy Values for Short-Lived Fission Products (C. W. Reich, R. L. Bunting)

The libraries of fission-product nuclear data utilized by "summation-calculation" codes to calculate the fission-product decay-heat source term incorporate data on large numbers (typically several hundred) of individual nuclides. For each nuclide, the radioactive-decay information required for these decay-heat calculations includes the half-life, decay modes and the average β and γ energy ($\langle E_\beta \rangle$ and $\langle E_\gamma \rangle$, respectively) emitted per decay. At the present time, a significant fraction of these data (especially the average decay-energy values) results from procedures other than direct experimental determination. For example, the Version-IV ENDF/B Fission-Product File contained data for 711 radioactive nuclear species. Of these, ~380 represented cases for which the experimental data were either non-existent or sufficiently sparse that the $\langle E_\beta \rangle$ and $\langle E_\gamma \rangle$ values could not be obtained directly. These nuclides were generally those with short half-lives, which, because of the attendant experimental difficulties, have remained relatively unstudied. Unfortunately, they are also the ones whose major contribution to the decay-heat source term occurs at relatively short times (~1 to ~10^3 s), which is the region of importance for the assessment of loss-of-coolant accidents (LOCA).

In the course of our decay-data evaluation for the Version-V Fission Product File of ENDF/B, we became aware of measurements[1] of the beta-strength functions of a number of short-lived fission-product nuclides. Many of these were nuclides for which no other information on the emitted β or γ radiation was available. It seemed to us that such data could be used to provide $\langle E_\beta \rangle$ and $\langle E_\gamma \rangle$ values for these nuclides, thus significantly expanding the base of "measured" data for ENDF/B-V. Accordingly, $\langle E_\beta \rangle$ and $\langle E_\gamma \rangle$ values were extracted from the β-strength data and incorporated into ENDF/B.

We have recently submitted for publication (in Nuclear Science and Engineering) a paper describing our procedure for obtaining average decay-energy values from the β-strength data and presenting these deduced values. We also have included in this paper a comparison, where possible, of our deduced $\langle E_\beta \rangle$ values with those obtained from conventional decay-schemes studies and direct β-spectrum measurements. We have found that, on the average, the β-strength-based values agree better with those from the direct β-spectrum measurements than does either of these with the values obtained from the decay-schemes studies. We further conclude that, from an experimental point

[1] K. Aleklett, G. Nyman and G. Rudstam, Nucl. Phys. A246, 425 (1975).

of view, the present status of the average decay-energy data for the short-lived fission-product nuclides is rather poor.

2. Mass-Chain Evaluation for the Nuclear Data Sheets (R. L. Bunting, C. W. Reich)

Through our participation in the International Nuclear-Structure and Decay-Data Evaluation Network, which has as its objective the establishment and maintenance of a four-year cycle time for the Nuclear Data Sheets, we have the responsibility for the ten mass chains in the region $153 \leq A \leq 162$. The mass-chain evaluations for A=157 and 153 have been completed and are now in the review process. Work on the next two A chains on our schedule, namely A=160 and 161, is underway.

B. APPLICATIONS OF NUCLEAR-DECAY AND GAMMA-SPECTROSCOPY DATA

1. Emission Probabilities and Energies of the Prominent Gamma-Ray Transitions from the ^{240}Pu Decay (R. G. Helmer and C. W. Reich)

As a part of our laboratory involvement in the work of the IAEA Coordinated Research Program to measure and evaluate required nuclear decay data for selected transactinium isotopes, we are making precise (overall accuracy $\lesssim 1\%$) measurements of the emission probabilities (absolute intensities) of the prominent gamma-ray transitions from isotopes of U and Pu of particular importance for fission-reactor technology. The first in this series of measurements involved the decay of ^{240}Pu. The abstract of the published article[1] on this work follows.

> To permit increased precision in the quantitative assay of ^{240}Pu by means of gamma-ray spectrometry, we have measured the emission probabilities of the three prominent gamma-rays associated with the decay of ^{240}Pu. The gamma-ray emission rates were measured using calibrated Ge spectrometers. The decay-rate calibration was based on a measurement of the alpha-emission rate by NBS. Precise values for the gamma-ray energies were also measured. The following results were obtained: 45.244(2), 104.234(6) and 160.308(3) keV for the gamma-ray energies, and 43.5(9), 7.18(7) and 0.402(4) photons per 10^5 decays for the respective gamma-ray emission probabilities.

2. Emission Probabilties and Energies of Gamma-Ray Transitions from the ^{239}Pu Decay (R. G. Helmer, C. W. Reich, R. J. Gehrke, J. D. Baker)

As a part of our laboratory involvement in the work of the IAEA Coordinated Research Program noted above, the second set of measurements was on the

[1] R. G. Helmer and C. W. Reich, International Journal of Applied Radiation and Isotopes 32, 829 (1981).

decay of ^{239}Pu. The abstract of the published article[1] on this work follows.

> To aid in the quantitative assay of ^{239}Pu by means of gamma-ray spectrometry, we have made precise measurements of the emission probabilities of six of the prominent gamma-rays associated with the decay of ^{239}Pu. The gamma-ray emission rates were measured using calibrated Ge spectrometers. The decay-rate calibration was based on a measurement of the alpha-emission rate by NBS. Gamma-ray energies were also measured. For six precisely measured lines the energy values obtained are 51.624(1), 129.296(1), 203.550(5), 332.845(5), 375.054(3) and 413.713(5) keV and the respective gamma-ray emission probabilities are 27.1(5), 6.41(5), 0.568(4), 0.492(4), 1.547(12) and 1.455(9) photons per 10^5 decays. Relative gamma-ray intensities were also determined for about 55 additional transitions.

3. <u>Emission Probabilities and Energies of the Prominent Gamma-Ray Transitions from the Decay of ^{238}Pu</u> (R. G. Helmer, C. W. Reich, J. D. Baker, R. J. Gehrke)

The third set of measurements in our involvement in the IAEA Coordinated Research Program noted above is on the decay of ^{238}Pu. The emission rates and energies of four prominent gamma rays have been measured on calibrated Ge spectrometers. The decay rate calibration was based on an alpha-emission-rate measurement done by NBS. The preliminary results are 43.498(1), 99.854(3), 152.720(2) and 766.37(3) keV for the gamma-ray energies and 38.6(8), 7.48(7), 0.944(12) and 0.0218(11) photons per 10^5 decays for the respective gamma-ray emission probabilities.

4. <u>Gamma-Ray Energies from the Decay of ^{99}Mo, ^{133}Ba and ^{210}Pb</u> (R. G. Helmer, A. J. Caffrey, R. J. Gehrke, R. C. Greenwood)

As a continuation of our effort to measure and evaluate gamma-ray energies for the calibration of gamma-ray spectra, we have published several new measurements. The abstract of this article[2] follows.

> The energies of gamma-rays from several radioactive sources have been measured to provide additional calibration lines for Ge semiconductor detectors. The energy values obtained are: for ^{99}Mo, 140.511(1) keV; for ^{133}Ba, 53.161(1), 276.398(2), 302.853(1), 356.017(2) and 383.851(3) keV; and for ^{210}Pb, 46.539(1) keV.

---

[1] R. G. Helmer, C. W. Reich, R. J. Gehrke and J. D. Baker, International Journal of Applied Radiation and Isotopes <u>33</u>, 23 (1982).

[2] R. G. Helmer, A. J. Caffrey, R. J. Gehrke and R. C. Greenwood, Nuclear Instruments and Methods <u>188</u>, 671 (1981).

5. Efficiency Calibration of a Ge Detector for 30-2800 keV Gamma Rays (R. G. Helmer)

As part of our effort to provide precise gamma-ray intensity measurements with Ge detectors, we have calibrated an 8 cm^3 planar detector. This calibration involved 19 sources, 18 nuclides and 58 gamma rays with energies from 14 to 2754 keV. These sources were obtained primarily from two metrology laboratories and from our own laboratory. Some deviations between the efficiency values from different nuclides and sources of the same nuclide are noted. The magnitudes of the necessary counting corrections and various components of the uncertainty are discussed. An observed variation of the efficiency with time is illustrated and discussed. A paper describing these measurements has been prepared for publication in Nuclear Instruments and Methods.

6. Gamma-Ray Emission Probabilties for the Decays of ^{141}La and ^{142}La (R. J. Gehrke)

Because the chain yields for masses 141 and 142 are high for the thermal neutron fission of ^{235}U (i.e., 4.82% and 5.87%, respectively), the gamma-ray emission probabilities of ^{141}La and ^{142}La are important in a number of reactor-related applications. The emission probability of the most intense gamma ray in the decay of ^{141}La (at 1354 keV) is not well established and only one direct measurement of the ^{142}La 641-keV gamma-ray emission probability has been reported (with an uncertainty of 4.8%).

In order to obtain precise values (approximately 1% uncertainty at the 1σ level) for the gamma-ray emission probabilities of ^{141}La and ^{142}La, we have measured the emission probabilities of the 1354-keV gamma ray emitted in the decay of ^{141}La and the 641-keV gamma ray emitted in the decay of ^{142}La. The abstract of this published work[1] follows.

> The emission probabilities of the 1354-keV gamma-ray emitted in the decay of ^{141}La and the 641-keV gamma-ray emitted in the decay of ^{142}La have been measured to be (1.643 ± 0.021) and (47.4 ± 0.5) gamma-rays per 100 decays, respectively. The half-lives were measured to be (3.92 ± 0.03) h for ^{141}La and (91.1 ± 0.5) min for ^{142}La.

7. Gamma-Ray Emission Probability for the Decay of ^{143}Ce (R. J. Gehrke)

The 57- and 293-keV gamma rays emitted from ^{143}Ce have been used in neutron dosimetry as well as in fission-yield determinations. Measurements of this type require that the emission probability of a strong gamma ray be known to an accuracy of approximately 1% as indicated in the request list of the ICRM Working Group of Non-Neutron Nuclear Data. Because there is no reported β^- feeding to the ^{143}Pr ground state in the decay of ^{143}Ce, it

[1] R. J. Gehrke, International Journal of Applied Radiation and Isotopes 32, 377 (1981).

is normally possible to determine the absolute gamma-ray intensities (gamma-ray emission probability) by setting the sum of the intensities of the gamma-ray transitions feeding the ^{143}Pr ground state to 100%. However, in the case of ^{143}Ce, the 57-keV transition, which depopulates the first excited state, is highly converted and the uncertainty in its conversion coefficient is too large to allow the precise determination of the emission probabilities in this manner.

For these reasons we have undertaken to measure the emission probabilities of these gamma rays emitted in the decay of 33.0-h ^{143}Ce by 4π β-γ coincidence counting and Ge(Li) spectrometric techniques. The emission probabilities of the 57- and 293-keV gamma rays were found to be (12.3 ± 0.3) and (42.8 ± 0.4) gamma rays per 100 decays, respectively. The relative intensities for 13 other gamma rays emitted in the decay of ^{143}Ce have also been measured. This work has been accepted for publication in the International Journal of Applied Radiation and Isotopes.

8. Delayed Neutron Spectral Measurements (A. J. Caffrey, R. C. Greenwood, L. O. Johnson)

The effort to measure the energy spectra of delayed neutrons from fission-product isotopes is continuing. A principal objective of this effort is to define the lower energy portion of such spectra, from a few keV up to approximately 300 keV. Because of their absence of thermal neutron sensitivity, and their good energy resolution in this region, hydrogen gas-filled proton-recoil detectors incorporating neutron-gamma pulse-shape discrimination circuitry are being used for this task. With such detectors, measurements of the delayed neutron energy spectra of ^{93}Rb, ^{94}Rb, ^{95}Rb, and ^{96}Rb, over the range of 10 to 1000 keV, have been completed using the TRISTAN on-line mass separator at Brookhaven National Laboratory.

9. Analyses of National Uranium Resources Evaluation Reference Materials from New Brunswick Laboratory[1] (J. R. Smith, A. J. Caffrey, R. G. Helmer, C. P. Willis and J W Rogers)

The National Uranium Resources Evaluation (NURE) project needs certified reference materials to assure reliability in its analytical measurements information. Consequently, an interlaboratory measurement program has been initiated in which New Brunswick Laboratory (NBL) Reference Materials (RM's) will be analyzed by several laboratories to (1) establish "consensus" uranium and thorium values for these RM's, (2) develop an RM reference data base for comparison of NURE measurements performed by various measurement methods, and (3) document the traceability of NURE measurements to the national measurement base. Of these three program objectives, the first two involve participation such as ours and the third will be met by certification by NBS of the NBL reference materials with respect to the nationally accepted reference materials.

[1] These results have been issued as U. S. DOE Report EGG-PHYS-5618 (Oct., 1981)

NBL has distributed these reference materials to several laboratories which have agreed to make analytical measurements on them. The RM's were (I) pitchblende ore diluted with silica, (II) monazite sand diluted with silica, (III) uranium (normal) oxide (U_3O_8), and (IV) silica. A variety of measurement techniques which are based on different assumptions have been applied. The first and most extensive set of experiments involved measuring the ^{235}U concentration in the uranium samples by counting delayed neutrons emitted following neutron irradiation. The counting system was calibrated by carrying out a similar experiment on a sample of a known amount of ^{235}U. This method provides excellent precision and, to the extent that the analysis of the calibration sample is accepted, excellent accuracy. These measurements provided ^{235}U concentrations for all five NBL samples, as well as the relative concentrations. This method could not be used on the thorium samples. In the second set of experiments, the relative concentrations of ^{235}U and ^{232}Th in the various samples were determined by passive gamma-ray spectroscopy. In the third set of experiments, the absolute concentrations of ^{235}U, ^{226}Ra and ^{232}Th in the highest concentration (1%) samples were determined by passive gamma-ray spectrometry.

In the gamma-ray measurements one must be concerned about where the gamma ray occurs in the series of daughter activities. This concern arises since the ^{222}Rn (3.8 day) gas could escape from the sample or chemical separation could occur in the handling of some samples. The pertinent decay chains are as follows (with the location and energy in keV of the gamma rays used in this study indicated):

$$^{232}Th \xrightarrow[\alpha]{} {}^{228}Ra \xrightarrow[\beta]{} {}^{228}Ac(911) \xrightarrow[\beta]{} {}^{228}Th,$$

$$^{235}U(185.7,205.3) \xrightarrow[\alpha]{} {}^{231}Th \text{ and}$$

$$^{238}U \xrightarrow[\alpha]{} {}^{234}Th \xrightarrow[\beta]{} {}^{234}Pa \xrightarrow[\beta]{} {}^{234}U \xrightarrow[\alpha]{} {}^{230}Th \xrightarrow[\alpha]{} {}^{226}Ra(186.2) \xrightarrow[\alpha]{}$$

$$^{222}Rn \xrightarrow[\alpha]{} {}^{218}Po \xrightarrow[\alpha]{} {}^{214}Pb(242,352) \xrightarrow[\beta]{} {}^{214}Bi.$$

This indicates that the 242- and 352-keV lines used in some of the measurements require the ^{222}Rn to be retained in the sample. Also, the use of the 186- and 911-keV gamma rays assumes that no chemical separation of the material has taken place.

C. NUCLEAR LEVEL-SCHEMES STUDIES

1. Levels in ^{152}Sm (R. C. Greenwood)

Work is currently in progress to obtain more detailed information on the nuclear level structure of ^{152}Sm from measurements of the $^{151}Sm(n,\gamma)$ reaction and the β^- decay of ^{152}Pm.

2. Levels in ^{184}W (W. F. Davidson (Ottawa), C. W. Reich, R. C. Greenwood)

In order to obtain more detailed information on the nature of the lowest-lying excited $K^{\pi}=0^{+}$ and 2^{+} bands (2 each) in ^{184}W, a cooperative program of research has been undertaken involving measurements of the ^{183}W(n,γ)-reaction gamma-rays with the curved crystal spectrometer systems at the Institute Laue-Langevin in Grenoble. Based on this work, a more complete picture has been obtained of the decay patterns of these bands. We are currently attempting to understand the structure of these bands using both a phenomenological band-mixing approach and the IBA model.

D. SHORT-LIVED FISSION-PRODUCT STUDIES UTILIZING He-JET TRANSPORT AND ^{252}Cf SOURCES

1. Identification of New Neutron-Rich Rare-Earth Nuclei Produced in ^{252}Cf Spontaneous Fission (R. C. Greenwood, R. J. Gehrke, J. D. Baker, D. H. Meikrantz)

A comprehensive program of nuclear structure studies of fission products using both on-line chemical and mass-separation techniques has recently been initiated at the INEL. A unique feature of this program, apart from the use of ESOL (Elemental Separation On Line) and ISOL facilities in combination, is the use of ^{252}Cf as the source of the fission products. Because of long-standing interest at this laboratory in the deformed rare-earth region, our initial experimental thrust has been to exploit the higher yields of the rare-earth fission-product isotopes available in ^{252}Cf. An abstract of the paper[1] describing this work which was presented at the "4th International Conference on Nuclei Far From Stability" follows.

> A program of systematic study of the decay properties of neutron-rich rare-earth nuclei with 30 s < $t_{1/2}$ < 10 min, produced in ^{252}Cf spontaneous fission, is currently underway using the Idaho ESOL (Elemental Separation On Line) Facility. The chemistry system used for the rare earth elemental separations consists of two high-performance chromatography columns connected in series and coupled to the ^{252}Cf fission source *via* a helium gas-jet transport arrrangement. The time delay for separation and initiation of gamma-ray counting with this system is typically 2-3 min. Significant results which have been obtained to date with this system include the identification of a number of new neutron-rich rare-earth isotopes including ^{155}Pm ($t_{1/2}$=48±4 s) and ^{163}Gd ($t_{1/2}$=68±3 s), in addition to 5.51 min ^{158}Sm which was identified in an earlier series of experiments.

---

[1] R. C. Greenwood, R. J. Gehrke, J. D. Baker and D. H. Meikrantz, CERN-Service d'information scientifique, CERN 81-09 (1981) pp. 602-607.

2. Advanced System for Separation of Rare-Earth Fission Products (J. D. Baker, R. J. Gehrke, R. C. Greenwood, D. H. Meikrantz)

A microprocessor-controlled radiochemical separation system, to perform ESOL (Elemental Separation On Line), has been further advanced to separate individual rare-earth elements from mixed fission products in times of the order of a few minutes. The fission source consists of two electrodeposited ^{252}Cf spontaneous fission sources which are coupled *via* He-jet transport to the automated chemistry system. Chemical separations were performed using two high performance liquid chromatography columns coupled in series. The first column separated the rare-earth group by extraction chromatography using dihexyldiethylcarbamoylmethylphosphonate (DHDECMP) adsorbed on Vydac C_8 resin. The second column isolated the individual rare-earth elements by cation exchange chromatography using Aminex A-9 resin with α-hydroxyisobutyric acid (α-HIBA) as the eluent. Significant results, which have been obtained to date with this advanced system, are the identification of several new neutron-rich rare-earth isotopes including $^{155}Pm(T_{\frac{1}{2}}=48\pm4$ s) and ^{163}Gd ($T_{\frac{1}{2}}=68\pm3$ s). In addition, a half-life of 41 ± 4 s is reported for ^{160}Eu.

3. Identification of a New Isotope, ^{168}Dy (R. J. Gehrke, R. C. Greenwood, J. D. Baker, D. H. Meikrantz)

As part of our program of systematic study of the decay properties of neutron-rich rare-earth nuclei we have identified with the ESOL facility a new isotope, 8.5 ± 0.5 min ^{168}Dy. The activity was produced in the spontaneous fission of ^{252}Cf and transported *via* a He jet system to a rapid radiochemical separative facility where the Dy fraction was removed from the mixed fission products. The assignment to ^{168}Dy decay was based on the presence of five gamma rays in the chemically separated Dy fraction which were associated with the decay of an 8.5-min activity and on the observation of the grow-in and then decay of the daughter, 2.98-min ^{168}Ho, with approximately an 8-min half-life. The gamma-ray emission probabilities have been determined.

4. Identification of a New Isotope, ^{155}Pm (R. C. Greenwood, R. J. Gehrke, J. D. Baker, D. H. Meikrantz)

The following is an abstract of a paper which has been accepted for publication in the journal Radiochimica Acta.

A new isotope ^{155}Pm has been identified using the Idaho ESOL facility. This isotope was identified in the Pm fraction separated using high-performance liquid chromatography from gross fission products resulting from spontaneous fission in ^{252}Cf. Five gamma rays could be assigned to this ^{155}Pm activity, which decays with a half-life of (48 ± 4) s. The assignment of this 48-s Pm activity to ^{155}Pm is based in part upon the observation of the grow-in of 22.4-min ^{155}Sm from a 48-s parent and in part on the fact that the 5 gamma rays could be placed in a ^{155}Sm level scheme which

is consistent with that obtained recently from studies of the ^{154}Sm(n,γ) reaction.

5. A New Isotope, ^{163}Gd; Comments on the Decay of ^{162}Gd (R. J. Gehrke, R. C. Greenwood, J. D. Baker, D. H. Meikrantz)

The following is an abstract of a paper which has been accepted for publication in the journal Radiochimica Acta.

A new isotope, ^{163}Gd, has been identified which was produced in the spontaneous fission of ^{252}Cf. The half-life of this isotope was measured to be (68$\pm$3) s and eleven gamma rays have been assigned to its decay. The assignment of this activity to ^{163}Gd is based on the presence of these gamma rays in the gadolinium fraction, which was chemically separated from mixed fission products, and on the observation of the growth and decay curve associated with gamma rays from 19.5-min ^{163}Tb, the daughter activity. Two new gamma rays have been identified by half-life as belonging to the decay of ^{162}Gd. Gamma-ray energies and intensities are reported for the ^{162}Gd and ^{163}Gd isotopes.

6. He-JET COUPLED ON-LINE MASS SEPARATOR (R. C. Greenwood, R. A. Anderl, V. J. Novick)

The mass separator at the INEL has been successfully coupled on-line to a source of ^{252}Cf fission products via a He-gas jet transport arrangement using solid aerosols of NaCl as activity carriers. Initial tests of the ISOL system on-line to an approximately 7 μg ^{252}Cf source were conducted using gamma-ray spectroscopic measurements of the separated ^{138,139}Cs, ^{141,142}Ba and ^{142}La activities. The measured transport efficiencies through the system of approximately 3% and approximately 0.3% for the Cs and Ba isotopes, respectively, are comparable with the results of earlier tests conducted at the INEL with the hollow-cathode ion source alone coupled to the He-gas jet transport arrangement.[2] Following these tests, a general survey of the mass-separated activities was conducted with the ISOL system on-line to an approximately 600 μg source of ^{252}Cf. Gross β-γ activity was measured for samples collected at 73 mass positions. Gamma-ray spectra were measured with a Ge(Li) detector for 29 of the mass positions. The survey experiments demonstrated the production of significant fission-product

[1] R. K. Smither, K. Schreckenbach, H. G. Börner, W. F. Davidson, T. von Egidy, D. D. Warner, R. F. Casten, M. L. Stelts, and A. I. Namenson, Argonne National Laboratory Report ANL-80-94 (1980) p. 90; and R. K. Smither, private communication.

[2] R. A. Anderl, V. J. Novick and R. C. Greenwood, NIM 186 (1981) 153.

activity for rare-earth and refractory (Pd, and possibly Mo, Tc, Ru) elements. The results of these studies were reported earlier.[1] Current emphasis is on implementing a moving-tape collector and automated data acquisition system for studies in the rare-earth and refractory element mass regions.

E. INTEGRAL REACTION-RATE AND CROSS-SECTION MEASUREMENTS

1. Capture and Fission Cross Sections for Actinides (R. A. Anderl)

Accurate neutron cross sections are required for a reliable prediction of the burnup and buildup of americium and curium isotopes in reactor fuels. Because of the sparcity of measured differential and integral data, the neutron cross section specifications for these isotopes in the intermediate and fast neutron energy regions has often been based primarily on theoretical calculations. Consequently, considerable uncertainty can be associated with predicting the inventory of the higher actinides in fast reactor systems.

To improve upon the fast reactor integral data base for use in cross-section evaluation, measurements of the integral capture and fission cross sections for ^{241}Am and ^{243}Am have been made using the fast neutron field of the Coupled Fast Reactivity Measurements Facility (CFRMF) and chemically pure and isotopically enriched samples. The integral cross sections were derived from measurements of the ^{241}Am(n,f), ^{241}Am(n,γ) ^{242g}Am, ^{243}Am(n,f) and ^{243}Am(n,γ) ^{244g}Am integral reaction rates using gamma-spectrometric and isotope dilution alpha spectrometric (IDAS) techniques.[2] Integral fission rates for both ^{241}Am and ^{243}Am were determined from measurements of the emission rates of prominent gammas (328, 487, 537, 815 and 1596) in the β^- decay of ^{140}Ba and ^{140}La using calibrated Ge(Li) spectrometers. A fission yield of 5.5$\pm$0.3 was used in the analysis. The integral capture rate for ^{241}Am was obtained from a measurement of the ^{242}Cm production cross section using IDAS. The integral capture rate for the ^{243}Am to ^{144g}Am ground state was determined by a measurement of the emission rates of the 744.1-keV and 898.2-keV gamma rays in the β^- decay of ^{244g}Am using calibrated Ge(Li) spectrometers. Mass analysis for all the samples was made using IDAS. Integral cross sections (in b) obtained from this work are as follows: 0.450$\pm$6.2% for ^{241}Am(n,f), 1.22$\pm$3.5% for ^{241}Am(n,γ) ^{242g}Am, 0.353$\pm$6.1% for ^{243}Am(n,f) and 0.0976$\pm$4.8% for ^{243}Am(n,γ) ^{244g}Am. Assuming ratios for ground state branching relative to total neutron capture of

---

[1] R. C. Greenwood, R. A. Anderl and V. J. Novick, "Development of a Gas-Jet Coupled ISOL Facility with a ^{252}Cf Spontaneous Fission Source," in Proc. of 4th International Conference on Nuclei Far From Stability, CERN 81-09 (July, 1981) p. 723.

[2] R. A. Anderl and N. C. Schroeder, "Integral Capture and Fission Cross Sections for ^{241}Am and ^{243}Am in the CFRMF," to be published early in 1982 as US DOE Report EGG-PHYS-5691.

0.787 for $^{241}Am(n,\gamma)$ and 0.109 for $^{243}Am(n,\gamma)$, total integral capture cross sections in barns derived from the partial cross sections are 1.55±3.5% for ^{241}Am and 0.895±4.8% for ^{243}Am. A comparison of the measured integral cross sections to those calculated using ENDF/B-V differential data and the central spectrum for the CFRMF gives the following ratios of calculated to experimental cross sections: 1.16 for $^{241}Am(n,f)$, 0.72 for $^{241}Am(n,\gamma)$, 1.18 for $^{243}Am(n,f)$ and 0.66 for $^{243}Am(n,\gamma)$. These integral test discrepancies indicate the need for re-evaluating the ENDF/B-V cross sections for these reactions over the regions of cross-section response in the CFRMF spectrum. A least-squares adjustment analysis is being done to identify the cross-section regions which are inconsistent with the measured integral data.

2. Capture Cross Sections for Fission Products (R. A. Anderl. Y. D. Harker)

Our program to provide integral cross sections of interest to the development of fast reactor systems has included measurements in the CFRMF and in EBR-II. These data are used primarily for integral testing of the capture and fission cross sections in ENDF/B.

Integral-capture reaction rates have been measured for enriched isotopes of ^{143}Nd, ^{144}Nd, ^{145}Nd, ^{147}Sm, ^{149}Sm, ^{151}Eu, ^{152}Eu, ^{153}Eu and ^{154}Eu irradiated in different neutron spectra in EBR-II. The integral data have been used in least-squares analyses with the FERRET code to determine adjustments to ENDF/B-IV cross sections which are required to achieve consistency with the measured integral data. The adjusted cross sections are in good agreement with recent differential data and with adjusted cross sections based on STEK integral data. This work has been documented in Ref. 1.

An integral-testing study[2] was done for ENDF/B-V fission-product capture cross sections. The integral data base used comprised 45 measured spectrum-averaged cross sections for 34 fission-product neutron capture reactions in both the CFRMF and EBR-II neutron fields. The study includes a detailed specification of the flux spectra and processed cross sections used in the calculation of spectrum-averaged cross sections and provides an estimate of the uncertainty in the calculated integral cross section due to flux spectrum uncertainties. Sources of discrepancy in integral data testing were examined. The results of the study indicate that the changes made in the fission-product capture cross sections in going from ENDF/B-IV to ENDF/B-V resulted in more consistency for 26 of the integral data, less consistency for 11 of the integral data and no change for 8 of the integral data.

---

[1] R. A. Anderl. F. Schmittroth, Y. D. Harker, "Integral Capture Measurements and Cross Section Adjustments for Nd, Sm and Eu," US DOE Report EGG-PHYS-5182, INEL (1981).

[2] R. A. Anderl, "INEL Integral Data-Testing Report for ENDF/B-V Fission Product and Actinide Cross Sections," US DOE Report EGG-PHYS-5405, INEL (1981).

Experiments are underway for remeasuring the integral cross sections in the CFRMF for ^{99}Tc, ^{103}Rh, ^{104}Ru, ^{109}Ag, ^{127}I and ^{147}Pm. This work will be completed in FY82.

3. Cross Sections for Neutron Dosimetry (R. A. Anderl)

An integral data testing study[1] was made for 23 ENDF/B-V dosimeter cross sections. This work included a compilation of up-to-date integral reaction rates for dosimeters irradiated in CFRMF and the derivation of a consistent set of spectrum-averaged cross sections. The neutron field of the CFRMF was characterized and spectra suitable for data testing were specified. Integral tests, as defined by the ratio of calculated-to-measured integral cross sections, were determined and assessed for each dosimeter reaction with respect to reaction energy response, uncertainty considerations, spectrum shape changes and weighting function effects.

The above study[1] was extended to include integral test computations for all dosimeter reactions on ENDF/B-V using spectra for the CFRMF, BIG-10 and Watt ^{235}U fission neutron benchmark fields. Discrepancies between measured integral data and the calculated spectrum-averaged cross sections indicate the need for re-evaluation of the following dosimeter cross sections: $^{6}Li(n,He)$ in the region of the 250-keV resonance, $^{10}B(n,He)$ above 10 keV, $^{27}Al(n,p)$, $^{47}Ti(n,p)$, $^{48}Ti(n,p)$, $^{58}Fe(n,\gamma)$ in both the resolved resonance region and above 10 keV, $^{197}Au(n,\gamma)$ above 10 keV and $^{237}Np(n,f)$ below 10 MeV.

F. THE ^{252}Cf $\bar{\nu}$ PROBLEM

1. The Half-Life of ^{252}Cf (J. R. Smith)

At a ^{252}Cf $\bar{\nu}$ workshop in November 1980, V. Spiegel reported the discovery of an error in the computation of the half-life of ^{252}Cf from his calibrations of a source in his manganese bath. The corrected value for the half-life became 2.654 yr. Because of the importance of the half-life in interpreting our ^{252}Cf $\bar{\nu}$ data, it was thought worthwhile to derive the half-life from fission-rate calibration of one of the sources used in the $\bar{\nu}$ measurements. Accordingly, our fission chamber #2 was recalibrated in June, 1981. When combined with the data from the calibrations performed in March and December, 1978, the new calibrations indicate a half-life for ^{252}Cf of 2.651 ± 0.004 sidereal years. The calibrations spanned a period of 1187 days and included corrections for the effects of the ^{252}Cf present in the sample. This new half-life value is in excellent agreement with the revised value of Spiegel.

[1] R. A. Anderl *et al.*, "INEL Integral Data-Testing Report for ENDF/B-V Dosimeter Cross Sections," US DOE Report EGG-PHYS-5608, INEL (1981).

[2] R. A. Anderl *et al.*, "Addendum to INEL Integral Data-Testing Report for ENDF/B-V Dosimeter Cross Sections," US DOE Report EGG-PHYS-5668, INEL (1982).

A. DECAY STUDIES OF FISSION PRODUCTS WITH TRISTAN AT THE HFBR AT BNL

The TRISTAN on-line isotope separator facility[1,2] became operational at the High Flux Beam Reactor at Brookhaven National Laboratory in 1980. Using an integral target surface-ionization source combination, mass-separated beams of Rb, Sr, Cs, Ba, Ce, and Pr fission products are available for study of the above elements and their daughters. Members of the Ames Laboratory group (Hill, Wohn, Sistemich, Wolf and Yamamoto) have collaborated with a number of other users from BNL, Clark University, University of Maryland, and University of Oklahoma in a wide variety of measurements. Experiments have involved decay scheme studies using γ-ray spectroscopy, Q_β measurements with high-purity Ge detectors, and γγ angular correlations using a four Ge detector system. In addition Dr. A. Wolf, a one-year visitor from Israel, is installing a system for the measurement of "g factors" of nuclear excited states using the technique of perturbed angular correlations. Results of TRISTAN studies on Q_β measurements and the decays of ^{141}Cs, ^{146}La, ^{148}La, ^{150}Pr, and ^{99}Sr are given below.

1. Decay of Mass-Separated ^{141}Cs to ^{141}Ba and Systematics of N=85 Isotones (Yamamoto *et al.*)

The decay of 24.9s ^{141}Cs was studied by x-ray and γ-ray spectroscopy and 192 γ rays were assigned to the decay. A decay scheme involving 187 γ rays placed in 72 levels was deduced. The decay scheme is characterized by a triplet of low-lying states: $3/2^-$ ground state, $5/2^-$ state at 48.5 keV, and $7/2^-$ state at 55.0 keV. The $3/2^-$ and $5/2^-$ states are consistent with zero β branching and the $7/2^-$ state has a 57% β branching. For transitions among these 3 levels, values of $|\delta|$(E2/M1) were deduced. Comparisons with level structures of other N=85 isotones are made and systematic trends in energies of states characteristic of these "quasi-$f_{7/2}$" nuclei are discussed in a report[3] on this study, which will be submitted soon.

---

[1] R. E. Chrien, M. L. Stelts, V. Manzella, R. L. Gill, F. K. Wohn, and J. C. Hill, Nuclear Spectroscopy of Fission Products, ed. by T. von Egidy, Inst. Phys. Conf. Ser. 51, 44 (1980).

[2] J. C. Hill, F.K. Wohn, R. L. Gill, D. A. Lewis, and R. E. Chrien, *ibid*, p. 53.

[3] H. Yamamoto *et al.*, to be submitted to Phys. Rev. C.

2. Decay of ^{148}La and Band Structure in ^{148}Ce (R. L. Gill *et al.*)

The decay of ^{148}La was studied by γ-ray spectroscopy. A preliminary report of the decay has been published.[4] A half-life of 1.05s for ^{148}La was determined from γ-ray multiscaling measurements. The level scheme deduced incorporates 52 of 54 identified γ rays into a scheme with 28 levels. Recent $\gamma\gamma(\theta)$ measurements have confirmed the 0^+ assignment of a level at 770.3 keV. The decay scheme of ^{148}La is consistent with zero β branching to the ^{148}Ce ground state. Band structures in even-even ^{148}Ce have been assigned and compared with level structures of other Ce isotopes and N=90 isotones.[4,5] A manuscript of this study is under preparation.

3. Precision Q_β-Value Determinations for Neutron-Rich Rb and La Isotopes (D. S. Brenner *et al.*)

Beta-ray end-point energies for Rb and La fission products were measured with a hyperpure-Ge Q_β spectrometer. Coincidence measurements were used to establish β feedings and to verify level schemes for daughter nuclides. Q_β values have been determined for ^{88,94,96,98}Rb and ^{146,148}La. The Rb values have been reported.[6] Our results will be compared with other experiments and with predictions of mass formulae in a manuscript which will soon be submitted to Phys. Rev. C.

4. Decay of ^{146}La and Band Structure in ^{146}Ce (F. K. Wohn *et al.*)

The decay of the low-spin isomer of ^{146}La to levels in even-even ^{146}Ce was studied by γ spectroscopy. More than 300 γ rays have been identified for this decay, which has a Q_β value of 6.4 MeV. No direct production of ^{146}La from the TRISTAN ion source has been established. Operation at low ion-source temperatures yields only ^{146}La from the β decay of even-even ^{146}Ba, hence the low-spin isomer (6.27s) of ^{146}La can be isolated for study. A preliminary report, focusing on levels in ^{146}Ce below 2 MeV, has been published.[7] Band structures in ^{146}Ce and comparisons with level structures of other Ce isotopes and N=88 isotones have been presented in Refs. 5 and 7. Recent $\gamma\gamma(\theta)$ and γ-multiscale measurements are under analysis.

---

[4] R. L. Gill *et al.*, 4th International Conference on Nuclei Far from Stability, ed. by P. G. Hansen and O. B. Nielsen (CERN) 81-09, Geneva, 1981, p. 569.

[5] W. B. Walters *et al.*, *ibid.*, p. 557.

[6] D. S. Brenner *et al.*, *ibid.*, p. 129.

[7] G. M. Gowdy *et al.*, *ibid.*, p. 562.

5. Decay of ^{150}Pr (J. C. Hill *et al.*)

A study is underway of the decay of ^{150}Pr to levels in ^{150}Nd. This study was made possible due to the ability of the TRISTAN ion source to directly separate Pr fission products. The ^{150}Pr has a half-life of about 6s. Gamma singles and preliminary $\gamma\gamma$ coincidence measurements revealed 28 γ rays which are assigned to a level scheme for ^{150}Nd with 14 excited states with energies up to 2069 keV. Also observed was a γ ray at 109 keV that has been tentatively assigned to ^{150}Ce decay indicating direct separation of Ce in our ion source at low efficiency.

6. Decay of ^{99}Sr (R. F. Petry *et al.*)

The decay of ^{99}Sr to levels in ^{99}Y has been studied. The nucleus ^{99}Y is of interest since it may be possible to describe the low-lying levels in terms of an odd proton coupled to a deformed ^{98}Sr core. Gamma singles and $\gamma\gamma$ coincidences revealed 70 γ rays. More than 90% of these have been placed in a level scheme for ^{99}Y consisting of 22 excited states up to 2314 keV. A half-life of 0.26s was measured for ^{99}Sr.

B. DECAY STUDIES AT THE KFA IN JÜLICH, GERMANY

One of us (Hill) spent a one-year sabbatical year at the KFA Nuclear Research Center while Dr. Sistemich from the KFA spent a year at the Ames Laboratory working with TRISTAN. Dr. Hill carried out studies on the decay of the fission product ^{102}Y at the gas-filled recoil separator JOSEF. The half-life was measured to be 0.34±0.04s. Analysis of the data is still in progress and more detailed information will be given in the next report. A study of the decay of neutron-rich ^{36}P was also carried out. Details are given below.

1. Identification and Decay of Neutron-Rich ^{36}P (J. C. Hill, H. R. Koch, and K. Shizuma)

We report the first study of the decay of ^{36}P to levels in the N=20 nucleus ^{36}S. The ^{36}P was produced through the ^{37}Cl(n,2p)^{36}P reaction. Fast neutrons were generated by stopping a beam of 70-MeV deuterons from the JULIC cyclotron in a thick Be target. The half-life of ^{36}P was measured to be 5.9±0.4s. Three gamma rays were observed with energies of 902.0, 1638.1, and 3290.7 keV and relative intensities of 77, 38, and 100 respectively. Beta feeding is principally through allowed transitions to negative parity states in ^{36}S above 4 MeV. This work will be published in Phys. Rev. C.[8]

---

[8] John C. Hill, H. R. Koch, and K. Shizuma, Phys. Rev. C, to be published in Mar. 1982.

The scope of our research capabilities was extended during this past year to include the measurement of neutron scattering differential cross sections at neutron energies of tens of kilovolts. The first measurement made was on ^{187}Os to determine the inelastic scattering cross section for the 9.7 keV first excited state, which is crucial to the use of ^{187}Re as a precise clock for measuring the age of universe. Similar measurements on other isotopes such as ^{183}W are contemplated for the future.

A. NEUTRON SCATTERING- ELASTIC AND INELASTIC

1. ^{187}Os(n,n') - Very low energy neutrons. (Hershberger, Macklin*, Hill*, Balakrishnan, McEllistrem)

The use of the decay of ^{187}Re as a means of dating the universe was advanced by D. D. Clayton[1] in 1964. The usefulness of this cosmochronometer is contingent on a knowledge of the s-process abundance of ^{187}Os which, by subtraction from the observed ^{187}Os abundance, gives the ^{187}Os produced by beta decay from ^{187}Re. This abundance depends on the prediction that the abundance of an isotope times its neutron capture cross section is a constant in an s-process chain, specifically

$$^{187}\mathrm{Os(slow)} = {}^{186}\mathrm{Os}\ \frac{\sigma(n,\gamma;186)}{\sigma(n,\gamma;187)}$$

However, at stellar temperatures most ^{187}Os nuclei are actually in the first excited level, and not in the ground state. Therefore one also needs the cross section for capture out of the excited level. While this cannot be measured, it can be inferred if one knows the inelastic neutron scattering cross section to this level at energies appropriate to stellar temperatures. This was the motivation for the present experiment. In order to increase the available neutron flux and also to improve the relative energy resolution it was decided to make the measurement at a neutron energy near 60 keV and then to extrapolate the results back to 30 keV, the assumed stellar temperature.

The neutrons were produced from a 2 keV thick LiF target using the ^{7}Li(p,n)^{7}Be reaction. The LiF targets were very uniform and stable enough to withstand many days bombardment by the 2 μa proton beam. To minimize the

---

*Oak Ridge National Laboratory

[1] D. D. Clayton, Astrophys. J., 139, 637 (1964).

effect of background, time-of-flight techniques were used to measure the neutron energy spectrum. The experiment used 2 gm of enriched ^{187}Os as the scatterer and 2 gm of enriched ^{188}Os as an equivalent scatterer for elastic scattering, but without inelastic scattering. A two photomultiplier assembly viewing a fast scintillator was used to monitor the zero degree neutron flux and energy, and consequently the energy setting of the Van de Graaff accelerator. The overall performance of this setup was so accurate that it was possible to maintain the accelerator energy constant within a precision of 100 to 150 eV. The distance of the sample from the neutron source was 4 cm and the scatterer to detector distance was 39 cm. A three-photo-multiplier scintillation detector with a majority coincidence logic was used to detect the 61 keV elastically scattered neutrons along with the spectrum of 51 keV neutrons inelastically scattered from the 9.76 keV first excited level of ^{187}Os. To increase the overall resolution of the time-of-flight spectrometer, the accelerator proton pulsing was increased from the normal 2 megacycle rate to 5 megacycles for this experiment. Since the sample size was extremely small when compared with the one generally used in neutron scattering experiments (0.01 moles as compared to 0.3 moles normally), several days of continued data collection was necessary to have an observable inelastically scattered spectrum. The very good accuracy attained in setting the energy of the accelerator, to within 100 eV, made it possible to add up several days of data without loss of resolution.

The resulting neutron spectra for ^{188}Os, ^{187}Os, and their properly normalized difference is shown in Figs. 1 to 3. Fig. 3 shows the difference between Figs. 1 and 2, and was a first crude effort to extract the inelastic scattering yield. Our analysis to date suggests an inelastic scattering cross section of $\sigma(n,n') \simeq 1.8 \pm 0.6$ b at $E_n = 61$ keV.

2. <u>Neutron-excess Effects in Neutron Scattering</u> (Harper, Weil, Brandenberger)

The differential cross sections for elastic and inelastic neutron scattering from five even-A tin isotopes have been measured at 1.0, 1.6 and 4.0 MeV, as well as the total cross sections in the energy range $0.3 \leq E_n \leq 5.0$ MeV. The purpose of this work was to investigate the effects of changing neutron excess in a sequence of isotopes with similar nuclear structure. A preliminary analysis[2] had indicated that fitting with both a spherical optical model (SOM) and an optical model with coupled channels (CC) resulted in a neutron excess dependence of the imaginary potential well depth that is 2-3 x larger than is found in most global analyses. The CC analysis is being redone with the most recently determined β_2 values for the first excited states, and it appears that now the imaginary well neutron-excess dependence will agree

---

[2]J. L. Weil, IEEE Transactions on Nuclear Science, NS-28, April, 1981, p.1255.

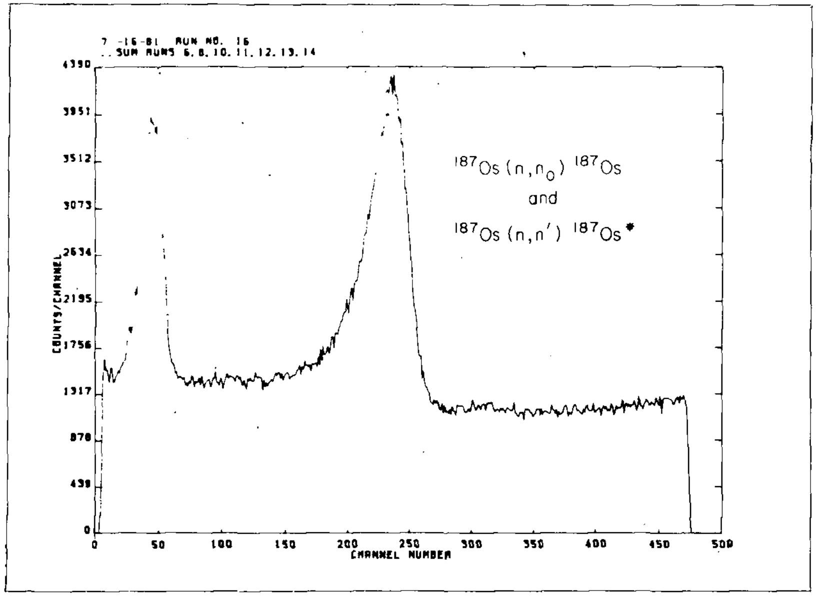

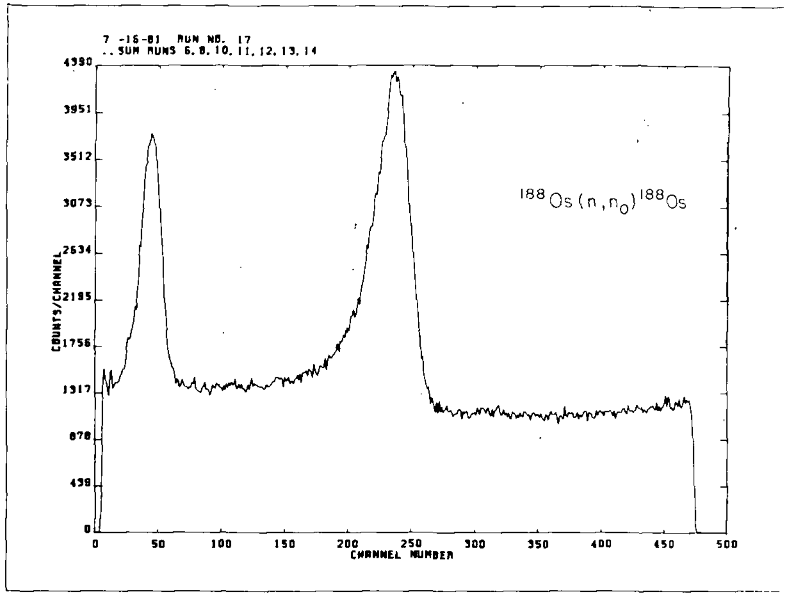

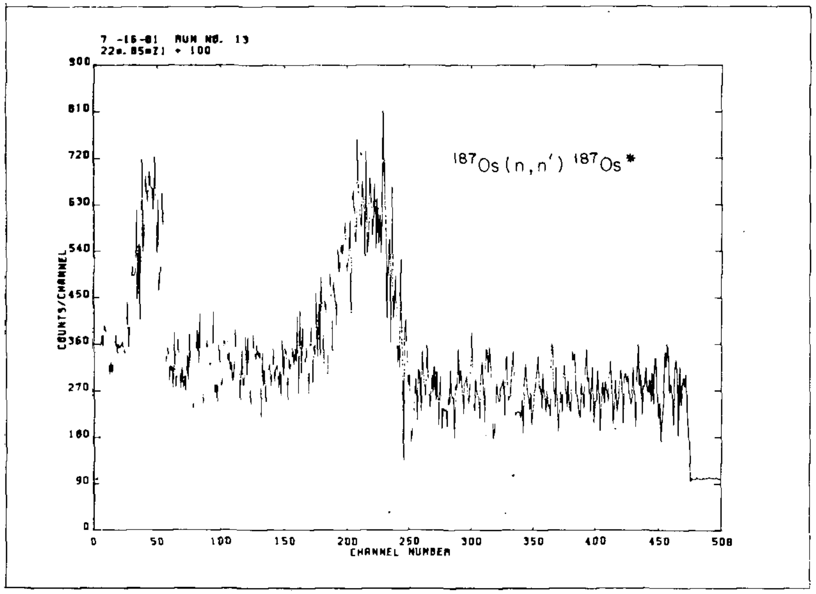

Fig. 1. (Upper left). Time-of-flight spectrum of neutrons scattered from ^{187}Os. The central peak is neutrons, and the left hand peak is gamma rays.

Fig. 2. (Upper right). Time-of-flight spectrum of neutrons scattered from ^{188}Os. Note that the neutron peak is narrower than for ^{187}Os because of lack of inelastic scattering.

Fig. 3. (Lower left). Time-of-flight spectrum of neutrons inelastically scattered from ^{187}Os. This is the difference between the above two spectra, after appropriate normalization.

with the global value of $W_1 \cong 15$ MeV.[3] Thus, it would appear that the difference in the values of W_1 obtained in the SOM and the CC analyses may be connected to the monatonic decrease in β_2 as A increases, which implies that even small changes in nuclear structure have a large effect on neutron-excess dependence if they are not carefully taken into account. In both the SOM and CC analyses, the real well depth has a neutron excess dependence that is consistent with that determined from global analyses.

3. ^{206,208}Pb(n,n') (Hanly, Coope, McEllistrem, Mirzaa)

Differential cross sections of ^{206}Pb(n,n') and ^{208}Pb(n,n') have been measured at $E_n = 7$ and 8.5 MeV with isotopically enriched scattering samples for the purpose of comparing the strength of the 3^- and 5^- collective excitations in these two nuclei. ^{206}Pb(n,n') data has also been taken which should help in determining the 5^- excitation strength in ^{206}Pb. Spectra are shown in Figs. 4 and 5. An unexpected qualitative difference in the scattering from these two isotopes is a very strong excitation of levels in ^{208}Pb at $E_x = 4$-5 MeV which has no analog in the spectra for ^{206}Pb(n,n'). From the resolution of the scattering to the 3_1^- and 5_1^- levels in ^{208}Pb, it appears that the equality of the cross sections for exciting the 3_1^- level in both ^{206}Pb and ^{208}Pb which was reported by Cranberg[4] is probably not correct. This could be due either to a difference in β_3 values or a difference in the imaginary well depth, W_D.

4. ^{190,192}Os(n,n') (McEllistrem, Yates, Mirzaa, Hanly, Weil)

As part of the on-going study of neutron scattering from shape transitional nuclei, the differential cross sections for ^{192}Os(n,n') have been measured at the two bombarding energies of 1.60 and 3.94 MeV. At the lower energy, inelastic scattering groups to the 2_1^+, 2_2^+, 4_1^+, 3_1^+, 4_2^+ were successfully resolved, while at the higher energy only the 2^+ inelastic scattering was measured with good enough statistics to be useful. A coupled channels analysis is expected to reveal differences in dynamical behavior between ^{192}Os and ^{194}Pt, for which the analysis is almost complete. Measurements of the differential cross sections of ^{190}Os(n,n') at 2 MeV and of both ^{190}Os(n,n') and ^{192}Os(n,n') at 5 MeV are now being planned to extend the scope of our study of nuclear structure in the A $\cong$ 190 region. With the expected sensitivity of neutron scattering at low energies to non-axial excitations, we may be able to provide information about the susceptibility of these isotopes to non-axial deformation when excited, a susceptibility not readily discerned from studies of excited levels and their γ-ray decays. There is good reason

---

[3]C. M. Perey and F. G. Perey, At. Data and Nuclear Data Tables 17, 1 (1976).

[4]L. Cranberg and C. D. Zafiratos, Phys. Rev. 142, 775 (1966).

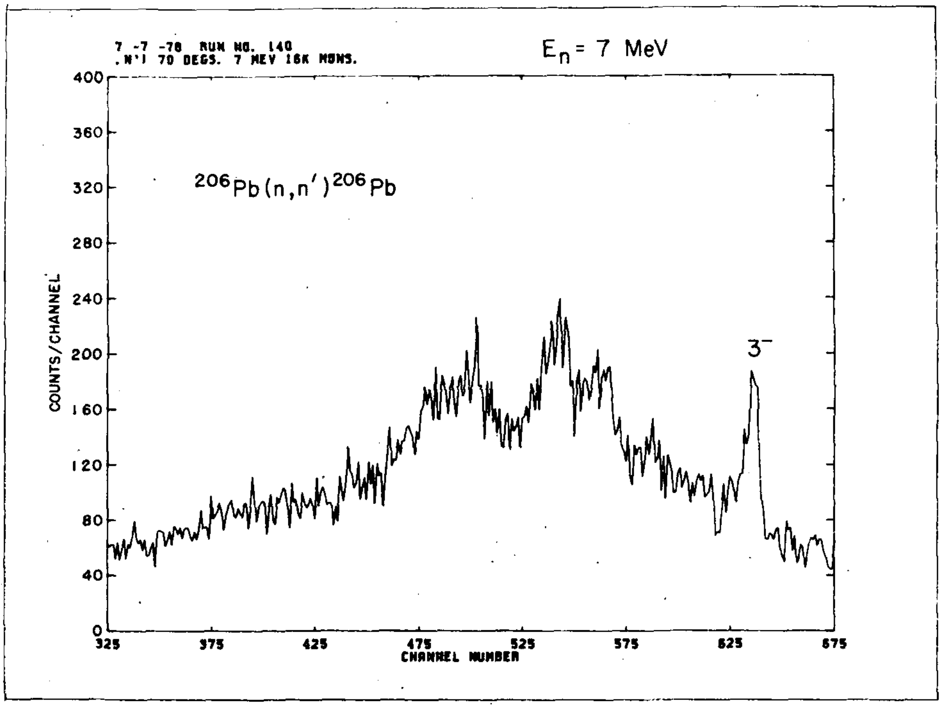

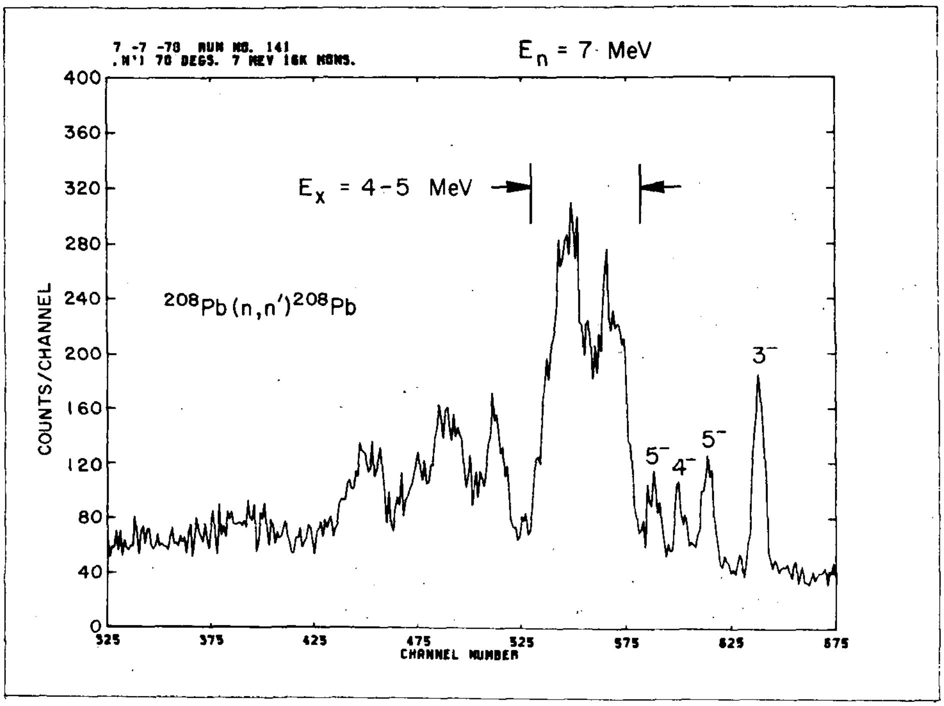

Figs. 4 and 5. Time-of-flight spectra of neutrons scattered from ^{206}Pb and ^{208}Pb.

to expect success since previous work[5] with the Sm isotopes has shown that axial quadrupole deformations can be reliably extracted from neutron total, elastic, and inelastic scattering cross sections.

B. NUCLEAR STRUCTURE STUDIES

1. Even-Even Nuclides - Mostly Shape Transitional (Kleppinger, Yates, Ghatak-Roy)

Data collection and analysis are complete for our study of ^{192}Os using the (n,n'γ) reaction. A level scheme incorporating 50 energy levels below 2.4 MeV has been constructed. Branching ratios have been calculated for these levels, and cross sections for (n,n'γ) at 2.5 MeV have been computed by comparison to the well-known cross section of the ^{56}Fe 847-keV γ ray. Angular distribution data and decay systematics have been instrumental in the assignment of spins to most of the observed levels.

Our results indicate that, while IBM, BET and the general collective model characterize the ^{192}Os quasi-ground and quasi-γ bands quite well, the predictions of these models show significant deviations from experimental values for the higher bands[6] (see Fig. 6). In particular, the energy of and branching from the 0_3^+ level are not correctly predicted by any model. This failure of the models suggests that some as yet uncharacterized shape transition within the larger Pt-Os transitional region is taking place at ^{192}Os.

A 45-g enriched (>97%) sample of ^{190}Os arrived in May. Detailed excitation function data from 1.3-3.0 MeV have been collected, as well as angular distribution data at 2.5 MeV. Our compiled list of γ rays attributable to ^{190}Os($\sim$150) indicates that many new transitions are being observed;[7,8] however, preliminary work implies that most of these new γ rays originate from energy levels above the pairing gap.

Data collection, including angular distributions and detailed excitation functions, has been completed for ^{200}Hg. A list of γ rays has been

---

[5]Ch. Lagrange, J. Lachkar, G. Haouat, R. E. Shamu, and M. T. McEllistrem, Nucl. Phys. A345, 193 (1980).

[6]R. Bijker, A. E. L. Dieperink, O. Scholten and R. Spanhoff, Nucl. Phys. A344 207, (1980); K. J. Weeks and T. Tamura, Phys. Rev. C 22 1323, (1980), Peter O. Hess, Joachim Maruhn and Walter Greiner, J. Phys. G 7 737 (1981).

[7]R. F. Casten, M. R. MacPhail, W. R. Kane, D. Breiting, K. Schreckenbach and J. A. Cizewski, Nucl. Phys. A316 (1979) 61.

[8]C. M. Lederer and V. S. Shirley, Table of Isotopes, 7th Ed. (1978).

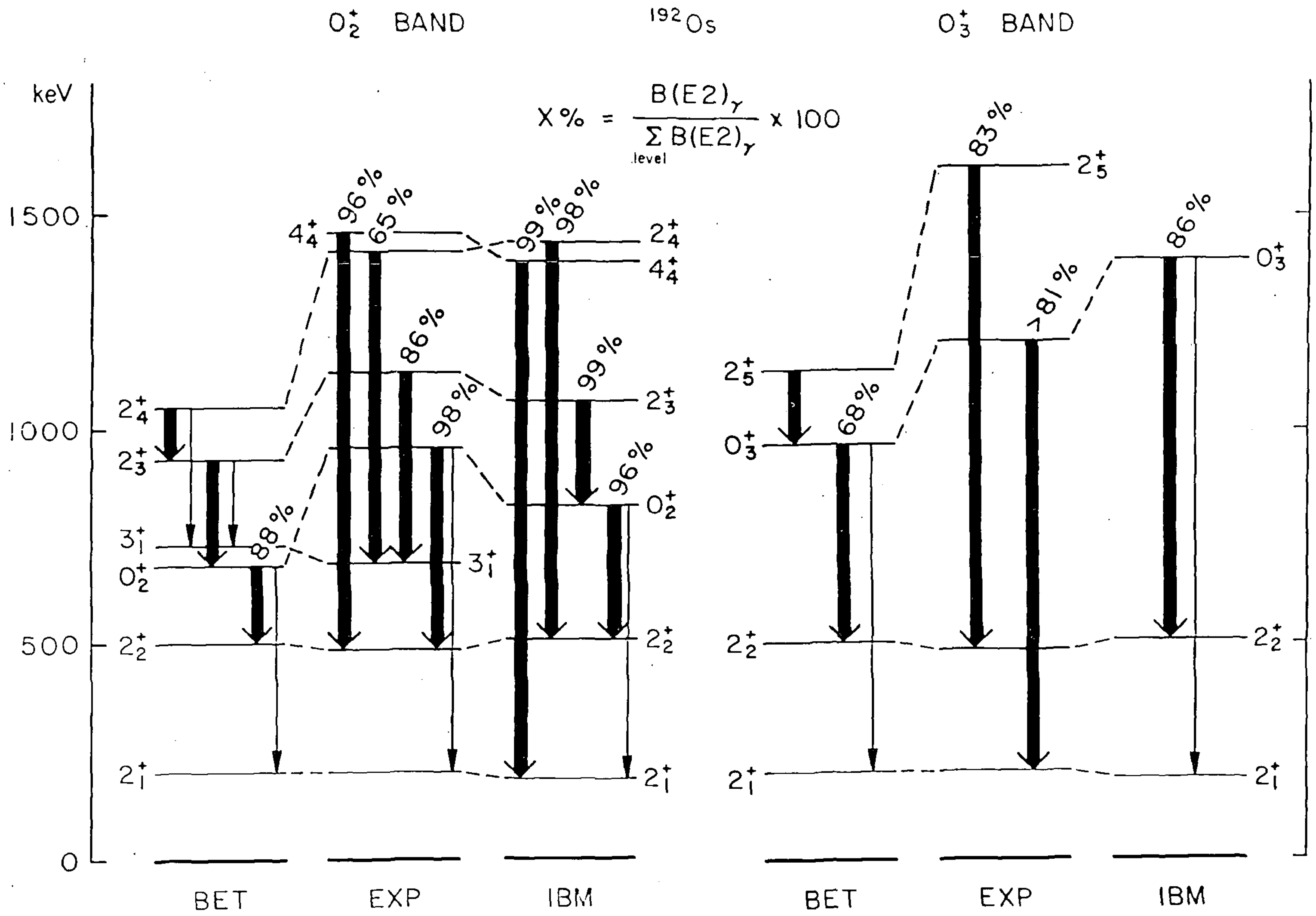

Fig. 6. Comparison between experimentally observed strong γ-decay modes of 0^+ bands in ^{192}Os and predictions of current models. Both models show serious disagreement with experiment.

compiled and further data analysis is in process.

2. Odd-mass Nuclides - Shape Transitional Region (Yates, Kahn, Kleppinger)

With the measurement of angular distributions this past summer, we have finished collecting data for ^{195}Pt. Data analysis is proceeding slowly, partially because the γ-ray spectra for this nucleus are very complex at all but the lowest energies (<0.8 MeV); at 2.5 MeV, over 400 γ rays are apparent.

Analysis of ^{191}Ir is in the preliminary stage. The γ-ray spectra are less complicated than those for ^{195}Pt, and excitation function data from 0.5-2.0 MeV are currently being analyzed for the placement of energy levels.

3. $^{118,120,122,124}Sn(n,n'\gamma)$ Reactions (Sa, Cao, Weil, Balakrishnan)

Excitation functions of the gamma rays from $^{124}Sn(n,n'\gamma)$ have been measured in the energy range $2.3 \leq E_n \leq 3.7$ MeV for more than 36 γ-rays. At least 18 of these are previously unobserved transitions which serve to locate 10, and possibly 11, new excited states in ^{124}Sn. Angular distributions of the γ-rays were measured at E_n = 2.60 and 3.40 MeV to aid in the assignment of levels spins, most of which are presently subject to considerable uncertainty.[8,9] A precision energy calibration was made with standard γ-ray sources and with $^{56}Fe(n,n'\gamma)$ to aid in the assignment of energies to the new γ-rays and levels. Preliminary measurements on $^{118}Sn(n,n'\gamma)$, $^{120}Sn(n,n'\gamma)$ and $^{122}Sn(n,n'\gamma)$ have also been made at four neutron energies in the above bombarding energy range. These preliminary data show many new γ-rays from the deexcitation of excited levels in these nuclei. Because of the unexpected impurity of the ^{124}Sn sample used, the analysis of data on $^{124}Sn(n,n'\gamma)$ is complicated by the presence of many extraneous gamma rays from other tin isotopes. The preliminary data on $^{118,120,122}Sn(n,n'\gamma)$ has been very helpful in identifying new transitions in ^{124}Sn.

C. PROTON STRENGTH FUNCTIONS (Flynn, Gabbard, Hershberger, Laird*, Smith)

The work on proton strength functions at sub-Coulomb bombarding energies has progressed well and there are some interesting new results. During the past year much analytical work, primarily with the program GENOA, has been done to verify and gain a more detailed understanding of the anomalous, but systematic, variation of W, the imaginary part of the optical model (OM) potential, vs. A in the range $88 \leq A \leq 130$. This analysis has been based on (p,n), (p,p) and (p,γ) measurements done in this lab on seven isotopes of Zr

---

[9] B. Fogelberg and P. Carle, Nucl. Phys. A323, 205 (1979).

and Mo. An earlier analysis by Johnson et al[10,11] which first demonstrated the anomaly was based almost entirely on (p,n) data alone.

Three important results of the Kentucky work to date are (1) the confirmation of Johnson's result[12,13] on the rapid variation of W with A in the mass range $88 \leq A \leq 130$; (2) confirmation of the persistence of rapid variation of W in this mass range when the isobaric analog states ($T_>$ states) are included in the analysis[14] by a coupled channels calculation using the Lane Model; and (3) observation of the persistence of the rapid change in W vs. A when computations of strength functions are carried out with a deformed nuclear potential (coupled channels) model in the absence of analog states.

Recent further study, largely through the continuation of the systematic O.M. analysis of three zirconium isotopes and three molybdeum isotopes, has yielded new and/or more detailed information about two nuclear phenomena. These phenomena are the joint variation (with VR^2 approximately invariant) of the real part of the O.M. potential and the variation of the proton absorption (as reflected in the imaginary potential W) in these six nuclei. The addition of a complete set of elastic (p,p) scattering measurements to the earlier (p,n) measurements as well as preliminary results for the (p,γ) cross sections in ^{90}Zr and ^{92}Zr has made this more detailed analysis possible.

As postulated by Lane, et al.[15] and others, W is related to the transition rate (Fermi's Golden Rule #2) into the states of the compound nucleus and the other "states" which cause protons to disappear from the beam

---

[10] C. H. Johnson, A. Galonsky, and R. L. Kernell, Phys. Rev. Lett. 39, 1604 (1977).

[11] C. H. Johnson, J. K. Bair, C. M. Jones, S. K. Penny, and D. W. Smith, Phys. Rev. C 15, 196 (1977).

[12] D. S. Flynn, R. L. Hershberger, and F. Gabbard, Phys. Rev. C 20, 1700 (1979).

[13] R. L. Hershberger, D. S. Flynn and F. Gabbard, Phys. Rev. C 21, 896 (1980).

[14] R. Schrils, D. S. Flynn, R. L. Hershberger, and F. Gabbard, Phys. Rev. C 20, 1706 (1979).

[15] A. M. Lane, J. E. Lynn, E. Melkonian, and E. R. Rae, Phys. Rev. Lett. 2, 424 (959). J. E. Lynn, Theory of Neutron Resonance Reactions, Clarenden Press, Oxford, ENG. (1969).

(absorption). Although these processes involve a complex array of reaction mechanisms, including compound nucleus formation, and direct excitation of rotational and vibrational states, the qualitiative description [$W = \text{const.} \times |\langle f|H'|i\rangle|^2 \rho(E)$ is generally understood.[15] The product of the level density and the square of the matrix element must be summed over all "types" of final states or intermediate states. The doorway (2p1h) states are of special significance in the process of compound nucleus formation and theoretical computations normally treat transitions through these states.[16] Collective states are normally treated theoretically through use of deformed potentials (coupled channels).

[16] S. M. Grimes, Phys. Rev. C 22, 436 (1980); Barry Block and H. Feshbach, Annals of Phys. 23, 47 (1963).

A. ISOTOPES PROJECT

E. Browne, J.M. Dairiki, R.B. Firestone, C.M. Lederer, and V.S. Shirley

In the past year we have made considerable progress in the area of nuclear structure data evaluation and compilation. Development continues on the Radioactivity Handbook, based on data taken from the international Evaluated Nuclear Structure Data File (ENSDF).[1] This file is maintained by the National Nuclear Data Center (NNDC) at the Brookhaven National Laboratory on behalf of the International Network for Nuclear Structure Data Evaluation. The Handbook will provide a compilation of recommended radioactive decay data for applied users. It will be published in a style similar to that of the Table of Isotopes[2] and will contain selected "best" values of γ-ray and level properties, independent of the decay parent, taken from ENSDF. The most up-to-date values of atomic properties, internal conversion coefficients, and electron radial wavefunctions will be used to generate associated x-ray and electron intensities. Programming to establish the best γ-ray properties from disparate data sets in ENSDF has been developed. Fluorescence yields from K, L_1, L_2, and L_3 vacancies are now well known, so the Handbook will provide the x-ray and auger-electron energies and intensities associated with these vacancies. Additional computer algorithms to check the data for uniformity of style and content are also being written.

Parallel to the Handbook development, the Isotopes Project is actively involved in evaluating mass-chains over the region A = 146-152, 163-194. Last year the mass-chains A = 185, 188, and 193 were published while A = 169, 187, 189, and 190 are in the final reviewing process. Currently masses A = 174, 181, and 192 are being updated. In addition, we have been actively developing the science of nuclear structure data evaluation and compilation. Our organization of the 1st Conference on Nuclear Structure Data Evaluation at Asilomar, CA, last year was a great success. It marked the beginning of a dialogue, in the international evaluation community, about the scientific problems associated with evaluating nuclear structure data. We have also continued to provide input to the NNDC and the Ad Hoc Subcommittee on Formats and Procedures on ways of improving the style and content of ENSDF and Nuclear Data Sheets. Finally, we are initiating new, innovative research into the systematics of nuclear data properties. This

[1]"Evaluated Nuclear Structure Data File", edited and maintained by the National Nuclear Data Center, Brookhaven National Laboratory, on behalf of the International Network for Nuclear Structure Data Evaluation. Summary of file contents and published documentation may be found on page ii of any issue of the Nuclear Data Sheets.

[2]"Table of Isotopes", 7th edition: C.M. Lederer and V.S. Shirley, editors; E. Browne, J.M. Dairiki, and R.E. Doebler, principal authors; A.A. Shihab-Eldin, L.J. Jardine, J.K. Tuli, and A.B. Buyrn, authors; John Wiley and Sons, Inc., New York (1978).

work has led to the creation of new guidelines for evaluation and is a significant contribution to the body of knowledge in nuclear physics. Examples of this evaluation research are outlined in the following contributions.

B. NUCLEAR STRUCTURE DATABASE
(R.B. Firestone and E. Browne)

The most up-to-date and uniform source of evaluated data on nuclear structure and radioactive decay was published in the 7th Edition of the Table of Isotopes[1]. Up to now, the use of this source for horizontal compilations was a tedious, manual task. We have incorporated all of the data used to generate the level scheme figures in the Table of Isotopes into an easily searchable database. The Nuclear Structure Database[2] contains adopted information about nuclear level properties and their modes of decay. It is divided into data files from nuclear reaction and from radioactive decay. In addition to the information from the Table of Isotopes, chemical properties (density, melting point, boiling point, and abundance)[3], atomic masses[4], thermal neutron cross sections (fission, absorption, and dispersion)[5], and fission yields for thermal and reactor neutrons[6] have been added.

The Nuclear Structure Database is useful for rapid searches on specific nuclear properties. It is organized to facilitate the writing of data retrieval programs and database management systems. The results of a typical search, for the lowest energy $2^+ \rightarrow 0^+$ E2 transition enhancements, is shown in figure B-1. Additional searches on logft values and γ-ray transition probabilities are discussed below. An interactive γ-ray energy binning routine has also been created.

In the future we plan to increase the scope and utility of the database. As ENSDF[7] becomes more current, that data will be incorporated into the database in association with production of the AENSDF file being created for the Radioactivity Handbook. Additional mass data, chemical information, and theoretical or experimental nuclear data will also be included. Although this file is currently primarily used for our research into nuclear decay systematics, it is hoped that at a later date we might provide a more general management system for use by the broader research community.

---

[1]"Table of Isotopes", 7th edition: C.M. Lederer and V.S. Shirley, editors; E. Browne, J.M. Dairiki, and R.E. Doebler, principal authors; A.A. Shihab-Eldin, L.J. Jardine, J.K. Tuli, and A.B. Buyrn, authors, John Wiley and Sons, Inc., New York (1978).

[2]R.B. Firestone and E. Browne, "Nuclear Structure Database", LBL-11089 (1980).

[3]V.S. Shirley, C.M. Lederer, E. Browne, J.M. Dairiki, R.E. Doebler, A.A. Shihab-Eldin, L.J. Jardine, J.K. Tuli, A.B. Buyrn, J.M.H. Chong, and D.P. Kreitz, "Nuclear Wallet Cards", produced by the Isotopes Project, Lawrence Berkeley Laboratory, on behalf of the U.S. Nuclear Data Network (1979).

[4]A.H. Wapstra and K. Bos, At. Nucl. Data Tables 19, 1 (1977).

[5]S.F. Mughahghab and D.J. Garber, BNL-325, Third Edition, Vol. 1 (1973).

[6]W.H. Walker, AECL 5105 (1975).

[7]"Evaluated Nuclear Structure Data File", edited and maintained by the National Nuclear Data Center, Brookhaven National Laboratory, on behalf of the International Network for Nuclear Structure Data Evaluation.

N \ Z	52	54	56	58	60	62	64	66	68	70	72	74	76	78	80	82	84	86	88	90	92	94	96	98	100
60																									
62																									
64																									
66		50																							
68	29	62																							
70	37	48	67																						
72	31	41	77	84																					
74	25	36	60	75																					
76	20	46	36	52																					
78	15	22	33																						
80			19																						
82			10	13	19	11																			
84				21	23																				
86			30		32	33																			
88			49	38	56	57	80		68	73															
90			57	79	116	140	159	149	110	90															
92				102		175	186	179	167	140															
94					87		197	193	200	169	126														
96							199	199	213	195	153														
98								208	209	205	181														
100									210	202	148														
102									207	207	149														
104										201	187				62										
106										178	157	147	126	126	44										
108											154	134	99	94											
110												118	97	83											
112												111	76	70											
114													73	62											
116													62	46	41										
118														45	30										
120														29	27										
122															19	4									
124															13	3									
126																									
128																									
130																									
132																									
134																		46	111						
136																		59	98	162					
138																			123	169	223				
140																			144	194	234				
142																				201	234				
144																				182	250	285			
146																					271	294			
148																						296	333		
150																						292	324		
152																							323		
154																								357	
156																									

Fig. B-1. E2 Weisskopf enhancements for the $2^+ \rightarrow 0^+$ transitions in even-even nuclei, Z = 52–100.

C. ß-DECAY Logft SYSTEMATICS
(R.B. Firestone)

A thorough reevaluation of ß-decay logft systematics has not been done for nearly ten years. The most recent evaluation by Raman and Gove[1] is the current basis for the logft spin assignment rules used for the preparation of the ENSDF[2] file in the production of Nuclear Data Sheets. These rules have served as useful guidelines in the past, but they are insufficient for several reasons. The present rules were derived from only a few, well-characterized transitions, and, as such, they represent a potentially biased subset of all transitions. Also, there were too few transitions available to investigate adequately the frequency with which logft values occur (especially near their lower limits). More generally, there is no use of ß-decay theory for establishing theoretical limits on logft values. Calculations have not been thoroughly performed to establish reasonable lower limits for all multipoles, and the influence of nuclear structure, as in shell effects, has not been considered.

Specifically, the rule for isospin forbidden $0^+ \rightarrow 0^+$ transitions appears to be insufficient due to the extraordinarily large nuclear matrix elements required for the fastest transition and uncertainties in the measurement upon which it is based. Also, logft values generally appear to have substantial shell model dependencies[3], which can be systematized to provide better spin assignment rules.

A reevaluation of the ß-decay logft systematics has been initiated using various sources including the Nuclear Structure Database from the Table of Isotopes[3] and ENSDF[2]. The systematics will be investigated for all known transitions as a function of nuclear structure and probability of occurrence. Fast transitions, within a given category, will be reevaluated to establish their reliability. A parallel theoretical study is also in progress aimed at building a realistic theoretical framework for the logft rules.

[1]S. Raman and N.B. Gove, Phys. Rev. C7, 1995 (1973).

[2]"Evaluated Nuclear Structure Data File", edited and maintained by the National Nuclear Data Center, Brookhaven National Laboratory, on behalf of the International Network for Nuclear Structure Data Evaluation.

[3]R.B. Firestone and E. Browne, "Nuclear Structure Database", LBL-11089 (1980).

D. γ-RAY TRANSITION PROBABILITY SYSTEMATICS
(E. Browne and R.B. Firestone)

The use of γ-ray transition probabilities for assigning multipolarities has been limited, in the past, by the fact that only gross lower limits to the half-lives had been suggested. These limits are derived primarily from the compilation of γ-ray transition strengths by Endt[1-3]. Recommended upper limits for the transition strengths have been suggested by Endt based on the fastest, reliably known transitions of a given multipole. These limits are valid, but they are too restrictive because they fail to account for the effects of nuclear structure. For more detailed systematics, one must look to the older works of Moszkowski[4] and of Goldhaber and Sunyar[5].

We have initiated a new, systematic study of γ-ray transition probabilities based on varied sources such as the Nuclear Structure Database from the Table of Isotopes[6], Endt's compilations[1-3], and ENSDF[7]. For each multipole the transition probabilities are being mapped out in terms of nuclear structure. An example is shown for the $g_{9/2} \rightarrow p_{1/2}$ M4 transitions near Z = 50 in figure D-1. These transition probabilities are observed to vary smoothly. The ability to avoid errors in evaluation by using these systematics has been demonstrated[8], and unmeasured transition half-lives can be accurately predicted.

---

[1]P.M. Endt, At. Nucl. Data Tables 23, 3 (1979).

[2]P.M. Endt, At. Nucl. Data Tables 23, 547 (1979).

[3]P.M. Endt, At. Nucl. Data Tables 23, 47 (1981).

[4]S.A. Moszkowski in "Alpha-, Beta-, and Gamma-ray Spectroscopy", edited by Kai Siegbahn (North-Holland, Amsterdam, 1965), Vol. 2, pp. 863-886.

[5]M. Goldhaber and A.W. Sunyar, ibid., pp. 931-944.

[6]R.B. Firestone and E. Browne, "Nuclear Structure Database", LBL-11089 (1980).

[7]"Evaluated Nuclear Structure Data File", edited and maintained by the National Nuclear Data Center, Brookhaven National Laboratory, on behalf of the International Network for Nuclear Structure Data Evaluation.

[8]E. Browne and R.B. Firestone in "Proceedings of the 1st Conference on Nuclear Structure Data Evaluation", edited by R.B. Firestone, V.S. Shirley, and J.M. Dairiki (LBL-14070, 1982).

E. ß-DECAY ENERGIES AND MASSES OF $^{103-105}$In

(J.M. Wouters, H.M. Thierens,* J. Aysto,** M.D. Cable, P.E. Haustein,† R.F. Parry, and Joseph Cerny

The study of the nuclidic mass surface in the vicinity of the doubly magic nucleus ^{100}Sn is of fundamental interest in providing information on the strength of the shell closure when Z = N = 50. A comparison of measured mass excesses with currently available model mass predictions can determine the accuracy with which the various models include the effects resulting from shell closures. As a further step in the extension of the known mass surface we have measured the decay energies of $^{103-105}$In using β-γ coincidence spectroscopy following on-line mass separations. The decay of

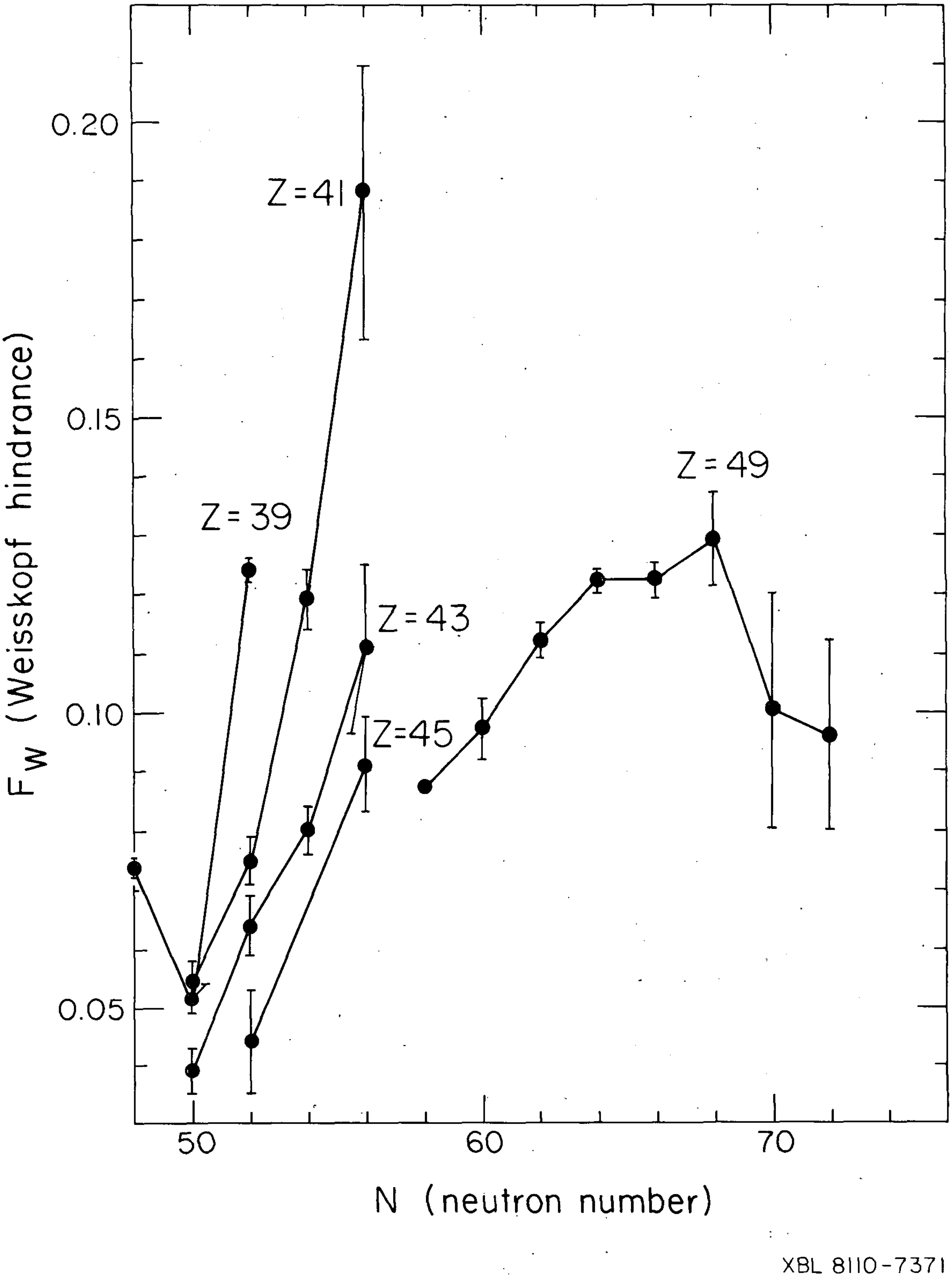

Fig. D-1. $g_{9/2} \rightarrow p_{1/2}$ M4 Weisskopf hindrances.

^{102}In[1] was also observed[1] but with inadequate statistics up to now to determine an accurate endpoint energy.

Heavy ion beams of ^{12}C, ^{14}N and ^{16}O from the 88-inch Cyclotron were directed onto various targets to produce indium isotopes via (HI,xn) and (HI,pxn) reactions. The recoils were transferred via a helium-jet to the RAMA on-line mass separator, where they were mass analyzed. The mass separated recoils were collected on a mylar tape and transported to the detector station for β-γ coincidence spectroscopy.

Table I presents a summary of the Q_{EC} determinations. A comparison was made of the predictions of the known indium masses with selected representatives of the different mass theories that are available. Those masses calculated according to the mass relations of the Garvey-Kelson[2] type and those calculated from the shell model formula of Liran-Zeldes[2] agree very well with the experimental results from ^{106}In to ^{125}In. For each of these mass models the root-mean-square deviation of theory from experiment for these nuclides is less than 200 keV. At ^{103}In, a strong deviation of about 1 MeV of the experimental value from the predictions of Liran-Zeldes and the different Garvey-Kelson type mass formulas suddenly appears. The predictions of those liquid drop models considered here differ more from the experimentally observed mass behavior than the results of calculations based on the Garvey-Kelson relations. For the models of Myers,[2] Groote, et al.,[2] Seeger-Howard[2] and Moller-Nix,[3] the root-mean-square deviation from all the indium mass data is 1070, 830, 780 and 630 keV, respectively. As was noted for those mass models, a sudden change in the systematic differences between the experimental and calculated masses also sets in for ^{103}In in the comparison with the liquid drop model predictions.

In conclusion, according to our results, ^{103}In is about 1 MeV more bound than predicted by the Liran-Zeldes and the different Garvey-Kelson type mass formulas. Other investigations of the mass surface near ^{100}Sn will show whether the observed deviation from the systematics for ^{103}In might have any possible relationship with the nearly double-shell closure.

---

*present address: University of Gent, Belgium

**permanent address: University of Jyvaskyla, Finland

†permanent address: Brookhaven National Laboratory, U.S.A.

[1]R. Beraud, J. Treherne, A. Charvet, R. Doffait, J. Genevey, A. Gizon, J. Gizon and M. Meyer, Z. Physik A299 (1981) 279

[2]At. Data Nucl. Data Tables 17, 41 (1976).

[3]P. Moller and J. Nix, Report LA-UR-80-1996.

Table I
Summary of the Q_{EC} Determinations

Nuclide	Gate	Q_{EC} (MeV) This work	Literature
^{103}In	188	5.41 ± 0.19	5.8 ± 0.5 (ref. 2)
^{104}In	658,834	7.41 ± 0.20	7.1 ± 0.2 (ref. 3)
^{105}In	131	5.16 ± 0.16	

F. OBSERVATION OF GIANT DIPOLE RESONANCES BUILT ON STATES OF HIGH ENERGY AND SPIN*

J.O. Newton, B. Herskind, R.M. Diamond, E.L. Dines, J.E. Draper, K.H. Lindenberger, S. Shih, C. Schück, and F.S. Stephens**

Studies of the GDR have been restricted mostly to coherent excitation from nuclear ground states that excites only the giant resonances built on them. Brink,[1] however, has proposed that every state in a nucleus has a GDR associated with it. A consequence of this idea is that the strength functions for electric dipole transitions from every state would have a Lorentzian-like shape as a function of γ-ray energy E_γ, with a magnitude determined from the E1 sum rule. Such a variation of strength with E_γ would affect the shape of the spectrum of γ rays emitted from a highly excited nucleus, particularly in the vicinity of $E_\gamma = E_G$, the energy of the GDR. We have observed this effect in the statistical γ rays following heavy-ion fusion reactions.

The present experiments make use of a sum-spectrometer-multiplicity technique that selects the γ rays from moderately high-spin (≈20-65ħ) states produced in heavy-ion compound nucleus reactions. The sum spectrometer consists of two 33 cm diameter by 20 cm thick NaI detectors facing the target 2.5 cm above and below the beam axis, each subdivided into four elements. Eight NaI (12.7 x 15.2 cm) detectors were placed 50 cm from the target at angles of ±160°, ±100°, ±80°, -135° and -45° and were shielded from each other and the beam slits by 5 cm of lead. Targets (∿1 mg/cm^2) of ^{82}Se, ^{110}Pd, and ^{124}Sn were bombarded with ∿10 nA of 170 MeV ^{40}Ar ions from the LBL 88-Inch Cyclotron. Spectra from the eight NaI detectors, associated with three regions of sum spectrometer energy E_s with the range ∿10-40 MeV, were added. Spectra for the ^{82}Se case are shown in figure F-1. In the energy interval from ∿2-8 MeV, the spectra show an exponentially falling tail, composed of the statistical transitions deexciting the product nuclei after neutron evaporation. All spectra rise considerably higher than this exponential at energies above ∿10 MeV, indicating a different source of γ rays. Beyond ∿20 MeV the spectra are flat and probably due to cosmic rays.

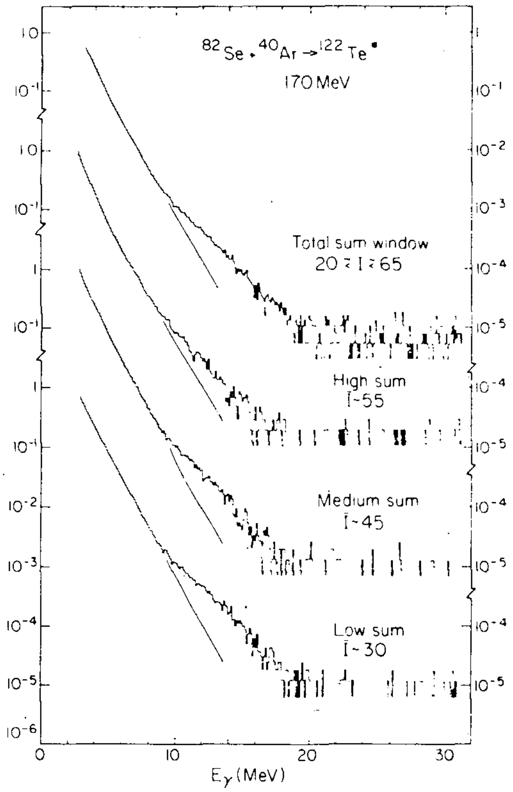

Fig. F-1. NaI spectra corresponding to $E_s = 10-40$ MeV and three windows within this range for the ^{82}Se + ^{40}Ar system. The sloping lines show exponential extrapolations of the lower E_γ parts of the spectra. The shapes of the true γ-ray spectra are not expected to differ greatly from these, and hence the ordinate in "transitions per MeV" should be approximately correct.

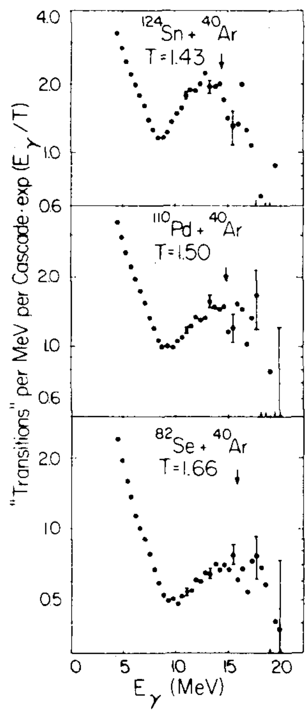

Fig. F-2. Background subtracted total-window spectra multiplied by $\exp(E_\gamma/T_e)$. Arrows indicate $E_\gamma = 78/A^{1/3}$ MeV, the centroid of the ground-state GDR.

The reason for the steep slopes in figure F-1 is that the level densities for the final states, to which the transition probabilities are proportional, vary approximately exponentially with E_x (and thus as $\exp(-E_\gamma/T)$). A rough way to see the shape of the γ-ray strength functions is to remove the level density dependence by multiplying by $\exp(E_\gamma/T_e)$, where T_e is an effective T. For the less interesting region with $E_\gamma \leqslant 8$ MeV, $T_e \approx 1$ MeV. Above 10 MeV the curves are flatter, indicating that these γ rays are emitted at much higher T_e. We have somewhat arbitrarily taken T_e = 1.43 MeV for ^{164}Er (^{124}Sn target), and adjusted the others for the expected mass dependence: $T \propto A^{-1/2}$. The data from the total sum window (with the flat high-energy background subtracted) multiplied by these exponentials are shown in figure F-2. The peaked structures have maxima ($\sim$14 MeV) and widths similar to those for the GDR based on ground states and strongly suggest GDR strength functions. In addition, the bump becomes higher in energy as the target mass decreases, as would be expected for the GDR ($E_G \propto A^{-1/3}$). These measurements demonstrate that one can study the GDR in the γ-ray deexcitation spectra following heavy-ion fusion reactions.

---

*Condensed from Phys. Rev. Lett. 46, 1383 (1981).

**Permanent addresses: Australian National University, Canberra, Australia (JON); Niels Bohr Institute, University of Copenhagen, Copenhagen, Denmark (BH); University of California, Davis (ELD, JED); Hahn-Meitner Institute, Berlin, W. Germany (KHL); Shanghai Institute of Nuclear Research, Shanghai, China (SS); and Centre de Spectrometrie Nucleaire et de Spectrometrie de Masse, Orsay, France (CS).

[1]D.M. Brink, doctoral thesis, University of Oxford (1955).

G. THE ß-STRENGTH FUNCTION

(R.B. Firestone, R.C. Pardo, R.A. Warner, W.C. McHarris, and W.H. Kelly)

The completion of our investigation of the β^+/e strength function for ^{145}Gd decay[1] provides strong evidence for the dominance of simple resonance structures in the decay of nuclei far from stability. From this detailed study of ^{145}Gd decay, 326 γ rays were placed deexciting 136 levels. This represents >98% of the total decay intensity. A plot of the ^{145}Gd ß-decay strength function is shown in figure G-1. This strength function is strongly peaked near 4.5 MeV, apparently due to shell effects, and confirms similar results obtained for ß-delayed neutron decay, for example, as observed by Kratz et al.[2]

These data cast strong doubts on the usefulness of the statistical model for the calculation of average ß-decay properties for experimentally unknown isotopes far from beta stability. The use of ß-decay strength functions that are constant[3] or slowly varying[4] should be considered as unreliable. It is clear that microscopic calculations such as those of Klapdor[5] are necessary to predict more adequately nuclear decay properties. An evaluation of the available experimental information on ß-decay strength resonances is currently in progress to investigate solutions to this problem using systematics.

[1]R.B. Firestone, R.C. Pardo, R.A. Warner, W.C. McHarris, and W.H. Kelly, Phys. Rev. C25, 527 (1982).

[2]K.T. Kratz, W. Rudolph, H. Ohm, H. Franz, M. Zendel, G. Herrmann, S.G. Prussin, R.M. Nuls, A.A. Shihab-Eldin, D.R. Slaughter, W. Halverson, and H.V. Klapdor, Nucl. Phys. A316, 335 (1962).

[3]J.C. Hardy, L.C. Carraz, B. Jonson, and P.G. Hansen, Phys. Lett. 71B, 307 (1977).

[4]F.M. Mann, C. Dunn, and R.E. Schenter, Phys. Rev. C25, 524 (1982).

[5]H.V. Klapdor and T. Odo, Astrophys. J. 242, L49 (1980).

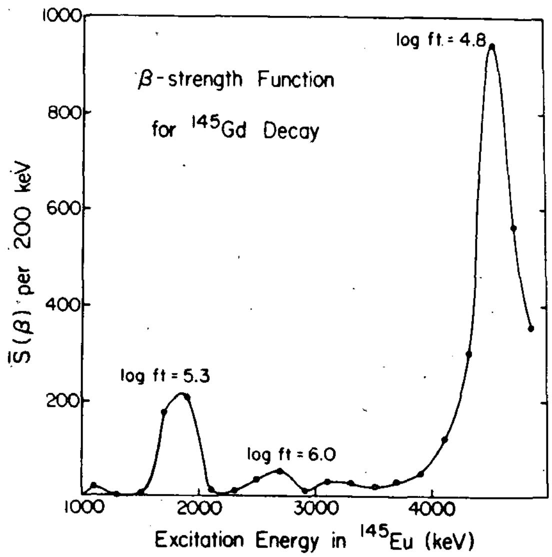

Fig. G-1. The β-strength function $\bar{S}(\beta)$ (per 200 keV) plotted as a function of excitation energy in ^{145}Eu. Here we define $\bar{S}(\beta)=b(E)/ft$, where $b(E)$ is the intensity fraction per 200-keV interval of excitation and ft is the standard β decay rate to that energy domain of the daughter. Broad resonances at 1.8-, 2.6-, and 4.5-MeV are observed, and the effective logft's to these resonances are shown.

A. NUCLEAR DATA APPLICATIONS - MEASUREMENTS

1. Transport of 14-MeV Neutrons Through Tritium Breeding Materials in Fusion Reactors (Hansen, Komoto, Pohl, Wong)

The neutron emission spectra from ^{6}Li, ^{6}LiD and ^{7}Li have been measured using the sphere transmission and time-of-flight (TOF) techniques for 14-MeV incident neutrons from the Livermore Insulated-Core-Transformer (ICT) accelerator. The radius of the spheres, 16.52 cm, corresponds to 1.1 mean-free paths (mfp) for the ^{6}Li and ^{7}Li spheres and to 1.93 mfp for the ^{6}LiD sphere for 14-MeV neutrons. The neutron emission spectra from a 0.8 mfp Be sphere (R = 12.58 cm) and 1.8 mfp CF_2 sphere (R = 16.52 cm) have also been measured. Be, used as a neutron multiplier in the tritium breeding blanket, can be present in metal form, as a flouride (molten salt blankets: LiF (47%), BeF_2 (53%) composition, known as "flibe"), or as a lithium compound (Be_2Li_2O).

The neutron spectra were measured for the energy interval of 1 to 15 MeV using a stilbene scintillator (5.08 cm - diam. x 5.08 cm - long) positioned at 26°, and a 10 m flight path. The calculations have been carried out with TARTNP, a coupled neutron-photon Monte Carlo Transport code with the ENDL and ENDF/B-V neutron and photon libraries.

Overall, the ENDF/B-V calculation for the ^{6}Li spheres is in better agreement with the measurements than the ENDL, with discrepancies no larger than 20% in the energy region 8 - 12 MeV of the emitted neutrons. The calculations for ^{6}LiD, ^{7}Li, Be and CF_2 spheres show discrepancies of 20 to 30% with the measured spectra in the energy distribution of the neutrons below the source peak. A detailed analysis of the elastic, inelastic, and total cross sections for these materials is being carried out to understand the discrepancies.

2. Neutron Differential Scattering Measurements at 14.4 MeV (Hansen, Pohl, Wong)

Elastic and inelastic differential cross sections have been measured for Be, C, Al, Fe, Co, Ta and Bi at 14.4 MeV incident energy. The source neutrons are produced at the LLNL Cyclograaff facility by the ^{2}H(d,n)^{3}He reaction using 12 MeV deuterons onto a 3.13 cm-long gas cell, 1 cm diam., pressurized to 2 atmospheres of deuterium. This cell is one of two identical cells mounted in a flip-flop mechanism which allows alternate measurements to be carried out with "gas-in" and "gas-out." The scattering samples are cylinders, 2.54 cm diam. by 5.08 cm high, and are suspended vertically 20 cm beyond the end of the cell. Scattered neutrons are detected using the neutron time-of-flight facility with sixteen NE213 scintillator detectors (11.4 cm diam. by 5.1 cm long) covering the angular region from 3 to 159° with a 10.75 m flight path. The detectors are shielded from the direct neutron source by a set of wedges (30 cm Pb and 70 cm Fe) positioned radially around the scattering sample.

The measured elastic neutron differential cross sections corrected for multiple scattering are in excellent agreement with measurements found in the literature.[1,2] The main purpose of these measurements has been to test the new experimental facility: twin gas cells, tritium handling, and shielding in preparation for neutron scattering measurements up to 35 MeV using the $^{3}H(d,n)^{4}He$ reaction with deuterons up to 20 MeV available at this facility.

3. The Angular Distribution of Photoneutrons for ^{17}O (Phillips, Rowley, Woodworth, Jury*, Watson*)

We have measured the photoneutron cross section of ^{17}O leaving ^{16}O in its ground state. Electron bremsstrahlung was used as the photon source with electron energies of 15, 17, 21, and 25 MeV. The angular distribution of photo neutrons was measured at 7 angles from 22-1/2 to 157-1/2 degrees. The ^{17}O cross sections were measured relative to the ^{2}H cross section. The data are being analyzed to obtain additional information on the quantum numbers of the isolated resonances below the giant dipole resonance in ^{17}O. Information on the giant dipole will also be obtained from the highest energy measurement.

4. Photoneutron Cross Sections for ^{29}Si and ^{30}Si (Pywell,** Thompson,*** McNeill,+ Jury,* Woodworth, Berman)

Following previous photoneutron-yield measurements carried out at Melbourne, we have measured the photoneutron cross sections for ^{29}Si and ^{30}Si from 13 to 33 MeV with monoenergetic photons produced by the annihilaton in flight of fast positrons from the LLNL 100 MeV Linear Accelerator. The (γ,n) cross section for ^{29}Si is relatively smooth, owing to its non-zero spin, and exhibits a giant dipole resonance (GDR) about 4 MeV wide, centered at 21 MeV. The $(\gamma,2n)$ cross section for ^{29}Si was consistent with zero from its threshold at 25.7 MeV to the highest energy measured. The GDR for ^{30}Si, as seen in the total photoneutron cross section $\sigma[(\gamma,n) + (\gamma,2n)]$, exhibits more structure, with peaks at about 17.5, 19.5, 20.5 and 22.5 MeV. The (γ,n) cross section drops to very small values a few MeV above the $(\gamma,2n)$ threshold at 19.1 MeV, then rises again as the $(\gamma,2n)$ cross section falls with increasing energy above its peak at about 23 MeV. This behavior has never been seen before, and probably indicates the increasing dominance of the (γ,pn) cross section a few MeV above its threshold at 22.9 MeV.

---

* Trent University, Peterborough, Ontario, Canada
** University of Saskatchewan, Saskatoon, Saskatchewan, Canada
*** University of Melbourne, Parkville, Victoria, Australia
\+ University of Toronto, Toronto, Ontario, Canada
1 Matoba et al., Nucl. Phys. A 204, 129 (1973).
2 M. Hyakutake et al., Jour. Phys. Soc. of Japan 38, 606 (1975).

5. Continuum Charged-particle Emission from Reactions Induced by Neutrons, Protons and Alpha-particles (Vonach*, Haight)

According to the Bohr hypothesis, a compound nucleus does not remember how it was formed except for the conservation of angular momentum. To test this hypothesis as well as to obtain more accurate level density information, we are studying the decay modes of the excited ^{51}Cr compound nucleus. In previous studies this nucleus was formed by 15 MeV neutrons on ^{50}Cr and the charged-particle emission spectra were measured.[3] Neutron emission following neutron bombardment of ^{50}Cr has not yet been measured but is technologically quite possible. We are now forming the ^{51}Cr compound system at the same excitation energy by alpha-particles on ^{47}Ti and protons on the rare isotope ^{50}V. The isobars ^{50}V and ^{50}Cr are related by such a slow beta-decay that both are found in nature. This unusual situation allows study of the same compound system $^{51}Cr^*$ by neutrons or protons incident on ^{50}Cr or ^{50}V respectively. Information on the angular momentum dependence is given by the ^{47}Ti plus alpha reaction products.

6. Coupled-Channel Calculations of Neutron Elastic and Inelastic Scattering on $^{76,80,82}Se$ (Brown, Grimes,** Madsen+, Poppe, Wong)

Using the Oregon State Coupled-Channel Code,[4] we have calculated[5] the elastic and 2+ inelastic scattering of 8 MeV neutrons on $^{76, 80, 82}Se$. Our calculations differ from previous work[6] in that we couple in explicitly the two-phonon states. Our fits to the neutron scattering data[6] result in a more reasonable value of 18.5 MeV for the imaginary isovector surface strength as compared to the previous value of 38 MeV.[6] The smaller imaginary isovector strength and the values of other optical parameters have been verified by calculating the $^{76, 80, 82}Se(p,n)$ reaction to the ground isobaric analog state and comparing with recent measurements at 19 MeV.[7] The good agreement (see Fig. A-1) confirms the validity of the smaller imaginary isovector strength and the importance of coupling in the two-phonon states in the selenium isotopes.

---

* On subbatical leave from Institut fur Radiumforschung und Kernphysik, Vienna, Austria.

** Present address: Ohio University, Athens, OH 45701.

\+ Summer Visitor, Permanent address: Oregon State University, Corvallis, OR 97331.

3 S.M. Grimes, R.C. Haight, K.R. Alvar, H.H. Barschall and R.R. Borchers, Phys. Rev. C19, 2127 (1979).

4 M.J. Stomp, F.A. Schmittroth and V.A. Madsen, USAEC Technical Report, Contract No. AT(45-1)-2227, Task Agreement No. 11(unpublished).

5 V.R. Brown, C. Wong, S.M. Grimes, C.H. Poppe and V.A. Madsen, Phys. Rev. C24, 2359 (1981).

6 J. Lachkar et al., Phys. Rev. C14, 933 (1976).

7 C. Wong, S.M. Grimes, C.H. Poppe, V.R. Brown and V.A. Madsen (UCRL-87165) (to be published in Phys. Rev. C).

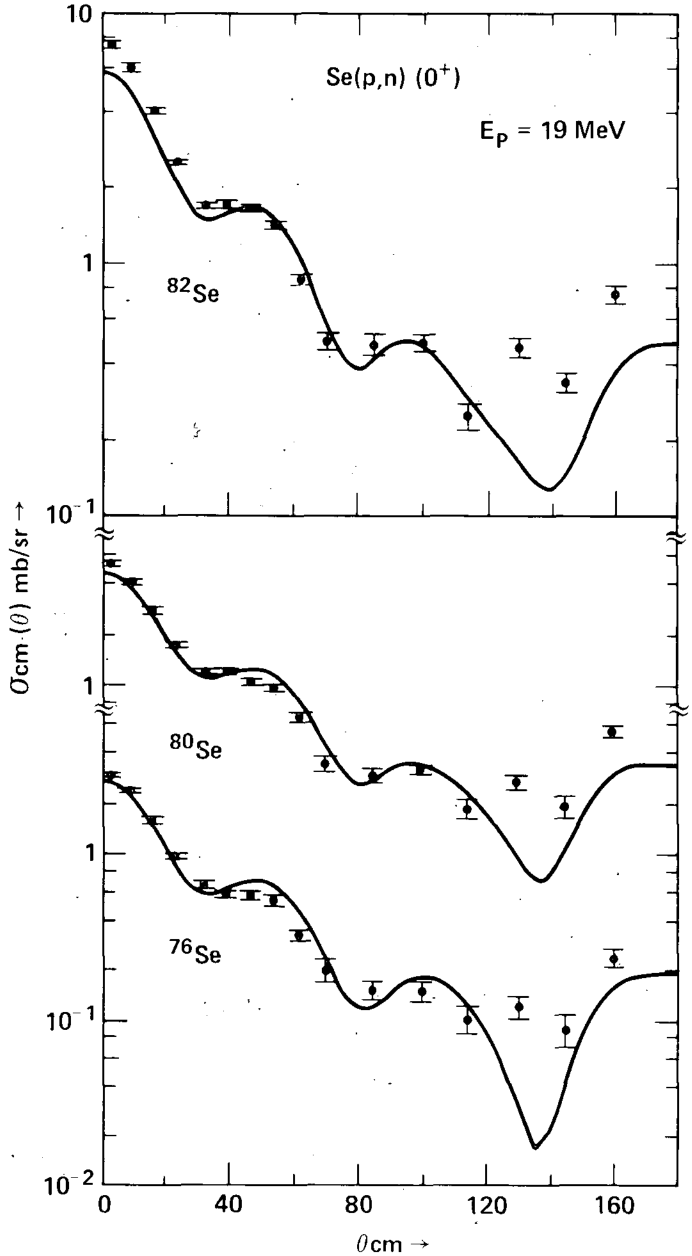

FIG. A-1. Measured and calculated angular distributions for the excitation of the 0^+ analog states in $^{76,80,82}Se$ (p,n) by 19 MeV protons. The neutron optical model parameters were derived from an analysis of neutron elastic and inelastic scattering data.

7. Neutron-Capture Resonances for ^{82}Se (Browne,* Berman)

We have investigated neutron capture resonances for ^{82}Se using the white neutron source from the LLNL 100 MeV Linac. Strong neutron-capture resonances for ^{82}Se were found at 3.63, 7.1, and 9.51 keV and weaker ones at 0.58, 1.15, and possibly 13.54 and 16.5 keV. None was found at lower neutron energies. Energies have been assigned to neutron-capture resonances up to 40 keV for all the other selenium isotopes as well.

8. Measurement of Fast-Neutron Cross Sections for ^{88}Y, ^{88}Zr, and ^{168}Tm (Nethaway, Smith, Prestwood,** Thomas**)

We have made several measurements of fast-neutron cross sections for the radioactive target materials ^{88}Y, ^{88}Zr, and ^{168}Tm. These measurements are difficult to make because of the intense radioactivity associated with their relatively short half-lives. The experimental results are valuable because they provide additional tests of the nuclear models used in the calculation of cross sections for neutron-deficient nuclides.

The tracer materials were produced by spallation of molybdenum and tantalum targets with 800-MeV protons at the Isotope Production Facility at LAMPF. The tracers were allowed to age until the short-lived products ^{87}Y and ^{167}Tm had decayed to negligible levels. We used targets containing up to 40 mCi ^{88}Y, 140 mCi ^{88}Zr, and 15 mCi ^{168}Tm. The fast-neutron irradiations were made at the ICT and RTNS-II facilities at Livermore, using neutrons in the 14-15 MeV range.

The ^{88}Y and ^{88}Zr measurements were made on the daughter nuclide ^{87m}Sr, which was separated as a function of time from Y and Zr fractions from the ^{88}Zr target, and from the ^{88}Y target itself. The ^{167}Tm measurements were made on the mass-167 fractions following single and double isotope separations of the ^{168}Tm target. Preliminary results are given in Table A-1.

9. Intermediate States in Nuclear Fission (Becker)

Nuclear states in the second minimum of the fission barrier reflect themselves in broad resonance structures in fission excitation functions and in anomalous fragment angular distributions. To study these intermediate states, we have measured simultaneously the excitation function and fragment angular distribution for the $^{232}Th(n,f)$ reaction, with a resolution of 0.16 nsec/m. A "white" neutron source produced by the Lawrence Livermore National Laboratory 100-MeV Electron Linac irradiated a thick ^{232}Th sample. Fission fragments were detected in a new array of multi-wire position sensitive counters designed to yield fragment angular distribution information.

---

* Present address: Los Alamos National Laboratory, Los Alamos, NM 87545.
** Los Alamos National Laboratory, Los Alamos, NM 87545.

The angular distributions, extracted after normalization to data collected with a ^{235}U(93%) foil in the place of the ^{232}Th sample, were parameterized by a Legendre Polynomial expansion, $W(\theta) = I_f \; (1 + A_2P_2 \; (\cos\theta) + A_4P_4(\cos\theta))$. The coefficients for different incident neutron energy regions obtained in a preliminary analysis are presented in Table A-2. Note that the angular distribution associated with the photofission process is peaked at 90° as expected, and that as the incident neutron energy increases over the second-chance fission threshold, the angular distribution becomes strongly forward peaked. In the region of $1.2 \leq E_n \leq 2$ MeV, the angular distribution exhibits both positive and negative coefficients. Further analyses and comparisons with other work are continuing.

10. <u>Excited Levels of ^{250}Bk From Spectroscopic Measurements of $^{249}Bk(n,\gamma)$ ^{250}Bk and $^{249}Bk(d,p)^{250}Bk$</u> Reactions (Hoff, Lougheed, Lanier, White,* Borner,** Davidson,** Schreckenbach,** Warner,** von Egidy,** Kouzes,+ Naumann,+ Dewberry+)

The gamma rays and conversion electrons emitted following neutron capture in ^{249}Bk targets have been measured by use of the GAMS, BILL, and three-crystal pair spectrometers at Grenoble. We have measured the proton spectrum from the $^{249}Bk(d,p)^{250}Bk$ reaction by use of a QDDD spectrometer at the Princeton AVF cyclotron. The data from these measurements have been combined with those from earlier studies of ^{254}Es alpha decay[8] to produce a more detailed level scheme for ^{250}Bk than before. Although the interpretation of our experimental data is not complete, we have identified 23 excited levels in ^{250}Bk (see Table A-3).

The average deviation between experimental bandhead energies for eight of these nine bands and values calculated from a simple model involving addition of excitations observed in neighboring odd-mass nuclei is 11 keV. Values for the Gallagher-Moszkowski splitting of each configurational pair were obtained from theoretical calculations.[9]

It is possible to distinguish unambiguously between the only two proton states used in the configuration assignments, 7/2[633] and 3/2[521], because of the large difference in rotational parameters. For the four configurational pairs observed in ^{250}Bk, the moment of inertia for each band with antiparallel alignment of odd-nucleon momenta is systematically larger than for its parallel-aligned mate. It is not clear whether this is a general phenomenon or peculiar only to the ^{250}Bk level scheme.

---

* Western Oregon State College, Monmouth, OR.

** Institut Max von Laue-Paul Langevin, Grenoble, France.

\+ Princeton University, Princeton, NJ 08540.

8 I. Ahmad, H. Diamond, J. Milsted, J. Lerner, and R. Sjoblom, Nucl. Phys. <u>A208</u>, 287 (1973); W. McHarris, F. Stephens, F. Asaro, and I. Perlman, Phys. Rev. <u>144</u>, 1031 (1966).

9 R. Piepenbring and J.P. Boisson, private communication (1978).

TABLE A-1. Preliminary results of fast-neutron cross sections measured for ^{88}Y, ^{88}Zr, and ^{168}Tm.

Reaction	Neutron energy (MeV)	Cross sections (mb)
$^{88}Y(n,2n)^{87}Y$	14.1	1140 ± 60 (a)
	14.8	1180 ± 60 (a)
$^{88}Zr(n,2n)^{87}Zr$	14.8	467 ± 24
$^{88}Zr(n,np)^{87}Y$	14.8	257 ± 26
$^{168}Tm(n,2n)^{167}Tm$	14.5	2100 ± 110

(a) The ^{87}Y isomer ratio, m/(m+g), was measured to be 0.72 0.05.

TABLE A-2. Angular distribution coefficients obtained in the $^{232}Th(n,f)$ reaction

En (MeV)	Δ En (MeV)	A_2	A_4
1.2	0.1	0.56 ± 0.34	-0.19 ± 0.45
1.3	0.1	0.40 ± 0.19	-0.41 ± 0.25
1.4	0.1	0.27 ± 0.16	-0.28 ± 0.21
1.5	0.1	-0.21 ± 0.12	-0.35 ± 0.17
1.6	0.1	-0.21 ± 0.12	-0.18 ± 0.16
1.7	0.1	0.43 ± 0.17	-0.57 ± 0.23
1.8	0.1	0.34 ± 0.08	-0.08 ± 0.02
1.9	0.1	0.11 ± 0.17	0.18 ± 0.24
3.0	1.0	0.10 ± 0.08	-0.02 ± 0.10
4.0	1.0	0.16 ± 0.10	0.11 ± 0.13
5.0	1.0	0.28 ± 0.11	-0.16 ± 0.15
6.0	0.5	0.56 ± 0.16	0.35 ± 0.18
6.5	0.5	0.44 ± 0.13	0.28 ± 0.16
7.0	0.5	0.69 ± 0.15	-0.06 ± 0.18
7.5	0.5	0.37 ± 0.14	0.22 ± 0.18
8.0	0.5	0.43 ± 0.19	-0.05 ± 0.23
8.5	1.5	0.39 ± 0.12	-0.01 ± 0.16
"photo-fission"		-0.32 ± 0.03	-0.06 ± 0.04

TABLE A-3. Experimental levels in ^{250}Bk and comparisons with simple model predicitions.

Configuration	Bandhead energy(keV) Exp.	Model	Rotational band levels I	E(keV)	$\hbar^2/2J$ (keV) Exp.	Model
3/2$^-$[521]p + 1/2$^+$[620]n	0	0	2^-	0	5.77	5.72
			3^-	34.472		
			4^-	80.258		
			5^-	137.32		
3/2$^-$[521]p - 1/2$^+$[620]n	104	109 $\pm$ 5	1^-	103.828	5.35	5.72
			2^-	125.007		
			3^-	157.391		
			4^-	203.637		
7/2$^+$[633]p + 1/2$^+$[620]n	36	40 $\pm$ 18	4^+	35.587	4.31	4.26
			5^+	78.326		
			6^+	130.492		
7/2$^+$[633]p - 1/2$^+$[620]n	115	96 $\pm$ 18	3^+	115.442	4.14	4.26
			4^+	148.595		
3/2$^-$[521]p + 7/2$^+$[613]n	97	101 $\pm$ 30	5^-	97.493	5.80	5.88
			6^-	167.089		
3/2$^-$[521]p - 7/2$^+$[613]n	146	144 $\pm$ 30	2^-	146.472	5.59	5.88
			3^-	179.990		
7/2$^+$[633]p - 7/2$^+$[613]n	175	107 $\pm$ 35	1^+	175.123	--	4.34
			0^+	215.944		
7/2$^+$[633]p - 3/2$^+$[622]n	212	213 $\pm$ 23	2^+	211.822	4.18	4.37
			3^+	236.739		
			4^+	270.461		
7/2$^+$[633]p + 3/2$^+$[622]n	316	295 $\pm$ 23	5^+	316.463	4.43	4.37
			6^+	369.61		

B. NUCLEAR DATA APPLICATIONS - CALCULATIONS

1. Development of Microscopic Optical Model for Neutron Elastic Scattering, with Application to ^{208}Pb (Dietrich, Howell, Phillips, Petrovich,*)

We have developed the capability of performing microscopic optical model calculations based on the folding of a complex density- and energy-dependent effective interaction with the nuclear density. The aim of these calculations is to reduce the number of parameters in this conventional optical model description, and ultimately to improve our understanding of the relation between the neutron and proton optical models and the (p,n) quasi-elastic reaction. The general approach is due to that of Brieva and Rook.[1] The free parameters that are adjusted to data are normalization factors for the real and imaginary central potentials and the real spin-orbit potential generated by the folding procedure. Fig. B-1 shows a fit to 25.7-MeV data for neutron scattering from ^{208}Pb. The central part of the effective interaction is that of Brieva, Rook, and von Geramb,[2] and the spin-orbit force from the M3Y interaction.[3] The nuclear charge density was taken as a two-parameter Fermi function fit to electron scattering,[4] and the neutron and proton densities were assumed to be proportional.

The quality of the fit is comparable to that with conventional optical models that use a common geometry over a wide energy range. The normalizing factors were 1.07, 0.92, and 1.28 for the real, imaginary and spin-orbit potentials, respectively, which indicates reasonable consistency of the model, at least at this energy. A test of the model over a wide neutron energy range (7 to 40 MeV) is presently under way.

2. A Strength Function Method for Calculating Level-densities (Bloom, Vonach,** Grimes,*** and Hausman+)

A new method for calculating level densities based on the Lanczos algorithm,[5] with the addition of a Monte Carlo (statistical) technique for sampling the full set of eigenvectors modeling the nucleus, has been developed and applied to the positive parity levels of ^{28}Si. A realistic Hamiltonian is used to generate the

---

* Permanent address: Florida State University, Tallahassee, FL 32306.

** On sabbatical leave from Institut fur Radiumforschung und Kernphysik, Vienna, Austria

*** Permanent address: Ohio University, Athens, OH 45701.

\+ Permanent address: Los Alamos National Laboratory, Los Alamos, NM 87545.

1 F.A. Brieva and J.R. Rook, Nucl. Phys. A291, 317 (1977).

2 H.V. von Gerarub, F.A. Brieva, and J.R. Rook in Microscopic Optical Potentials, H.V. von Geramb, ed., Lecture Notes in Physics No. 89, Springer Verlag, Berlin, 1979, p.104.

3 G. Bertsch et al., Nucl. Phys. A284, 399 (1977).

4 D. E. Bainum et al., Phys. Rev. C16, 1377 (1977).

5 R. R. Whitehead, A. Watt, and D. Kelvin, Phys. Letters 89B, 313 (1980).

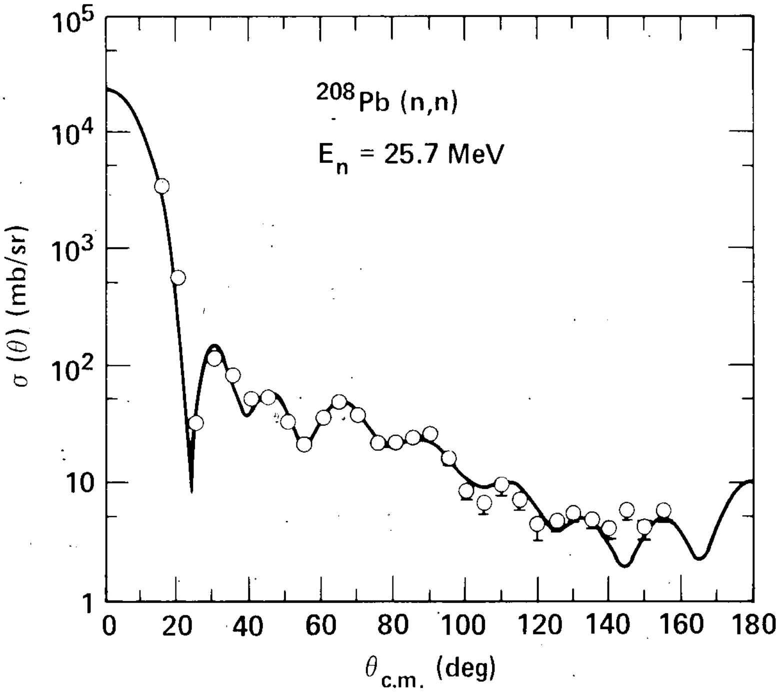

FIG. B-1. Calculated angular distribution of 25.7 MeV neutrons elastically scattered by ^{208}Pb. The optical potential was obtained by the folding model. The experimental data are from Ref. 4.

sampled model space. The number of levels in the model for ^{28}Si was 69,000; a rather large statistical sample of 24,000 states was used in these calculations. Spin cutoff parameters have also been calculated.

Preliminary comparisons with experimental data are quite encouraging for the level densities calculated at excitation energies of 8-15 MeV. In this region the calculated level densities are expected to be independent of the model size.

3. Parameterization of the E1 Strength Function (Gardner, Gardner)

The reparameterization of an energy-dependent Breit-Wigner model of the E1 gamma-ray strength function, $f_{E1}(E)$, has been investigated using a more general expression for the Breit-Wigner line shape function, $G(E_\gamma, E_R, \Gamma_R)$. For a giant dipole resonance (GDR) with one peak or two peaks of equal height,

$$f_{E1}(E_\gamma) = 3.3 \times 10^{-6} \frac{NZ}{A} \frac{F_{SR}}{E_\gamma} \frac{\sum G_i(E_\gamma, E_{Ri}, \Gamma_{Ri})}{\sum \Gamma_{Ri}} \; MeV^{-3}$$

Here E_R and Γ_R are the peak energy and width of the GDR, and E_γ is the gamma-ray transition energy. F_{SR} incorporates the extent to which the dipole sum rule is exhausted. For neutron and low-energy proton capture, we define this in terms of the isopin splitting of the GDR, $F_{SR} \doteq [T_o/(T_o + 1)]\,[1 + 3/2\, A^{-2/3}]$, where $T_o = (N-Z)/2$.

The line shape function now employs a product of a constant width, Γ_R, and an energy-dependent width, $\Gamma(E_\gamma)$

$$G(E_\gamma, E_R, \Gamma_R) = \frac{\Gamma_R \Gamma(E_\gamma)/4}{(E_\gamma - E_R)^2 + \Gamma_R \Gamma(E_\gamma)/4}$$

The energy-dependent width has the form

$$\begin{aligned} \Gamma(E_\gamma) &= \Gamma_R E_\gamma^2 \left(\frac{2}{E_x + E_R}\right)^2 \quad ; \quad E_\gamma \le (E_x + E_R)/2 \\ &= \Gamma_R \quad ; \quad E_\gamma > (E_x + E_R)/2 . \end{aligned}$$

There is one free parameter, E_x, for which the value of 5 MeV seems to fit a wide range of masses. The E_γ^2 dependence of $\Gamma(E_\gamma)$ tends to agree with a number of experimental photoabsorption measurements. In addition, we have compared our new predictions with the extensive survey of dipole radiative strength functions derived from neutron resonance data by McCullagh, Stelts and Chrien.[6] This comparison is shown in Fig. B-2, where the E1 strength function is expressed as

$$S_{E1} = f_{E1}(E_\gamma)\, E_\gamma^{-2}\, A^{-8/3}.$$

The dashed-line band shows a range of calculated values from our original treatment.[7] The solid line shows the present results which constitute a significant improvement, although the new parameterization may still overpredict the magnitude of f_{E1} by about 30% in some mass ranges.

4. Evaluation of Macroscopic Fission Barrier Models (Blann, Komoto)

Fission barriers may be represented as the sum of a microscopic and macroscopic component. The microscopic component is related to the position and spacing of single particle levels as a function of nuclear deformation; the macroscopic component is related to the interplay between coulomb and surface energies versus nuclear deformation. Below $Z \approx 82$ the macroscopic component is much larger than the microscopic component; therefore this region is well suited to testing macroscopic barrier models. However significant fission cross sections result in $Z < 82$ nuclides only when moderately large angular momenta are present, e.g., in heavy ion induced reactions.

---

6 C.M. McCullagh, M.L. Stelts, and R.E. Chrien, Phys. Rev. C23, 1394 (1981).

7 D.G. Gardner, M.A. Gardner, and F.S. Dietrich, "A Study of Gamma-Ray Strength Functions," UCID-18759 (August 7, 1980).

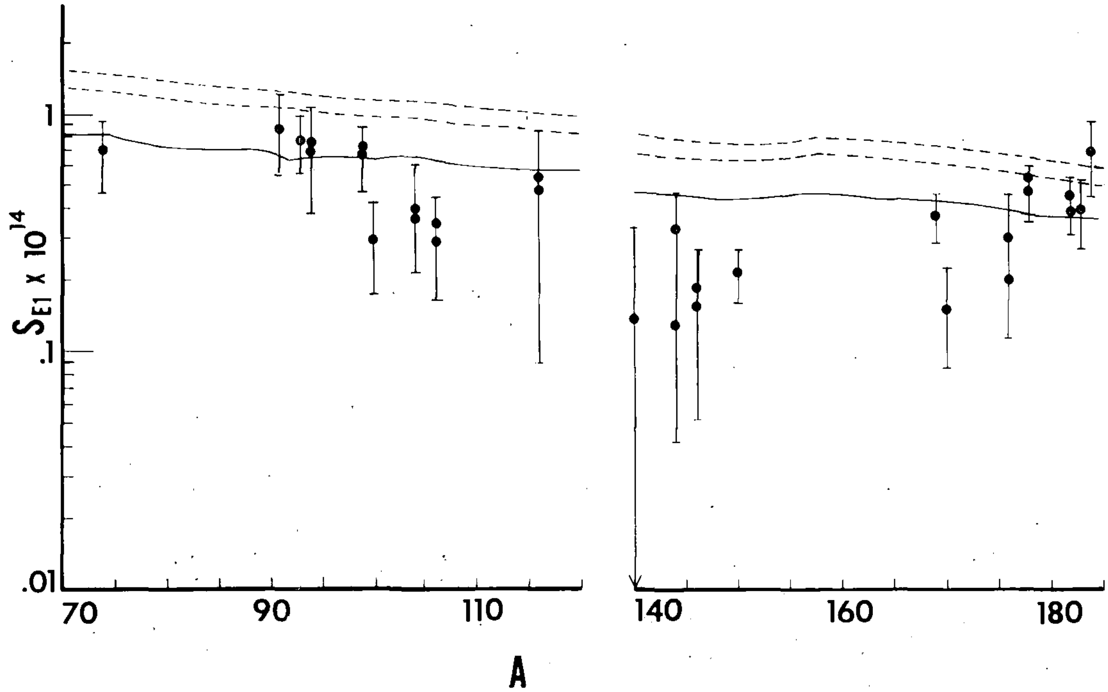

FIG. B-2. E1 strength function as a function of atomic mass numbers. The dashed band is from the original energy-dependent Breit-Wigner model.[7] The solid line is the result of the pressed model. Experimental data points are from McCullagh et al.[6]

The main model invoked to predict the macroscopic barriers versus angular momenta is the rotating liquid drop model (RLDM).[8] This has been found in many comparisons with data to overestimate the angular momentum dependent fission barriers.[9] The errors were qualitatively in the direction predicted by Krappe et al., due to finite range effects at the saddle point; however the latter correction was predicted only for non-rotating nuclei, making comparisons with results deduced for rotating systems unclear.[10]

We have analyzed a large body of (HI,f) data with a new Hauser-Feshbach code in order to determine the magnitudes of differences between macroscopic fission barriers and the RLDM predictions. These barrier decrements may be compared to first order with finite range model predictions if the abscissa is a total disruptive parameter consisting of both coulomb and centrifugal components. A comparison is shown in Fig. B-3 between predictions of the finite range model and experimentally deduced decrements from RLDM barriers. A very strong correlation may be seen, with a suggestion that the finite range correction may be around 1 MeV low in the parameter range of comparison.

---

8 S. Cohen, F. Plasil and W.J. Swiatecki, Ann. Phys. (N.Y.) 82, 557 (1974).
9 M. Beckerman and M. Blann, Phys. Rev. C17, 1615 (1978).
10 H.J. Krappe, J.R. Nix and A.J. Sierk, Phys. Rev. 20, 992 (1979).

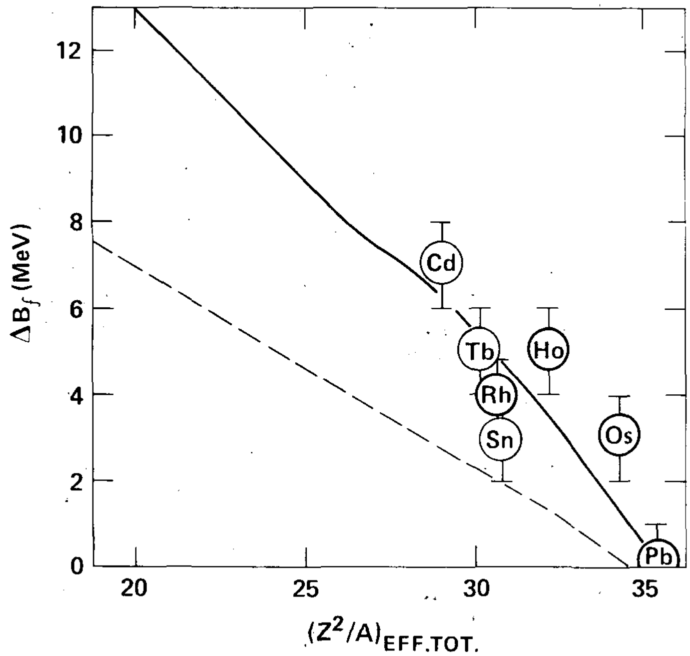

FIG. B-3. Corrections deduced to RLDM barriers for various compound systems versus the effective Z^2/A of the compound systems. The solid curve is the finite range correction prediction of Ref. 10, calculated for stable nuclei. The dashed curve is the lower finite range correction prediction of Ref. 10.

A detailed description of the calculations performed, computer code capabilities, and range of data analyzed has been reported.[11] The present results suggest that extensions and refinements of the finite range approach may provide a good basis for more accurate macroscopic descriptions of the fission process.

5. Fission Barriers of Rotating Nuclei (Mustafa, Baisden, and Chandra)

Fission barriers of rotating nuclei have been calculated with a new macroscopic model.[12] The model explicitly includes the effects of the finite range of nuclear forces and diffuse nuclear surface in all the terms contributing to fission barriers. The model also allows for triaxial shape variations and a continuous transition from ground state to saddle to scission shapes.

---

11 M. Blann and T. Komoto, "Statistical Fission Parameters for Nuclei at High Excitation and Angular Momenta," UCRL-87112 (1982).

12 M.G. Mustafa, P.A. Baisden, and H. Chandra, Lawrence Livermore National Laboratory, Livermore, CA, UCRL-85260. Rev. 1, (1982).

The predictions of our model can be tested by heavy-ion experiments and utilized in the de-excitation of a compound nucleus by particle emission and fission.

C. NUCLEAR DATA FOR REACTOR SAFETY

1. Determination of Fission Yields by Continuous Chemistry (Meyer, Henry, Massey, Rengan)

We have used our ethylene gas-jet system[1,2] to measure independent fission yields of short-lived selenium fission products. In these experiments, a mixture of ethylene and nitrogen was used to thermalize and carry the fission products from a ^{235}U target chamber in a gas jet. The selenium isotopes of mass 83-88 were selectively collected in a quartz-wool trap in about 750 ms after fission (or later when an additional delay line is used).[3] The gamma-ray spectra of the mixture of selenium isotopes obtained under equilibrium conditions were used to determine the fission yield of ^{85}Se. Using the known ^{84}Se yield, the absolute yield of ^{85}Se was calculated.

Results of three different experiments were used. The collection of Se started at 750, 870, and 940 ms, respectively. A correction for the decay of As precursors during the time before collection was made on the assumption that the Se species, formed as a result of As decay, behave similar to those formed directly in fission. The values for the independent yields of ^{85}Se to ^{88}Se are summarized in Table C-1. The independent-yield values calculated for ^{85}Se from the three experiments with different delays agree fairly well with each other and with the value reported by Kratz and Herrmann.[4]

2. Experimental Test of High-Energy Beta Strength Functions: S_β for $^{84}As(\beta^-)^{84}Se$ with Q_β of Approximately 10 MeV (Henry, Lien, Meyer)

We have used the AUTOBATCH fast chemistry system[5] to isolate rapidly the short-lived As isotopes from mixed fission products. Over 10,000 targets were irradiated, chemically separated, and counted during the ^{84}As gamma-ray coincidence and high-energy singles experiments.

---

1 Nuclear Chemistry Division Annual Report, UCAR-10062, p. IV-B-2, 1980.
2 R.A. Meyer, Energy & Technology Review, Lawrence Livermore National Laboratory, Livermore, CA, UCRL-52000-80-5 (1980) p.8.
3 K. Rengan, J. Lin, T.N. Massey, M. Zendel, and R.A. Meyer, submitted to J. Inorg. Nucl. Chem. (1981).
4 J.V. Kratz and G. Herrmann, IAEA Symp. Phys. Chem. Fission, 2, 95 (1973).
5 O. G. Lien, P. C. Stevenson, E. A. Henry, R. P. Yaffe, and R. A. Meyer, Lawrence Livermore National Laboratory, Livermore, CA, UCRL-84371 (1980) Nucl. Inst. and Methods (in press).

TABLE C-1. Fission Yields of Short-Lived Selenium Isotopes

Delay (milliseconds)	Independent Yield 85-Se (31s)	86-Se (15s)	87-Se (5.6s)	88-Se (1.5s)
750	0.97	0.68	(0.0662·B)[b]	(0.0537·C)[b]
870	0.99	0.72	(0.0666·B)[b]	(0.0537·C)[b]
940	1.00	0.72	(0.0668·B)[b]	(0.0552·C)[b]
Literature (Batch-Chem)	1.08	None	None	None
Precursor Half life	2.03s	0.9s	0.3s	Unk.

a All values have an error of approximately 5%.

b The final value for these await the determination of the absolute intensity of the respective fiducial gamma ray: B is 468-keV gamma-ray absolute intensity of ^{87}Se, and C is the 158-keV gamma-ray absolute intensity of ^{88}Se.

The experimental beta strength function deduced from the ^{84}As decay scheme can be compared to that calculated by a statistical model where the beta strength function is assumed to be proportional to the level density (calculated using the Gilbert and Cameron formalism[6]). The most significant differences are that the experimental beta transition intensity has an excess of about 16% near 2700 keV and a deficit of the same size above 6.8 MeV compared to calculated beta transition intensities. Above 7.0 MeV the calculated beta intensity is approximately four times that which can be estimated by the procedures described below. Over the energy range from 3 to 6.8 MeV the experimental beta strength function deduced from discrete gamma rays fluctuates about but follows the general trend of the calculated strength function.

Since a large part of the beta strength function at all energies is determined by gamma rays which populate the 1455-keV level, the gamma rays in coincidence with the 1455-keV level can serve as a useful probe to determine if the general shape of the spectrum of gamma rays into this level can be reproduced by a statistical model.

---

6 A. Gilbert and A.G.W. Cameron, Can. J. Phys. 43, 1446 (1965).

Shown in Fig. C-1 is a comparison of the experimental gamma-ray intensity into the 1455-keV level compared to that calculated using the statistical beta strength function. It is assumed in the calculation that levels with J = 3, 4, and 5 are populated by the beta decay and that these levels decay by dipole transitions. Above 5 MeV of excitation, levels were grouped into 200 keV bins, while below 5 MeV the experimental levels were used in the calculation. The total intensity into each bin or level included the beta intensity and the sum of all gamma-ray intensity from higher levels. It is seen that such a calculation cannot account for the observed gamma-ray intensity into the 1455-keV level.

The gross coincidence spectra of other strong gamma rays show results similar to, though less easily quantifiable than those indicated by the 1455-keV coincidence gate. They show in most cases a discontinuity at a gamma-ray energy commensurate with an excitation energy of 6.5 MeV. These quantitative and qualitative results from the gross coincidence spectra indicate that the experimental beta strength functions derived from discrete gamma rays underestimate the strength near 6.5 MeV. No evidence is found for sufficient additional gamma-ray intensity to account for all of the 16% beta intensity discrepancy between experiment and calculation above 6.8 MeV. Finally, we observe that the gamma-ray intensity distribution to low-lying levels is not reproduced by a statistical distribution.

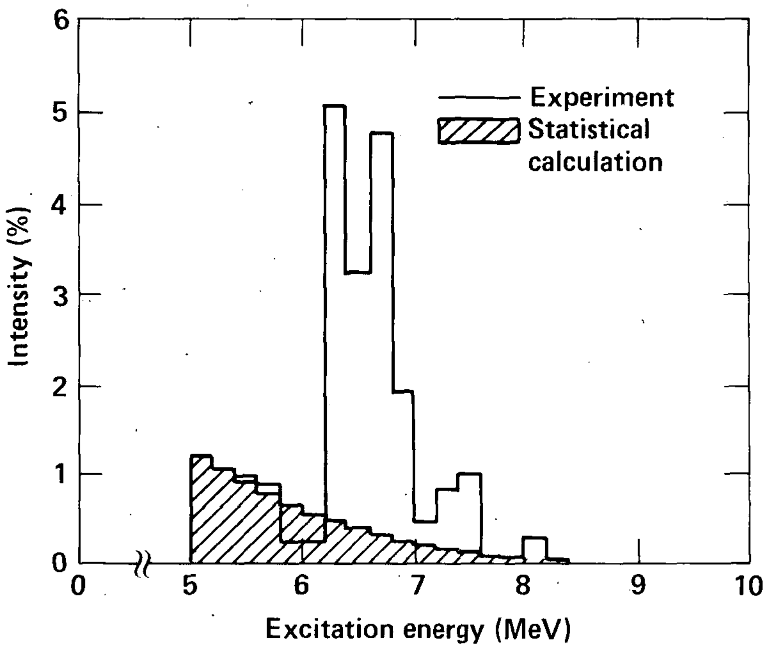

FIG. C-1. Comparison of experimental gamma-ray intensity into the 1455-keV level to that calculated using a statistical beta strength function.

A. NUCLEAR DATA MEASUREMENTS

1. Low-Energy Fusion Cross Sections (Jarmie, Brown, Hardekopf, Toevs)

The goal of this project is to measure cross sections for interactions between hydrogen isotopes in the bombarding energy range 10-120 keV. Such cross sections are fundamental to the operation of future controlled fusion systems.

During the past year we have made final calibrations of the target system using the D(p,p)D reaction at 10 MeV. Following this we completed our first data runs for the D(t,α)n system at triton bombarding energies of 15, 20, 40, and 80 keV. The alpha spectra have a very low background. We were able to obtain a statistical uncertainty of $\pm$ 10% in 80 minutes for the 15 keV data point. The absolute accuracy for the cross sections is about 15%, limited at present by our knowledge of the beam intensity.

Our goal in the coming year is to improve the beam intensity measurement, and then to make final measurements of the D(t,α)n and the D+D reactions with an uncertainty of $\pm$ 5%. We then expect to make preliminary observations in other few-nucleon systems such as the T+T reaction, ^{3}He(d,p)^{4}He, and D(t,γ). The D(t,γ) reaction has the potential for being an important diagnostic reaction for studying D+T plasmas, but its cross section is virtually unknown.

2. Differential Cross Sections of the Reaction ^{4}He(t,n)^{6}Li Between 8.5 and 16.5 MeV and the n-^{6}Li Cross-Section Standard (Drosg, Drake, Hardekopf, Hale)

We have measured the ^{6}Li(n,α)t cross section using the inverse reaction (triton beam on a ^{4}He gas target). The reaction ^{6}Li(n,t)^{4}He has long been used as a standard for measuring the neutron flux in a great variety of experiments.

Our results, after transformation into the ^{6}Li(n,t)^{4}He system, are in excellent agreement with R-matrix analysis in both shape and angular distribution over the 0.24-MeV resonance (Fig. A-1).

In addition to the 0.24-MeV resonance we have data corresponding to 2.99 and 5.37 MeV incident neutrons. For these data, the cross sections are larger than the R matrix predictions.

Detailed results of this experiment can be found in Los Alamos report LA-9129 MS.

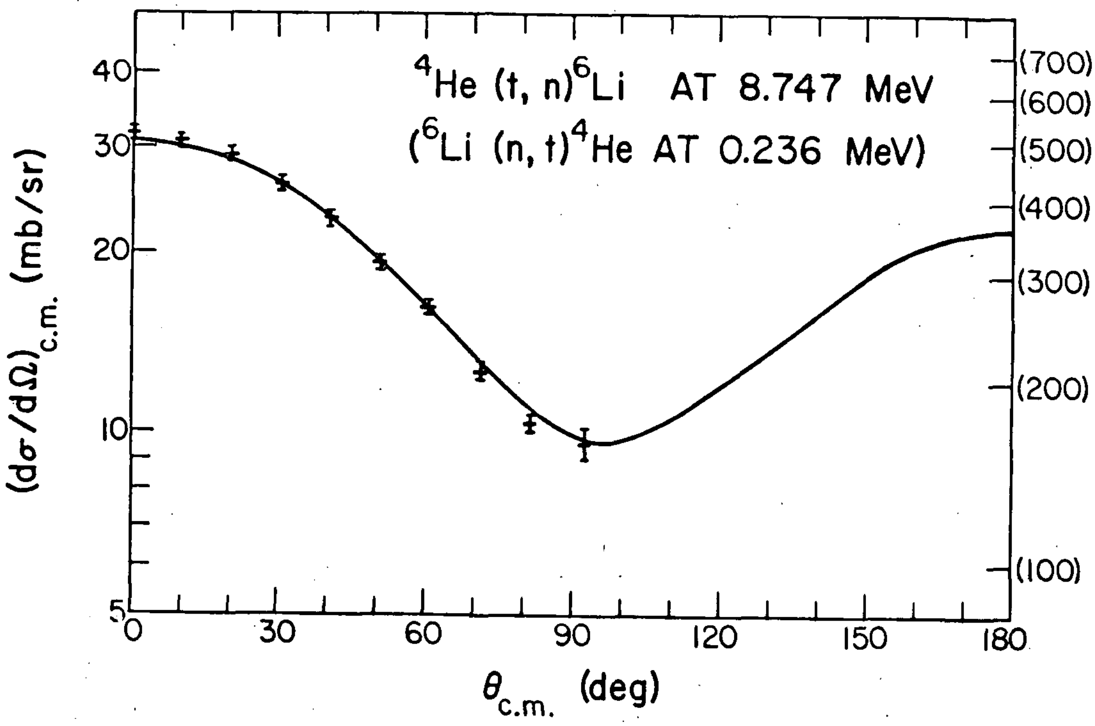

Fig. A-1. Angular distribution at 8.747 MeV for ^{4}He(t,n)^{6}Li [at 0.236 MeV for ^{6}Li(n,t)^{4}He]. The curve is the R-matrix prediction; the right scale is for n-^{6}Li.

3. ^{169}Tm(n,γ) Cross Section from 2.6 keV to 2 MeV (R. L. Macklin, ORNL; Drake, Malanify, Arthur, Young)

We have measured the neutron capture cross section for ^{169}Tm from 2.6 keV to 2 MeV. Two separate running periods were required to collect the data over this energy region. In order to extend the measurements to 2 MeV a uranium absorber was placed in the neutron beam line to reduce the ORELA gamma flash. Individual resonance parameters were derived for resonances from 2.6 to 4.2 keV, and average resonance parameters were obtained from the energy averaged data from 2.6 to 100 keV. The data are compared with compound nucleus calculations in Fig. A-2. Resonance parameters and average cross sections are presented in tabular form in Los Alamos report LAUR-82-69.

4. Neutron-Capture Cross Sections of the Tungsten Isotopes ^{182}W, ^{183}W, ^{184}, and ^{186}W From 2.6 to 2000 keV (R. L. Macklin, ORNL; D. Drake, and E. Arthur)

We have measured the neutron-capture cross sections for the four major isotopes of tungsten using the 40-m station at ORELA. In the region of isolated resonances, 2.6 keV to about 7 keV, we have deduced individual resonance parameters. In cases in which we can deduce both Γ_n and Γ_γ, our data agree well with the Γ_n's of Camarda.[1] We have made the usual parame-

[1] H. S. Camarda, et al, Phys. Rev. C8, 1813 (1973).

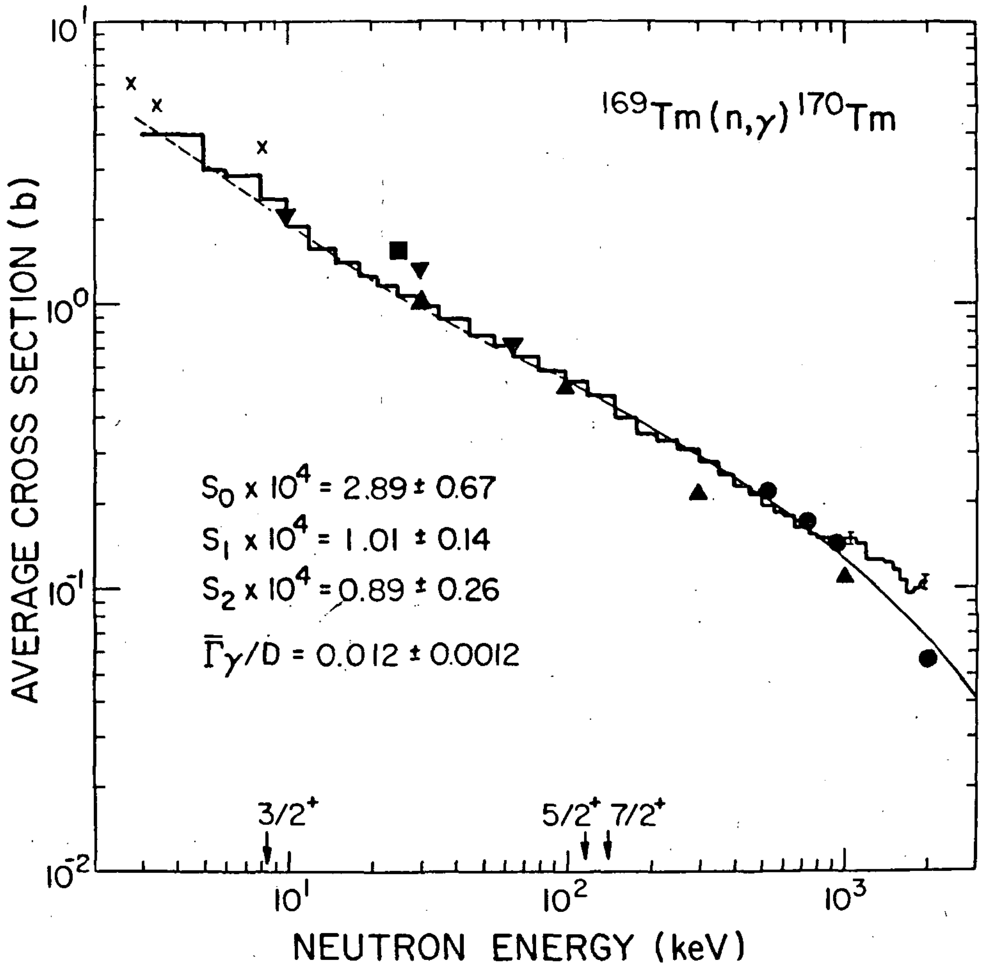

Fig. A-2. A Histogram plot of the average ^{169}Tm(n,γ)^{170}Tm cross section as a function of incident neutron energy. The dashed curve was calculated from the average resonance parameters shown in the figure. The solid triangles, ▲, are from Ref. 1, the solid circles, ●, are from Ref. 2, the crosses, x, are from Ref. 3, the inverted solid triangles, ▼, are from Ref. 4, and the solid square, ■, is from Ref. 5. The heavy solid curve represents the compound nucleus calculation. This curve is not plotted below 100 keV because it is essentially the same as the dashed curve.

1. J. A. Holmes, S. E. Woosley, W. A. Fowler, and B. A. Zimmerman, Atomic and Nuclear Data Tables 18, 316 (1976).
2. S. Joly, J. Voignier, G. Grenier, D. M. Drake, and L. Nilsson, Nucl. Sci. Eng. 70, 53 (1979).
3. R. C. Block, G. G. Slaughter, L. W. Weston, and F. C. Vonderlage, Conference on Neutron Time of Flight Methods, Saclay, 203, (1961).
4. J. H. Gibbons, R. L. Macklin, P. D. Miller, and J. H. Neiler, Phys. Rev. 122, 182 (1961).
5. K. Siddappa, M. Sriramachandra Murty, and J. Rama Rao, J. Phys. A. 5, 871 (1972).

tric fit to the averaged data from 2.6 to 100 keV. Figure A-3 shows the averaged data, the parametric fit (parameters are given in the figure), and predictions from a compound nucleus calculation for ^{182}W. Los Alamos report LA-9200 presents the data in tabular form.

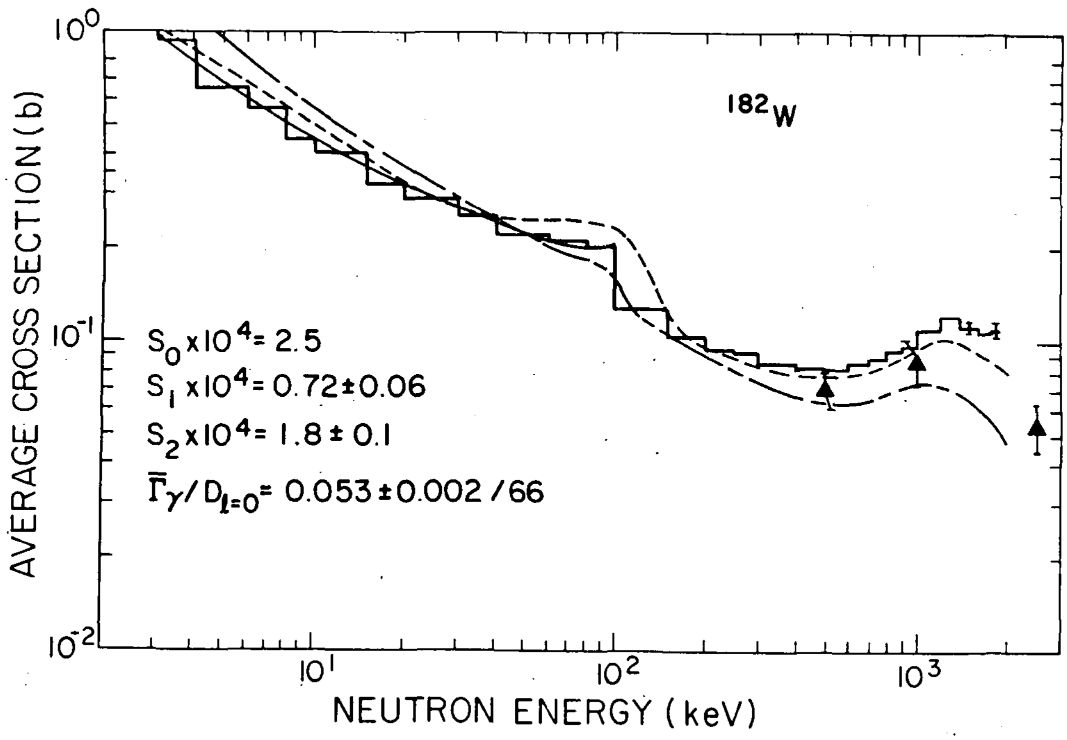

Fig. A-3. Average capture cross sections for ^{182}W. The histogram represents the present data; the smooth line was computed from the strength functions shown in the figure. The short dash-long dash line was taken from BNL 325 (1973). The dash-dash curve is the compound nucleus calculation and the solid triangles are from Ref. 2.

5. Nature of the Coupling in Subthreshold Fission of ^{238}Np
(Auchampaugh, Exterman, Moore, Olsen, Moses; N. Hill, ORNL)

High-resolution measurements of the total and fission cross section of (^{237}Np+n) in the region of the subthreshold fission structure near 40 and 120 eV have been made with samples at liquid nitrogen temperature. The previously accepted normalization of the fission cross section is found to be too low by a factor of three. Analysis of these data clearly show the presence of an "intruder" state in the region below 40 eV, with properties that are similar to the other states nearby. This suggests that the coupling between states in the first and second wells of the double-humped fission barrier is moderately weak (rather than very weak, as has been generally assumed), and that the outer barrier is less penetrable than the inner one.

[2] G. Grenier, et al., Proc. Int. Conf. Nucl. Cross Sections for Technology, Knoxville, TN (1979), p. 323.

6. Fission Cross Sections of ^{242}Pu and ^{244}Pu (M. S. Moore, C. E. Olsen; J. A. Wartena, CBNM; H. Weigmann, Geel)

Normalization of the fission cross sections of ^{242}Pu and ^{244}Pu measured on the electron linear accelerator at Geel (GELINA) has been completed. The normalization was done in two ways: 1) by alpha counting and spontaneous fission counting of a small, thin sample that had been prepared by C. Olsen at the same time as the production samples, and 2) by using the resonance-region ^{239}Pu normalization for the ^{242}Pu sample. The flux shape was obtained with a ^{235}U fission sample, measured simultaneously, and the effects of neutron absorption in the fission chamber were eliminated by taking the average value of two independent series of runs made with the chambers reversed in the neutron beam. The final data sets showed reasonable agreement with previous measurements for ^{242}Pu, and were 11% higher than previous results of ^{244}Pu in the region above threshold.

Twenty Class-II states were observed in the fission of (^{244}Pu + n) below 100 keV. We carried out a Monte-Carlo simulation study of these data, concluding that the properties of these resonances will permit us to determine barrier parameters for ^{245}Pu fission, although the data are not of high enough quality to tell if the p-wave barrier is lower than the s-wave, as postulated by Bjornholm and Lynn.

7. Excitation Functions for Reactions Induced by Spallation (Reedy)

The energetic neutrons produced in the beam stop of a high-energy accelerator simulate well the neutrons made in meteorites and the moon by the cosmic rays. To better understand the cosmic-ray production of nuclides in extraterrestrial matter, we are doing irradiations at several locations near the main beam stop of the LAMPF accelerator. Activities for a number of products with known neutron-induced cross sections [e.g., Lu(n,xn) or Au(n,xnP] or spallation systematics (e.g., ^{46}Sc, ^{48}V, etc., from Fe) will be unfolded to get the neutron fluence and spectrum for energies above a few MeV. We also will irradiate several elements that are important targets in extraterrestrial matter and measure the activities of a number of long-lived cosmic-ray-produced nuclides. Comparisons of these measured activities with production rates calculated from estimated excitation functions and the neutron spectrum will be used to get revised excitation functions. Preliminary irradiations of a large number of foils were made recently in the Radiation Effects Stringer at LAMPF. Although a large number of neutron-capture products were made, many nuclides made by energetic particles were observed, including ^{7}Be, ^{22}Na, and ^{46}Sc from Fe and several (p,n) products (e.g., ^{43}V from Ti and $^{56-58}$Co from Fe).

B. NUCLEAR DATA EVALUATION

1. Calculations of Neutron Spectra from the n+d Reaction (G. M. Hale)

Spectra for light-particle reactions leading to three-body final states are important in many applications because such reactions can occur at relatively low energies. Typically, these spectra consist of relatively narrow peaks on top of broad, underlying structures commonly attributed to "three-body phase space" contributions. However, such structure can also come from kinematically-broadened resonance effects, as, for instance, the contribution from the n-α resonance in the ^{6}Li(n,n')dα spectra calculations described in a previous report.[1]

We have calculated neutron spectra from the n+d reaction using a resonance model similar to that described in Ref. 1, except that interference between the direct and exchange amplitudes has been taken into account, and an approximate integral of the exchange contribution over the angles of the undetected particle has been replaced by the exact expression. The calculations for 14.1-MeV incident neutrons are compared in Fig. B-1 with spectra measured at two laboratory angles. The calculations are normalized to the data at forward angles, and there the agreement is good. At back angles, the calculated spectra overpredict the data considerably. Some of the assumptions and approximations that remain in the model are being relaxed in an effort to improve the calculated spectra at back angles.

---

[1]G. M. Hale, "Resonance Model for Three-Body Final States," Los Alamos Report LA-7200-PR, p. 2 (1978).

2. Charged-Particle Elastic Cross Sections (G. M. Hale, J. C. DeVeaux)

The slowing down of charged particles in a plasma has, in the past, concerned particles with energies sufficiently low to assume that the dominant mechanism is Coulomb elastic scattering. However, current fusion studies are sometimes concerned with the slowing down of fast ions, in which the nuclear components of the scattering are important at large angles, and enter even at small angles through interference with the Coulomb amplitude. Using a format developed at Los Alamos which allows an exact Legendre polynomial representation of $\sigma_{NI}(\mu)$, the difference of the elastic scattering cross section and the Rutherford (or "pure Coulomb") cross section at $\mu = \cos \theta_{CM}$, we are constructing a file of elastic cross sections for most of the possible interactions between light ions from protons through alpha particles, at energies up through several MeV.

The cross sections are calculated from parameters obtained over the years from the extensive Los Alamos program of R-matrix analyses of light systems, and are generally based on large data bases that contain many other measurements in addition to elastic cross sections. R-matrix theory provides an explicit separation of nuclear and Coulomb effects in the cross section, and reasonable extrapolations to low energies, particularly in the presence of low-lying resonances, as in the case of d-T scattering.

In Fig. B-2 are shown results of various integrals involving $\sigma_{NI}(\mu)$ for d-T scattering, compared to evaluations at Livermore reported by Perkins and Cullen.[1] The solid curves are the Livermore results and the dashed curves are the Los Alamos calculations. In both cases, the upper limits of the integrals over μ are given by min (.94, μ_o), where $\sigma_{NI}(\mu_o) = 0$, in order to define values of the integrals that correspond to positive integrated cross sections. The integral quantities are seen to disagree substantially in the region of the low-energy d-T resonance where the Livermore extrapolations to zero energy are somewhat over-simplified due to the lack of elastic cross-section data.

---

[1] S. T. Perkins and D. E. Cullen, Nucl. Sci. and Eng. 77 (1981) 20.

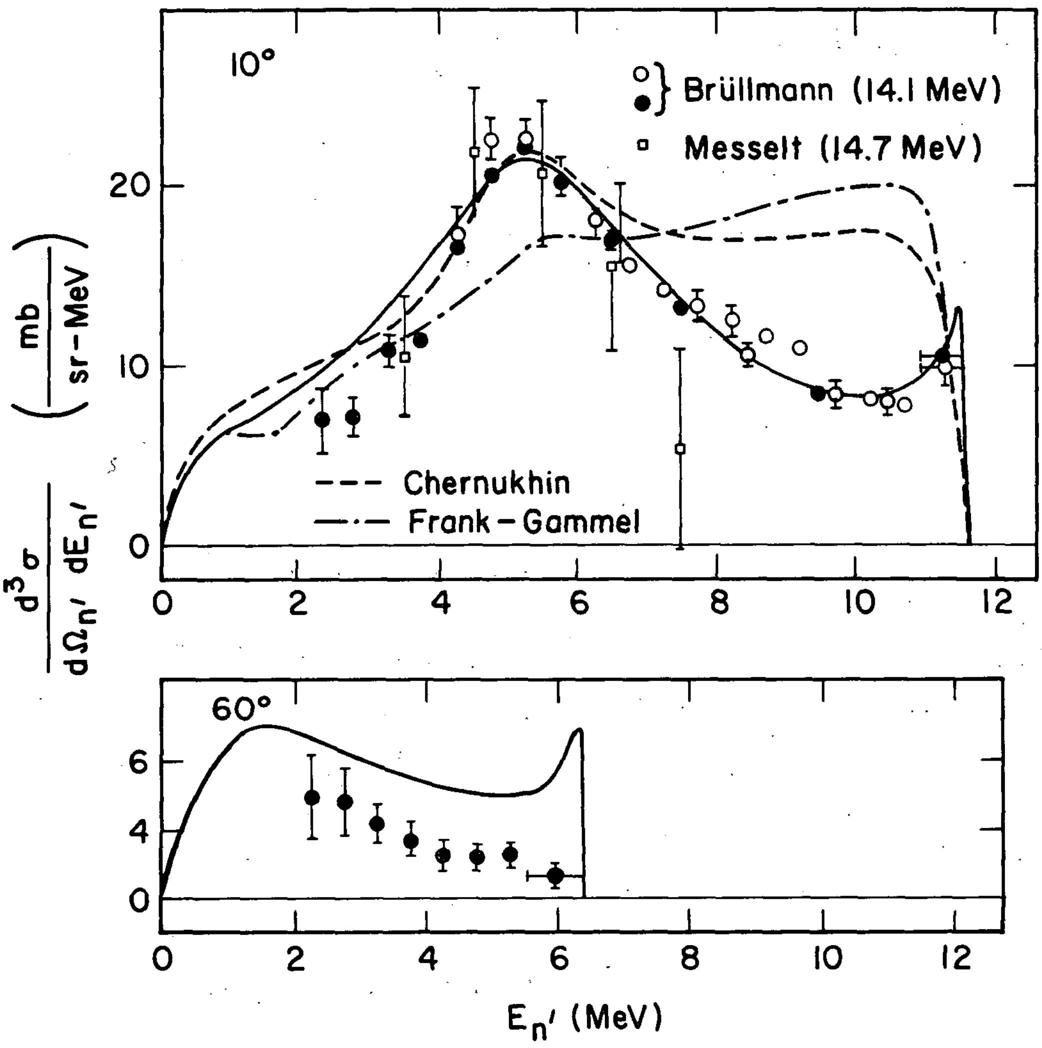

Fig. B-1. Resonance model calculations (solid curves) compared to measured n+d neutron spectra at θ_{LAB} = 10 and 60 degrees for 14.1 MeV incident neutrons. The dashed and dot-dashed curves at 10 degrees are other calculations, and the circles and squares are measured values.

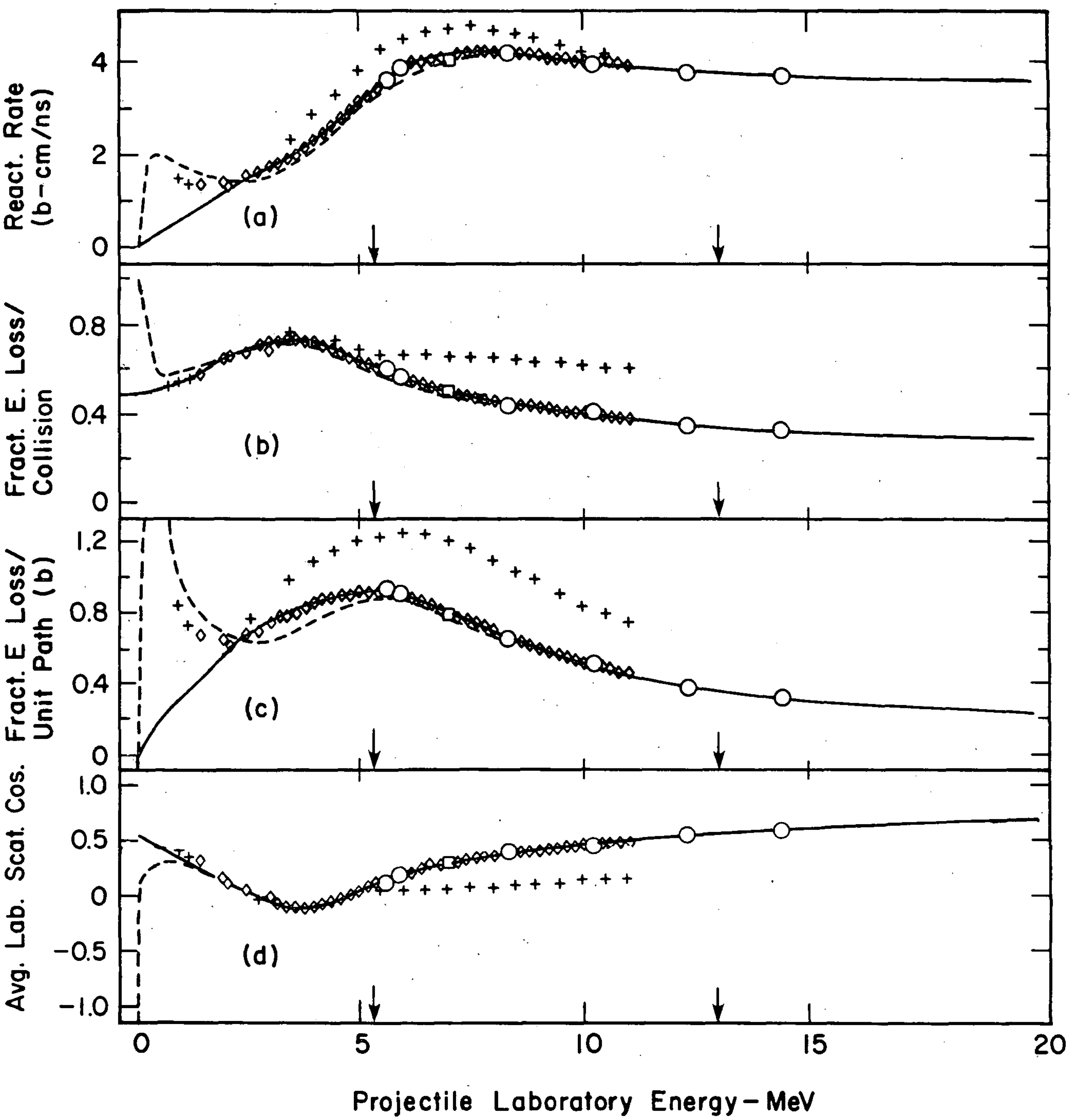

Fig. B-2. Integrals of $\sigma_{NI}(\mu)$ for dT scattering. The solid curves are the evaluations of Perkins and Cullen; the dashed curves are calculated from Los Alamos cross sections; and the points represent experimental data.

3. Analysis of n+^{7}Li Reactions Using Variance-Covariance Techniques (P. G. Young)

A new evaluation of n+^{7}Li nuclear data has been completed for the neutron energy range 0.1-20 MeV.[1] The analysis utilized the GLUCS[2] code system to perform variance-covariance analyses of each of the individual cross-section types for which experimental data exist. The results from the GLUCS analysis were then combined using the ALVIN[3] code under the constraint that all partial reactions sum to the total cross section, with full account being taken of all covariances. The results for the ^{7}Li(n,nt) reaction cross section (Fig. B-3) are some 15% lower than ENDF/B-V at 10 MeV and 10% lower at 14 MeV.

Other features of this new evaluation are a complete reanalysis of all elastic and inelastic angular distributions, a division of the (n,nt) cross section into a series of excitation energy bins that permit inclusion of accurate energy-angle correlations for emission neutrons, and complete covariance files for all cross-section data, including emission neutrons. The results of this evaluation have been submitted for Revision 2 of ENDF/B-V.

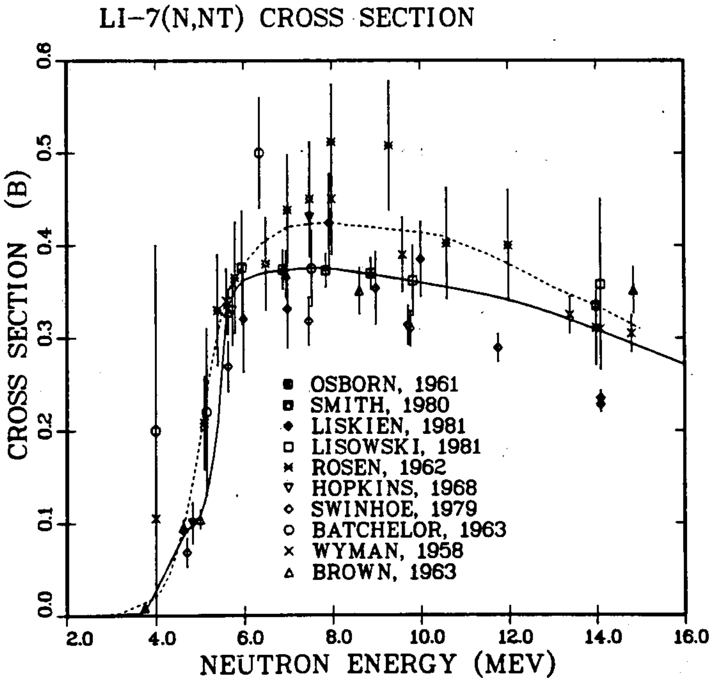

Fig. B-3. Evaluated and experimental ^{7}Li(n,nt) cross sections. The solid curve is the present result, and the dashed curve is ENDF/B-V.

[1]P. G. Young, Trans. Am. Nuc. Soc. 39, 272 (1981).

[2]D. M. Hetrick and C. Y. Fu, "GLUCS: A Generalized Least-Squares Program for Updating Cross-Section Evaluations with Correlated Data Sets," ORNL/TM-7341 (ENDF-303), Oak Ridge National Lab. (1980).

[3]D. R. Harris, W. A. Reupke, and W. B. Wilson, "Consistency Among Differential Nuclear Data and Integral Observations: The ALVIN Code for Data Adjustment, Sensitivity Calculations, and for Identification of Inconsistent Data," LA-5987, Los Alamos National Lab. (1975).

4. Calculation of n+^{169}Tm Reactions (P. G. Young, E. D. Arthur, C. Philis,* P. Nagel,* M. Collin*)

As part of an effort to calculate nuclear data for several unstable Tm isotopes, a theoretical analysis of experimental data for n+^{169}Tm reactions is in progress. Deformed optical model parameters have been determined using both ^{165}Ho and ^{169}Tm experimental data through use of an isospin term in the real and imaginary well depths along with appropriate adjustment of the β_2 and β_4 deformation parameters based on systematics. Using transmission coefficients from this analysis, preliminary Hauser-Feshbach statistical theory calculations have been carried out for the ^{169}Tm(n,γ) reaction, and for the ^{169}Tm(n,2n) and ^{169}Tm(n,3n) reactions with appropriate preequilibrium corrections. The results for the (n,2n) reaction up to 23 MeV are shown in Fig. B-4.

---

*Centre d'Études de Bruyères-le-Châtel, Montrouge, France

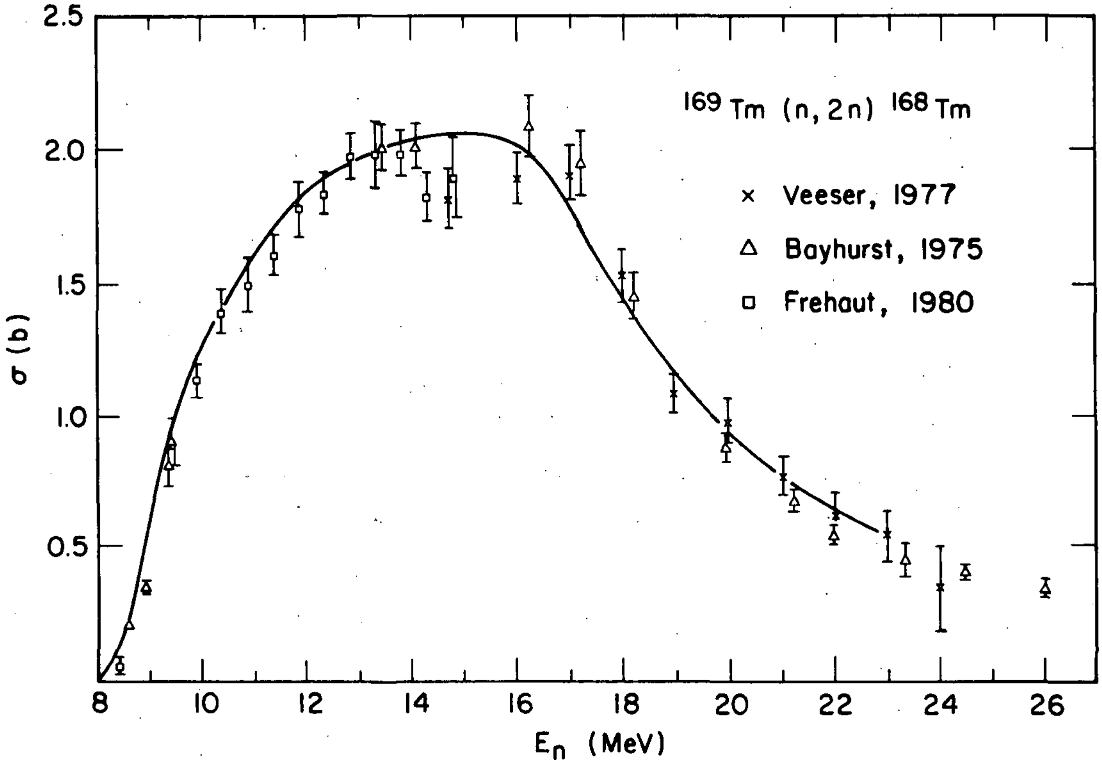

Fig. B-4. Calculated and measured ^{169}Tm(n,2n) cross sections.

5. Calculated Neutronic Properties of Prompt Fission Fragments (Foster, Arthur)

We have completed calculations of the neutronic properties of the "average prompt fission fragment" from fast-neutron-induced fission of ^{235}U and ^{239}Pu. "Prompt" means before significant beta decay has occurred (<0.1 s after fission). We have approximated the ensemble of real fission fragments by a weighted average over individual nuclides selected from the peaks and half-height portions of the fission-yield curves. Even this minimal approximation to the overall average requires 44 nuclides in the calculations, for which we determined nuclear-model parameters using Arthur's procedure.[1]

These 44 nuclides suffice to cover all neutral-particle emission for incident-neutron energies from 1 keV to 20 MeV, which includes reactions up to (n,3n) and the associated photon emission. The calculations for this energy range were performed primarily with the nuclear-model codes COMNUC and GNASH. We have supplemented these calculations with a simple approximation based on the yield of ^{135}Xe, in order to cover the incident-energy range from 10^{-5} eV to 1 keV. Results for ^{235}U are shown in Fig. 5.

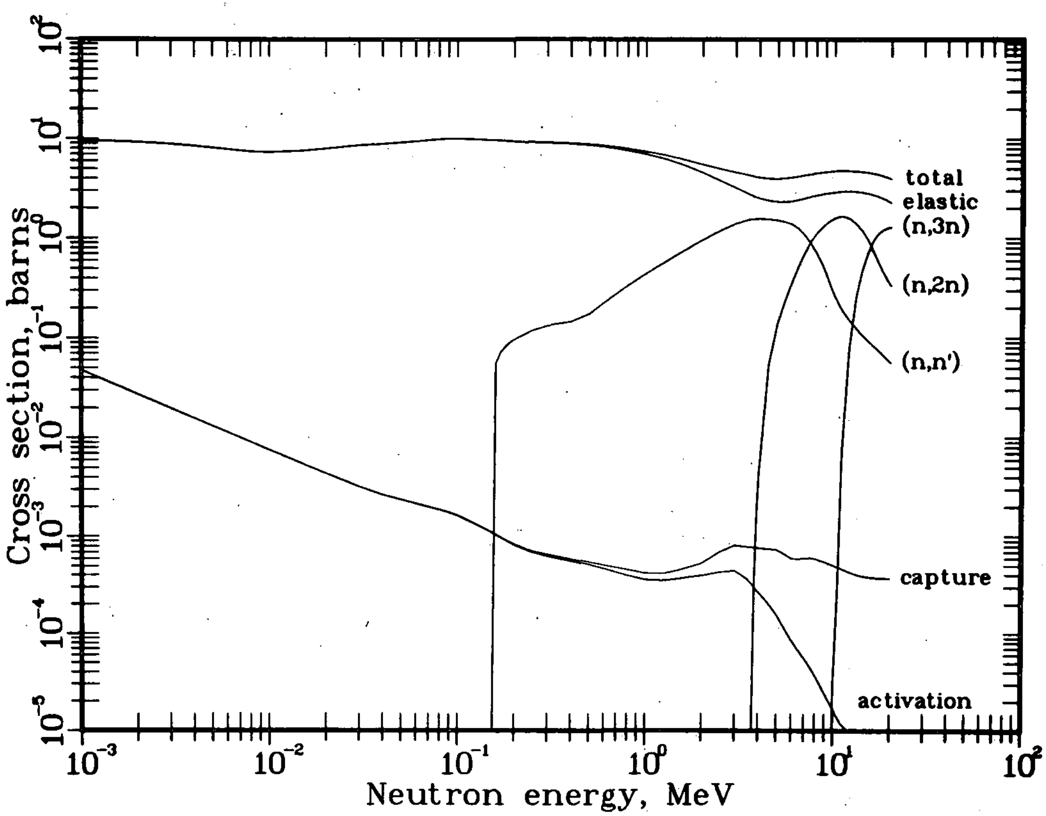

Fig. B-5. Neutron cross sections above 1 keV for the average prompt fission fragment from fast fission of ^{235}U.

---

[1]E. D. Arthur, Nucl. Sci. Eng. 76, 137 (1980).
[2]D. G. Foster, Jr., and E. D. Arthur, Los Alamos National Laboratory report LA-9168-MS (1982).

6. Neutron Cross Section Calculations for ^{235,238}U and ^{239,242}Pu (E. D. Arthur)

We calculated neutron cross sections for ^{235,238}U and ^{239,242}Pu for energies between 0.01 and 5 MeV with primary interest being determination of inelastic cross sections, particularly those for ^{239}Pu. Coupled-channel and Hauser-Feshbach statistical models were used. To calculate fission cross sections within the Hauser-Feshbach model, an improved fission channel was added to the COMNUC code. This replaced the simple Hill-Wheeler single-humped barrier with a more realistic double-humped barrier model approximated by three coupled or two uncoupled oscillators. Enhancements to transition state densities, calculated phenomenologically, were incorporated to account for nuclear symmetry effects[1] existing at the barriers. Corrections to the fission width based on the presence of Class II states in the second well were also included. With this model we could reproduce well measured (n,f) data, thereby introducing valuable constraints on other calculated quantities. Additionally, the resulting barrier parameters and enhancements were in general agreement to published values.[2,3]

Figure B-6 compares our calculated cross section for inelastic neutron scattering from the 0.057 MeV state in ^{239}Pu to that currently existing in the ENDF-B/V evaluation. The major cause of the large difference shown occurs because of direct-reaction effects included in our calculations for the ground-state rotational band members. Similar direct-reaction calculations are now underway for levels of higher-lying bands. When this is complete these results can be used to upgrade the present ENDF-B/V evaluation for ^{239}Pu.

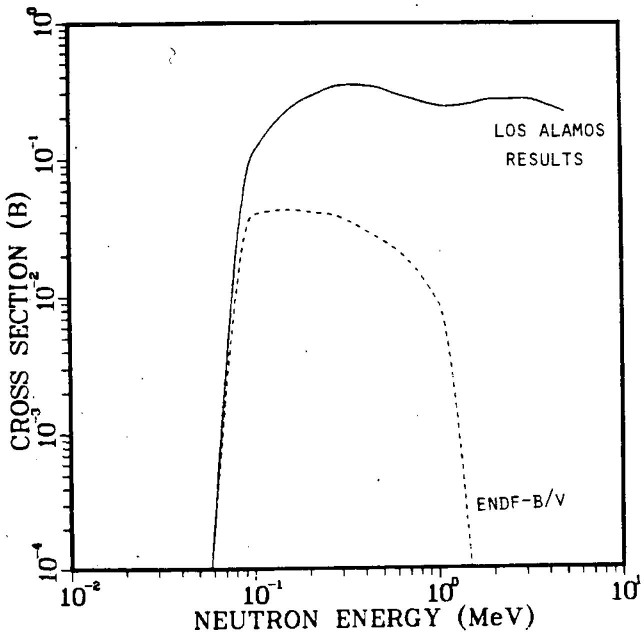

Fig. B-6. A comparison of the calculated ^{239}Pu(n,n') cross section to the .057 MeV state with ENDF/B-V

[1]A. Gavron et al., Phys. Rev. C13, 2374 (1976).

[2]B. B. Back et al., Phys. Rev. C10, 1948 (1974).

[3]A. S. Jensen, "Recent Developments in the Theory of Nuclear Level Density," Proc. Int. Conf. Neutron Physics and Nuclear Data, Harwell, p. 378 (1978).

7. Prompt Fission Neutron Spectrum Matrix for ^{235}U (D. G. Madland, J. R. Nix)

The prompt fission neutron spectrum for ^{235}U has been calculated as a function of both incident and outgoing neutron energy using a newly developed theory by Madland and Nix.[1] The matrix $N(E,E_n)$ was calculated for incident neutron energies (E_n) in the range 0-15 MeV and for secondary energies (E) ranging from 10^{-5} MeV to 50 MeV. The effects of and competition between first-chance, second-chance, and third-chance fission are included in the calculation. The results are illustrated in Fig. B-7 in the form $R(E,E_n) = N(E,E_n)/N(E,E_n = 0)$.

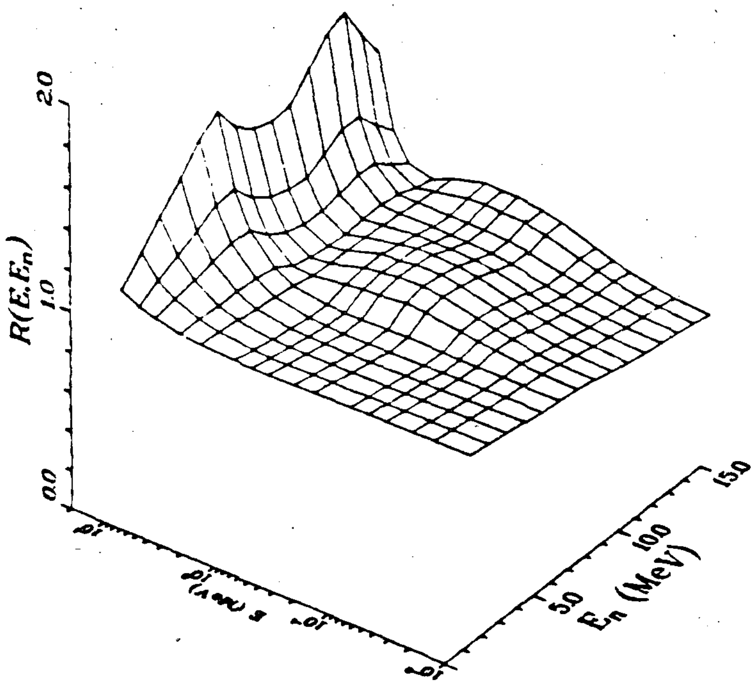

Fig. B-7. Ratio matrix of the prompt fission neutron spectrum for the neutron-induced fission of ^{235}U. The quantity plotted is $R(E,E_n) = N(E,E_n)/N(E,0)$, where $N(E,E_n)$ is the prompt neutron spectrum matrix, E is the laboratory energy of the emitted neutron, and E_n is the incident neutron energy.

[1] D. G. Madland and J. R. Nix, "New Calculation of Prompt Fission Neutron Spectra and Average Prompt Neutron Multiplicities," Los Alamos preprint LA-UR-81-2968, October 1981, and submitted for publication in Nuc. Sci. and Eng.

8. Determination of Average Resonance Parameters: The Ribon Exercise [M. S. Moore; M. Caner, Y. Gur (SOREQ, Israel); H. Derrien, E. Fort (CEN, Cadarache); F. Fröhner (KFK, Karlsruhe); H. Gruppelaar (ECN, Petten); G. Rohr, H. Weigmann (CBNM, Geel); J. S. Story (AEE Winfrith); P. Ribon, N. Tubbs (CEN and NEA, Saclay)]

Participants in the international comparison of methods for determining average resonance parameters met at the NEA Data Bank in Saclay, France, on October 15-16 to discuss the results of the second exercise supplied by Ribon. While the very large discrepancies revealed in the first exercise have been largely eliminated, the results still showed systematic discrepancies of perhaps 20% in the most critical parameter, the S-wave level density. The most reliable methods appear to be capable of giving about 5% accuracy in this parameter. At the meeting it was felt that certain of the methods tested were limited in usefulness because of user's subjectivity; i.e., a high degree of expertise and judgement was required in order to obtain reliable results. Other codes were thought to require an excessive amount of computer time.

Participation in the exercise showed up several deficiencies in the various codes. Perhaps the most serious is the neglect of a correction for resonance overlap in the input data. Our code has since been modified to take account of this effect, optimized to the point that it runs in a few seconds instead of minutes, and is provided with an iterative procedure that allows the user to obtain reasonable solutions for all the test problems provided, without any user interaction. The revised code has been submitted to the NEA Data Bank for distribution to interested users. We expect that the results and conclusions of the international intercomparison will be reported at the Specialists' Meeting on Fast Neutron Capture at Argonne National Laboratory in April, 1982.

9. Resonance Parameterization of (^{235}U + n) below 100 eV [M. S. Moore; G. de Saussure (ORNL)]

At the May 1981 meeting of the U. S. Cross Section Evaluation Working Group (CSEWG), it was recommended that in the region below 100 eV for (^{235}U+n), a multilevel representation should be used to replace the single-level Breit-Wigner description currently in the ENDF/B-V evaluation. There have been several new measurements, perhaps the most important being the polarized-neutron and polarized-sample fission cross-section measurements of Keyworth et al.[1] We also find evidence that certain of the scission point variables may be correlated with variations in the quantum number K, the projection of angular momentum on the nuclear symmetry axis. One of these scission-point variables is $\bar{\nu}$, the number of neutrons emitted per fission, which shows a small but significant variation with neutron energy (± 0.5%) in the low energy resonance region. We have carried out a correlation analysis of $\bar{\nu}(E)$, the fragment mass distribution variation, the fragment kinetic energy variation, and the J and K quantum numbers, and conclude that $\bar{\nu}$ depends on the fission channel properties rather than on the resonance spin for (^{235}U+n).

In order to include the calculation of such variations in the resonance description, a new parameterization is required. We began with the reduced R-matrix, fitting the spin-separated fission cross sections of Keyworth et al. from 1-100 eV. Included as a constraint in the fitting were the angular anisotropy measurements of Pattenden and Postma,[2] which had been reduced to give the variation of the K quantum number from resonance to resonance. We still need to include total and capture cross-section data in the fitting, and carry out the analysis in the region below 1 eV.

[1]G. A. Keyworth, C. E. Olsen, J. D. Moses, J. W. T. Dabbs, and N. W. Hill, in "Nuclear Cross Sections and Technology," NBS Spec. Pub. 425 (1975), Vol. II, p. 576; see also M. S. Moore, J. D. Moses, G. A. Keyworth, J. W. T. Dabbs, and N. W. Hill, Phys. Rev. C18, 1328.

[2]N. J. Pattenden and H. Postma, Nuc. Phys. A167, 225 (1971).

10. Time-Grouped Delayed Neutron Spectra [T. R. England, W. B. Wilson; R. E. Schenter, F. Mann (Hanford Engineering Development Laboratory)]

Using ENDF/B-V fission yields, emission probabilities (Pn) for 105 precursors[1] and recent (1981) spectra for 29 emitters,[2] the delayed neutron equilibrium spectra has been calculated in the conventional six time groups for eleven fissionable nuclides. The 29 emitters account for 70-87% of the total $\bar{\nu}_d$ (82% for ^{235}U); therefore, the spectral shapes are expected to be an improvement over current ENDF/B-V evaluated spectra. The calculations extend over the full energy range of 0-3 MeV. Fig. B-8 shows the group and total values for 10 keV divided by the calculated $\bar{\nu}_d$ for ^{235}U (= 0.0177) up to 1 MeV.

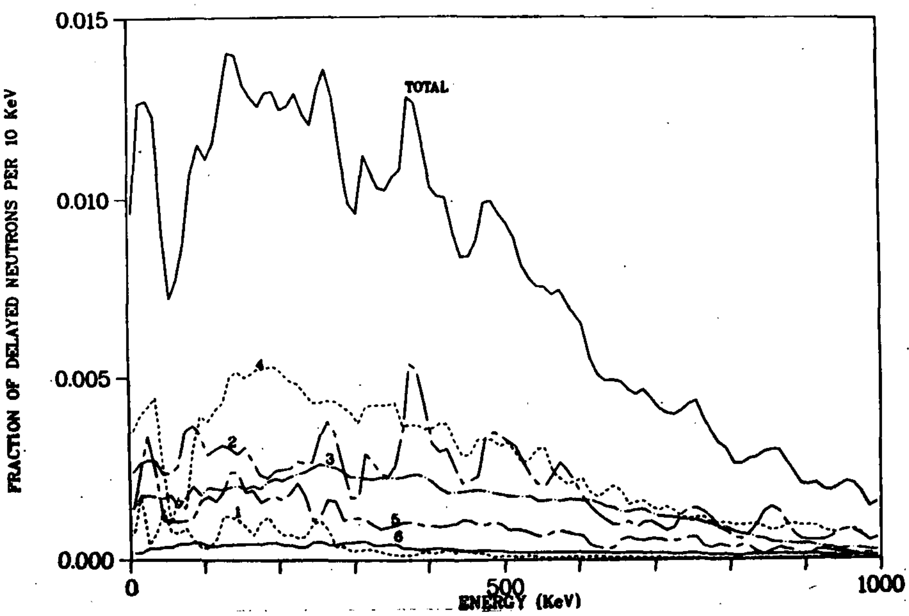

Fig. B-8. ^{235}U Delayed Neutron Spectra (Thermal Fission)

[1]T. R. England, R. E. Schenter, and F. Schmittroth, Proc. Int. Conf. on Nuclear Cross Sections for Technology, NBS Special Publication 594, p. 800 (1980).

[2]G. Rudstam, personal communication (November 1981).

UNIVERSITY OF LOWELL

A. NEUTRON CROSS SECTIONS FOR ^{232}TH AND ^{238}U

1. Recent Measurements (L.E. Beghian, G.H.R. Kegel, G.P. Couchell, J.J. Egan, A. Mittler, D.J. Pullen, W.A. Schier, C.A. Ciarcia, and J. Shao)

Neutron scattering cross sections for levels between 680-1500-keV excitation energy in Th-232 and U-238 have been measured by the (n,n') time-of-flight technique. Incident neutrons generated by the ^{7}Li(p,n)^{7}Be reaction had a typical energy spread of 8-10 keV. Measurements of 125°-differential scattering cross sections were performed over the incident neutron energy range 0.90-2.10 MeV, in approximately 50-keV increments. The sample shape and scattering geometry were chosen to optimize energy resolution for 0.2- to 0.5-MeV outgoing neutrons. Over this outgoing energy range, an overall energy resolution of less than 15 keV was maintained. The relative neutron fluence was determined by rotating the main detector used in the 125°- scattering measurements to 0° to view the primary neutron flux. Relative normalization was achieved by measuring the direct neutron flux from the lithium target by a second overhead monitor detector held fixed in both measurements. The energy response of the main detector was determined by comparing it with a U-235 fission chamber of known efficiency.

These measurements have produced inelastic cross sections in the region 0.2-0.5 MeV above threshold for many levels above the ground-state rotational band in Th-232 and U-238. Estimates of the EO transition strength can be determined by comparing the cross section values for (n,n'γ) and (n,n'). In Th-232 we have found EO branching ratios as high as 40%. Some discrepancies are still unresolved, in instances where the (n,n'γ) and (n,n') cross sections are different although the EO transition is forbidden on the basis of spin selection rules.

2. Data Analysis (G.H.R. Kegel, G.P. Couchell, C.A. Ciarcia and J. Shao)

The spectra obtained from our (n,n') studies often consist of many overlapping peaks due to the high density of levels near 1 MeV in excitation for both Th-232 and U-238. In formulating a new spectrum analysis procedure one usuallyrequires extensive preparatory work and testing before detailed prescriptions can be set down. The interactive code ARITH, written in our laboratory, assists in this initial task. It performs ordinary arithmetic operations (+, -, /, *) on two spectra, on a channel-by- channel basis. Spectra may also be integrated, convoluted with $\exp(t/\tau)$, smoothed, truncated, displayed, plotted, listed or expanded in orthogonal functions (Hermite or Laguerre) as requested by the user.

To unfold these spectra, we use a two step approach: first, we generate simulated response functions for each of the neutron groups involved; and secondly, we approximate the measured spectrum, in a least-squares fashion, by a superposition of response functions using our code TINA.

The response functions are based on three sets of data. We measure prompt profiles of the main detector, i.e., we determine the response of the main detector to monoenergetic neutrons from E_n = 200 keV to E_n = 1900 keV, using a thin ($\sim$1 keV) Li target. Measurements are done in 100- or 200-keV steps. Our code LAGUE parameterizes these measurements, interpolates between parameters, if necessary and constructs a prompt profile for any desired intermediate energy. The prompt profiles include the contributions of finite (detector and accelerator) time resolutions and that of the scintillator thickness.

Secondly, we use our code IMBUI[1] to generate simulated TOF spectra; these spectra include the contributions of target and scatterer kinematics and angular distributions, of geometric effects and of neutron attenuations. IMBUI also provides us with the quantity dT/dE_o (T = flight time, E_o = primary neutron energy) which is needed to transform the target thickness spectrum (an energy distribution) into a time spectrum. This target thickness spectrum is the third datum, and the least known one. Our knowledge of this spectrum derives from a detector placed at 0°, which monitors the prompt neutron resolution during the lithium target-making evaporation and also during the course of the scattering measurements. Code LAPA finally performs the convolution of the three time spectra providing the required response function. Figure A-1 shows two measured doublets and their decomposition using TINA.

3. Theoretical Investigations

a. Theoretical Calculations of Neutron Inelastic Scattering Cross Sections for Th-232 and U-238 (E. Sheldon and D.W.S. Chan)

Angle-integrated cross sections for inelastic scattering of fast neutrons from 0.8 to 2.5 MeV on Th-232 and U-238, proceeding to higher collective (quadrupole and octupole vibrational) states in the residual nuclei, have been computed in a "standard" and a "unified" approach; the resulting excitation functions have been compared with our experimental data. In all calculations, a consistent set of optical potential and deformation parameters, as derived by Haouat and Lagrange of the Bruyeres group, was used. The "standard" formalism employed an incoherent sum of compound-nucleus (CN) and coupled-channels direct-

---

[1] G.H.R. Kegel, Computer Physics Communications, 24 (1981).

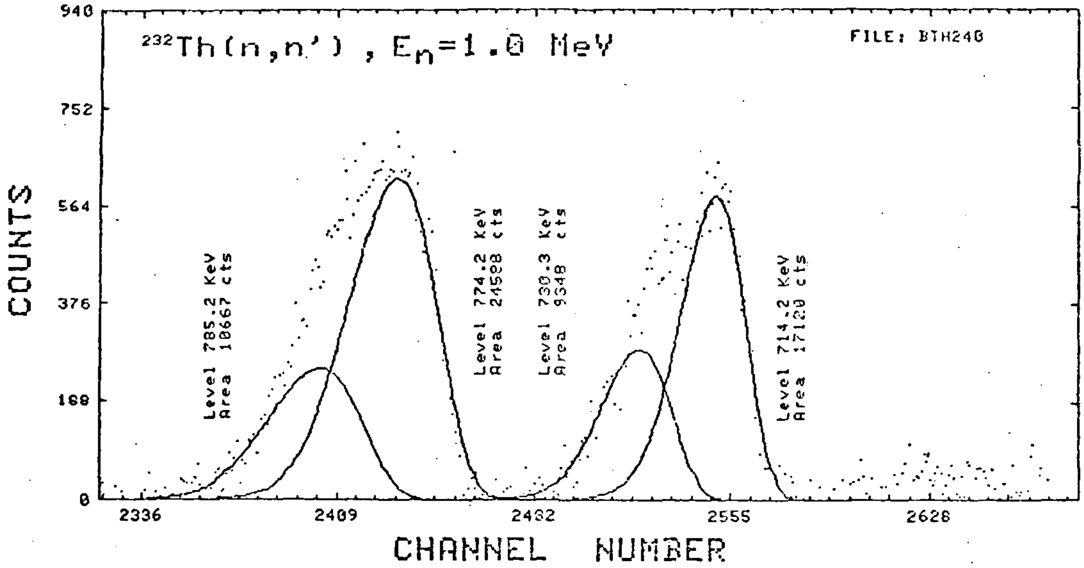

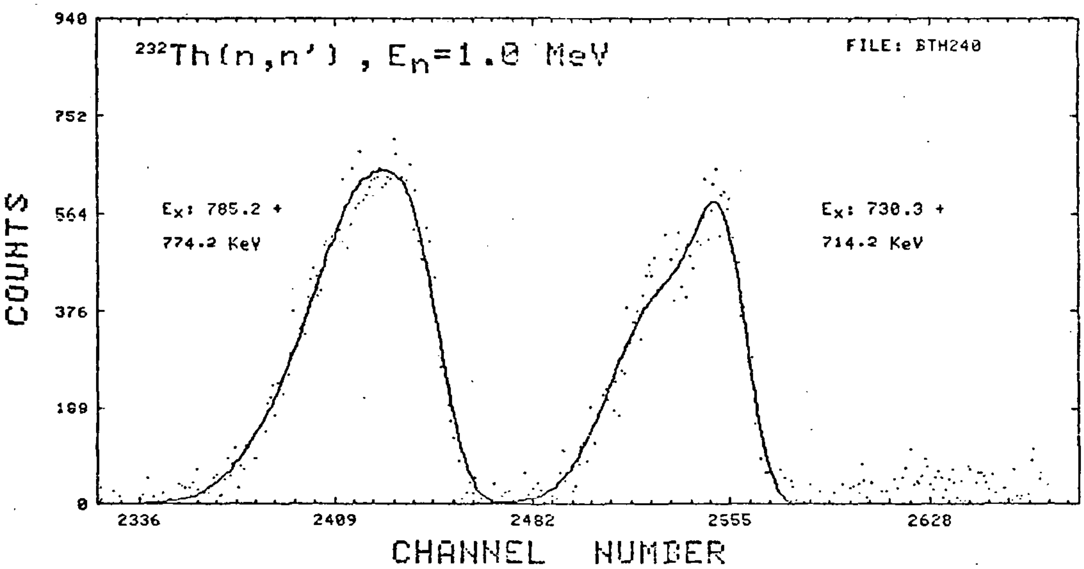

Figure A-1: Inelastic neutron TOF spectrum at E_n = 1.0 MeV after background subtraction and corresponding to the two doublets at E_x = 714.2+730.3 keV and 774.2+785.2 keV in Th-232. The measured data are represented by the dots. The curves show the decomposed and combined best fits to the measured neutron profiles calculated with the unfolding code TINA.

interaction (DI) cross sections, evaluated with the programs "CINDY" and "KARJUP" (Karlsruhe version of "JUPITOR") respectively. Provision was made for the effect of level-width fluctuations and for competing neutron exit channels. The results in general compared well with the measured values, but in several instances disagreed significantly with the ENDF/B-V evaluation.

Still better agreement ensues from the use of the "unified" formalism based upon energy-averaged second moments of transformed S-matrix elements in a statistical approach developed by Weidenmuller et al. and embodied within a new fluctuation program "NANCY" with coupled channels and competing channels to generate and manipulate the grand ensemble of S-matrix elements. With only the coupling strengths as adjustable parameters, this offers a promising, reliable means of analysis well suited to the interpretation of neutron scattering on deformed actinide nuclei.

Figure A-2 shows a sample of the results comparing the experimental excitation functions for Th-232(n,n') as deduced from (n,n'γ) measurements to the predictions of unified statistical S-matrix theory (solid curves, for various values of the relative coupling strength as indicated beside the respective curves) and of standard (CN + DI) theory (broken curves, with "best-fit" values of the coupling strength as indicated). These preliminary analyses, along with those for U-238(n,n') applied to the members of the $K = 0^-$ octupole vibrational bands in the residual actinide nuclei, suggest that the unified formalism is in principle able to provide a perceptibly better fit to experimental data than that attainable with the standard (CN + DI) approach. The detailed results of the unified analysis applied to the entire set of Th-232 and U-238 levels are being prepared for publication.

4. Future Studies

Additional measurements of inelastic neutron scattering from the high-lying states of Th-232 and U-238 are to be carried out. We will investigate the incident neutron energy range of 1.5 to 2.1 MeV, looking specifically at outgoing neutron energies in the interval 0.8 - 1.4 MeV. Data will be taken in incident energy increments of 100 keV and with an overall energy resolution of 15 keV using thin scattering samples. Our (n,n'γ) results for this excitation region suggest the possibility of a direct interaction contribution to the scattering process. If this indication is further borne out by the (n,n') measurements then additional measurements, namely angular distributions, will be necessary to obtain angle-integrated cross sections.

Measurements on the ground-state rotational band for incident energies in the region 400 keV to 1 MeV will be taken on Th-232 and U-238.

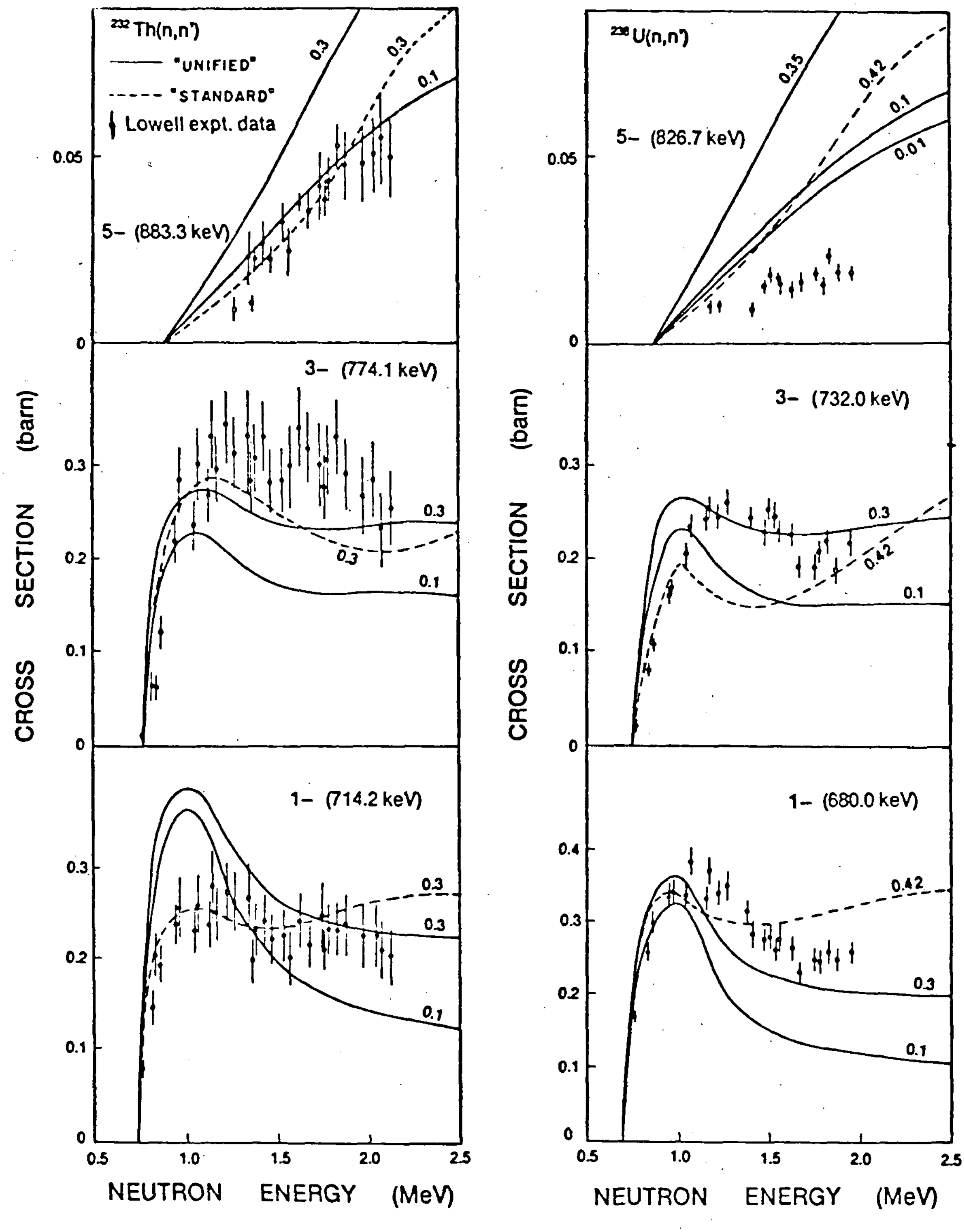

Figure A-2: Comparison of "Unified" and "Standard" calculated cross sections to experimental results for Th-232

Low energy measurements will be performed to determine elastic and inelastic cross sections for Th-232 and U-238 at incident neutron energies of less than about 200 keV (down to near 40 keV). Particular care will be used to reproducibly achieve fine increments in the incident energy, especially where resonance behavior is observed. Some elastic angular distributions will be measured. Inelastic studies at these low energies will probably be done using our ring geometry technique, which employs large but thin scatterers shaped so as to conform with isochronous time-of-flight surfaces. This is achieved by compensating for the energy dependence of the ^{7}Li(p,n) reaction with angle by using neutron flight paths of approximate length to achieve a constant time-of-flight.

A study of additional actinides will begin this year, namely U-233, U-235 and Pu-239. These samples must first be fabricated. Some technical developments aimed at improving our system's resolution are expected in the near future. We will also adapt our data analysis codes so that they will handle encased scatterers.

B. DELAYED-NEUTRON ENERGY SPECTRA OF FISSIONABLE ISOTOPES

(G.P. Couchell, W.A. Schier, J.J. Egan, G.H.R. Kegel, A. Mittler, D.J. Pullen, C.S. French, Q. Sharfuddin, A.W. Bielech, K.E. Patton, and N.M. Sampas)

We have undertaken a study of delayed-neutron spectra following neutron-induced fission, with special emphasis on the low-energy region (measurements extending to as low as 10 keV), where present data show large discrepancies. Delayed-neutron spectra will be determined by the neutron time-of-flight technique using beta-neutron correlations for timing purposes (the precursors of delayed-neutron emitters always decay by beta emission). Both plastic and lithium (enriched in ^{6}Li) glass scintillators will be used for neutron detection, giving us a high detection efficiency and good time resolution for both high- and low-energy neutrons. By employing a fast transfer system for transporting the fission fragments to the neutron spectrometer, we will also study the time dependence of the delayed-neutron spectrum. By the proper choice of counting-time intervals following fission, the contribution of each delayed neutron group can be enhanced in a particular spectrum. In this manner, it is possible to decompose each spectrum into its various components, assuming six groups of delayed neutrons and the known fractional yield, β_i, and decay constant, λ_i, of each group. It is expected that this study will represent the first direct measurement of the delayed-neutron spectra for the two shortest lived components (groups 5 and 6) with half-lives of 0.5 and 0.2 sec.

The following summarizes the progress during the first year of our project to study delayed neutron spectra following neutron-induced fission of U-235 and Pu-239. During this period we have completed the fabrication and assembly of the experimental system, and all major components have been tested and their design parameters optimized. Preliminary delayed-neutron measurements involving the complete system have begun.

Experimental Systems Development

Neutrons are generated by the $^{7}Li(p,n)^{7}Be$ reaction using the University of Lowell 5.5-MV Van de Graaff Accelerator. We employ an infinitely thick lithium target to produce neutrons spanning a broad energy band from 0 to 3.5 MeV. These studies will be supplemented by measurements performed with the University of Lowell 1-MW swimming pool reactor, where the thermal column will be used for thermal neutron irradiation.

Our initial studies concentrate on U-235 and Pu-239 because of their importance in proposed fast breeder reactor systems. Preliminary measurements are now under way using infinitely thick (to fission fragments) U-235 fission foils. Major components of the overall experimental arrangement are depicted in Fig. B-1. (This drawing is not to scale.)

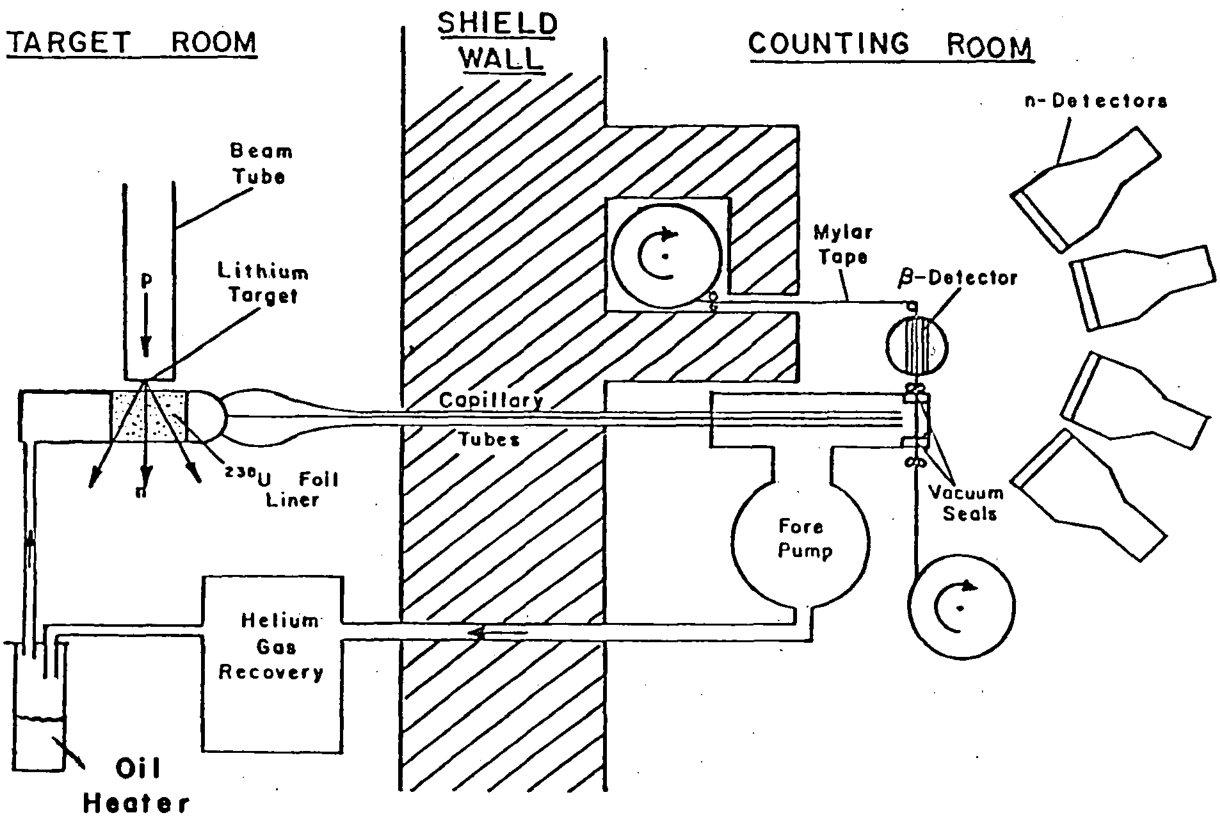

Figure B-1: Overall experimental arrangement

One of the main difficulties besetting delayed-neutron measurements is caused by the intense background of incident and prompt fission neutrons. Typically 10^{10}/s neutrons incident on the fission foil produce approximately 10^6/s prompt fission neutrons and only 10^4/s delayed neutrons. The problem of separating the delayed neutrons from this intense background has been solved by the following two techniques: 1) construction of a radiation cave in the wall of our accelerator target room which houses the fission chamber and target assembly and eliminates accelerator neutrons and prompt fission neutrons from the counting room, and 2) use of a helium-jet transfer system to rapidly transport the fission products away from the fission chamber to a low-radiation counting room where the neutron spectrometer is located. A second major background consideration is the high gamma-ray activity in the counting room associated with the fission fragments themselves. This activity is typically 100 times larger than that due to delayed neutrons. Our neutron time-of-flight spectrometer has been designed to eliminate all but about ¼-½% of the gamma-ray activity from the delayed-neutron portion of the spectrum.

As depicted in Fig. B-1, fission fragments are stopped by high-pressure helium gas filling the fission chamber. The fragments are quickly flushed out of the fission chamber by the helium jet stream and transferred into the counting room, where they are sprayed onto a moving tape. The tape will pass through a series of these beta detectors in the actual spectrometer. These detectors signal the emission of a beta particle, which is in turn correlated with the emission of a neutron or a gamma ray. The velocity of the emitted neutron or gamma is determined by measuring the time between the beta emission and the arrival of the neutron/gamma at one of four neutron detectors equally spaced from the transport tape. Each beta detector samples fragments of different average delay time following fission. The delay time and dwell time of the tape in passing through each beta detector is controlled by the detector geometry and tape speed. The fission fragment production rate exceeds 10^6 fission fragments per second. Approximately half of these fragments are stopped in the helium atmosphere of the fission chamber and the remainder are embedded in the walls.

A two-stage transfer process is required for these measurements. The first stage rapidly and efficiently transfers the fission fragments from the fission chamber to the counting room. The second stage provides sufficient delay to optimize activities in a particular range of halflives.

The helium jet process has been chosen for the first stage of the transfer system. The second stage is produced by the tape transport system.

To study the transfer efficiency of the helium jet process, a test cell was built to house a bare Cf-252 spontaneous fission source. After an attempt to optimize transfer efficiency by cooling the test cell we decided on an alternate technique of saturating the helium transfer gas with fore pump oil vapors and this has proven to give consistently high transfer efficiencies. In this approach, the fission fragment provides a nucleation site onto which the oil vapors condense. Massive clusters are formed which are little effected by the thermal motion of the helium and move rather with the macroscopic motion of the gas.

The transfer efficiency was measured with a continuous tape arrangement. Fission fragments could be deposited onto the tape either directly by placing the Cf-252 nearly in contact with the tape, or by transferring the fission fragments by means of the helium jet through 15 m of capillary tubing before depositing them onto the tape at the same location. The efficiency is then simply the ratio of the count rates above their respective backgrounds in a well-shielded detector which views a portion of the tape.

The transfer efficiency associated with this 15 m capillary tube is shown in Fig. B-2 as a function of helium pressure in the test cell. Falloff on the low pressure side is interpreted as being due to insufficient stopping in the gas, whereas falloff on the high pressure side probably arises from turbulence setting in near the entrance to the capillary tube.

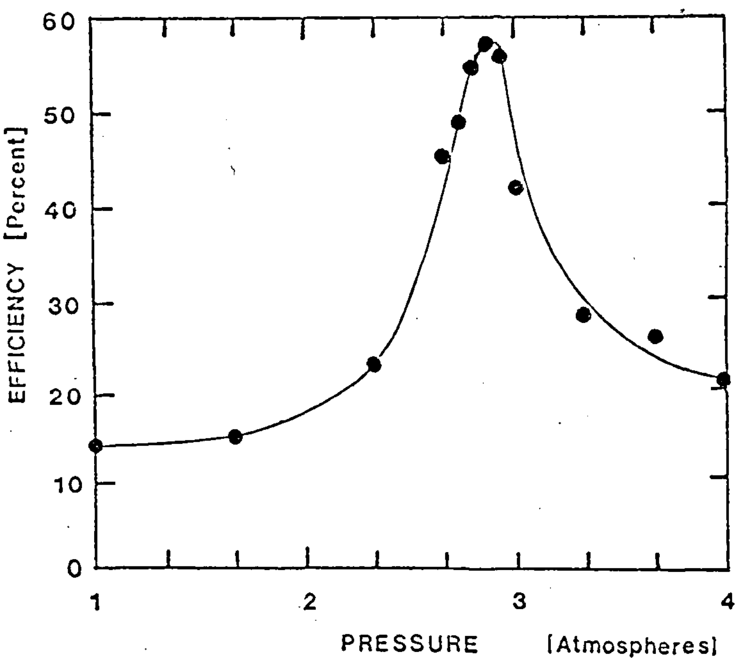

Figure B-2: Transfer efficiency of the helium jet utilizing a 15 meter capillary tube

To measure the helium jet transfer time of the fission fragments from the fission chamber to the counting room, the proton beam was mechanically chopped to produce a pulse of neutrons at the lithium target and thus a pulse of fission fragments from the U-235 foil in the fission chamber. The helium jet transferred these fragments to a rapidly moving tape in the counting room. The moving tape viewed with a beta detector through a narrow window gave good time resolution of the transferred activity. The beta counts were recorded as a function of time by operating the multichannel analyzer in the multiscaling mode and initiating the cycle with every other target current pulse.

The transferred activity is shown in Fig. B-3 as a function of time. This time dependence is primarily associated with the time required to flush the chamber of activity laden carrier gas and displace this volume with fresh helium. One observes that the activity builds up with the beam on and falls off with the beam removed. At least 60% of the activity is transferred in 0.7 seconds. Furthermore the system is sensitive to the two shortest halflives (0.23 and 0.61 seconds) in the six-group approach. This transfer time of 0.7 seconds can probably be reduced by a factor of two by extending the helium diffuser, thus halving the active volume of the chamber.

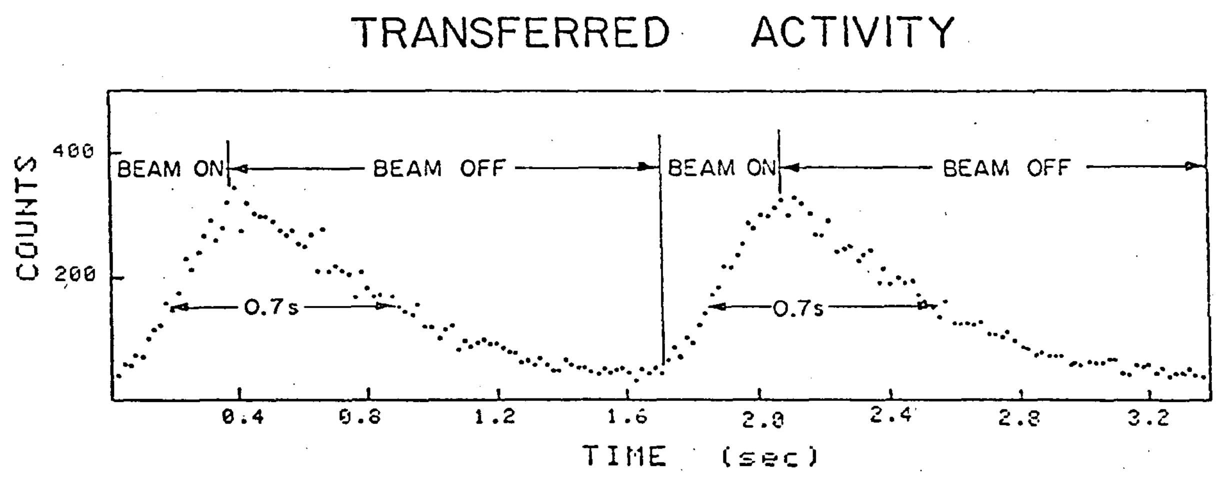

Figure B-3: Measured time dependence of the transferred activity from neutron induced fission

Fission fragments were also sprayed from the transfer capillary directly onto the thin scintillator of the beta detector to study beta count rates for neutron induced fission of U-235. The beta detector in this case subtends only a 2Π solid angle. At a fission production rate 20% of the maximum, the beta detector count rate was 50,000 cts/s. With a 4Π detection geometry and maximum fission fragment production, the beta count rate would be 500,000 cts/s.

Neutrons or gamma rays are detected by four 4½"-diamter by ¼"-thick scintillators mounted on RCA-8854 low-noise photomultiplier tubes. Delayed neutron spectra will be measured in two stages, by 1) using Pilot U plastic scintillators for the region $E_n \geq 40$ keV, and 2) using lithium-6-loaded glass scintillators for the energy range 10 keV $\leq E_n \leq$ 300 keV.

Future Schedule

We expect accelerator measurements on U-235, employing an incident neutron beam of broad energy range (E_n = 0-3.5 MeV), to be completed by the end of June 1982. Beginning July 1982, U-235 fission initiated by reactor-thermal-column neutrons will be studied. The next stage of the project involves making similar broad-energy-band and thermal-energy neutron studies with Pu-239 fission foils. If we observe a considerable difference in the corresponding spectra obtained in the fast-versus-thermal neutron measurements, we hope to undertake a more detailed study of the neutron energy dependence of delayed-neutron spectra in a future program.

The software for data reduction and spectral stripping is currently in use on our HP model-2100 computer. A computer program for decomposing each delayed-neutron spectrum into its various six-group components is now being written. All software for data analysis is expected to be completed by the end of July 1982.

THE UNIVERSITY OF MICHIGAN
Department of Nuclear Engineering

A. INTRODUCTION

Two series of measurements were completed over the past year that made use of our photoneutron laboratory. These concerned the capture cross sections of In-115 and Th-232, and are summarized in the sections that follow. No further experiments are active at the present time, but we are maintaining the photoneutron facilities, including the manganese bath, in a state that will permit reactivation in the future.

We have shifted our major emphasis to a newly-established laboratory for 14 MeV neutron measurements. Measurements are nearly complete on the fission cross sections of U-235 and Pu-239, and on the angular distribution of the fission fragments from these isotopes. Additionaly work is planned on some (n,p), (n,α), and (n,2n) reactions in structural materials of interest in fusion technology, fast neutron dosimetry, and neutron diagnostics. These efforts are being carried out in collaboration with Professor J. C. Robertson of The University of New Mexico.

B. CAPTURE CROSS SECTION MEASUREMENTS ON IN-115 (D. J. Grady, and G. F. Knoll)

The $In^{115}(n,\gamma)^{116m1}In$ cross section has been absolutely determined at neutron energies of 23, 265, and 964 keV. These energies are the median neutron energies of the photoneutron sources, Sb-Be, Na-D_2C, and Na-Be, utilized in this work. The measurements are independent of other cross section data except for corrections amounting to less than 10%.

Independent determinations of the reaction rate, detector efficiency, neutron source strength, scalar flux and target masses were performed. Reaction rates were determined by beta counting of the $^{116m1}In$ decay activity using a 4π gas flow proportional counter. The detector efficiency was measured using $4\pi\beta$-γ coincidence counting techniques. A correction factor for non-ideal detector behavior and the complex decay scheme effects was performed using the foil absorber method of efficiency extrapolation. Photoneutron source emission rates were determined by intercomparison with ^{252}Cf spontaneous fission neutron source in The University of Michigan Manganese Bath. The ^{252}Cf source was itself calibrated against NBS-II, the secondary national neutron standard. The normalized scalar flux was calculated from the neutron emission angular distribution results of the Monte Carlo computer program used to model neutron and gamma transport in the source. Target mass determinations were made with a microbalance.

Four major correction factors were determined. Neutron in-scatter from the experimental package to the target foil was calculated using a point approximation and limited scattering reaction anisotropy. Neutron backscatter from the traget foil holder was determined using a Monte Carlo calculation of the average path length through the foil for neutrons scattered in the backing. A correction for the activity induced in the foils due to room-return neutrons was derived from a plot of the saturated ^{116m}In activity per target atom versus the spacing-dependent scalar flux. The y-intercept is the activity associated with the spacing-independent room-return. Finally, the measured capture cross sections were normalized to the photoneutron source median energies using the calculated neutron energy spectra and $^{115}In(n,\gamma)^{116m}In$ cross-section shape data.

The absolute cross sections obtained for the $^{115}In(n,\gamma)^{116m1}In$ reaction were 588$\pm$12, 196$\pm$4, and 203$\pm$3 millibarns at 23, 265, and 964 keV, respectively.

C. MEASUREMENT OF THE CAPTURE CROSS SECTION IN THORIUM AT 23 keV (G. T. Baldwin, and G. F. Knoll)

Measurement has been made of the thorium radiative capture cross section using Sb-Be photoneutrons and an absolute activation method. The average of two determinations gave a value of 604 mb at 23 keV neutron energy with a 4% estimated error from all sources ($\pm 1\sigma$).

In each experiment, a cylindrical shell target of natural thorium metal was irradiated for approximately two weeks by a centrally-positioned Sb-Be source. The accumulated 27-day half-life ^{233}Pa, activated by neutron capture in thorium, was recovered by solvent extraction with diisobutylcarbinol after first dissolving the target in hydrochloric acid.

Ninety percent recovery of protactinium was obtained, as measured by isotopic tracing with ^{232}Pa. The 1.3-day half-life ^{232}Pa had to be produced immediately before each use. A thin thorium foil was irradiated with 11 MeV protons using a tandem van de Graaff accelerator. The ^{232}Pa was the recovered by chemical separation.

The ^{233}Pa activity was measured by counting the 312-keV decay gamma with a Ge(Li) detector. Detector efficiency was determined by indirect calibration against a ^{237}Np deposit assayed by alpha counting at the National Bureau of Standards.

The Sb-Be source strength was measured by the manganese bath method, using a ^{252}Cf source for calibration, traceable to the NBS II neutron standard. Flux per unit source strength was determined by Monte Carlo modelling of the source/target irradiation geometry.

D. ABSOLUTE MEASUREMENTS OF FISSION CROSS SECTIONS AT 14 MeV NEUTRON ENERGY (M. Mahdavi and G. F. Knoll)

Since our last progress report, we have carried out a significant part of the measurement program aimed at determining the fission cross sections of U-235 and Pu-239 at 14 MeV. At the completion of these experiments, we plan to extend the techniques to U-233, Np-237, and U-238. In all cases but the last, the target foils are the same as those used in our previous photoneutron cross sections measurements.

As well as using the same target foils, these fission measurements at 14 MeV employ many other techniques developed in our lower energy measurements. These include:

a) Registration of fission fragments through a limited solid angle defined by an aperture in the forward direction.

b) Manual counting of fission fragments from tracks etched in polyester track-etch film.

c) Use of supplementary fission fragment angular distribution measurement to relate forward fragment yield to total fission rate.

d) Careful treatment of room-return neutrons, including use of a low-albedo laboratory and multiple measurements with variable source-target spacing.

A major departure from our previous work is in the determination of the neutron flux. To replace the manganese bath calibration of our photoneutron sources, we rely on a combination of flux monitoring techniques for the 14 MeV measurements. To date, these have concentrated on the use of activation foils of aluminum and iron, and assuming values for these capture cross sections at 14 MeV. This relative measurement technique will be refined in the future by developing more accurate techniques including proton recoil flux determination and/or associated particle techniques.

Our work to date has focussed in four major areas:

1) Measurement of the fission rate and monitor foil activation

2) Absolute efficiency determination of the 4π beta detector and its K correction

3) Fission fragment angular distribution measurements

4) Measurement of the neutron energy

1. Fission Rate and Activation Foils

A positioning jig was assembled to provide a highly precise spacing between the target foil, activation foils, and detector films. Care was exercised in the design of these components to minimize mass and the associated neutron scattering. Means are provided to routinely vary the neutron target-target foil spacing so that a series of measurements can be carried out to determine the contribution of room-return neutrons as in our earlier photoneutron measurements.

As the primary flux monitor, square activation foils of 99.95% pure iron were utilized. Thicknesses of 2 and 3.6 mils were used, with masses accurately determined by weighing. As a secondary standard, aluminum foils of 1 inch diameter and 99.991% purity were also employed. Thicknesses of 5 and 10 mils were chosen, with masses also determined by microbalance weighing. Masses of the fission foils were determined several years ago as part of our photoneutron cross section series. Three independent methods were used in these determinations, including microbalance weighing, absolute alpha counting, and fission ratio measurements made at the National Bureau of Standards.

Neutrons were produced by deuterium bombardment of tritiated targets produced by Safety Light Corporation. These targets show a noticeable depletion of tritium over the course of a typical irradiation (several hours) and so it is necessary to monitor the neutron yield as a function of time.

In order to relate the absolute neutron flux at the fission foils to that at the position of the monitor foils, several computer codes were developed to determine the average scalar neutron flux per source strength for our specific irradiation geometry.

The computer codes were also used in the design of the experiment. Specifically, choices were made of the various spacing and geometric sizes to keep the variation of neutron flux with geometric uncertainties to a minimum. Some of these uncertainties include the physical spacing between various components (measured by gauge block and micrometer techniques), and the possible wandering of the deuteron beam spot during the course of the measurement. Because of the limited solid angle counting of the fission fragments, uncertainties in the fragment angular distribution will also directly affect the detector efficiency calculation.

The neutron yield was inferred by measuring the activity induced in foils of pure aluminum or iron. Because of the short half life of the induced activities, it is necessary to take into account any time variation of the neutron yield that takes place over the irradiation period. Because of the noticeable depletion of our tritium targets, we observe a significant drop off of the neutron yield over the course of a typical irradiation period (1 to 4 hours). As a result we have developed a monitoring system that consists of a long counter kept in a fixed location in the laboratory whose output is recorded over the entire length of the irradiation by using a multichannel analyzer in multi-scale mode. These data then are used directly in a simple computer code which relates the total induced activity in the activation foil at the end of the measurement to the integrated neutron yield.

2. Beta Detector Efficiency and K Correction

One element of the neutron flux determination is the absolute counting of the activity induced in the iron and aluminum foils. The techniques that were used are similar to those employed previously in the series of measurements on the activation cross section of indium using our photoneutron sources. The same detector is used here, and the approach involves measurement of the K correction to account for the complex decay schemes of aluminum and iron. The beta detector efficiency was varied through the use of a series of aluminum absorbers covering the activated foils. Results obtained for the iron foils compare quite favorable with results of Robertson and Ryves[(1)] using an independent efficiency measurement method.

---

1. J. C. Robertson, Journal of Nuclear Energy, 27 (1972) 139

3. Angular Distribution of Fission Fragments

We are now employing an extension of experimental techniques described earlier[2] as part of our photoneutron measurements. In this case, however, we are able to make these measurements directly in our own laboratory, rather than using accelerator facilities at Argonne National Laboratory as in our previous work. We are using the same support structures that position the track etch film along an arc with the fission foil at its center. These measurements have been detailed in previous progress reports and do not differ significantly from our earlier efforts. We have already carried out irradiations for U-235 and Pu-239, and are in the process of counting the etched films and analyzing the resulting data.

---

2. S. T. Hsue, G. F. Knoll and J. Meadows, "Angular Dist. of Fission Fragments from Fast Fission of Uranium - 235", Nuclear Sci. and Eng. 66, 24-28 (1978).

NATIONAL BUREAU OF STANDARDS

A. NEUTRON DATA MEASUREMENTS AND DETECTORS

1. Absolute Measurements of the ^{235}U Fission Cross Section From ∿ 300 to 3000 keV Neutron Energy (A. Carlson, J. Behrens)

This experiment is being performed at the NBS Neutron Time-of-Flight facility. The neutron flux is being measured with a large plastic scintillator ("Black Detector") located 200 m from the neutron target. Monte Carlo calculations of the efficiency of this detector were verified experimentally[1] for neutron energies below 900 keV using a T(p,n)^{3}He associated particle spectrometer. On the same beam line at 68 m from the target a well-characterized[2] thin film ^{235}U fission chamber is used to measure the reaction rate. Time dependent backgrounds for both detectors have been reduced to negligible levels with shielding and the use of special data acquisition methods. Two parameter (time-of-flight and pulse height) data is being obtained for both detectors and stored on a million word disk for convenient analysis.

Final data for this experiment is now being taken and the data is being analyzed for preliminary cross section values. After this measurement has been completed, the black detector efficiency at 2.6 MeV will be determined with the D(d,n)^{3}He associated particle spectrometer being assembled at the NBS Van de Graaff facility. Comparison with the calculated efficiency will permit an evaluation of the uncertainty in the neutron flux at the higher neutron energies employed in the fission cross section measurements.

2. Absolute ^{235}U(n,f) Cross Section at 2.6 MeV (K. C. Duvall, M. Dias, O. Wasson)

A measurement of the ^{235}U(n,f) cross section at 2.6 MeV using the time-correlated associated particle technique with the ^{2}H(d,n)^{3}He reaction is in progress at the 3 MV Van de Graaff laboratory. The same ^{235}U fission deposits used in the 14 MeV measurement are utilized. This measurement will reduce the uncertainty in this cross section in the 2-3 MeV interval where there is a 10% scatter in various results and for which recent measurements[3,4] differed by approximately 5%.

---

1 M. M. Meier, *Proceedings of a Symposium on Neutron Standards and Applications,* National Bureau of Standards Special Publication 493, 221 (1977).

2 O. A. Wasson and M. M. Meier, Nucl. Instrum. Methods 190, 571 (1981).

3 Cancé, Grenier, Gimat, and Parisot, Bruyeres-le-Chatel Progress Report, NEANDC(E) 211 (March 1981).

4 R. Arlt *et al.* Technical University of Dresden Report 05-43-80 (To be published in Kernenergie).

3. Summary of Previous $^{235}U(n,f)$ Measurements (O. A. Wasson)

The $^{235}U(n,f)$ cross section measurements performed on the NBS linac using the H_2 gas flux monitor and the absolute measurements performed at the NBS 3 MV Van de Graaff facility using the Black Neutron Detector and the time-correlated associated particle technique have been reassessed and submitted for publication.[5,6] The results have also been sent to the National Nuclear Data Center. The cross section at 14.1 MeV agrees within 0.2% with the ENDF/B-V evaluation while the results in the 200-1200 keV region are approximately 2% less than the evaluation.

4. ^{237}Np:^{235}U and ^{232}Th:^{235}U Fission Cross Section Ratio Measurements in the MeV Region (J. W. Behrens, J. C. Browne,* J. C. Walden,** E. Ables**)

Final results are published[7] or will soon be published[8] on the fission cross-section ratios for ^{237}Np and ^{232}Th relative to ^{235}U in the neutron energy ranges from 0.02 to 30 MeV and from 0.7 to 30 MeV, respectively. These measurements were conducted at the Lawrence Livermore National Laboratory 100 MeV electron linac. Our measurements provide fission cross section ratios for these two isotopes that fill gaps in the MeV range where past experimental data were lacking.

5. Inferred MeV Fission Cross Sections for Unmeasured Actinides (J. W. Behrens)

During the past decade considerable effort has been spent in extending the measurements of fission cross sections of the actinides in the MeV range. Measured data now exist for over 24 nuclides. This set is now sufficiently large to justify an attempt to infer the fission cross section for unmeasured nuclei from systematics of neighboring nuclei.

There is a good theoretical basis for the usefulness of such inferences at the higher energies. Any calculation of the fission cross section must begin with an optical model prediction of the compound nucleus formation cross section. This cross section is known to very slowly with neutron energy and atomic mass from a number of total cross section measurements. The fission cross section is obtained from a calculation of the competition of decay by fission with the other modes of decay. For the neutron energies above a few

---

* Los Alamos National Laboratory, Los Alamos, NM.

** Lawrence Livermore National Laboratory, Livermore, CA.

5 Wasson, Carlson, and Duvall, Nucl. Sci. Eng. 80, 282 (1982).

6 Wasson, Meier, and Duvall, Nucl. Sci. Eng., In press (1982).

7 Behrens, Browne, and Walden, Nucl. Sci. Eng. 80, 393 (1982).

8 Behrens, Browne, and Ables, to be published in Nucl. Sci. Eng. (1982).

MeV the excitation is well above all fission barriers associated with lower angular momenta. Therefore, the details of the barrier shape are expected to have a reduced effect on fission probability and the fission probability should be a slow function of the neutron energy. Also, at high energies a wide range of angular momenta are available so that the fission channel width and width for all other decay channels should not be changing rapidly. It is, therefore, reasonable to believe that unmeasured fission cross sections can be inferred from appropriate, well-measured nuclei with an accuracy perhaps better than 10%.

The method is illustrated for the case of ^{238}Pu whose fission cross section can be inferred from two avenues: the first from the neighboring isotopes of plutonium, ^{244}Pu, ^{242}Pu, and ^{240}Pu and the second from the isotopes ^{236}U and ^{237}Np with all measured data compared in terms of excitation energy rather than neutron energy. Predictions of the cross section from these two approaches are shown as a function of neutron energy in columns 2 and 3 of Table A-1. The average of the two predictions are shown in the 4th column. The 5th and 6th column show the measurement and the % difference between prediction and measurement. In this case, prediction appears to have about the same accuracy as the measurement. The accuracy of the inferred data should improve with higher neutron energy. The accuracy probably can be improved with some procedural refinements. It appears that inferred cross sections can be made on the following isotopes ^{234}Th, ^{233}Pa, ^{230,231,232,237,239,240}U, ^{235,239}Np, ^{236,237,238,243}Pu, ^{239,242,245}Am and ^{240,242}Cm.

6. Progress in the Investigation of Structure in (n,α) Cross Sections of Li Glass in the eV Energy Region (A. Carlson)

New measurements of the ratio of the (n,α) cross sections of $^{10}BF_3$ and Li glass will begin this year. For these measurements the relative gamma ray background in the Li glass detector will be reduced significantly compared with previous[9] measurements by using highly enriched (in ^{6}Li) lithium glass. To reduce the uncertainties in these data due to the large self-shielding corrections, the ^{6}Li content of the new scintillator was measured. The ^{6}Li determination was made from transmission measurements of the glass at the thermal column of the NBS reactor. Measurements were also made of the ^{6}Li content of the glass used in a previous[9] experiment; however, for that experiment the self-shielding corrections were small.

[9] J. B. Czirr and A. D. Carlson, Proc. of the Int. Conf. on Nuclear Cross Sections for Technology, U. of Tennessee, National Bureau of Standards Special Publication 594, 84 (1980).

Table A-1. The $^{238}Pu(n,f)$ Cross Section

E_n (MeV)	Constant Z	Constant N	Avg.	Measurement	Difference $\left(\frac{\text{Avg. Meas.}}{\text{Meas.}} \times 100\%\right)$
1.4	1.90	2.30	2.10	2.10*	0.0
2.4	2.32	2.41	2.37	2.30*	+ 3.0
3.4	2.15	2.15	2.15	2.15*	0.0
4.4	1.70	2.03	1.87	2.10*	-10.9
5.4	1.80	1.98	1.89	2.05*	- 7.8
6.4	2.12	2.12	2.12	2.35*	- 9.8
7.4	2.58	2.66	2.62	2.75*	- 4.7
8.4	2.58	2.73	2.66	2.80*	- 5.0
9.4	2.63	2.68	2.66	2.75*	- 3.3
10.4	2.58	2.40	2.49		
11.4	2.46	2.46	2.46		
12.4	2.50	2.43	2.46		
13.4	2.54	2.50	2.52		
14.4	2.68	2.62	2.65	2.67†	- 0.7
15.4	2.74	2.47	2.60		
16.4	2.56	2.52	2.54		
17.4	2.49	2.29	2.39		
18.4	2.53	2.34	2.44		
19.4	2.63	2.33	2.48		

* Knitter, Budtz-Jørgensen, and Smith, CBNM Report CBNM/VG/35/81 (1981).

† Barton & Koontz, Phys. Rev. 162, 1070 (1967).

7. International Intercomparison Measurements at 14 MeV (K. C. Duvall)

The NBS has participated in two recent international intercomparisons of fast neutron fluence determinations at 14 MeV. The International Bureau of Weights and Measures (BIPM) sponsored intercomparison utilized the $^{115}In(n,n')^{115}In^m$ activation as a transfer device. Natural indium samples were irradiated in the NBS 14 MeV standard neutron field using the $T(d,n)\alpha$ source reaction and the associated particle method for accurate determination of the neutron fluence. The induced sample activity was measured here with a high resolution GeLi detector. The results of the measurements were submitted with an overall accuracy of ±1.5% which will be compared with results from other laboratories. Results from the BIPM intercomparison measurement will be used to determine an absolute cross section value for the $^{115}In(n,n')^{115}In^m$ activation. The NBS participation in the National Physical Laboratory (NPL) sponsored fast neutron dosimetry intercomparison involved the irradiation of a Zr/Nb sample in the NBS 14 MeV neutron field. The activated sample was sent to NPL for the activity measurement and analysis. The neutron fluence received by the sample was reported to NPL with an accuracy of ±1.5%.

8. Multichannel Plate Neutron Detector (R. A. Schrack, R. G. Johnson)

The multichannel plate neutron detector has been utilized to provide radiographic images of selected isotopes. By gating the detector to be sensitive only to neutrons having an energy corresponding to an absorption line for a particular isotope, images have been generated of a selected isotope in a complex matrix of other isotopes. Neutrons in the energy region 1 to 40 eV were produced by the NBS Linac using a water-moderated source. The 5 meter flight path was utilized. Figure A-1 shows the electronics utilized. The computer reconstructed images obtained are shown in Fig. A-2. Figure A-2a shows the radiograph produced from a pattern made of gold foil about 0.15 mm thick. The image was produced by recording events only for those neutrons having an energy of the gold resonance at 4.91 eV. The resolution of the system is about 0.51 mm. The image shown is 2.5 cm in diameter, each letter is 6 mm wide. This figure represents 259,331 detected neutrons. Fig. A-2b shows variations in the thickness of a silver braze between sheets of stainless steel and brass which are each 0.64 cm thick. The average thickness of the silver is 0.02 mm. The 5.19 eV resonance in ^{109}Ag was used to produce this image. Instrumentation is now being developed to allow the simultaneous imaging of several isotopes.

9. Development of an Absolute Neutron Flux Detector for the 1-20 MeV Energy Region (M. S. Dias†)

An absolute neutron flux detector has been built at the NBS to be used in the energy range between 1 and 20 MeV. The detector consists of two thin NE110 plastic scintillators coupled to phototubes. The escape of protons, which is the main correction, is eliminated experimentally by means of the dual configuration of the detector. This is done by adding the single pulses produced by protons that lose all its energy in the first scintillator with the sum pulses produced by protons that lose part of their energy in each scintillator. The detector has been optimized in order to have a good light collection uniformity. The absolute efficiency of the detector has been checked at 14.1 MeV, using the 3 MV Positive Ion Van de Graaff of the NBS as the source of neutrons. The results are presently being compared with theoretical calculations based on a Monte Carlo code. The next steps will be (a) the check of the absolute efficiency at 2.6 MeV and (b) the use of the detector as a flux monitor for a precision measurement of the $^{235}U(n,f)$ cross section at 2.6 MeV.

† Ph.D. student from the Instituto de Pesquisas Energéticas e Nucleares - São Paulo - Brazil

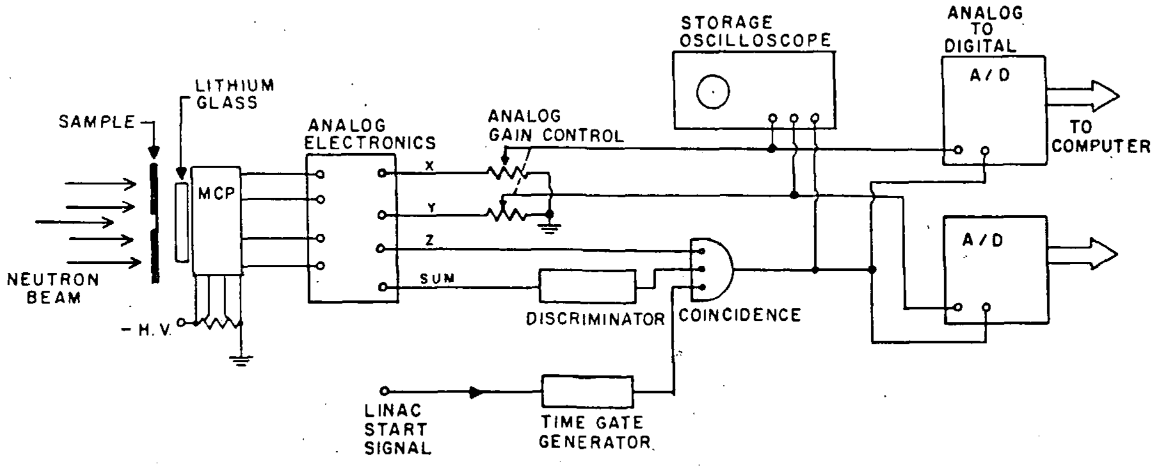

Fig. A-1. Electronic circuit of data collection system for Resonance Neutron Radiography using the microchannel plate position sensitive neutron detector.

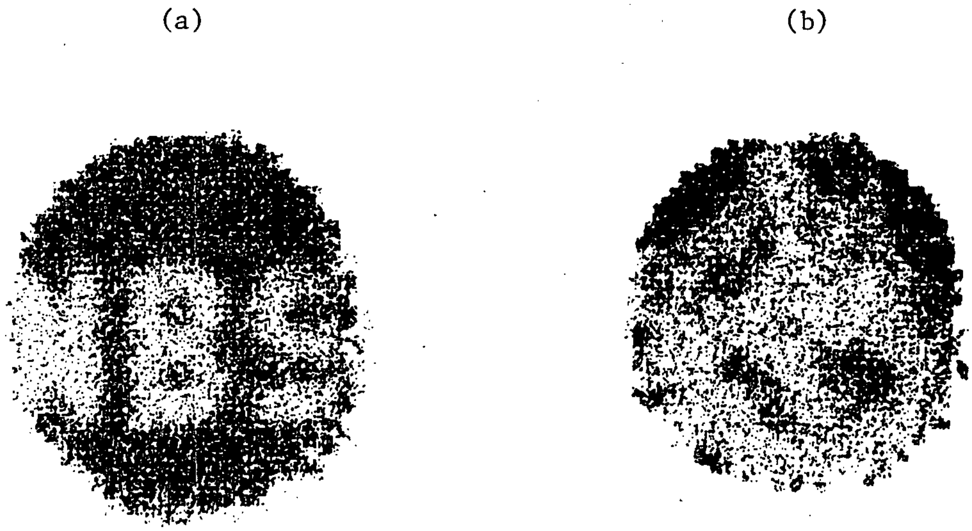

Fig. A-2. (a) Radiographic image of gold object made by 4.91 eV neutrons.

(b) Radiographic image of silver distribution made by 5.21 eV neutrons.

B. NEUTRON PHYSICS

1. Atomic Excitation Induced by Neutrons (C. D. Bowman and R. G. Johnson)

No generally useful method presently exists for calculating the probability of atomic excitation induced by neutron-nucleus scattering. We have calculated the probability that an atom will remain in its ground state when the nucleus is struck by a neutron and subtracted this from unity to get the combined probability of excitation or ionization. The quantity calculated is the matrix element

$$M_{11} = \prod_j \langle\psi_1 \,|\exp[-i(m_e/M)(\vec{Q}.\vec{r}_j)]\,|\psi_1\rangle$$

where ψ_1 is the ground state wave function of the atom, m_e is the electron mass, M the nuclear mass; $\vec{Q}$ the momentum transfer, $\vec{r}_j$ the vector from the nucleus to the jth electron and M_{11} the matrix element for remaining in the ground state. The probability for any type of excitation P_e is therefore

$$P_e = 1 - (M_{11})^2$$

In order to calculate the matrix element we use approximate electron wave functions having the shape of Gaussians with the same average radial electron position and the same standard deviation as the hydrogenic wave function. We use an effective charge Z^* to account for screening. For a particular electron we find

$$M_{11} = 1-[(m_e/M)(Qa_o/Z^*)]^2[n^2(n^2+2)-\ell^2(\ell+1)^2].$$
$$.\ \{[3n^2-\ell(\ell+1)]^2/[n^2(n^2+2)-\ell^2(\ell+1)^2]+5\}$$

where a_o is the Bohr radius and n and ℓ are the principle and orbital quantum numbers, respectively. We believe that the calculational accuracy increases with increasing n and ℓ. A few results from the calculation are given in Table B-1 for 1 keV incident neutrons and a scattering angle of 90°. Generally the probability increases linearly with the neutron energy. Studies are underway to determine whether this additional small channel for energy loss significantly influences neutron moderation in practical systems. Experiments are being planned to check the accuracy of these predictions.

Table B-1. Excitation Probability for 1 keV Neutrons (90°).

Atom	Electron	Neutron Z^*	Excitation Probability	Energy for Electron Removal (eV)
H	1S	1	.074	13.6
N	2P	1.5	0.014	14.5
Na	3S	1	0.029	5.1
Ar	3P	1.5	0.023	15.8
K	4S	1	0.030	4.3

2. Molecular Excitations Induced by Neutrons (R. G. Johnson and C. D. Bowman)

The electronic excitation of molecules can occur exactly as in the case of atoms as discussed above, i.e., excitation due to the recoil of the center-of-mass. However, the scattering of the neutron by one of the nuclei of the molecule can also cause excitation of internal molecular motions. The excitation of these vibrations and rotations contribute to the inelastic cross section. In addition, because of weak coupling between the motions of the nuclei and the electrons of the molecule another mechanism for electronic excitation exists.

Measurements of inelastic scattering of neutrons in the electron volt region is continuing. Work has concentrated on improving the signal to background for the resonant-capture detector and improving the overall count rate. The signal to background ratio has been improved by a factor of ~ 3 with a somewhat better energy resolution.

Work has also been directed at obtaining a better understanding of inelastic neutron scattering in the eV range. For the excitations of vibrations and rotations the results of this work will appear in a forthcoming publication.[10] In collaboration with S. W. Lovesey of the Rutherford and Appleton Laboratories, a calculation of electronic excitations in homonuclear diatomic molecules through the coupling of the nuclear motions with electronic states has been completed. The calculation is performed by including the leading non adiabatic corrections in the Schrödinger equation for the molecule. The total probability for an electronic excitation in the H_2 molecule calculated by this formalism is, for example, 0.3% at a momentum transfer of ~ 100 Å^{-1}.

[10] R. G. Johnson and C. D. Bowman, Inelastic Scattering Measurements of eV Neutrons, Phys. Rev. Letters, submitted for publication.

Continued experimental and theoretical developments for this interesting problem are planned. For example, coincidence measurements will probably be required to observe the small cross sections involving electronic excitations by neutron scattering.

C. DATA COMPILATION

1. Photon and Charged Particle Data Center

The X-Ray and Ionizing Radiation Data Center and the Photonuclear Data Center have been combined into a Photon and Charged Particle Data Center. Current work deals with charged particle stopping powers (M. J. Berger and S. M. Seltzer), photon attenuation and atomic cross section data (J. H. Hubbell and H. Gerstenberg) and photonuclear cross section data (E. G. Fuller and H. Gerstenberg). Members of the new center will continue participation in the Cross Section Evaluation Working Group. Improved input data and methods have been developed for the calculation of charged particle collision stopping power[11] and radiation stopping power.[12] Work on electron and proton stopping power tables is in progress. Improved tables of photon attenuation and energy-absorption coefficients for energies 1 keV to 20 MeV have recently been prepared.[13] An updated version of the Photonuclear Data Index[14] will be presented and distributed at the August 1982 Gordon Conference.

2. New Compilation of Data for the Efficiency Calibration of Gamma-Ray Spectrometers (Dale D. Hoppes and Francis J. Schima)

A recent NBS Special Publication, SP 626, compiles the results of selected radionuclidic data measurements by 14 U.S. and international laboratories, including the NBS Radioactivity Group. The compilation was initiated by the Alpha-, Beta-, and Gamma-Ray Spectrometry Group of the International Committee for Radionuclide Metrology, with the goal of collecting carefully measured recent values of half-lives and gamma- and x-ray probabilities per decay for radionuclides useful for calibrating the efficiency of germanium spectrometry systems as a function of energy.

---

[11] S. M. Seltzer and M. J. Berger, Evaluation of Collision Stopping Power of Elements and Compounds for Electrons and Positrons, Int. J. Appl. Rad. & Isotopes (in press).

[12] S. M. Seltzer and M. J. Berger, Procedure for Calculating the Radiation Stopping Power for Electrons, Int. J. Appl. Rad. & Isotopes (in press).

[13] J. H. Hubbell, Photon Mass Attenuation and Energy-Absorption Coefficients from 1 keV to 20 MeV, Int. J. Appl. Rad. & Isotopes (in press).

[14] E. G. Fuller and H. Gerstenberg, Photonuclear Data Index, Suppl. 2 to NBS Spec. Publ. 380 (in press).

The contributors to SP 626 were asked to specify uncertainties in such a way that evaluators can check for consistency and arrive at a meaningful overall uncertainty.

A summary table contains data for 62 radionuclides for which two or more laboratories supplied values.

A. CROSS SECTION MEASUREMENTS

1. Capture Cross Sections

a. Direct Capture in the $^{34}S(n,\gamma)^{35}S$ Reaction with Thermal Neutrons* (R. F. Carlton,** S. Raman, and E. T. Jurney†)

The partial capture cross sections for primary γ rays in the $^{34}S(n,\gamma)^{35}S$ reaction with thermal neutrons are in reasonable agreement with the direct capture predictions of Lane and Lynn.

b. Neutron Resonance Study of ^{86}Kr* (B. Fogelberg,‡ J. A. Harvey, R. L. Macklin, S. Raman, and P. H. Stelson)

The level density in ^{87}Kr and the effective capture cross section of ^{85}Kr have been deduced from a neutron resonance study.

c. Resonance Neutron Capture in $^{86,87}Sr$¶ (G. C. Hicks,§ B. J. Allen,◊ A. R. de L. Musgrove, and R. L. Macklin)

The neutron capture cross sections of $^{86,87}Sr$ have been measured with high energy resolution from 3 to several hundred keV using the capture cross-section facility of the 40-m station on the Oak Ridge Electron Linear Accelerator. Individual resonances were analyzed to 37 keV for ^{86}Sr and to 14 keV for ^{87}Sr, and the average resonance parameters were deduced on the basis of assumed divisions between s- and p-wave resonances. The average radiative widths obtained on this basis are consistent with a capture mechanism which is predominantly statistical in nature.

d. Parity of the 398-eV Resonance in ^{35}Cl* (A. Z. Hussein, S. Raman), and J. A. Harvey)

The 398-eV resonance in the capture of neutrons by ^{35}Cl is definitely shown to be a p-wave resonance through neutron transmission measurements.

---

*Proceedings of Fourth International Symposium on Neutron-Capture Gamma-Ray Spectroscopy and Related Topics, Grenoble, France (September 1981).

**Middle Tennessee State University, Murfreesboro, Tennessee 37132.

†Los Alamos National Laboratory, Los Alamos, New Mexico 87545.

‡The Studsvik Science Research Laboratory, S-611 82 Nyköping, Sweden.

¶Submitted to Aust. J. Phys.

§Department of Physics, James Cook University Old 4811

◊AAEC Research Establishment, Private Mail Bag, Sutherland, NSW 2232

e. Thermal Neutron Absorption Cross Section of Sulfur and the ^{252}Cf $\bar{\nu}$ Problem* (E. J. Jurney,** S. Raman, and R. R. Spencer)

The thermal neutron absorption cross section for natural sulfur was measured to be 513 ± 15 mb. Any discrepancy between $MnSO_4$ bath and liquid scintillator measurements of ^{252}Cf($\bar{\nu}$) cannot be attributed to a discrepancy in this cross-section value.

f. Electric Dipole Transitions From Neutron Capture in ^{173}Yb Resonances† (O. Shahal, S. Raman, G. G. Slaughter, C. Coceva‡ and M. Stefanon‡)

Primary neutron capture γ rays have been studied from 49 neutron resonances in ^{173}Yb in the 10-530 eV energy range. These resonances are assigned J=2 and J=3 on the basis of the intensity ratios of suitable pairs of low-energy γ rays. The measured intensities of the high-energy primary γ rays have been converted to partial radiation widths. These widths have been subjected to a correlation analysis against reduced neutron widths, with the result that convincing evidence was not found for previously reported nonstatistical behavior in this nucleus. The ratio of the average population of a particular low-lying level from J=3 resonances to its population from J=2 resonances was found to be in satisfactory agreement with a cascade model. Resonances in the 10-200 eV range were noted to exhibit an enhancement of E1 transition probabilities to K=2 final states as compared to K=0 states. A level scheme for ^{174}Yb was constructed, and the neutron separation energy for this nucleus was deduced as 7464.5 ± 1.0 keV.

g. Test of Axel-Brink predictions in the ^{167}Er(n,γ)^{168}Er Reaction* (S. Kahane, G. G. Slaughter, and S. Raman)

The average radiation widths of primary γ rays in the reaction ^{167}Er(n,γ)^{168}Er are in reasonable agreement with the Axel-Brink predictions based on a giant dipole resonance model.

h. ^{99}Technetium Neutron Capture Cross Section¶ (R. L. Macklin)

The ^{99}Tc(n,γ) average cross section was measured at the Oak Ridge Electron Linear Accelerator (ORELA) from 2.65 to 2000 keV with an estimated uncertainty ranging from 4.0% to 4.9%. Individual resonance parameters were fitted by least-squares adjustment to the capture yield data from 2.65 to 5.08 keV. The average cross-section data agree with the ENDF/B 5 Mod 1) evaluation above 900 keV and lie within ±15% of the JENDL-1 evaluation below 700 keV.

---

*Proceedings of Fourth International Symposium on Neutron-Capture Gamma-Ray Spectroscopy and Related Topics, Grenoble, France (September 1981).
**Los Alamos National Laboratory, Los Alamos, New Mexico 87545.
†Submitted to Phys. Rev. C.
‡Comitato Nazionale Energia Nucleare, Bologna, Italy.
¶Submitted to Nucl. Sci. Eng.

i. ^{133}Cesium Neutron Capture Cross Section* (R. L. Macklin)

The $^{133}Cs(n,\gamma)$ cross section was measured at the Oak Ridge Electron Linear Accelerator (ORELA) from 2.66 keV to 600 keV with 3-4% uncertainty. Individual resonance parameters were determined by least-square adjustment to fit the yield data below 6 keV and the average cross section derived up to 600 keV.

j. Dipole and Quadrupole Radiation Strengths from Discrete States of ^{208}Pb** (S. Raman)

Information regarding the M1, E1, M2, and E2 radiation strengths from approximately 170 states in ^{208}Pb to the ground state is now available from a variety of experiments. Recent high-resolution neutron capture, transmission and scattering measurements carried out at the Oak Ridge Electron Linear Accelerator (ORELA) have contributed significantly in determining the strengths, and spin and parity assignments for approximately 110 states in the 7.37-8.40-MeV region. The M1 strengths are highly fragmented; the two strong 1^+ states expected from earlier (RPA) theoretical calculations are missing, and the strength in the 7.2-7.9 MeV region is far below previous estimates. An understanding of the M1 distribution in ^{208}Pb is crucial for pinning down the $\sigma_1 - \sigma_2$ interaction. The discrete 1^- states exhaust 3.4% of the classical sum rule strength. The bound states account for 1.4% and the resolved, unbound states in the 7.4-10.2 MeV region for the additional 2.0%. The M2 strengths from (e,e') measurements are, just as in the M1 case, significantly lower than RPA estimates employing bare operators. The measured E2 widths from 55 states in the excitation energy region between 7.37 and 8.17 MeV are reasonably consistent with those expected from the rising tails of giant quadrupole resonances located at higher energies.

k. The $^{36}S(n,\gamma)^{37}S$ Reaction with Thermal Neutrons† (S. Raman, W. Ratynski,‡ and E. T. Jurney¶)

The $^{36}S(n,\gamma)^{37}S$ reaction has been studied for the first time. Four primary transitions account for >95% of the thermal neutron capture cross section of 230 ± 20 mb.

---

*Submitted to Nucl. Sci. Eng.
**Proceedings of Second International Symposium on Neutron-Induced Nuclear Reactions, Smolenice, Czechoslovakia (June 1979).
†Proceedings of Fourth International Symposium on Neutron-Capture Gamma-Ray Spectroscopy and Related Topics, Grenoble, France (September 1981).
‡Institute of Nuclear Research, Otwock-Swierk, Poland.
¶Los Alamos National Laboratory, Los Alamos, New Mexico 87545.

l. Anomalous Transitions in ^{144}Nd and ^{146}Nd in "2-keV" (n,γ) Measurements[*] (S. Raman, O. Shahal, D. A. McClure,[**] and M. J. Kenny[**])

In "2-keV" (n,γ) measurements, anomalously strong E1 transitions have been observed to known 2^+ levels in ^{144}Nd and ^{146}Nd.

m. Statistical Properties of Complex States of $^{67}_{30}$Zn[†] (J. B. Garg, V. K. Tikku, J. A. Harvey, R. L. Macklin, and J. Halperin)

n. Stable Isotope Capture Cross Sections from Oak Ridge Electron Linear Accelerator[‡] (R. L. Macklin and R. R. Winters)

o. Gold Neutron Capture Cross Section from 100 to 2000 keV[¶] (R. L. Macklin)

p. Test of Axel-Brink Predictions by a Discrete Approach to Resonance-Averaged (n,γ) Spectroscopy[§] (S. Raman, O. Shahal, and G. G. Slaughter)

q. Enhanced Primary Dipole Transitions in the ^{89}Y(n,γ) Reaction[◊] (S. Raman, O. Shahal, A. Z. Hussein, G. G. Slaughter, and J. A. Harvey)

r. keV Neutron Capture in ^{141}Pr[♦] (R. B. Taylor, B. J. Allen, A. R. de L. Musgrove, and R. L. Macklin)

2. Total Cross Sections

a. Measurement of the Neutron Total Cross Section of Natural Nickel from 24 keV to 20 MeV[●] (D. C. Larson, J. A. Harvey, N. W. Hill, and C. H. Johnson)

The neutron transmission through a 2.54-cm sample of natural nickel has been measured for neutron energies between 24 keV and 20 MeV. The Oak Ridge Electron Linear Accelerator (ORELA) was used to provide the neutrons which were detected at the 200-m flight path by a NE-110 proton recoil detector. A selective gating system was utilized to minimize background

---

[*] Proceedings of Fourth International Symposium on Neutron-Capture Gamma-Ray Spectroscopy and Related Topics, Grenoble, France (September 1981).
[**] Brookhaven National Laboratory, Upton, New York 11973.
[†] Phys. Rev. C 24, 1922 (1981).
[‡] Nucl. Sci. Eng. 78, 110 (1981).
[¶] Nucl. Sci. Eng. 79, 265 (1981).
[§] Phys. Rev. C 23, 1794 (1981).
[◊] Phys. Rev. C 23, 2797 (1981).
[♦] Aust. J. Phys. 32, 551 (1979).
[●] Abstract of ORNL/TM-8203 (1982).

effects due to phototube afterpulsing in the detector. The experimental results are tabulated and compared with the total cross section in the ENDF/B-V file for nickel.

b. Transmission Measurements on Ti, Cr, and Mo (D. C. Larson, J. A. Harvey, and N. W. Hill)

Transmission measurements have been performed on samples of natural Ti, Cr, and Mo from ∿10 keV to 30 MeV at the 200-m flight path. The ORELA was run at 780 pulses per second with a 7-ns burst width. The data are being reduced to cross sections and will be compared with current ENDF/B-V evaluations for these materials.

c. Neutron Resonance Parameters of $^{68}_{30}$Zn+n and Statistical Distributions of Level Spacings and Widths* (J. B. Garg,** V. K. Tikku,** J. A. Harvey, J. Halperin, and R. L. Macklin)

Discrete values of the parameters (E_o, $g\Gamma_n$, J^{π}, Γ_{γ} etc.) of the resonances in the reaction $^{68}_{30}$Zn+n have been determined from total cross section measurements from a few keV to 380 keV with a nominal resolution of 0.07 ns/m for the highest energy and from capture cross-section measurements up to 130 keV using the pulsed neutron time-of-flight technique at ORELA with a neutron burst width of 5 ns. The cross-section data were analyzed to determine the parameters of the resonances using R-matrix multilevel codes. These results have provided values of average quantities as follows: S_o = (2.01 ± 0.34), S_1 = (0.56 ± 0.05), S_2 = (0.2 ± 0.1) in units of 10^{-4}, D_o = (5.56 ± 0.43) keV and D_1 = (1.63 ± 0.14) keV. From these measurements we have also determined the following average radiation widths: $(\overline{\Gamma_{\gamma}})_{\ell=0}$ = (302 ± 60) meV and $(\overline{\Gamma_{\gamma}})_{\ell=1}$ = (157 ± 7) meV. The investigation of the statistical properties of neutron reduced widths and level spacings showed excellent agreement of the data with the Porter-Thomas distribution for s- and p-wave neutron widths and with the Dyson-Mehta Δ_3 statistic and the Wigner distribution for the s-wave level spacing distribution. In addition, a correlation coefficient of ρ = 0.50 ± 0.10 between Γ_n^o and Γ_{γ} has been observed for s-wave resonances. The value of $\langle\sigma_{n\gamma}\rangle$ at (30 ± 10) keV is 19.2 mb.

d. ^{206}Pb+n Resonances for E=600-900 KeV: Neutron Strength Functions† (D. J. Horen, J. A. Harvey, and N. W. Hill)

*Accepted for publication by Phys. Rev. C.
**State University of New York, Albany, New York 12222.
†Phys. Rev. C 24, 1961 (1981).

3. Scattering and Reactions

a. ^{57}Fe (n,n'γ) Gamma-Ray Production (Z. W. Bell, J. K. Dickens, and D. C. Larson)

Measurements have been made of gamma-ray yields following neutron excitation of a 7-g sample of iron enriched in the isotope ^{57}Fe for incident neutron energies between 0.2 and 2 MeV. A Ge(Li) detector was used. Incident neutrons were obtained from the ORELA. Excitation functions for the dominant 122- and 352-keV gamma rays, and for weaker gamma rays which can be differentiated from Ge(n,n'γ) background, will be extracted.

b. ^{56}Fe(n,n'γ) E_γ = 846 keV Gamma-Ray Production (Z. W. Bell, J. K. Dickens, and D. C. Larson)

Preliminary measurements indicate that yields of this gamma ray are sufficient for accurate measurements for E_n between threshold and 30 MeV at the 20-m station of flight-path no. 8 of the ORELA despite the rapid decrease of the incident neutron flux with increasing energy. A careful study of the timing characteristics of the 90-cm^3 coaxial Ge(Li) detector as a function of recorded gamma-ray energy was made, and we have confirmed that we can readily differentiate neutron-induced 846-keV photons from scattered gamma-flash photons. Incident-neutron flux measurements have also been completed.

c. ^{206}Pb Level Structure from ^{206}Pb(n,n'γ) Measurements* (J. K. Dickens)

A study of gamma-ray data produced by neutron inelastic scattering from a lead sample enriched in the isotope ^{206}Pb has resulted in placements, or tentative placements, of 146 gamma rays as transitions among 112 known or postulated levels of the ^{206}Pb level structure.

4. Actinides

a. Fission-Product Energy Release for Times Following Thermal-Neutron Fission of Plutonium-239 and Plutonium-241 Between 2 and 14 000 s** (J. K. Dickens, T. A. Love, J. W. McConnell, and R. W. Peelle)

b. Yields of Fission Products Produced by Thermal-Neutron Fission of ^{249}Cf† (J. K. Dickens and J. W. McConnell)

---

*Abstract of ORNL/TM-8137 (1982).
**Nucl. Sci. Eng. 78, 126 (1981).
†Phys. Rev. C 24, 192 (1981).

c. Beta and Gamma Decay Heat Measurements for Fast and Thermal Reactors, Particularly for Pu-239* (J. K. Dickens)

Results of recent experiments and calculations for decay heat for ^{239}Pu are reviewed and compared. Comparisons with decay heat for thermal-neutron fission of ^{235}U and ^{241}Pu are also shown.

d. Yields of Short-Lived Fission Products of Thermal-Neutron Fission of Thorium-239** (J. K. Dickens, J. W. McConnell, and K. J. Northcutt)

The absolute yields of 39 fission products representing 30 different mass chains produced by thermal neutron fission of ^{229}Th and having half-lives between 15 and 4600 s have been determined using Ge(Li) spectroscopy methods. Spectra of gamma rays emitted in the decay of the fission products between 25 and 2400 s after a 15-s irradiation were obtained. Gamma rays were assigned to the responsible fission products by matching gamma-ray energies and half-lives. Fission product yields were then obtained from the data by first determining the appropriate gamma-ray activity as of the end of the irradiation, correcting for detector efficiency and gamma-ray branching ratio, and, finally, dividing by the number of fissions created in the sample.

The resulting fission product yields are compared with previous measurements and with recommended yields given in the recent ENDF/B evaluation. Relative uncertainties assigned to the present results range between 6 and 65%, with an absolute normalization uncertainty of 13%. The present uncertainties are smaller than or comparable to uncertainties assigned to previous experimental or evaluated yields for 16 mass chains.

e. Fission Product Yields for Thermal-Neutron Fission of Curium-243† (David G. Breederland)

Cumulative fission yields for 25 gamma rays emitted during the decay of 23 fission products produced by thermal-neutron fission of ^{243}Cm have been determined. Using Ge(Li) spectroscopy, 33 successive pulse-height spectra of gamma rays emitted from a 77-ng sample of ^{243}Cm over a period of approximately two and one-half months were analyzed. Reduction of these spectra resulted in the identification and matching of gamma-ray energies and half-lives to specific radionuclides. Using these results, 23 cumulative fission-product yields were calculated. Only those radionuclides having half-lives between 6 hours and 65 days were observed. Prior to this experiment, no fission-product yields had been recorded for ^{243}Cm.

---

*Conf.-810975-1, NTIS Pc A02/MF A01, NEACRP-A-464, prepared for the 24th Meeting of the NEACRP, Winfrith, Sept. 14-18, 1981.

**Nucl. Sci. Eng. (in press, 1982).

†Abstract of ORNL/TM-8168 (January 1982).

f. Yields of Fission Products Produced by Thermal-Neutron Fission of ^{229}Th (J. K. Dickens and J. W. McConnell)

Absolute yields have been determined for 47 gamma rays emitted in the decay of 37 fission products representing 25 mass chains created during thermal-neutron fission of ^{229}Th. Using a Ge(Li) detector, spectra were obtained of gamma rays between 15 min and 0.4 y after very short irradiations of thermal neutrons of a 15-μg sample of ^{229}Th. On the basis of measured gamma-ray yields and known nuclear data, total chain mass yields and relative uncertainties were obtained for 27 masses between 84 and 149. The absolute overall normalization uncertainty is <8%. The measured A-chain cumulative yields from the present program make up 84% of the total light-mass ($A \leqslant 115$) yield and 72% of the total heavy-mass yield. The results are compared with fission-product yields previously measured with generally good agreement. On this basis, and using other measurements for masses not observed in the present experiment, a complete mass distribution for A between 76 and 152 was deduced.

The data were analyzed to obtain values of most-probable charge (Z_p) and charge-dispersion (σ) parameters. Based upon new insight gained from study of similar data obtained for thermal-neutron fission of ^{235}U, we postulate a simple functional dependence $\sigma = \sigma(Z_p)$, and using this dependence obtain values of $Z_p(A)$ for 15 mass chains. Values of $Z_p(A)$ were estimated for other mass chains based upon results of a recent study of $Z_p(A)$. Charge distributions determined, using the deduced mass distribution and the deduced sets of $Z_p(A)$ and $\sigma(Z_p)$, are in very good agreement with recent measurements, exhibiting a pronounced even-odd effect in elemental yields. These results may be used to predict unmeasured yields for ^{229}Th fission.

g. Electron Antineutrino Spectrum for $^{235}U(n,f)$* (J. K. Dickens)

The $\overline{\nu}_e$ spectrum has been computed for fission-product decay following a 30-d irradiation of ^{235}U by thermal neutrons. Estimated uncertainties lie in the range (7-15)% for $E_{\overline{\nu}}<6$ MeV. Analysis relied on comparisons of calculated β-ray data with recently obtained experimental β-ray spectra. The $\overline{\nu}_e$ spectrum is softer than all other calculated $\overline{\nu}_e$ spectra. Cross sections (10^{-44} cm^2/fission) were calculated as $\sigma(\overline{\nu}_e + p \rightarrow n + e^+) = 58 \pm 3$, $\sigma(\overline{\nu}_e + d \rightarrow n + p + \overline{\nu}_e) = 2.7 \pm 0.2$, and $\sigma(\overline{\nu}_e + d \rightarrow n + n + e^+) = 1.04 \pm 0.13$.

h. Energies and Intensities of Gamma Rays from Decay of ^{229}Th and Daughters of Equilibrium** (J. K. Dickens and J. W. McConnell)

Energies and intensities of 52 γ-rays having energies between 31 and 1567 keV have been measured and compared with previous measurements for ^{229}Th, ^{225}Ra, ^{225}Ac, ^{221}Fr, ^{217}At, ^{213}Bi, and ^{209}Tl. Two new excited states of ^{213}Po have been postulated.

*Phys. Rev. Lett. 46, 1061 (1981).
**Radiochem. Radioanal. Lett. 47, 331 (1981).

i. Actinide Newsletter (S. Raman)

The fifth issue will appear in early 1982 and has 58 contributions from 28 laboratories in 14 countries. The IAEA Advisory Group on Transactinium Isotope Nuclear Data at its second meeting in Cadarache, France, in May 1979, made a strong recommendation for the continuation of the Actinide Newsletter and for persons working in this field all over the world to make contributions to it. The publication schedule is expected to be one issue per year in the future.

j. ^{238}U Self-Indication Ratio Measurements in the Resonance Region* (J. T. Yang,** J. L. Munoz-Cobos,† and G. de Saussure)

The purpose of this paper is to compare a set of self-indication ratio measurements, performed at ORELA over a wide range of ^{238}U sample thicknesses, with a calculation based on the ENDF/B-V evaluated data over the resolved resonance region. The present self-indication ratio measurements appear to be generally consistent with the results of the ENDF/B-V calculation.

k. Thorium S-Wave Neutron Widths from 21 to 20006 eV‡ (D. K. Olsen, R. W. Ingle, and J. L. Portney)

A ^{232}Th total cross-section measurement in the resolved resonance region has been requested with a 2% accuracy to obtain resonance parameters with a 5% accuracy. To improve the differential data base, we have measured neutron transmission spectra through eight samples of ^{232}Th. Fits to these data up to 440 eV, which concentrated on the capture widths, have been previously reported. In this paper, we report the results of extending these fits to 2.0 keV and discuss the result in terms of the s-wave strength function and the dilute-capture resonance integral.

l. Resolved Resonance Parameters for ^{238}U from 4 to 6 keV¶ (P. S. Meszaros and D. K. Olsen)

The ^{238}U shielded-capture cross sections are one of the most important nuclear data for reactor application. Nevertheless, a precise knowledge of these cross sections over a fast-reactor spectrum remains somewhat illusive. In this abstract, we report the results from a resonance analysis of the ORELA 150-m ^{238}U transmission data, allowing an extension of the resolved resonance region to higher energies. The resultant s-wave strength function from 4 to 6 keV is substantially smaller than that from 0 to 4 keV.

*American Nuclear Society, Kiamesha Lake, New York, Sept. 22-24, 1982.
**Department of Nuclear Engineering, University of Tennessee, Knoxville, Tenn.
†Universidad Politechnica de Valencia (Spain).
‡Trans. Am. Nucl. Soc. 38, 647 (1981).
¶American Nuclear Society Meeting, Los Angeles, California, June 6-11, 1982.

m. Measurement of Neutron Transmission Spectra Through ^{232}Th from 8 meV to 4 keV* (D. K. Olsen and R. W. Ingle)

Neutron transmission spectra through room-temperature ^{232}Th samples have been measured using the time-of-flight technique, the ORELA pulsed neutron source and a 1-mm-thick Li-glass detector. The measurement and data reduction are described in detail. The 40-m transmission spectra through eight samples are directly compared from 15 to 4000 eV with resolution-broadened transmission spectra calculated from the ENDF/B-V total cross section. Two sets of 22-m transmission spectra through five samples are combined into one total cross section from 0.008 to 15.0 eV and compared with the ENDF/B-V evaluation.

n. Measurement of the Average Number of Prompt Neutrons Emitted per Fission of ^{233}U Relative to ^{252}Cf for the Energy Region 500 eV to 10 MeV and Below 0.3 eV** (R. Gwin, R. R. Spencer, and R. W. Ingle)

The energy dependence of the average number of prompt fission neutrons emitted per fission, $\overline{\nu}_p(E)$, has been measured for ^{233}U relative to $\overline{\nu}_p$ for ^{252}Cf over the neutron energy ranges 500 eV to 10 MeV and below 0.3 eV. A large Gd-loaded liquid scintillator was used to detect neutrons and the samples of ^{233}U and ^{252}Cf were contained in fission chambers. The present results for $\overline{\nu}_p(E)$ for ^{233}U are in accord with the experimental results of Boldeman and the evaluated results of Lemmel in the thermal energy range, but in the neutron energy region between 100 keV and 1 MeV the present data are 1% or more larger than other experimental values.

o. Neutron Fission Cross Section of Pu-239 and Pu-240 Relative to U-235 (L. W. Weston and J. H. Todd)

The ratios of the neutron fission cross sections of Pu-239 and Pu-240 to that of U-235 have been measured simultaneously with a multi-plate ionization fission chamber using the Oak Ridge Electron Linear Accelerator as a neutron source. The neutron energy range for these ratio measurements was from 5 keV to 20 MeV. The data is basically in agreement with ENDF/B-V from 200 keV to 10 MeV. Below 200 keV, there is a discrepancy between the present Pu-239 ratio data and ENDF/B-V. The agreement of the Pu-240 ratio is reasonably good. From 10 to 20 MeV the agreement of the Pu-239 ratio with ENDF/B-V is poor. These ratios are important for thermal and fast reactor applications.

---

*Abstract of ORNL/TM-7661, ENDF-307 (1981).
**Abstract of ORNL/TM-7988, ENDF-315 (November 1981).

p. Neutron Fission Cross Sections of Pu-239 and U-235 Relative to $^{10}B(n,\alpha)$ (R. Gwin, R. R. Spencer, S. W. Scoles, R. W. Ingle, and J. H. Todd)

Measurements of the energy dependence $\sigma_f(E)$ the neutron fission cross sections have been made for ^{235}U and ^{239}Pu. For ^{235}U the energy interval covered in the experiments was from 0101 eV to 30 keV and for ^{239}U the range was 0.01 to 60 eV. The experiments which included the ^{239}Pu were performed during a program designed to measure $\overline{\nu}_p(E)$ the energy dependence of the average number of prompt neutrons emitted in fission of ^{235}U and ^{239}Pu relative to $\overline{\nu}_p$ the average number of prompt neutrons emitted in spontaneous fission of Cf-252.

The results for $\sigma_f(E)$ for ^{239}Pu obtained in the $\overline{\nu}_p(E)$ experiments were in good agreement (1-2%) with previous measurements by Gwin et al., where as for ^{235}U $\sigma_f(E)$ values obtained in the same work were 4% larger in the resonance region ($E > 1$ eV) than previously obtained. In addition, the results for $\sigma_f(E)$ for ^{239}Pu were in good agreement ($\sim$1%) with the work of Deruytter and Wagemans, but for ^{235}U the present values were about 3% larger obtained by Deruytter and Wagemans.

q. Measurement of Neutron Transmission Through Samples of Pu-240 1.9- and 0.4-cm Thick in the Neutron Energy Range 4 keV to 2 MeV (R. Gwin)

Measurements have been made of the energy dependence of neutron transmission through samples of ^{240}Pu 1.89 and 0.43 cm thick. Fifteen to twenty percent of the Pu in a fast breeder reactor may be ^{240}Pu and the primary motivation for these experiments was to measure the total neutron cross section for ^{240}Pu over the neutron energy region of importance to breeder reactor design 10 keV to 2 MeV.

The present measurements covered the neutron energy range from 2.5 eV to 6 MeV. Experimental results were obtained in the resonance energy region to provide a measure of the potential cross section, to compare with other data, and to serve as a check on the relative concentration of impurity isotopes such as ^{241}Pu and ^{241}Am in the Pu sample.

r. Some Spectroscopic Properties of the Fine Structures Observed Near the $^{231}Pa(n,f)$ Fission Threshold* (S. Plattard, G. F. Auchampaugh, N. W. Hill, G. de Saussure, J. A. Harvey, and R. B. Perez)

s. K-Components for the $\sim$1.4, $\sim$1.6-, and $\sim$1.7-MeV Structures in $^{232}Th + n$** (G. F. Auchampaugh, S. Plattard, N. W. Hill, G. de Saussure, R. B. Perez, and J. A. Harvey)

*Phys. Rev. Letters 46, 633 (1981).

**Phys. Rev. C 24, 503 (1981).

t. The Radiative Capture Yield of Thorium-232 from 100 to 4000 eV* (R. B. Perez, G. de Saussure, R. L. Macklin, J. Halperin, and N. W. Hill)

u. Neutron Capture Cross Section of ^{237}Np** (L. W. Weston and J. H. Todd)

v. Neutron Total Cross Section and Resonance Parameters of ^{231}Pa† (A. R. Z. Hussein, J. A. Harvey, N. W. Hill, and J. R. Patterson)

w. The Radiative Capture Yield of Thorium-232 from 100 to 4000 eV‡ (R. B. Perez, G. de Saussure, R. L. Macklin, J. Halperin, and N. W. Hill)

x. Thorium Resonance Neutron Capture (2.6-10 keV)¶ (R. L. Macklin)

5. Experimental Techniques

a. TPASS, A Gamma-Ray Spectrum Analysis and Isotope Identification Computer Code§ (J. K. Dickens)

The gamma-ray spectral data-deduction and analysis computer code TPASS is described. This computer code is used to analyze complex Ge(Li) gamma-ray spectra to obtain peak areas corrected for detector efficiencies, from which are determined gamma-ray yields. These yields are compared with an isotope gamma-ray data file to determine the contributions to the observed spectrum from decay of specific radionuclides. A complete FORTRAN listing of the code and a complex test case are given.

b. ISOLR - An Isometric Plotting Package for Use with ORPLOT◊ (Z. W. Bell)

An isometric plotting package is described. It is written entirely in FORTRAN and is designed to work in conjunction with ORPLOT, a general purpose plotting package in use at the ORELA PDP-10. The isometric plotter supports views from any point in space, logarithmic scales, and hidden lines.

---

*Nucl. Sci. Eng. 80, 189 (1982).
**Nucl. Sci. Eng. 79, 184 (1981).
†Nucl. Sci. Eng. 78, 370 (1981).
‡Nucl. Sci. Eng. 80, 189 (1981).
¶Nucl. Sci. Eng. 79, 118 (1981).
§Abstract of ORNL-5732 (March 1981).
◊Abstract of ORNL/TM-8192 (1982).

c. Tests on a Digital Neutron-Gamma Pulse Shape Discriminator with NE213* (Z. W. Bell)

d. Gamma-Ray Response for an NE213 Detector for $5 \leqslant E_\gamma \leqslant 25$ MeV (Z. W. Bell)

The gamma-ray response of an NE213 detector has been measured for $5 \leqslant E_\gamma \leqslant$ MeV, $\Delta E_\gamma < 200$ keV, using the University of Illinois Bremsstrahlung Monochromator. The data are being compared to calculations using the EGS computer code (RSIC, CCC-331). Preliminary analysis indicates that $^{12}C(\gamma,p)$ ^{11}B with subsequent detection of the photoproton is a significant detection process for $19 \leqslant E_\gamma \leqslant 24$ MeV (the Giant Dipole Resonance region in ^{12}C).

e. Digital Pulse-Pair Detecting Circuit (Z. W. Bell, J. W. McConnell, and E. D. Carroll)

We have constructed a completely digital pulse-pair detecting circuit using MECL 10000 and MECL III integrated circuits. A 50-MHz temperature compensated crystal controlled oscillator is used for the internal time base and the inspection interval is variable from 100 ns to 1.3 ms in 20-ns steps. Tests indicate reliable operation at input rates up to 25 MHz.

f. The Use of Oxide Targets in 2-keV Average Neutron Capture Measurements** (J. S. Tang and S. Raman)

Large samples ($\approx$10-100 grams) are usually required for "2-keV" filtered-beam measurements and such samples invariably come in the oxide form. Monte Carlo calculations show that the resulting neutron spectrum is degraded by $\approx$ 0.2 keV in a $^{145}Nd_2O_3$ sample. Otherwise, oxide samples are acceptable for such measurements.

g. Low-Energy Proton and Electron Responses of an n-Octane Liquid Scintillator† (M. H. Wood, S. M. Blankenship, T. P. Long, F. T. Avignone III, G. L. Morgan, and S. Raman)

B. DATA ANALYSES

1. Theoretical Calculations

a. A Calculation of Neutron and Gamma-Ray Production Cross Sections for Calcium from 8 to 20 MeV‡ (D. M. Hetrick and C. Y. Fu)

---

*Nucl. Instr. Meth. 188, 105 (1981).

**Proceedings of Fourth International Symposium on Neutron-Capture Gamma-Ray Spectroscopy and Related Topics, Grenoble, France (September 1981).

†Nucl. Instrum. Methods 188, 75 (1981).

‡ORNL/TM-7752, ENDF-308.

b. User's Guide for BAYES: A General-Purpose Computer Code for Fitting a Functional Form to Experimental Data* (N. M. Larson)

This report is intended as a users' manual for a general purpose computer program BAYES to solve Bayes' equations for updating parameter values, uncertainties, and correlations. Bayes' equations are derived from Bayes' theorem, using linearity and normality assumptions. The method of solution is described, and details are given for adapting the code for a specific purpose. Numerous examples are given, including problem description and solution method, FORTRAN coding, and sample input and output. A companion code LEAST, which solves the least-squares equations rather than Bayes' equations, is also described.

c. s-Process Studies in the Light of New Experimental Cross Sections: Distribution of Neutron Fluences and r-Process Residuals** (F. Käppeler, H. Beer, K. Wisshak, D. D. Clayton,† R. L. Macklin, and R. A. Ward‡)

A best set of neutron-capture cross sections has been evaluated for the most important s-process isotopes. With this data base, s-process studies have been carried out using the traditional model which assumes a steady neutron flux and an exponential distribution of neutron irradiations. The calculated σN-curve is in excellent agreement with the empirical σN-values of pure s-process nuclei. Simultaneously, good agreement is found between the difference of solar and s-process abundances and the abundances of pure r-process nuclei. We also discuss the abundance pattern of the iron group elements where our s-process results complement the abundances obtained from explosive nuclear burning. The results obtained from the traditional s-process model such as seed abundances, mean neutron irradiations, or neutron densities are compared to recent stellar model calculations which assume the He-burning shells of red giant stars as the site for the s-process.

d. Application of Group Theory to Data Reduction or Group Theoretical Foundation of Physical Probabilities (F. G. Perey)

The analysis within the framework of a theory of what was observed in experiments is essential to the testing of theories and is fundamental to physics. It is shown in this paper how group theory can be used to provide a general method of data reduction whereby only the laws of a particular theory are used in the analysis of observations. This application of group theory involves introducing a group of transformations of the physical system upon which the observations were made. This group of transformations leaves invariant the entities of the theory corresponding to the observations made

---

*Abstract of ORNL/TM-8185, ENDF-323.

**Abstract of KfK 3210, Kernforschungszentrum Karlsruhe GmbH, Karlsruhe.

†Max-Planck-Institut für Kernphysik, Heidelberg and Rice University, Houston, Texas.

‡Max-Planck-Institut für Physik und Astrophysik, München.

but transforms the entities that were not observed from what they are presumed to be in this theory into what they are not, called possibilities for what they are. This group of transformations is called the possibilities-generating group for the entities for which the observations are being reduced. Since possibilities for entities of theories so obtained are functionals of a known group of transformations, their subsequent use in the theories must be made consistent with the theory of representations of groups. There is a well-known invariant associated with possibilities for entities so generated which is invariant with respect to the parameterization of this group. It is the normalized volume measure in the group manifold of the possibilities-generating group. This invariant measure of the possibilities for entities of theories obtained in experiments is called the physical probabilities of the possibilities since it is a probability measure which has a Borel algebra. The above proposed method of data reduction allows us to deal unambiguously with the uncertainties in entities of physical theories obtained from all of the observations made in experiments and the distinction between systematic and statistical uncertainties disappears. Concrete realizations of possibilities-generating groups are given and explanations in group theoretical terms are offered for several important intuitive notions related to probabilities.

2. ENDF/B Related Evaluations

a. Evaluation of Neutron and Gamma-Ray-Production Cross Sections for Natural Iron (ENDF/B-V MAT 1326)* (C. Y. Fu and F. G. Perey)

b. Experience in Using the Covariances of Some ENDF/B-V Dosimetry Cross Sections** (C. Y. Fu and D. M. Hetrick)

Recent ratio data, with carefully evaluated covariances, were combined with eleven of the ENDF/B-V dosimetry cross sections using the generalized least-squares method. The purpose was to improve these evaluated cross sections and covariances, as well as to generate values for the cross-material covariances. However, certain problems were encountered, but not unexpectedly. These problems were traced to three areas of deficiencies in the covariances of the ENDF/B-V evaluations. First, some of the ratios calculated from the resulting combining process lie outside the interval defined by the ratio data and the ratios calculated from the ENDF/B-V evaluations. Some examples are: ratios of ^{46}Ti(n,p), ^{54}Fe(n,p), and ^{58}Ni(n,p) to ^{238}U(n,f) near 10 MeV. These results, though theoretically possible, suggest unrealistically large correlation in some of the input evaluations. Second, an unduly large energy range of full correlation enhances propagation of discrepancies. For example, both ^{46}Ti(n,p) and ^{235}U(n,f) have a fully correlated range from 4 to 10 MeV, so that a local discrepancy between ratio data and evaluations near 4 MeV propagates all the way up to 10 MeV. Third, changes in evaluated cross-section values larger than one standard deviation are present in most energy ranges. This implies that uncertainty estimates were

*ORNL/TM-7523, ENDF-302 (November 1980).
**Fourth ASTM-EURATOM Symposium on Reactor Dosimetry, Gaithersburg, Md, (1982).

generally too small in the ENDF/B-V evaluations and possibly in the ratio data too. For example, the output $^{63}Cu(n,\alpha)$ cross sections from 8 to 11 MeV changed from the input by three standard deviations. Such large changes, if due to an oversight in one evaluation, would adversely affect other evaluations through the ratio data and/or through the cross-material correlations. Remedies to these three deficiencies are being sought and tested. Success of this effort would lead to substantially improved cross sections as well as realistic and usable covariances.

c. Summary of ENDF/B-V Evaluations for C, Ca, Fe, Cu, and Pb and ENDF/B-V Revision-2 for Ca and Fe* (C. Y. Fu)

This report, together with documents already published, describes the ENDF/B-V evaluations of the neutron and gamma-ray production cross sections for C, Ca, Fe, Cu, and Pb and the ENDF/B-V Revision-2 for Ca and Fe.

d. On The ENDF/B Unresolved Resonance Region Formalism Representation** (R. B. Perez, G. de Saussure, J. L. Munoz-Cobos†, J. Barhen, and R. Q. Wright)

A considerable amount of effort has gone into the development of neutron cross-section representations in the unresolved resonance region. The central question about the ENDF/B representation of the unresolved resonance region is whether or not that representation leads to a correct estimate of resonance self-shielding. The purpose of this work is to present a test of the validity of the ENDF/B treatment of the unresolved resonance region, taking the ENDF/B-V ^{238}U, MAT 1398 as an example. Over 1-keV intervals, the unresolved resonance model appears to overestimate systematically the self-shielded capture cross section. If it can be assumed that in the interval from 4 to 10 keV, the discrepancies are of the same magnitude and same sign as in the interval from 1 to 4 keV, then this effect could explain, at least in part, the longstanding discrepancy between measured and computed values of the capture rate in ^{238}U-containing assemblies.

e. Problems and Progress Regarding Resonance Parameterization of ^{235}U and ^{239}Pu for ENDF/B‡ (M. S. Moore,¶ G. de Saussure, and J. Richard Smith§)

The procedures used to obtain the resolved and unresolved resonance parameterization of ^{235}U and ^{239}Pu contained in the U.S. Evaluated Nuclear Data File ENDF/B-V are reviewed. For ^{235}U, recommendations are made

*Abstract of ORNL/TM-8283, ENDF-325.

**American Nuclear Society Meeting, San Francisco, Calif. (November 1981).

†Universidad Politecnica de Valencia-Spain.

‡Joint IAEA/NEA Consultants Meeting on U and Pu Resonance Parameters, Vienna, September 28 - October 2, 1981.

¶University of California, Los Alamos National Laboratory, P. O. Box 1663, Los Alamos, NM 87544.

§EG&G, Idaho, Inc., P. O. Box 1625, Idaho Falls, Idaho 83401.

to improve the representation by including information on resonance spins and fission-channel vector orientations, and some preliminary results are presented. We review evidence that it is the fission channels rather than the spins of the resonances that lead to differences in fission mass distributions, the number of neutrons emitted per fission, and fission kinetic energies. The improved parameterization may thus have physics content that will prove of interest in future applications.

f. Comparison of the ENDF/B-V and SOKRATOR Evaluations of ^{235}U, ^{239}Pu, ^{240}Pu and ^{241}Pu at Low Neutron Energies (G. de Saussure and R. Q. Wright)

The U.S. and U.S.S.R.'s most recent evaluations of ^{235}U, ^{239}Pu, ^{240}Pu, and ^{241}Pu are compared over the thermal region and over the first few resonances. The two evaluations rest on essentially the same experimental data base and the differences reflect different approaches to the representation of the cross sections or different weightings of the experimental results. It is found that over the thermal and resolved ranges the two evaluations are very similar. Some differences in approaches are briefly discussed.

g. Representation of the Neutron Cross Sections of Several Fertile and Fissile Nuclei in the Resonance Regions* (G. de Saussure and R. B. Perez)

In this paper we review several problems related to the measurement, analysis, and evaluation of the neutron cross sections of the main fertile and fissile nuclides in the resonance region. In particular, we discuss the ENDF/B-V representation of these cross sections.

In recent years little progress has been made in improving our knowledge of the resolved resonance parameters of the fertile nuclei. We suggest that this absence of progress is due to a lack of adequate methodologies to deal with the systematic errors arising from uncertainties in the analysis of the measurements.

We comment on the ENDF/B treatment of the unresolved resonance region and recommend the validation of the unresolved resonance range evaluations with appropriate transmission and self-indication measurements.

h. An Evaluation of the Resolved-Resonance-Region Cross Sections of ^{232}Th** (D. K. Olsen)

An evaluation of the neutron-induced, resolved-resonance-region (5 to 4000 eV) cross sections of ^{232}Th is described in terms of explicit resonance parameters and pointwise cross sections. The evaluation average capture width, 24.4 ± 2.0 MeV, and 0-to-4 keV, s-wave strength function,

*Abstract of ORNL/TM-7945, ENDF-312.
**Abstract of ORNL/TM-8056, ENDF-319.

$0.826 \pm 0.037 \times 10^{-4}$ are appreciably larger than those of the ENDF/B-V evaluation. The present evaluation, together with the ENDF/B-V thermal and unresolved resonance region cross sections give a dilute-capture resonance integral of 86.1 b. The bound levels of ENDF/B-V are retained and pointwise cross sections are given to smoothly connect this evaluation to the ENDF/B-V thermal cross sections.

i. Evaluation of Neutron and Gamma-Ray Production Cross Sections for Calcium from 20 to 40 MeV (D. M. Hetrick, C. Y. Fu, and D. C. Larson)

Nuclear model codes were used to compute cross sections for neutron-induced reactions on ^{40}Ca for incident energies from 20 to 40 MeV. The input parameters for the model codes were determined through analysis of experimental data in this energy region. Computed cross sections along with emission spectra for each product were combined into an Evaluated Nuclear Data File (ENDF) using the proposed format for charged-particle reactions. Discussion of the models used, the resulting calculations, and the final evaluated data file are included in this report.

j. Evaluation of the $^{23}Na(n,2n)^{22}Na$ Reaction for ENDF/B-V* (D. C. Larson)

C. NUCLEAR DATA PROJECT ACTIVITIES - 1981 (Y. A. Ellis, B. Harmatz,** M. J. Martin, M. R. McGinnis,† J. T. Miller,‡ and M. R. Schmorak)

1. Data Evaluation

As part of the international network, for nuclear structure data evaluation, the Nuclear Data Project has continuing responsibility for mass chains in the region $A \geqslant 195$. Revised nuclear data sheets for 22 mass chains were prepared during 1981. In addition to its evaluation responsibility, NDP is committed to maintaining uniform, high standards for ENSDF by providing the position of editor-in-chief for Nuclear Data Sheets. The Nuclear Data Project provided review and editing for 15 mass chains during 1981. NDP staff members have also organized training seminars for new data evaluators in order to introduce them to NDP evaluation techniques, analysis programs, and conventions used in ENSDF and Nuclear Data Sheets.

---

*Nucl. Sci. Eng. 78, 321 (1981).
**Deceased.
†Technical support staff.
‡Technical support staff to mid-1981 only.

2. Evaluated Nuclear Structure Data File

The Evaluated Nuclear Structure Data File (ENSDF), developed and implemented by the NDP, contains a documented summary of the current status of nuclear measurements. The ENSDF now contains ∿8500 distinct sets of evaluated nuclear information. This includes:

∿2000 sets of adopted level properties (41,000 nuclear levels)
∿2200 decay schemes
∿4300 nuclear reaction data collections.

All decay scheme information in ENSDF is now at least as complete as the most recent Nuclear Data Sheets. Normalization information is included wherever available, and details of electron capture and internal conversion have been added systematically, so that complete tables of atomic and nuclear radiations can be assembled for more than 1600 decay schemes.

The ENSDF computer format has been adopted as an international standard for the systematic storage and exchange of nuclear structure data. NNDC at BNL is now responsible for the maintenance and dissemination of this file to other evaluation centers in the international network of data centers. NDP maintains a copy of this file for the use of its evaluators and other researchers at ORNL.

3. Nuclear Structure References

Nuclear Data Project's Nuclear Structure References (NSR) file contains about 75,000 entries. Approximately 5000 indexed new research works are added each year. About half of the additions are journal publications; the other half consists of reports, conference abstracts, preprints, etc. Each month an SDI (Selective Dissemination of Information) service is provided from new entries to the NSR file. NNDC at BNL is now responsible for the maintenance and dissemination of this file to other evaluation centers in the international network of data centers. NDP maintains a copy of this file for the use of its evaluators and other researchers at ORNL.

4. Publications

Five issues of the journal Nuclear Data Sheets (over 900 pages) were prepared and published in 1981. These included complete manuscripts (drawings, tables, reference lists) for 18 revised mass chains. The publication reponsibility was assumed by the National Nuclear Data Center at BNL in June of 1981. They will continue to have this responsibility.

5. Information Services

The NDP responded to over 40 requests for specific information by means of searches of the Nuclear Structure Reference File (NSR) printout from the Evaluated Nuclear Structure Data File (ENSDF) and personal consultation.

6. Special Activities

A collection of systematic level properties in the lead region was published.

An article containing updated listings of radiations from selected nuclides has been submitted to the Encyclopedia of Chemical Technology. This article, entitled "Radioisotopes," is in press.

OHIO UNIVERSITY

A. NEUTRON SCATTERING

1. The Ohio University Beam Swinger Facility* (Finlay, Brient, Carter, Marcinkowski, Mellema, Randers-Pehrson, Rapaport)

The Michigan State University beam swinger magnet (1) has been installed in the Ohio University Tandem Van de Graaff laboratory. A new time-of-flight system based on the beam swinger and the OU-8000 Minicomputer (2) has been developed and used in a variety of neutron scattering experiments employing the D(d,n), T(d,n) and T(p,n) source reactions. Principal features of the new system are improved resolution and counting rate, reduced background, increased angular range (8° to 160° in scattering experiments), and automatic or semi-automatic control of swinger magnet and scattering sample position. A complete description of the system has been accepted for publication by Nuclear Instruments and Methods.

2. Structure of ^{13}C from an R-Matrix Analysis of ^{12}C+n Scattering and Reaction Cross Sections (Knox, Lane)

Differential cross sections for ^{12}C+n elastic and inelastic scattering and for the $^{12}C(n,\alpha)^9Be$ reaction, together with high resolution total cross section data were analyzed by means of a multilevel multichannel R-matrix program to determine J, π, and $\gamma_{\lambda c}$ for states in ^{13}C up to E_x = 13.5 MeV. Good overall fits to the data were obtained throughout this large energy range. Spin and parity assignments for thirteen states above E_x = 9.5 MeV for which there had been either no previous J^π assignments or only tentative assignments have been made in this study. The present results are in good agreement with previous analyses and model calculations. A paper describing this work has been accepted for publication in Nuclear Physics.

3. Elastic and Inelastic Scattering of 20 - 26 MeV Neutrons from ^{12}C** (Meigooni, Finlay, Randers-Pehrson, Brient, Marcinkowski, Kurup, Rapaport, Mellema)

Elastic and inelastic scattering of 20.8 and 26 MeV neutrons from ^{12}C were studied at the Ohio University beam swinger time-of-flight spectrometer. The

---

* Supported in part by the Ohio University 1804 Fund, the U.S. Department of Energy and the National Science Foundation.

(1) R.K. Bhowmik et al., Nucl. Instrum. Methods 143, 63 (1977)

(2) D.E. Carter, Nucl. Instrum. Methods 160, 165 (1979)

** This investigation was supported by Grant Number CA25193, awarded by the National Cancer Institute, and by NSF Grant PHY 81-08456.

low background and high efficiency of the new spectrometer permit the observation of scattering to α-particle unstable states above 9 MeV. Complete differential cross sections for the ground state, the 2^+ (4.43 MeV) and 3^- (9.63 MeV) have been measured. Partial angular distributions or upper limits for the 0^+ (7.65) state and for more highly excited states have been obtained. Results have been analyzed together with earlier measurements (3) made with conventional techniques at 24 MeV.

4. <u>^{13}C+n</u> (Resler, Koehler, Lane, Knox, Randers-Pehrson)

Differential elastic cross sections for neutrons scattered from ^{13}C have been measured at 37 incident energies from 7.55 MeV to 11.00 MeV. At each energy cross sections were measured at 11 angles between 15° and 160°. These 407 cross sections required less than 2 weeks time on the new TOF facility. Neutrons were produced via the D(d,n) reaction. The source-to-sample distance was 20.5 cm and the flight path was 4.2 m. The scattering sample was 40.75 grams of ^{13}C enriched to 98% and the detector was one 4" x 8" NE213 liquid scintillator coupled to an RCA-4522 photomultiplier tube. Analysis of these elastic data is currently underway and measurements of inelastic cross sections will be made at selected energies in this region later. An R-matrix analysis of these data is planned.

5. <u>^{18}O(n,n)^{18}O and ^{18}O(n,n')^{18}O*</u> (Koehler, Lane)

The study of levels in ^{19}O by means of differential elastic and inelastic scattering of neutrons from ^{18}O is being undertaken to develop a better understanding of the shell model near the opening of the 2s-1d shell. Above E_n = 2.5 MeV ($E_x \cong 6.4$ MeV) no assignments of J or π are known for ^{19}O. The channel ^{18}O+n is essentially the only way to study ^{19}O by a compound nucleus reaction. Preliminary measurements with an enriched $H_2{}^{18}O$ sample were encouraging in several respects, but showed the need for a sample made from a different compound of oxygen so that the weaker inelastic groups from ^{18}O(n,n')^{18}O* could be observed free of the very large scattering peak from hydrogen. Following an extensive search the compound $Si^{18}O_2$ was judged to give the best overall properties for these measurements. The chemistry of preparation of $Si^{18}O_2$ from $H_2{}^{18}O$ such that only very small amounts of hydrogen or other contaminants remain is tedious and time consuming. However, with the collaboration of Professor D. Hendricker of our Chemistry Department, a sample of $Si^{18}O_2$ believed to be low in hydrogen has been produced. Initial elastic and inelastic scattering measurements in the range of $E_n \simeq 5 - 7$ MeV are now underway to determine whether or not the hydrogen contamination is sufficiently low for proper analysis of the weak inelastic peaks.

---

(3) R.W. Finlay *et al.*, Proc. Fourth Sym. on Neutron Dosimetry, Munich (1981), p. 361.

6. Comparison of $|Mn/Mp|^2$ for First and Second 2^+ States of ^{26}Mg* (Tailor, Rapaport, Finlay)

Neutron scattering data from ^{26}Mg at 24 MeV were measured using the Ohio University time-of-flight spectrometer. Coupled-channel analysis of these neutron elastic and inelastic scattering data have been completed. This analysis combined with the similar analysis of proton scattering data (4) at the same energy gives neutron to proton matrix element ratio (Mn/Mp). These results have been compared with those reported by use of various probes along with the most recently revised EM measurements (5).

7. Strong Coupling and Isospin Effects in Neutron Scattering from Se* (Kurup, Finlay, Randers-Pehrson, Brient, Marcinkowski†)

The even isotopes of selenium possess increasing neutron excess but decreasing collectivity as a function of increasing mass. Thus they provide an opportunity to study the competition between isovector and strong coupling effects. Earlier measurements of inelastic neutron scattering (6) and (p,n) reaction (7) have been difficult to explain in this framework (8). The present study attempts to extend the measurements of inelastic neutrons scattering to two-phonon and other higher excited states. $^{80}Se(n,n')$ has been measured at 8 MeV and further experiments are planned. Analysis is in progress.

8. Interaction of 11 MeV Neutrons with ^{89}Y* (Yan **, Brient, Finlay, Randers-Pehrson, Marcinkowski†, Tailor, Rapaport)

Differential cross section for scattering of 11 MeV neutrons by ^{89}Y were measured using the Ohio University beam swinger time-of-flight facility. Measurements were taken in the angular range between 15° and 145°. Empirical optical model parameters have been obtained from the measured elastic scattering data. Deformation parameters were obtained for low-lying excited states using these optical model parameters in a DWBA collective formalism. Comparisons with deformation parameters in neighboring even-even nuclei ^{88}Sr and ^{90}Zr have been made. The weak-coupling model is able to give a qualitative interpretation of neutron inelastic scattering by ^{89}Y.

---

(4) P.F.W. Alons, H.P. Block et al., Nucl. Phys. A367, 41 (1981)

(5) T.K. Alexander et al., Bull. Amer. Phys. Soc. 26, 1127 (1981)

(6) J. Lachkar et al., Phys. Rev. C14, 933 (1976)

(7) Wong, Grimes, Poppe, Brown and Madsen (to be published)

(8) V. Brown et al., Phys. Rev. C24, 2359 (1982)

* Supported in part by National Science Foundation Grant PHY 78-09911.

** Permanent address: Beijing Normal University, Beijing, People's Republic of China.

† Permanent address: Institute for Nuclear Research, Warsaw, Poland.

9. Elastic Scattering of 7.2- and 24-MeV Neutrons from ^{208}Pb* (Dietrich, Kurup, Finlay, Randers-Pehrson, Brient, Meigooni, Marcinkowski**, Mellema, Rapaport)

We have measured differential elastic cross sections from ^{208}Pb using the Ohio University beam-swinger time-of-flight facility (9). These measurements were motivated by conflicts in existing data near 7 MeV (10) and by insufficient differential data at the higher energies to obtain a clear picture of the energy dependence of the optical model. The data were taken in angular steps of 2° and 4° over the angular range 8° to 158°. The high precision of the 7.2 MeV data provides a very strong constraint on the parameters in a conventional optical model analysis. A microscopic folding-model calculation using a density- and energy-dependent central force and the M3Y spin-orbit force yields reasonable agreement with a preliminary analysis of the 24 MeV data and with analyzing-power data (11).

10. Inelastic Scattering to the Continuum* (Marcinkowski**, Randers-Pehrson, Mellema, Meigooni, Kurup, Brient, Tailor, Finlay)

Inelastic scattering of 25.7 MeV neutrons to unresolved final states with excitation energies up to ∿ 13 MeV were measured for monoisotopic samples of ^{51}V, ^{56}Fe, ^{65}Cu, ^{93}Nb and ^{209}Bi. Neutrons were produced via the T(d,n)^{4}He reaction in a gas cell that provided a background-free source spectrum above E_n = 12 MeV. Time-of-flight spectra were taken at seven angles between 25° and 145° using the beam-swinger spectrometer. The technique of dynamic biasing was very valuable in providing maximum detector efficiency and low background throughout the broad range of neutron energies. Data were converted to energy spectra, corrected for detector efficiency, averaged over 1 MeV bins and corrected for sample attenuation and multiple scattering. Analysis of the "pre-equilibrium" angular distributions in terms of the generalized-master-equation model is in progress.

11. Time-of-Flight Resolution in Fast Neutron Scattering Experiments† (Mellema, Finlay, Randers-Pehrson, Graham)

As part of the development of a new time-of-flight spectrometer with improved efficiency and energy resolution, experiments were carried out to identify separate, describe analytically, and to fold together properly the various

---

* Supported in part by National Science Foundation Grant PHY 81-08456.

(9) R.W. Finlay et al., Nucl. Instrum. Methods (to be published)

(10) W.E. Kinney and F.G. Perey, ORNL-4904 (1974)

(11) C. Wong et al., Phys. Rev. 128, 2339 (1962)

** Permanent address: Institute for Nuclear Research, Warsaw, Poland.

† Supported by the National Science Foundation.

contributions to time (and energy) resolution. Measurements and analysis involve: neutron energies from approximately 5 to 25 MeV; flight paths from 3 to 20 meters; and detectors using liquid scintillators ranging from 2" thick by 4½" diameter to 4" thick by 7 3/8" diameter. Results have been used to develop a computer code TOFSIM which simulates time-of-flight experiments and predicts energy and time resolution.

B. NEUTRON REACTIONS

1. Differential Cross Sections for the $^{6}Li(n,\alpha)t$ Reaction (Knox, Koehler, Resler, Randers-Pehrson, Graham, Lane)

Differential cross sections for the $^{6}Li(n,\alpha)t$ reaction have been measured at E_n = 2.0 MeV and 2.5 MeV. The measurements were made using high purity ^{6}LiF and BaF_2 targets on gold backings obtained from Micromatter (Seattle, WA). Analysis of these data is currently underway. These measurements will be extended to higher incident neutron energies later this spring.

2. (n,z) Measurements on ^{58}Ni and Stainless Steel (Graham, Randers-Pehrson, Grimes)

Measurements of (n,p) and (n,alpha) from targets of ^{58}Ni and 316-Stainless Steel were taken at a neutron energy of 8.0 MeV. Measurements were taken at angles of 0, 60 and 120 degrees, and outgoing particles with energies as low as 2 MeV were detected. Later measurements will be made at 9.5 and 11.0 MeV using a technique of subtracting out the D(d,n) breakup neutrons from the source reaction by the neutron yield from the $^{3}He(d,n)$ reaction, as described in a forthcoming paper (12).

3. Carbon Foil Thickness Determination by Proton Backscatter* (Graham, Randers-Pehrson)

Carbon foils of nomial thickness 0.5 to 4 mg/cm^2 on tantalum backings were used in a recent $C(n,\alpha)$ experiment. In order to obtain the proper cross section and to correct for the energy loss of the outgoing α particles, more precise values of the foil thicknesses were desired. The foils were used as targets for 2.0 and 4.0 MeV proton beams, with the thicknesses of the foils determined by the energy shift of protons backscattered through the carbon foils from the tantalum backings as compared with the proton backscattered from bare tantalum, similar to the method of Childs and Lenz (13). Back-scattering from the carbon foil itself was observed as well as structure in the ^{13}N system.

---

(12) Grimes, Grabmayr, Finlay, Graham, Randers-Pehrson and Rapaport, submitted to Nucl. Instrum. Methods

* This investigation was supported by Grant Number CA-25193, awarded by the National Cancer Institute, DHEW.

(13) W.A. Childs and G.H. Lenz, Nucl. Instrum. Methods 95, 441 (1971)

4. A Technique to Correct for Backgrounds Caused by Break-Up Neutrons from the D(d,n) Reaction (Grimes, Grabmayr, Finlay, Graham, Randers-Pehrson, Rapaport)

Use of the D(d,n) reaction as a monoenergetic neutron source for bombarding energies of 5 MeV and higher is complicated by the presence of neutrons lower in energy than those in the monoenergetic peak. These "break-up" neutrons are more numerous than those produced by foils and beam stop. A technique for simulating this spectrum by bombarding a ^{3}He target with deuterons has been developed.

A new target assembly having two gas cells (one filled with D_2 and the other with ^{3}He) has been developed. This assemply allows either of the two cells to be brought on the beam axis and permits deuterium runs to be alternated with ^{3}He runs without having to pump out gas each time.

A paper describing this work has been submitted to Nuclear Instruments and Methods.

C. ANALYSES AND MODEL CALCULATIONS

1. R-Matrix Studies

a. R-Matrix Code Development (Knox)

The original Ohio University R-Matrix Analysis Program (ORMAP) for analyzing neutron elastic scattering data has undergone several revisions in the last few years to include the neutron inelastic scattering channel and neutron induced charged particle reactions in structure studies. During the past year an additional option was added to the code, namely, the calculation of neutron polarization for the neutron elastic scattering channel. Work is now underway to include in the program the additional option of calculating charged particle elastic scattering cross sections. With the completion of this work the resulting code will be one of the most sophisticated in existence, allowing future structure studies to include both neutron and charged particle channels leading to states in the compound nucleus.

b. Studies of the ^{7}Li System (Knox, Lane, Sadowski)

The most recent evaluation (14) of the ^{6}Li(n,α)t reaction provides cross sections recommended for standard uses below 100 keV. Over the 240 keV resonance integrated cross sections from this evaluation are unitarily consistent and in agreement with experimental data. Predictions for the differential ^{6}Li(n,t)α cross section are, however, not in agreement with existing

---

(14) G.M. Hale in Neutron Standards Applications (NBS Special Publication 493) (1977) p. 30

data in some energy regions. On the high energy side of this resonance the current evaluation fails to give the proper forward-to-backward cross section ratio when compared with the measurements of Brown et al. (15) of $\sigma_{n,t}(0°)$ and $\sigma_{n,t}(180°)$ from the $T(\alpha,{}^6Li)n$ reaction and of Overley et al. (16) from ${}^6Li(n,t)\alpha$ reaction. This disagreement is probably due to the omission from the analysis of some as yet unknown level (or levels) at higher excitation energies.

With a better understanding of the structure of the ${}^7Li$ system and consequent better cross section evaluations, the range of applicability of the ${}^6Li(n,t)\alpha$ reaction as a standard might be increased. To this end a comprehensive R-matrix analysis of the ${}^7Li$ system has been undertaken. The neutron elastic, inelastic and (n,t) channels are currently being analyzed and with program additions described above, the t-α channel will be included later.

c. ${}^{11}B(n,n){}^{11}B$ and ${}^{11}B(n,n'){}^{11}B^*$ (2.12, 4.45, 5.02 MeV) (Koehler, Resler, Lane, Knox)

In the past year we have carried out extensive R-matrix analysis on our elastic and inelastic (2.12 MeV) differential cross section results as well as the previous elastic data of White et al. (17) for $2 \leq E_n \leq 8$ MeV. These new results are generally in agreement with the previous results of White et al. which were obtained by fitting differential elastic data only. All but one of the levels used by White et al. are present in our new R-matrix analysis. However, the large size of the 2.12 MeV level Legendre coefficients B_0 and B_2 necessitated the inclusion of several new levels for $E_n \geq 5$ MeV.

These new results from the R-matrix analysis are being compared to shell model calculations performed by J. Millener of Brookhaven National Laboratory. There is fairly good agreement between theory and experiment for $E_x \lesssim 7$ MeV. The spin and parities as well as reduced widths for most of the levels up to this energy are in good agreement although the energies of the negative parity states appear to be consistently low for the shell model calculations while the calculated positive parity states are consistently high though by a lesser amount. Above $E_x \approx 7$ MeV it appears that the levels in ${}^{12}B$ are many and the mixing may be strong. Comparison between theory and experiment is difficult. Both theory and experiment agree that this energy region in ${}^{12}B$ appears to be dominated by many negative parity states, though a level by level comparison is not easily made.

---

(15) Brown, Ohlsen, Hagland and Jarmie, Phys. Rev. C16, 513 (1977)

(16) Overley, Sealock and Ehlers, Nucl. Phys. A221, 573 (1974)

(17) White, Lane, Knox and Cox, Nucl. Phys. A340, 13 (1980)

From an applied point of view, since the inelastic cross sections for the 2.12 and 4.45 MeV levels are of considerable size, our survey of this region should help provide a good knowledge of the inelastic cross sections for ^{11}B needed for proper shielding design for fusion reactors employing boron ($\sim$ 80% ^{11}B) as a shielding constituent.

2. Model Calculations

a. Microcomputer Usage (Resler, Carter)

During the past several months we have been doing shell model calculations on the Los Alamos National Laboratory computer system, using a telephone modem connected to a terminal at Ohio University. We have recently adapted an Intel* SDK-85 System Design Kit to interface our terminal, the Ohio University IBM 370-IBM 4341 system via a hardwired modem and the Los Alamos computer system via a telephone modem. This system is built around an Intel 8085 microprocessor, three Intel 8251A programmable communication interfaces, 4K of ROM and $4\frac{1}{2}$ K of RAM. An operating system has been developed which allows the user at the terminal to do various tasks with the microcomputer. Three main modes of operation are defined as follows: (1) using the terminal with the OU computer system; 2) using the terminal with the Los Alamos computer system via the telephone modem; and 3) using the terminal with the Los Alamos computer system while recording the session on the OU computer system. We also have the ability to transfer files from one computer to the other. This allows us to prepare input files on our computer before using the phone connection to Los Alamos, thus minimizing telephone expenses. Also we are able to transfer output to our computer system from Los Alamos so we can get line printer output here. Possible system functions for the future might include such things as having our computer automatically calling up the Los Alamos computer system to start a job and then later check on its completion. This automation will further reduce telephone expenses.

b. Shell Model Calculations (Grimes, Lane, Resler, Koehler, Knox)

Through a telephone link, calculations utilizing the shell model code VLADIMIR are now being carried out at the Los Alamos National Laboratory. This code was originally developed at Livermore and the author, R.F. Hausman, is now at Los Alamos and has the code operational there.

We are presently testing two-body matrix elements and single particle energies for nuclei near A = 16. The calculations will eventually focus on ^{14}C and ^{19}O (to interpret the n+^{13}C and n+^{18}O reactions). A closed ^{4}He core is assumed. Our first goal is to adjust the shell model parameters to fit the spectra of ^{15}O and ^{17}O; with these values for the single particle energies and two-body matrix elements we will calculate the spectra for ^{14}C and ^{19}O. This work is being carried out in collaboration with G.F. Auchampaugh of Los Alamos.

* Intel Corporation, 3465 Bowers Avenue, Santa Clara, CA 95051.

We are also continuing development of a series of sub-routines to facilitate use of VLADIMIR in level density calculations. This work will utilize moment expansions to calculate level densities with complete inclusion of two-body effects. Collaborators in this work are S.D. Bloom and H. Vonach of Livermore and R.F. Hausman of Los Alamos.

PACIFIC NORTHWEST LABORATORY

A. DELAYED NEUTRON STUDIES

1. Delayed Neutron Emission Probabilities (P_n) (P. L. Reeder and R. A. Warner)

Measurements of P_n values will be performed at the TRISTAN on-line mass separator facility at Brookhaven National Laboratory using a beta-neutron coincidence counting technique. This technique eliminates the beta counting efficiency and its associated uncertainty from the expression used to calculate P_n values.

2. Delayed Neutron Average Energies ($\bar{E}$) (P. L. Reeder and R. A. Warner)

Our 1978 measurements of the average energies of neutrons from Rb and Cs precursors have now been published.[1] We have also published a compilation of average energy measurements for individual precursors. The "best values" for delayed neutron average energies were weighted by the fission yields and P_n values and then summed to give average energies of group and equilibrium delayed neutron spectra.[2]

The neutron counter used in our ring ratio technique to get average energies has been recalibrated to obtain the efficiency and ring ratio as a function of neutron energy. Monoenergetic neutrons were obtained by the $^{51}V(p,n)^{51}Cr$ and $^{57}Fe(p,n)^{57}Co$ reactions. Neutrons were counted with the detector on-line. Residual radioactivity in the targets was counted off-line. The efficiency curve is now defined by 12 points in the energy region 10-1300 keV instead of the 3 points in the previous calibration with photoneutron sources.

3. Delayed Neutron Half-Lives (P. L. Reeder and R. A. Warner)

Additional delayed neutron decay curves have been measured at the TRISTAN facility this year to determine whether Sr, Y, Ba, and La isotopes at mass numbers 97, 98, 99, 146, 147, 148 are delayed neutron precursors. The present results give little support for the existence of Sr and Ba precursors at these mass numbers. We do have evidence for delayed neutrons from ^{97}Y, ^{99}Y, ^{147}La, and ^{148}La. Measurements of P_n and $\bar{E}$ for these precursors are in progress.

---

[1] P. L. Reeder and R. A. Warner, "Measurement of Average Neutron Energies by a Counting Rate Ratio Technique" Nucl. Instrum. Methods 180, 173 (1981).

[2] P. L. Reeder and R. A. Warner, "Average Energy of Delayed Neutrons from Individual Precursors and Estimation of Equilibrium Spectra," Nucl. Sci. Eng. 79, 56 (1981).

4. Beta-Delayed Two-Neutron Emission (P. L. Reeder and R. A. Warner)

Beta-delayed two-neutron emission has been observed in ^{98}Rb. The probability per beta decay for emission of two neutrons is 0.060±0.009%. The results have been published.[3]

A search for two-neutron emission at mass numbers 96, 97, and 99 gave negative results. The upper limits on two neutron emission are <0.004, <0.008, and <0.024% for ^{96}Rb, ^{97}Rb, and ^{99}Rb, respectively. These results were reported at the International Conference on Nuclei Far From Stability.[4]

5. Gamma Rays Following Delayed Neutron Emission (P. L. Reeder and R. A. Warner)

Gamma rays in coincidence with delayed neutrons provide information on which levels in the final nucleus are populated by delayed neutron emission. In some cases, neutron emission goes to levels which are not fed by direct beta decay. Theoretical calculations based on various models of beta decay can predict the neutron intensity to these various levels. The partial neutron emission probability to a particular level, P_n^i, is a more sensitive test of the model chosen than just the P_n alone.

We have recently measured gamma rays in coincidence with delayed neutrons by placing a Ge detector inside our high efficiency neutron counter. Rb and Cs precursors from the TRISTAN on-line isotope separator were deposited on a moving tape system at a spot close to the Ge detector. Gamma spectra have been obtained for $^{95-98}$Rb and $^{143-147}$Cs precursors. The number of gamma rays in coincidence with neutrons varies from 1 in the case of ^{143}Cs to more than 35 in the case of ^{146}Cs. The spectra are currently being analyzed to obtain partial neutron emission probabilities, P_n^i.

---

[3] P. L. Reeder, R. A. Warner, T. R. Yeh, R. E. Chrien, R. L. Gill, M. Shmid, H. I. Liou, and M. L. Stelts, Phys. Rev. Letters 47, 483 (1981).

[4] P. L. Reeder, R. A. Warner, T. R. Yeh, R. E. Chrien, R. L. Gill, H. I. Liou, M. Shmid, and M. L. Stelts, Int. Conf. Nuclei Far From Stability, Helsingor, Denmark, June 7-13, 1981, CERN 81-09.

B. <u>ISOMER YIELDS</u> (P. L. Reeder and R. A. Warner)

Experiments are currently in progress to measure independent isomer yield ratios for thermal neutron induced fission of ^{235}U. Fission products from a neutron pulse from a TRIGA reactor are mass analyzed by the SOLAR on-line mass spectrometer. The first cases being studied are ^{90}Rb and ^{138}Cs. The half-lives of these isomers are long enough so that samples will be collected on a catcher foil and counted off-line to determine the yield ratios. Future experiments will include measurements on In, Br and I isomers.

C. <u>GAS SCINTILLATION PROPORTIONAL COUNTER FOR NEUTRON SPECTROMETRY</u> (R. A. Warner, H. E. Palmer, and P. L. Reeder)

A high efficiency, high resolution neutron spectrometer based on the gas scintillation proportional counter principle is currently under development. Neutrons will be captured in a high pressure, large volume cell of ^{3}He plus a small amount of Xe. Scintillation light from the Xe will be detected by a photoionization counter containing Tetrakis-(dimethylamino)-ethylene (TMAE). This detector will be used for a variety of neutron spectrometry experiments including coincidence measurements on delayed neutron precursors.

"REPORT FOR DOE-NDC 2/12/82"

UNIVERSITY OF PENNSYLVANIA

A. COMPLETED WORK

1. "Energy levels of Light Nuclei: A = 13-15"

   This paper has been published in Nuclear Physics A360 (1981) p. 1-186.

   F. Ajzenberg-Selove

2. "Energy levels of Light Nuclei: A = 16-17"

   This paper has been published in Nuclear Physics A375 (1982) p. 1-168.

   F. Ajzenberg-Selove

B. WORK IN PROGRESS

A review paper on A = 18-20 is being prepared, to be submitted for publication in July or August 1982. The preliminary version of A = 18 has been sent out as a preprint (PPP 4-81) in August 1981; A = 19 was sent out as PPP 5-81 in December 1981. The preliminary version of A = 20 is completed and will be sent out for comments as PPP 1-82 in March 1982. Our work is proceeding on schedule.

F. Ajzenberg-Selove and G. C. Marshall

RENSSELAER POLYTECHNIC INSTITUTE

A. NUCLEAR DATA

1. Fission Cross Section Measurements of ^{244}Cm, ^{246}Cm and ^{248}Cm+

(C.R.S. Stopa, H.T. Maguire, Jr.*, D.R. Harris, R.C. Block, R.E. Slovacek (KAPL), J.W.T. Dabbs (ORNL), R. Hoff, R. Lougheed (LLL)

The RINS (Rensselaer Intense Neutron Spectrometer) system, which includes a 75-ton lead slowing-down-time spectrometer and the RPI 100-MeV electron linac, has been used to measure the neutron-induced fission cross section of ^{244}Cm, ^{246}Cm and ^{248}Cm.(1,2,3) These isotopes have either large spontaneous fission background (e.g., ^{248}Cm) or large alpha decay rates (e.g., ^{244}Cm), and it required the high neutron intensity of the RINS System to carry out these measurements. Preliminary measurements of ^{248}Cm(2) and ^{246}Cm and ^{248}Cm(3) have been reported previously, and this paper includes the earlier results, combined with the results of a recent measurement in which all three isotopes were measured simultaneously. The fission chamber consists of five pairs of hemispherical electrodes contained in 2 atm of methane, and for the latest measurements the electrodes were coated with ^{244}Cm (5.2 μg), ^{246}Cm (17 μg), ^{248}Cm (35 μg), ^{235}U and ^{252}Cf. The ^{235}U chamber was used for normalization, and the ^{252}Cf chamber monitored any effects caused at early slowing-down times by the linac gamma flash or by RF pickup from the pulsing of the accelerator.

These measurements span the energy range from 0.1 eV to 100 keV. The data below ∿20 eV are the first obtained in this energy range, and the data above ∿20 eV complement the nuclear explosion time-of-flight measurements.(4) Low energy resonances have been resolved at 7.7, 17, 23 and 35 eV in ^{244}Cm; 4.3 and 15 eV in ^{246}Cm, and 7.3, 27 and 76 eV in ^{248}Cm. Parameters will be determined for these resonances.

*Now at Westinghouse Electric Corporation, Pittsburgh, PA

---

[1] R. E. Slovacek, D. S. Cramer, E. B. Bean, J. R. Valentine, R. W. Hockenbury and R. C. Block, Nucl. Sci. and Eng., 62, 445 (1977).

[2] H. T. Maguire, Jr., C. R. S. Stopa, D. R. Harris, R. C. Block, R. E. Slovacek, R. W. Hoff and J. W. T. Dabbs, Trans. Amer. Nuc. Soc., 38, 648 (1981).

[3] R. C. Block, H. T. Maguire, Jr., C. R. S. Stopa, D. R. Harris, R. E. Slovacek, R. W. Hoff, R. Lougheed and J. W. T. Dabbs, Trans. Amer. Nuc. Soc., 39, 876 (1981).

[4] M. S. Moore and G. A. Keyworth, Phys. Rev. C, 3, 1656 (1971).

B. SAFEGUARDS AND FISSILE ASSAY

1. The Applicability of the Lead Slowing Down Spectrometer For Non-Destructive Assay of Commercial-Size Fuel Elements

(F.W. Bornt, Jr.*, D.R. Harris and R.C. Block)

Fissile assay sensitivity measurements were carried out with the 75-ton Slowing Down Time Assay Device and a 10-cm-dia. cylinder of depleted U_3O_8, which simulates a 1/3 section of a PWR fuel element. A 26 gram sample of 93.3% enriched ^{235}U was placed inside and at various positions on the surface of the U_3O_8 cylinder, and the assay sensitivity for ^{235}U detection in the center relative to the surface of the cylinder exceeds 90% over the range of neutron interrogation energies from 0.1 to 1500 eV. Further measurements are planned for a simulated full section of a fuel element to determine the sensitivity to fissile assay at any position inside of a fuel element.

*Now at Westinghouse Electric Corporation, Pittsburgh, PA

A. NEUTRON PHYSICS

1. Helium Generation Cross Sections for 14.8-MeV Neutrons

(D. W. Kneff, B. M. Oliver, M. M. Nakata, and Harry Farrar IV)

Neutron-induced helium generation is a major consideration in the development of materials for fusion reactor components. Rockwell International is engaged in two programs to measure total helium generation cross sections for fast neutrons. The Department of Energy's Office of Basic Energy Sciences is sponsoring the measurement of the cross sections of a large range of separated isotopes and their associated pure elements for fast (8-15 MeV) monoenergetic neutrons. The Office of Fusion Energy is supporting cross section measurements of other fusion-related materials in the ~14.8-MeV T(d,n) neutron field, plus helium generation cross section measurements in the broad energy spectrum of the Be(d,n) neutron environment.

The OBES cross section measurements are made by irradiating small (~10-20 mg) samples of a wide range of pure elements and separated isotopes in a nearly monoenergetic neutron spectrum. The amount of helium generated in each sample is subsequently measured by high-sensitivity gas mass spectrometry. The neutron fluence distribution for the irradiation volume is mapped using a comprehensive set of radiometric plus helium accumulation neutron dosimeters, and then combined with the helium generation measurements for multiple samples of each material to deduce cross sections. Absolute fluence normalization is based on the ^{93}Nb(n,2n)^{92m}Nb cross section; the fluence mapping is the dominant source of uncertainty in the cross section measurements.

Irradiations performed to date have utilized the ~14.8-MeV neutron spectra from the T(d,n) Rotating Target Neutron Sources-I and -II (RTNS-I,II) at the Lawrence Livermore National Laboratory. Previous 14.8-MeV cross section measurements, based on two RTNS-I irradiations, have been summarized in earlier Reports to the DOE Nuclear Data Committee.[1,2] Since the last report, cross sections have been determined for V and Zr from RTNS-I, and for 13 pure elements and 18 separated isotopes from RTNS-II. The RTNS-II results are given in Table A-1. Also given in Table A-1 are our adopted cross section values, based on helium production measurements from both RTNS-I and RTNS-II irradiation experiments.

Helium production measurements for Li, ^{6}Li, ^{7}Li, O, F, and Cr from RTNS-II are also near completion. These materials (with the exception of chromium) were irradiated as polycrystalline compounds (e.g., LiF, PbF_2, PbO)

[1] Kneff, Oliver, Nakata, and Farrar, BNL-NCS-27800, p. 181 (1980)

[2] Kneff, Oliver, Nakata, and Farrar, BNL-NCS-29426, p. 155 (1981)

TABLE A-1

Total Helium Generation Cross Sections for ~14.8-MeV Neutrons

Material	Cross Section (mb) RTNS-II Measurement	Adopted Value[a]	Material	Cross Section (mb) RTNS-II Measurement	Adopted Value[a]
Si	218 ± 11	218 ± 11	Zr	10.1 ± 0.7	10.1 ± 0.7
V	18.5 ± 1.3	18.6 ± 1.3	Nb	14 ± 1	14 ± 1
Fe	49 ± 3	48 ± 3	Mo	14 ± 1	14 ± 1
^{54}Fe	94 ± 7	91 ± 7	^{92}Mo	31 ± 2	31 ± 2
^{56}Fe	47 ± 3	46 ± 3	^{94}Mo	22 ± 2	22 ± 2
^{57}Fe	33 ± 2	33 ± 2	^{95}Mo	17 ± 1	17 ± 1
^{58}Fe	20 ± 2	20 ± 2	^{96}Mo	12 ± 1	12 ± 1
Co	40 ± 3	40 ± 3	^{97}Mo	10 ± 1	10 ± 1
Ni	101 ± 7	100 ± 7	^{98}Mo	22 ± 2[b]	--
^{58}Ni	126 ± 9	121 ± 8	^{100}Mo	3.8 ± 0.3	3.8 ± 0.3
^{60}Ni	80 ± 6	80 ± 6	Sn	1.5 ± 0.1	1.5 ± 0.1
^{61}Ni	49 ± 4	51 ± 4	Pt	0.74 ± 0.11	0.74 ± 0.11
^{62}Ni	22 ± 2	22 ± 2	Au	0.50 ± 0.04	0.50 ± 0.04
^{64}Ni	9 ± 1	9 ± 1	Pb	0.62 ± 0.05	0.62 ± 0.05
Cu	51 ± 4	51 ± 3			
^{63}Cu	64 ± 5	65 ± 5			
^{65}Cu	17 ± 1	17 ± 1			

[a] Based on both RTNS-I and RTNS-II measurements.

[b] Isotopic material suspect

in platinum capsules. Other irradiated materials include Be, B, N, Mn, W, and selected separated isotopes of B, Ti, Cr, Sn, W, and Pb. The analyses of several of these materials have been initiated.

TRIANGLE UNIVERSITIES NUCLEAR LABORATORY

A. NEUTRON SCATTERING EXPERIMENTS

1. Brief Overview (A. Beyerle,* R. C. Byrd, J. Dave, J. P. Delaroche,** C. E. Floyd, P. P. Guss, C. R. Gould, G. Honore, C. Howell, S. M. El-Kadi,*** H. W. Lewis, K. Murphy, H. Pfutzner, R. Pedroni, F. O. Purser,+ L. W. Seagondollar, P. Thambidurai,++ G. Tungate,+++ R. L. Walter)

Measurements and analysis of neutron elastic and inelastic scattering have been conducted in the energy range 8 to 17 MeV for nuclei between A=10 and A=208. One aspect involves optical model analysis of elastic scattering data and coupled channels analysis of discrete inelastic scattering data for low lying states. Another aspect involves measurements of neutron evaporation spectra following inelastic scattering to unresolved highly excited states.

Major programs in polarized neutron scattering and in (p,n) reaction studies are carried on with much of the same apparatus and with many of the same personnel. Information gained from these research efforts has been incorporated into reaction model analyses, and has lead to improved parameterizations and evaluations of experimental results obtained here and elsewhere. These programs and the fast neutron radiative capture work are discussed in the TUNL progress report for 1981 (TUNL XX) but are not discussed further here.

The mechanical parts of the time-of-flight system continue to be improved. Simultaneous measurements at 16° on either side of the beam line are now possible following modifications to the detector support carts. Light emitting diodes have been glued on either side of the neutron detector faces and provide a precise visual location of the detectors inside the collimating shields. This makes positioning of the tungsten shadow bars much easier.

All data acquisition and analysis is carried out on the new

*. Present address: EG and G, Inc., San Diego, Cal.
**. Permanent address: Centre d'Etudes de Bruyeres-le-Chatel, France.
***. Present address: Al Fatah University, Tripoli, Libya.
+. Present address: LANL, Los Alamos, New Mexico.
++. Presently associated with the ^{11}C project at TUNL.
+++. Present address: Max Planck Institute, Heidelberg, West Germany.

VAX-11/780 computer. Codes to handle both polarized and unpolarized neutron scattering experiments have been developed. Simulation programs have been written to analyze the various factors entering into the resolution observed in neutron time of flight experiments. The Monte Carlo codes used to correct for multiple scattering and finite source size effects have been installed on the VAX. The corrections for the neutron evaporation spectra measurements are particularly involved and the code for making these calculations is under test.

2. Studies in the 1p Shell Between 7 and 15 MeV (Gould)

a. ^{10}B, ^{11}B Cross Sections

The ^{10}B and ^{11}B results have been accepted for publication in Nucl. Sci. and Eng. The abstract follows:

"Neutron cross sections have been measured for ^{10}B and ^{11}B. Elastic angular distribution data for ^{10}B are reported for incident neutron energies of 8.0, 9.0, 10.0, 11.0, 12.0, 13.0 and 14.0 MeV. Elastic scattering data and inelastic scattering data for states at excitation energies of 2.14, 4.46 and 5.04 MeV in ^{11}B are reported for incident neutron energies of 8.0, 9.0, 9.7, 9.9, 11.0, 12.0, 13.0 and 14.0 MeV. Legendre coefficients for angular distributions are obtained. All data are corrected for finite geometry and multiple scattering effects through a light element Monte Carlo code. The angle-integrated data for ^{11}B are in disagreement with ENDF-IV for the higher neutron energies."

Additional cross-section data on ^{10}B and ^{11}B were obtained at 15 MeV to complement an analysis of the spin-orbit interaction in light nuclei. These data will also be used in the extension of the Lane model from ^{9}Be to the boron isotopes.

b. ^{13}C Cross Section

This work has been submitted for publication in Nuclear Science and Engineering. The abstract is as follows:

"Fast neutron scattering cross sections have been measured for ^{13}C. Angular distributions for elastic scattering over an angular range from 20° to 155° are presented for incident neutron energies of 9.97, 11.96, 13.94, 15.94 and 17.92 MeV. Inelastic scattering data were obtained at 9.97 MeV for states at excitation energy 3.09 MeV and for the unresolved states at 3.68 and 3.85 MeV. The data were corrected for finite sample and source effects using a Monte Carlo simulation. Legendre polynomial coefficients for angular distributions and Optical Model fits to the elastic scattering data are reported."

The integrated elastic cross sections are compared to the total neutron cross section results of Auchampaugh et al.[1] and Cohn et al.[2] in Fig. A-1.

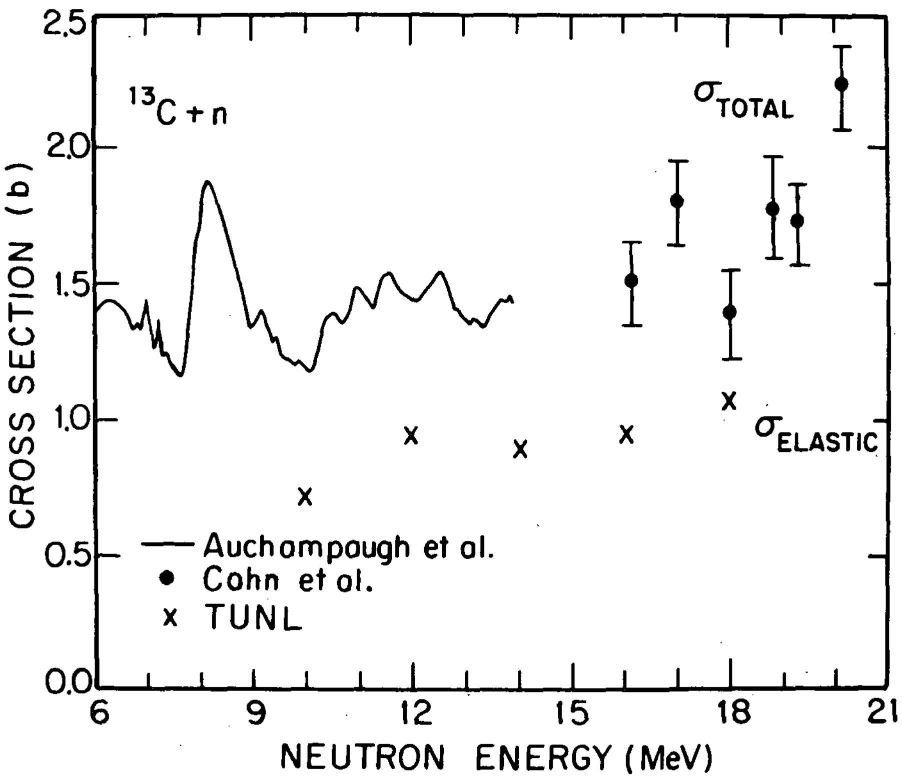

Fig. A-1. Extracted total elastic cross section compared to total elastic plus inelastic cross section.

1. G. F. Auchampaugh et al. , Nucl. Sci. and Eng. 69 (1979) 30.
2. H. O. Cohn et al. , Phys. Rev. 122 (1961) 534.

c. Optical Model Calculations for 1p-shell Nuclei

The applicability of the Spherical Optical Model (SOM) to nucleon scattering from light nuclei continues to be investigated at TUNL. The model reproduces experimental cross sections well when the total neutron cross sections vary smoothly with energy. The agreement is not as good when resonance structure is present, however the model still reproduces the gross features adequately.

The total neutron cross section for ^{13}C exhibits moderate structure throughout the 10 to 18 MeV region. SOM calculations were attempted using the computer code GENOA of F. Perey. The potential has the standard Woods-Saxon real term, derivative Woods-Saxon surface imaginary term and a spin-orbit term. Fig. A-2 depicts the best fit obtained to the experimental data. The parameters found for ^{13}C are:

$$
\begin{aligned}
V_o &= 55.23 - 0.514E \\
r_o &= 1.204 \\
a_o &= 0.520 \\
W_d &= 7.54 + 0.134E \\
r_i &= 1.366 \\
a_i &= 0.221 \\
V_{so} &= 5.500 \\
r_{so} &= 1.120 \\
a_{so} &= 0.380
\end{aligned}
$$

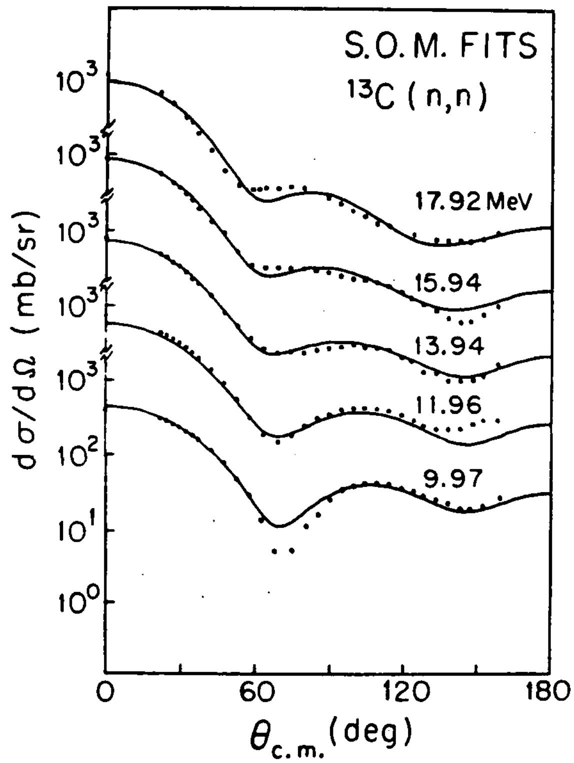

Fig. A-2. Spherical optical model fits of the data using "averaged geometry" parameters for n + ^{13}C.

A search for an SOM parameter set which varied smoothly with bombarding energy and target mass and which reproduced the general features of nucleon scattering for several nuclei was also attempted. An extensive search using 45 neutron scattering angular distributions from 1p-shell elements was carried out. Fits obtained using fixed geometry were not satisfactory, so a linear mass dependence to the parameter r_o was introduced. This improved the fits considerably. All the parameters were comparable to those obtained for heavy nuclei except the imaginary diffuseness term, which was found to be unusally small.

The best agreement was obtained for neutron scattering from ^{6}Li, ^{7}Li, ^{9}Be, ^{10}B and ^{11}B. The discrepancies observed for ^{12}C, ^{13}C and ^{16}O were not surprising since resonance structure in the total cross section is quite prominent for these nuclei. Predictions for proton scattering from ^{10}B, ^{9}Be and ^{6}Li were also in reasonable agreement with the experimental data. The global parameters obtained are:

$$
\begin{aligned}
V_o &= 45.14 - 0.0204E + 23.48(N\pm Z)/A + V_c \\
r_o &= 1.508 - 0.0133A \\
a_o &= 0.5 \\
W_d &= 11.32 + 0.237E + 16.08(N\pm Z)/A \\
r_i &= 1.353 \\
a_i &= 0.200 \\
V_{so} &= 5.5 \\
r_{so} &= 1.15 \\
a_{so} &= 0.5 \\
r_c &= r_o
\end{aligned}
$$

where the positive sign applies to protons and negative sign applies to neutrons. The Coulomb correction term ($V_c = 0.4Z/A^{1/3}$) drops out for neutron scattering. These results are currently being prepared for publication.

3. Neutron Scattering from Medium Mass Nuclei (Walter)

a. ^{40}Ca Cross Sections

In collaboration with W. Tornow, E. Woye and G. Mack from Tübingen, cross-section data were obtained for elastic scattering from ^{40}Ca at 10, 12, and 14 MeV. The data and related calculations have been submitted for publication in Nuclear Physics. Dr. H. Leeb of Vienna collaborated in this work. The abstract follows:

"The analyzing power and differential cross section for elastic neutron scattering from calcium have been measured at 9.9, 11.9 and 13.9 MeV using the $^{2}H(d,n)^{3}He$ source reaction and neutron time-of-flight techniques to detect the scattered neutrons. Polarized neutron beams were produced via the polarization transfer reaction $^{2}H(\vec{d},\vec{n})^{3}He$ at $\Theta = 0^{o}$. The data have been corrected for finite geometry and multiple scattering effects. None of the global neutron-nucleus optical model parameter sets usually referred to in the literature reproduces the present cross-section and analyzing power data. Individual as well as global fits of the data resulting from new optical model searches are presented. It is shown that a recent empirical determination of the real part ΔV_C of the Coulomb correction term is probably in question. Our imaginary Coulomb correction term ΔW_C agrees quite well with both a very recent empirical determination and theoretical studies. Although the quality of the fits to the data can be improved by adding ℓ-dependent potentials to the general optical potential, no definite conclusions can be drawn from the present data as to whether or not ℓ-dependent potentials are important in neutron-calcium scattering in the energy range investigated. The data have also been analyzed using a Fourier-Bessel-series description of the real central optical potential. Comparing the χ^2 values, the experimental data are better reproduced by the Fourier-Bessel method than by our Woods-Saxon optical model analyses. The Fourier-Bessel potentials obtained show strong deviations from the standard Woods-Saxon shape but are in good agreement with calculations using the nuclear structure approach."

b. Elastic and Inelastic Scattering from $^{54,56}Fe$ and $^{63,65}Cu$

Cross-section measurements for the isotopes $^{54,56}Fe$ and $^{63,65}Cu$ comprised the major portion of the thesis of S. M. El-Kadi (Duke University). The abstract follows:

"Neutron differential elastic and inelastic scattering cross sections have been obtained for an incident neutron energy range between 8 and 14 MeV for ^{54}Fe, ^{56}Fe, ^{63}Cu and ^{65}Cu. These measurements provide cross section data for nuclear fusion reactor design.

Elastic scattering cross sections have been analyzed using a spherical optical model to obtain global parameters that can predict necessary neutron elastic scattering cross sections in the mass and energy ranges of the present work.

The global parameters have been used to calculate the volume integral and the rms radius of the central real potential. The matter radii as well as the neutron radii then have been deduced.

Coupled channels (CC) calculations were performed for elastic and inelastic scattering data assuming the harmonic vibrational model. The anharmonicity effect on the predictions of the cross section has been considered for ^{56}Fe by inserting the reorientation matrix element in the CC calculations. Good fits have been obtained for both elastic and inelastic scattering cross sections of ^{54}Fe and ^{56}Fe. The quadrupole deformation parameters obtained are in good agreement with those deduced from Coulomb excitation measurements.

The coupled channels calculations for ^{63}Cu and ^{65}Cu isotopes have been carried out using the weak particle-core coupling model. The quadrupole deformation parameters obtained are comparable with the corresponding deformations for the even core nuclei."

The analysis of the data involved coupled-channels calculations and use of the code ECIS79 written by J. Raynal of France. Test calculations were done in August (1980) during a visit of J. Raynal to TUNL, and the first cross-section analyses were initiated in January (1981) during a visit of J. P. Delaroche of Bruyeres-le-Chatel, France.

c. $^{58,60}Ni$ Cross Sections

Cross-section data for $^{58,60}Ni$ have been obtained at 8, 10, 12, and 14 MeV. The data were reported at the Baltimore APS Meeting. Spherical optical model and coupled-channels calculations have been made to describe these data, as well as 24 MeV data obtained at Ohio University (R. W. Finlay, private communications) and polarization data obtained at 10 and 14 MeV at TUNL. Samples of the cross-section data and calculations are shown in Fig. A-3.

Both models, SOM and CC, give a reasonable description of available $^{58,60}Ni(n,n)$ data for σ and $A(\Theta)$. The energy range covered in our searches is 8 to 24 MeV. From the CC analyses, values were derived for β_{nn} and β_{so}. Earlier Ni(p,p) data were reanalyzed using a Lane-consistent approach so that comparison could be made between β_n and β_p. Reasonable descriptions were found for both types of Ni(N,N) processes.

The CC analysis followed the SPRT method developed at Bruyeres-le-Chatel, but an inverse procedure from that customarily used was employed by us. Nevertheless, we obtained a fairly good description of the total cross section from 100 keV to 30 MeV with our potential parameters.

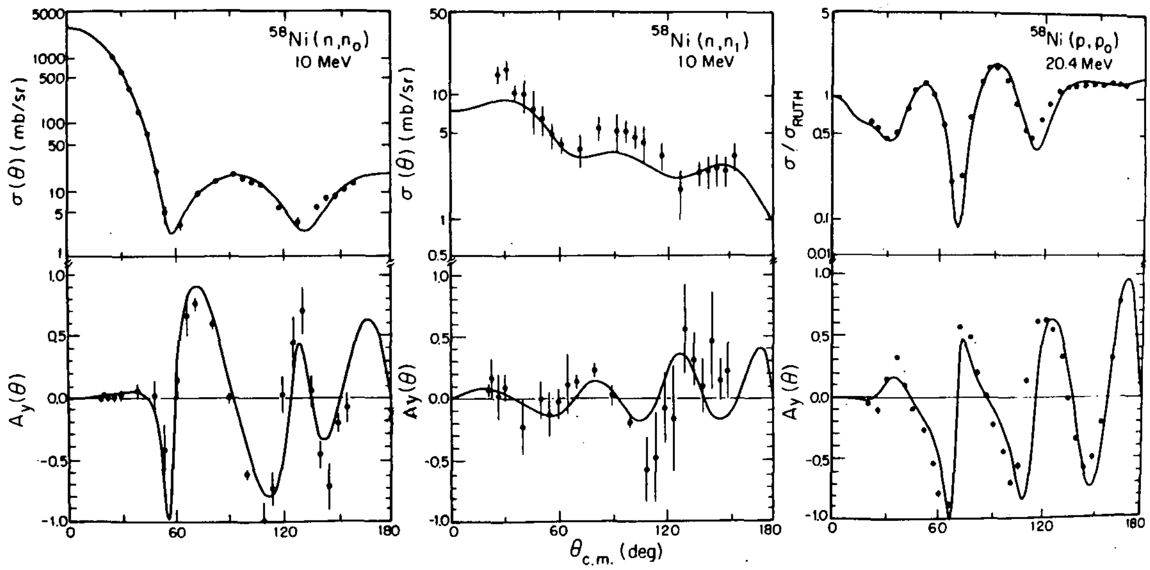

Fig. A-3. Data and coupled-channels calculations for ^{58}Ni(N,N).

d. $^{116,120}Sn$ Cross Section

Cross-section data for $^{116,120}Sn$ at 10 and 14 MeV and for ^{120}Sn at 17 MeV are now in final form. Due to an error in the input to the Monte Carlo multiple scattering code, the data at 14 and 17 MeV had to be reprocessed. These data along with TUNL polarization data at 10 and 14 MeV are being used in spherical and deformed optical model studies.

e. ^{208}Pb Cross Section

The measurements for ^{208}Pb at 10 and 17 MeV have been completed. This gives TUNL data sets at 10, 14 and 17 MeV to complement the previously reported 9, 11, 20 and 26 MeV data of Rapaport et al. at Ohio University. All these data plus TUNL polarization results at 10 and 14 MeV were incorporated in optical model studies. Some cross-section results are compared to SOM calculations in Fig. A-4.

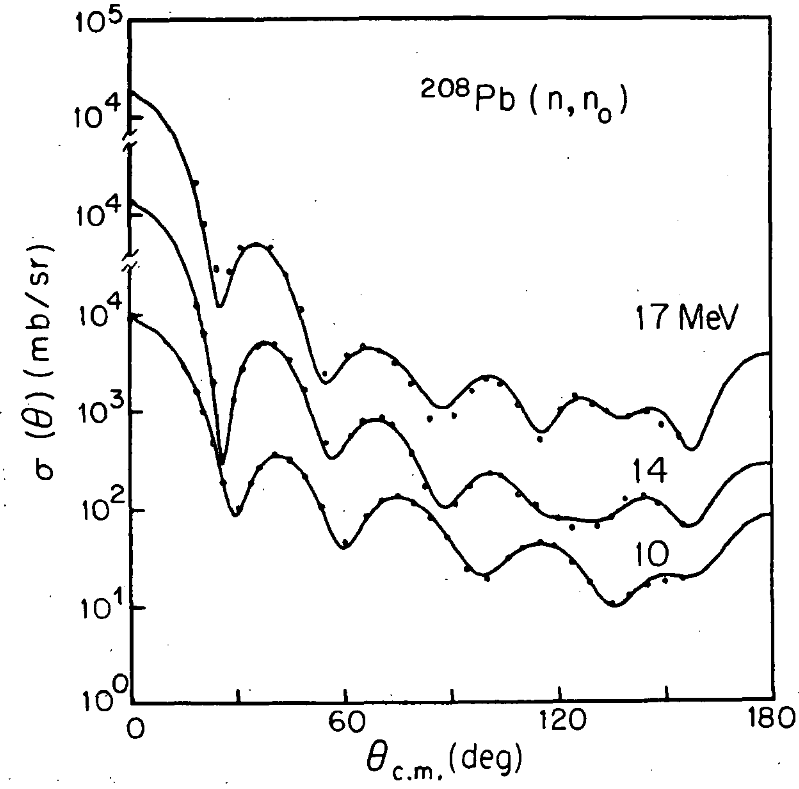

Fig. A-4. Measured cross sections for $^{208}P(n,n)^{208}Pb$.

B. NEUTRON SOURCE REACTION STUDIES

1. Tritium Break-up Contribution to the Neutron Source Reaction $^3H(p,n)$ from 9 to 14 MeV (P. Thambidurai, A. Beyerle, C. R. Gould, F. Purser)

This work has been submitted for publication in Nucl. Instr. and Methods. The abstract is given below:

> "Zero-degree neutron emission spectra have been measured in the $^3H(p,n)$ reaction for bombarding energies from 9.77 to 14.77 MeV in 1-MeV stops. Double differential cross sections for neutrons resulting from tritium break-up reactions have been extracted and compared to previous work. The break-up cross sections are small in comparison to the $^3H(p,n)^3He$ source neutron cross sections, but are not negligible. The effect of these break-up neutrons should be considered in evaluating measurements of neutron evaporation spectra induced by neutrons in the 10 to 14 MeV energy range."

The integrated cross sections range from 0.91 mb/sr at 9.77 MeV to 10.87 mb/sr at 14.77 MeV and are in good agreement with the measurements of Drosg and Auchampaugh.[1]

2. The $^1H(^7Li,n)$ Reaction as an Intense Neutron Source (J. W. Dave, C. R. Gould, S. Shafroth, S. Wender)

Reactions induced by protons and deuterons have long been used to make beams of neutrons for nuclear physics experiments. Two specific examples are the $^7Li(p,n)$ reaction, employed as a neutron source in the few-MeV range, and the $^9Be(d,n)$ reaction, used as a white neutron source in the 1 to 20 MeV energy range. Recent developments in heavy-ion source technology have made it possible to accelerate a wide variety of heavy-ion beams with moderate intensity. It is interesting to consider reversing these reactions therefore, and investigate the possibilities for neutron production by heavy ion bombardment of hydrogen targets.

We have recently studied one such example, namely $^1H(^7Li,n)$ from threshold up to E_{Li}=22 MeV. The main feature to emerge for negative-Q reactions such as this is that, near threshold, kinematic

---

1. M. Drosg and G. Auchampaugh Nucl. Instr. and Meth. 140 (1977) 515.

focussing confines the neutrons to a narrow forward going cone. As a result the neutron flux is high and self collimated. Such a source has advantages in experiments with detectors which are especially sensitive to neutron damage, for example (n,n'γ) studies with Si(Li) detectors or (n,γ) studies with Ge(Li) detectors. The large effective cross section for neutron production near threshold could also be of value in hydrogen depth profiling.

The neutrons were produced in a 3-cm long gas cell filled with 1/2 atm of hydrogen gas. The entrance foil was 3-micron thick nickel foil and the beam dump was a thin tantalum disk. Lithium beam energy losses in the entrance foil ranged from 1.9 MeV at 16 MeV to 1.4 MeV at 23 MeV. Beam-energy losses in the gas ranged from about 400 keV at 16 MeV to 300 keV at 23 MeV.

The characteristics of the source are illustrated by the zero-degree neutron time-of-flight spectra of Fig. B-1. These spectra were obtained with pulsed ^{7}Li beams of 10 nA intensity and are

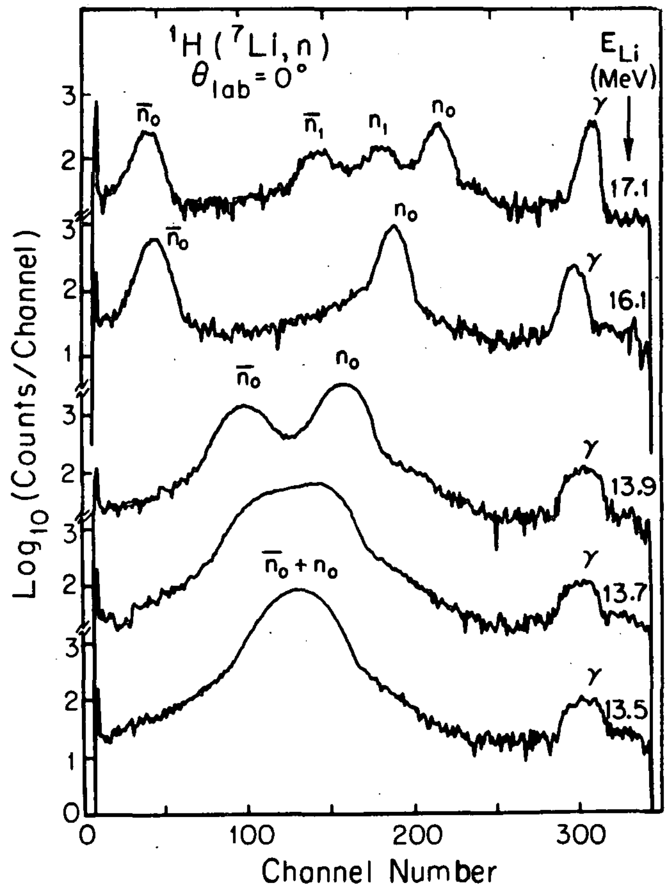

Fig. B-1. Zero degree neutron time-of-flight spectra from ^{7}Li bombardment by hydrogen.

for equal amounts of beam current on target. The bombarding energies range from just above threshold for the ^{1}H(^{7}Li,n)Be reaction to above threshold for the ^{1}H(^{7}Li,n)^{7}Be* reaction. As the lithium energy increases the two ground state neutron groups n_0 and $\bar{n}_0$ become well separated. Their intensity decreases rapidly above threshold. At 17.1 MeV the ^{7}Be* channel is open and the four possible neutron groups are clearly seen. The effective cross sections are large. For example, at 13.5 MeV the cross section for the sum of the n_0 and $\bar{n}_0$ groups (average energy about 1.5 MeV) is about 4 b/sr. The measured cross sections agree reasonably well with the values predicted from the known cross sections for the inverse ^{7}Li(p,n) reaction.

The ^{1}H(^{7}Li,n) reaction is a particularly favorable case because (p,n) cross sections are large for quasi elastic processes. The neutron energy is low at threshold however. Higher energy neutrons can be obtained with reactions with more negative Q-values, for example ^{1}H(^{12}C,n). The (p,n) cross sections for such T=0 targets are much smaller however.

The results have been submitted for publication in Nucl. Inst. and Methods.

A. ALPHA,N YIELDS (Patrick J. Grant, Gene L. Woodruff, & David L. Johnson)

Neutron yields from (α,n) reactions are plotted in Fig. 1 for oxygen, beryllium, flourine, and carbon for alpha energies ranging from 3 to 10 MeV. The measurements were performed using targets of elemental beryllium and carbon, PbO and PbF_2. The data plotted represent yields from materials of interest and/or targets for which previously repeated results are available.[1] The target conversions were made using corrections for atom fractions and dE/dx values. All of the results reported here involved the use of the 1.5 m graphite stack with Fe multiplier, and a constant efficiency of 5.5% has been assumed. The efficiency of the assembly varies at higher neutron energies, and calibration data are still under analysis. The data in Fig. 1 are not expected to be significantly changed by the results of the calibrations at high neutron energies.

In general the yield curves in Fig. 1 have the same shape as those reported in Ref. 1. Our results are consistently about 20% higher with the exception of the data for UC. In this case our yields are lower by approximately 10% at 4 MeV and converge at higher energies. There is little disagreement above about 6 MeV. In addition to uncertainties in efficiency values, there may be inconsistencies in the target conversion procedures. These would not apply, however, to the Be data.

[1] J. K. Bair and J. Gomez del Camp, Nuc. Sci. Eng. 21, 18 (1979)

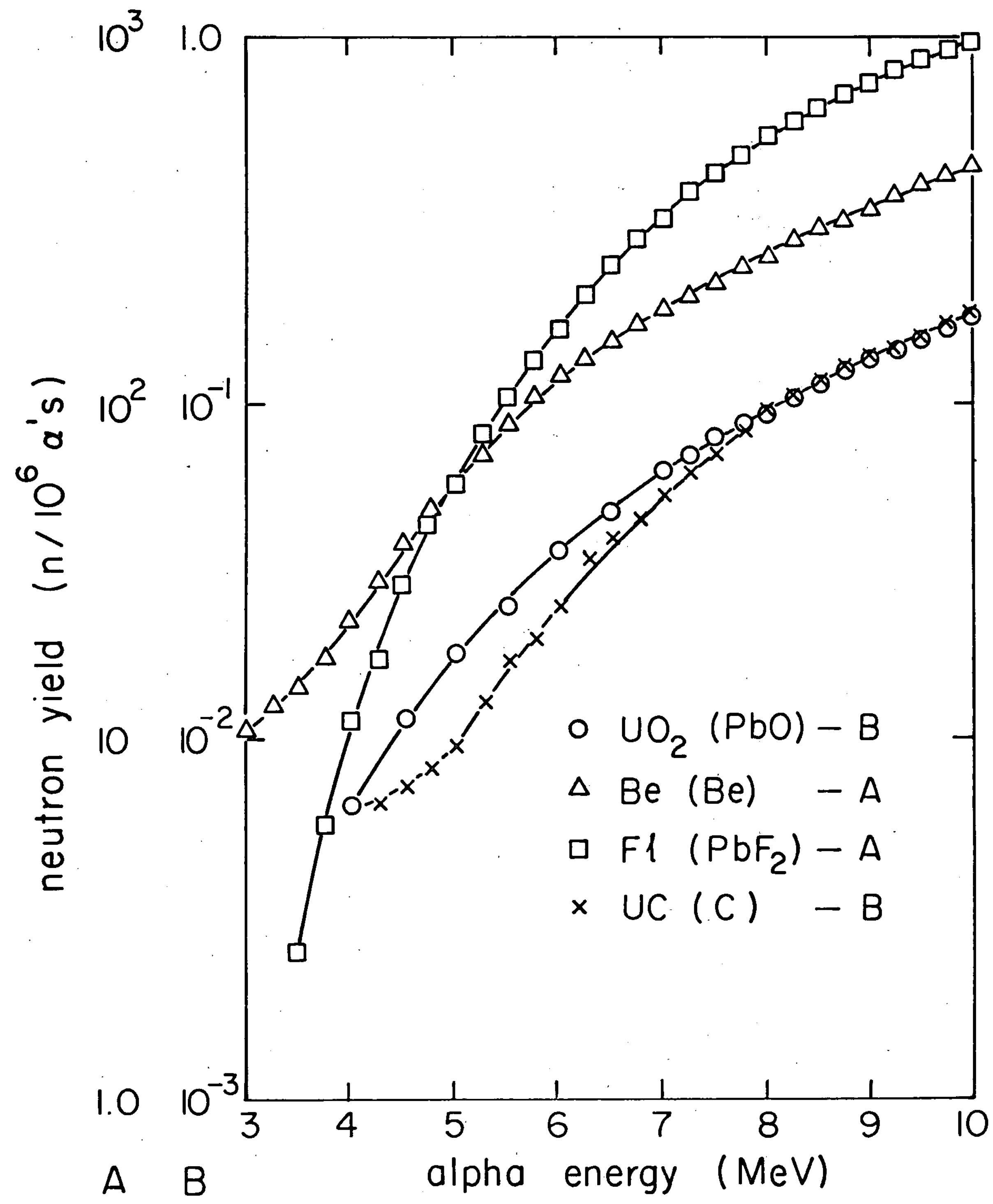

Fig. A-1 Neutron Yield vs Alpha Energy-Target Matrices are given in Parenthesis.

A. NEUTRON PHYSICS

1. Studies of the $^{209}Bi(\vec{n}, n)$ Interaction at Wide Angles in the Neutron Energy Range Between 2 and 4 MeV (M. Ahmed and F. W. K. Firk)

We have measured the asymmetry of polarized neutrons elastically scattered from ^{209}Bi at neutron energies between 2 and 4 MeV and at thirteen angles between 30° and 160°. The measurements have been corrected for the effects of multiple scattering and finite geometry using a Monte Carlo method, to give the point analyzing powers. The results have been included in a global optical model analysis.

2. Studies of the Differential Cross Section in n-^{209}Bi Elastic Scattering Between 2 and 4 MeV (M. Ahmed and F. W. K. Firk)

We have measured $\sigma(E, \theta)$ for $^{209}Bi(n, n)$ elastic scattering between 2 and 4 MeV at twenty angles between 20° and 160°. Corrections for the effects of multiple scattering and finite geometry have been made. The differential cross sections was measured relative to the standard $^{12}C(n, n)$ differential cross section throughout the region of interest.

3. An Optical Model Analysis of the n-^{209}Bi Interaction Between 2 and 4 MeV (M. Ahmed and F. W. K. Firk)

We have combined our measurements of the analyzing power and differential cross section of ^{209}Bi for elastically scattered neutrons between 2 and 4 MeV with published measurements of the neutron total cross section, differential cross section and total inelastic cross section in a global optical model analysis. Using the results of the optical model analysis of Tanaka et al. as a starting point, we have been able to refine the analysis to the point where an acceptable fit is obtained to all the observed quantities. At all angles, Mott-Schwinger scattering is taken into account using the Born phase-shift method.

4. Angular Distribution Measurements of n-^{NAT}Pb and n-^{209}Bi Scattering in the keV-Region (J. Kruk, M. Ahmed and F. W. K. Firk)

As part of our continuing effort to set an improved limit on the electric polarizability of the neutron, we have made measurements with high resolution of the angular distribution of neutrons scattered from Pb and Bi at energies from 500 eV up to 250 keV. In these challenging experiments, anisotropies at the 1%-level are to be expected.

A. NEUTRON PHYSICS

1. Total Inelastic-Neutron-Scattering Cross Sections of ^{232}Th, ^{233}U, ^{235}U, ^{238}U, ^{239}Pu and ^{240}Pu

(A. B. Smith and P. Guenther)

Differential-neutron-emission cross sections of ^{232}Th, ^{233}U, ^{235}U, ^{238}U, ^{239}Pu and ^{240}Pu were measured between 1.0 and 3.5 MeV with sufficient angle and magnitude detail to obtain the angle-integrated cross sections to < 3% accuracies. Emitted-neutron energy resolutions were quanitatively defined and varied from $\approx$ 0.1 to 0.35 MeV. The experimental results were corrected for fission-neutron contributions and the non-elastic cross sections determined to within well defined energy resolutions. These experimental results imply total-inelastic-scattering cross sections which are compared with the comparable quanitites deduced from ENDF/B-V in Fig. 1. Good general agreement is noted for ^{232}Th, ^{233}U, ^{235}U and ^{238}U inelastic scattering, poor agreement is oberved for ^{240}Pu and a serious discrepancy exists in the case of ^{239}Pu. The impact of such inelastic changes upon integral calculations is being assessed. A report of this work is in press (ANL/NDM-63).

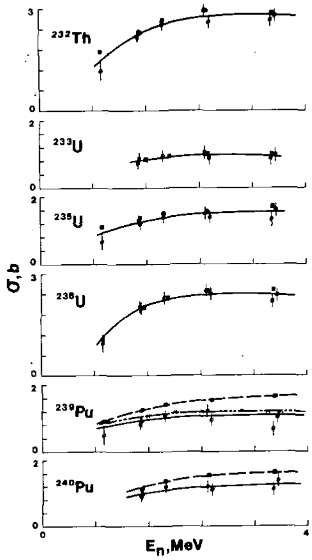

Fig. 1. Neutron total-inelastic-scattering cross sections of ^{232}Th, ^{233}U, ^{235}U, ^{239}Pu, and ^{240}Pu. Values deduced from the present measurements are noted by O. Comparable values derived from ENDF/B-V and the evaluation of ref. 1 are indicated by ■ and X, respectively. Curves are "eyeguides" referenced as follows;——— present results, —— —— —— ENDF/B-V, and ——— — — ——— the evaluation of ref. 1.

---

1 Antsipov et al., INDC (ccp) 166/CHJ (1981).

2. Structural Materials

2a. Fast-neutron Total and Scattering Cross Sections of ^{58}Ni

(Carl Budtz-Jorgensen,[a] Peter T. Guenther, Alan B. Smith and James F. Whalen)

Neutron total cross sections of ^{58}Ni were measured at 25 keV intervals from 0.9 to 4.5 MeV with 50-100 keV resolutions. Attention was given to self-shielding corrections to the observed total cross sections. Differential elastic- and inelastic-scattering cross sections were measured at 50 keV intervals from 1.35 to 4.0 MeV with 50-100 keV resolutions. An illustrative example of the results is given in Fig. 2. Inelastic excitation of levels at 1.458 ± 0.009, 2.462 ± 0.010, 2.791 ± 0.015, 2.927 ± 0.012 and 3.059 ± 0.025 MeV was observed. The experimental results were interpreted in terms of optical-statistical and coupled-channels models. A report of this work has been submitted for journal publication.

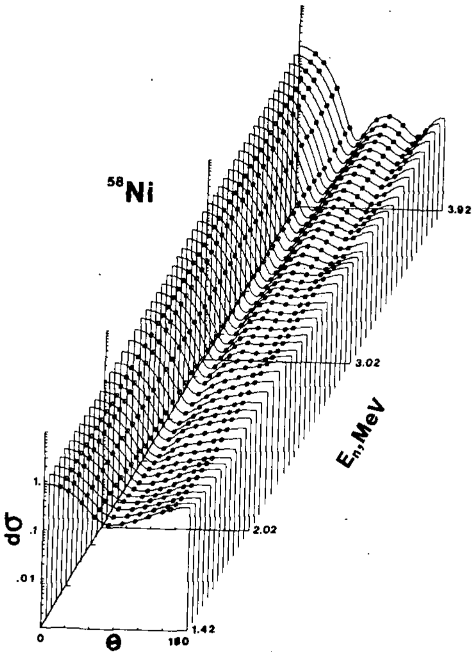

Fig. 2. Differential neutron elastic-scattering cross sections of ^{58}Ni. 200 keV averages of the present measured values are indicated by data symbols. Curves denote the results of spherical model calculations. The dimensionality is cross section in b/sr and scattering angle in lab degree.

[a] Visiting scientist from the Central Bureau for Nuclear Measurements Geel, Belgium.

2b. Fast-neutron Total and Scattering Cross Sections of ^{54}Fe
(P. T. Guenther, D. L. Smith, A. B. Smith and J. F. Whalen)

Broad resolution neutron total and scattering cross sections of ^{54}Fe have been measured from 0.5 the 4.0 MeV using time-of-flight techniques. Complimentary (n;n',gamma) measurements have been completed over the same energy range. The experimental results are now being processed.

3. Neutron Cross Sections of Fission Products

Portions of the comprehensive program outlined in the previous report are now coming to completion. Three illustrative examples being prepared for publication are the following.

3a. Low-MeV Neutron Cross Sections of Yttrium
(C. Budtz-Jorgensen[a], A. Smith, P. Guenther and J. Whalen)

Neutron total and scattering cross sections of elemental Yttrium have been measured from $\approx$ 1-4 MeV at intervals of $\leq$ 50 keV with broad resolutions. Differential-scattering cross sections were determined at ten or more scattering angles distributed between 20 and 160°. Inelastically-scattered neutrons were observed corresponding to the excitation of levels at: 909 ± 23, 1504 ± 20, 1747 ± 16, 2567 ± 26, 2889 ± 12 and 3104 ± 10 keV. The experimental results were examined in the context of a spherical optical potential and compared with comparable values given in ENDF/B-V. A report of this work is preparation.

3b. Fast-Neutron Total and Scattering Cross Sections of Elemental Palladium (A. Smith, P. Guenther and J. Whalen)

Neutron total cross sections of palladium have been measured from 0.5 to 4.5 MeV with resolutions of 30-70 keV at intervals of less than 50 keV. Differential neutron elastic- and inelastic-scattering cross sections have been measured from 1.5 to 3.8 MeV at intervals of 50-100 keV and at 10 to 20 neutron-scattering angles distributed between 20 and 160°. The experimental results being interpreted in terms of a generalized optical potential applicable to this mass-energy region.

3c. Fast Neutron Scattering Cross Sections of ^{115}In
(A. Smith and P. Guenther)

Neutron scattering measurements have been completed from 1.5 to 3.8 MeV. As a part of the above noted generalized model development for the neutron interaction in this mass-energy region, an optical potential

[a] Visiting scientist from the Central Bureau for Nuclear Measurements, Geel, Belgium.

has been obtained from the measured values. The quality of the measured quantities and the model description is illustrated in Fig. 3.

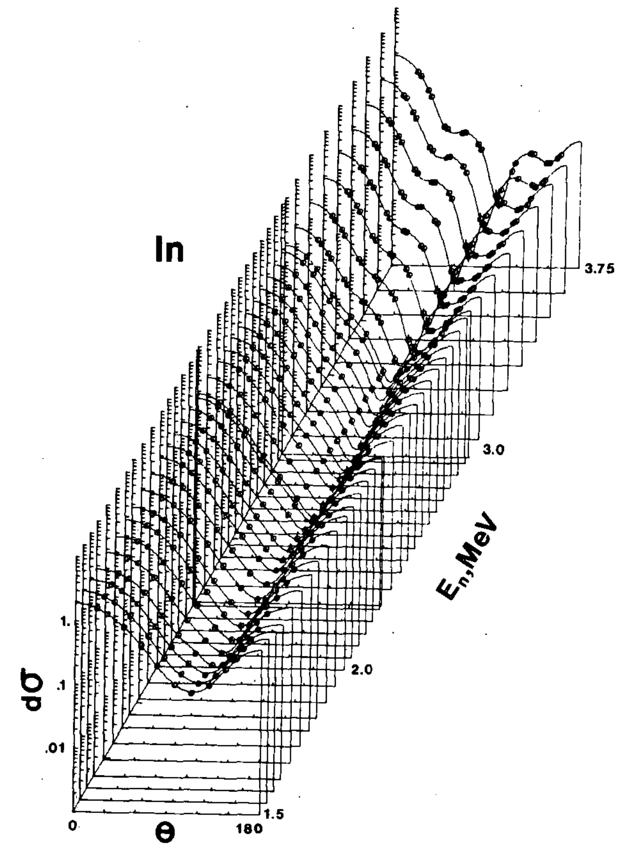

Fig. 3. Differential elastic-scattering cross sections of ^{115}In. The data symbols indicate the measured values and the curves the results of model calculations.

4. <u>Elastic Scattering of MeV Neutrons from Elemental Calcium</u> (A. Smith and P. Guenther)

Neutron differential-elastic-scattering cross sections of elemental calcium were measured from 1.5 to 4.0 MeV at intervals of $\approx$ 50 keV with broad resolutions. The measured scattering angles were distributed between 20 and 160°. The experimental results are illustrated in Fig. 4. The resulting angle-integrated elastic-scattering cross sections are in good agreement with the values given in ENDF/B-V but the differential distributions show considerably more detail and fluctuation. Monte-Carlo integral calculations suggest that this additional detail does not substantively effect shielding applications. The experimental results were used to deduce an optical potential for this doubly-magic nucleus. The results of this work are in press (Report ANL/NDM-65).

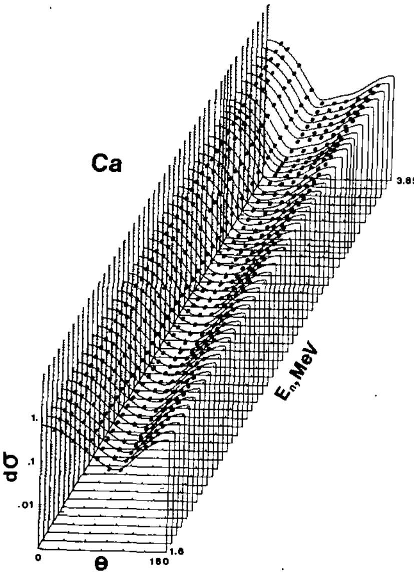

Fig. 4. Differential-elastic-scattering cross sections of calcium. The present experimental results, averaged over 250 keV, are noted by data symbols. Curves indicate the results of model calculations. The dimensionality is scattering angle in degree and cross section in b/sr, expressed in the laboratory system.

5. Fast-Neutron Activation of 48.6-min Cd-111M (D. L. Smith, J. W. Meadows, P. A. Moldauer and W. P. Poenitz)

Cross-section measurements for the activation of ^{111m}Cd have been performed using elemental Cd samples as well as samples enriched in ^{110}Cd and ^{111}Cd. The ^{111}Cd excitation function for elemental Cd was measured from 0.135-10.01 MeV as shown in Fig. 5. The potential of this activation process for dosimetry was also investigated. Isotopically-enriched samples were used in measurements to determine isotopic cross sections for ^{110}Cd(n,γ) ^{111m}Cd and ^{111}Cd(n,n') ^{111m}Cd at several energies below 1.6 MeV as shown in Figs. 6 and 7, respectively. Optical-model, statistical-model and gamma-ray cascade-decay model calculations were performed in order to interpret the experimental results. Reasonable agreement with the data was achieved using model parameters reported in the literature.

6. Capture Cross Sections of Zr and Mo Isotopes at Thermal and 30 KeV Energies (W. P. Poenitz and J. M. Wyrick)

Capture cross sections of ^{94}Zr, ^{96}Zr, ^{98}Mo and ^{100}Mo were measured at thermal and 30 keV neutron energies. The activation technique was used and measurements were made relative to the capture cross section of

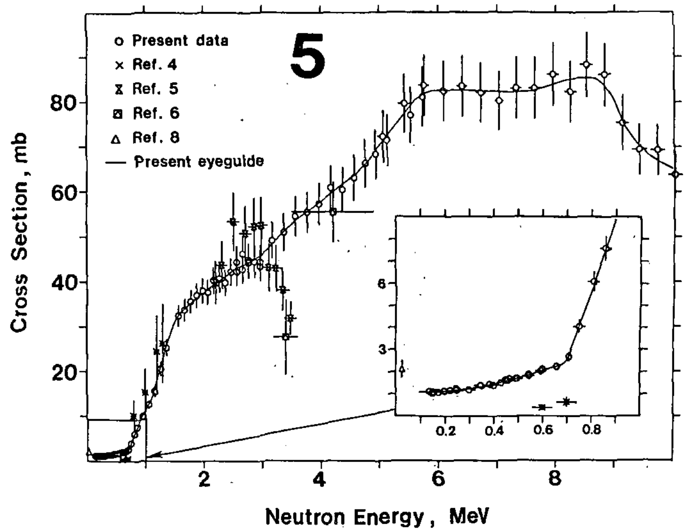

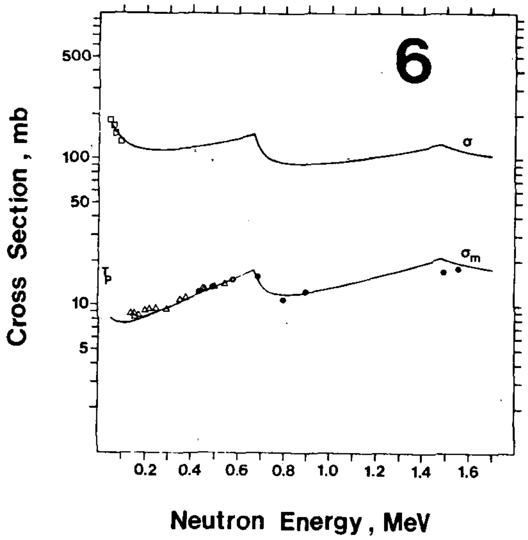

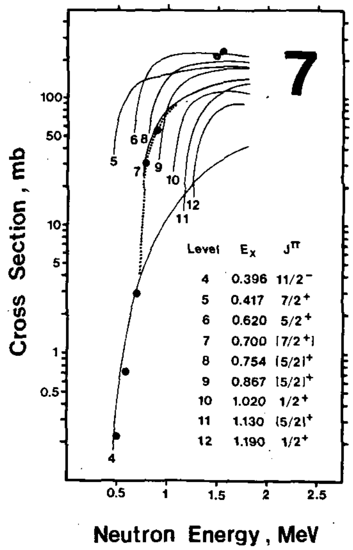

Fig. 5. Cross sections for ^{111m}Cd excitation in fast-neutron bombardment of elemental Cd. Present data are the open circles (O). The solid curve is an eyeguide to the present data.

Fig. 6. Capture (σ) and capture-activation data (σ_m) for ^{110}Cd. Present data are indicated by solid circles (O) and triangles (Δ). Solid curves are model-calculation results for the capture (σ) and capture-activation (σ_m) cross sections.

Fig. 7. Inelastic-activation cross sections for ^{111}Cd. Present data are indicated by solid circles (O). Solid curves are results of model calculations for discrete inelastic excitation of the indicated ^{111}Cd levels. The dotted curve is the isomer cross section derived by combining the discrete inelastic cross sections with empirically estimated gamma-ray branching ratios.

gold. The present results depend on decay scheme information; however, comparison at thermal energy with some of the previously available data shows good agreement. The results are given below;

	Thermal	30 KeV
^{94}Zr	49.4 ± 1.7 (mb)	25.2 ± 3.6 (mb)
^{96}Zr	20.3 ± 0.6	12.0 ± 0.7
^{98}Mo	131.7 ± 5.3	84.3 ± 3.6
^{100}Mo	188.8 ± 0.9	115.0 ± 15.0

7. ^{6}Li Total, Scattering and (n,α) Cross-Section Measurements Below 0.5 MeV (W. P. Poenitz)

The ^{6}Li cross sections are now rather well know above ≈ 500 keV[1]. However, some problems persist at lower energies. There is specifically a lack of scattering data over and below the 240 keV resonance. Scattering data available below ≈ 200 keV are uncertain or grossly discrepant. Experimental total cross sections in the resonance peak are persistently lower than corresponding R-Martrix fits used for ENDF/B-V and (n,α) cross-section values around 100 keV differ from ENDF/B-V values by more than desirable for a standard cross section. Measurements were carried out to obtain consistent total, scattering and (n,α) cross-section values between ≈ 70 keV and 500 keV. A new detector was designed for the measurements of the integrated scattering cross section; based on the Black Neutron Detector principle but detecting scattered neutrons in 4π geometry. A total cross section of ≈ 11.4b was obtained in the resonance peak which is higher than any previously measured value but in agreement with results by Smith et al.[1] and Knitter et al. [2]. Additional measurements and analysis are required to complete this work.

---

1 A. B. Smith et al., Nucl. Phys. A373, 305 (1982).
2 H. H. Knitter et al., Euratom Report EUR5726e (1977).

8. Studies of the n;n',γ) Process in ^{186}W (P. Guenther and D. L. Smith)

The interpretation of previous neutron experiments has been confused by uncertainties as to the excited levels of ^{186}W. In order to resolve these uncertainties, the (n;n',γ) process in ^{186}W has been experimentally examined up to incident energies of 2.0 MeV. The experimental results are now being interpreted.

B. FISSION PHYSICS

1. Fragment Angular Distributions and Total Kinetic Energies for the ^{235}U(n,f) Reaction (J. W. Meadows and C. Budtz-Jorgensen*)

A gridded ion chamber[1] was used to measure the fission fragment angular distribution and average kinetic energy for the ^{235}U(n,f) reaction from 0.18 to 8.81 MeV neutron energy. The results of the angular distribution measurement are shown in Fig. 8. Energy loss in the uranium deposits made the kinetic-energy measurement dependent on fragment angle and consequently on the angular distribution. This effect was eliminated by dividing the cosθ-energy distribution into equal intervals in cosθ. The average fragment energy in each cosθ interval at each neutron energy was compared with the average fragment energy in the corresponding cosθ interval for thermal neutron induced fission of ^{235}U. The results are shown in Fig. 9 for cosθ = 0.125.

The most prominent feature of these data is the sudden decrease in fragment energy near 4.5 MeV neutron energy. This may be caused by a decrease in shell effects with increasing excitation energy that results in a more elongated configuration at the scission point. With the charge centers further apart the coulomb repulsion is decreased and there is a corresponding decrease in the kinetic energy. A scission point model developed by Wilkins et al.[2] suggests that such a change may occur quite suddenly.

---

*Visiting scientist from the Central Bureau for Nuclear Measurements, Geel, Belgium.

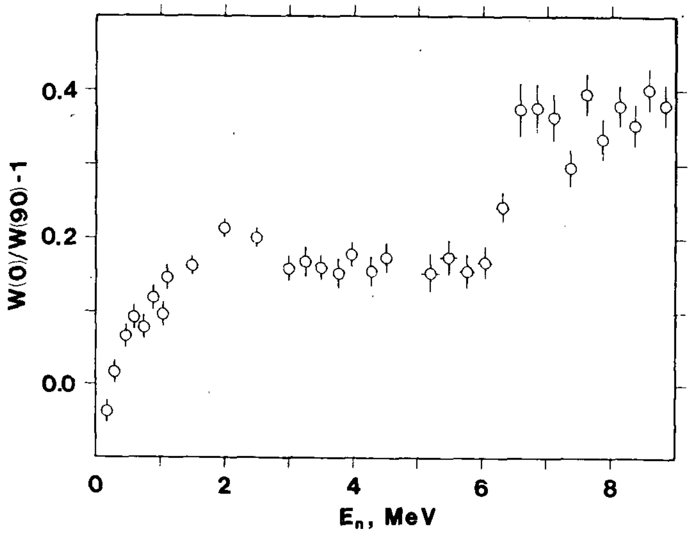

Fig. 8. The anisotropy of the ^{235}U(n,f) reaction as a function of neutron energy.

---

1 H. H. Knitter and C. Budtz-Jorgensen, Proc. Int. Conf. Nucl. Cross Sections and Tech., NBS Special Pub. 594 (1980).

2 B. Wilkins, E. Steinberg and R. Chasman, Phys. Rev., C14 1832 (1976).

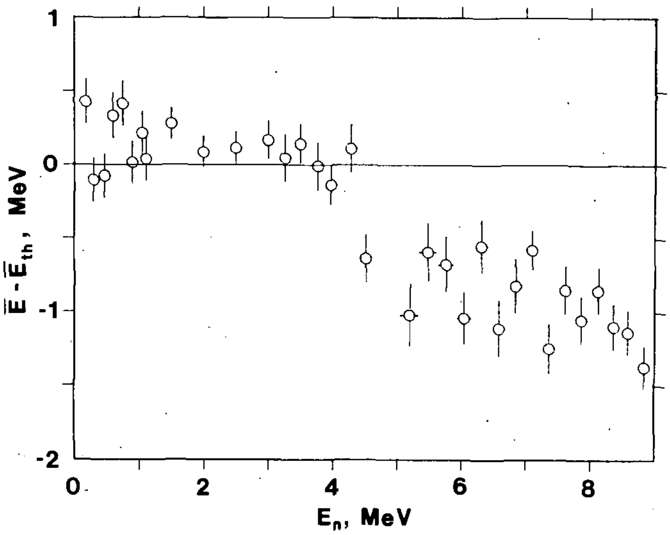

Fig. 9. The change in the average total kinetic energy relative to the value for thermal neutron induced fission.

2. Angular Distribtuion and Total Kinetic Energy for ^{232}Th(n;f) (C. Budtz-Jorgensen[a] and J. W. Meadows)

A measurement of the ^{232}Th(n;f) fission-fragment angular distributions with incident neutron energies from 1.5 to 1.8 MeV and energy spread of ± 8 keV has been made. A channel analysis based on the measured angular distributions has been completed. The fragment total kinetic energies (TKE) were measured simultaneously and a dramatic TKE variation of $\approx$ 1 MeV was observed over the ^{232}Th(n;f) resonance of 1.6 MeV. A report of this work will be published in the Proceedings of the International Symposium on Nuclear Fission and Related Collective Phenomena, Bad Honnef, October 1981.

[a] Visiting scientist from the Central Bureau for Nuclear Measurements, Geel, Belgium.

3. Product Yields from Monoenergetic-Neutron-Induced Fission of ^{235}U and ^{239}Pu (L. E. Glendenin, J. E. Gindler, D. H. Henderson and J. W. Meadows)

Yields of 37 fission products were determined for fission of ^{235}U induced by monoenergetic neutrons of energies 0.17, 0.55, 1.0, 2.0, 4.0, 5.5, 6.3, 7.1 and 8.1 MeV. Fission-product activities were measured with high resolution (Ge-Li) gamma-ray spectrometry of the neutron irradiated targets and with chemical separation of fission-product elements followed by beta counting and/or gamma-ray spectrometry. Results are published in Physical Review C24, 2600 (1981) A similar study is in progress for ^{239}Pu, and yields for 26 fission products were determined at a neutron energy of 3.4 MeV. Further measurements at 0.1, 0.5, 1.0, 2.0, 5.0, 6.5 and 8.0 MeV are planned.

4. ^{252}Cf-Spontaneous-Fission-Neutron-Spectrum Investigations
(W. P. Poenitz and T. Tamura)

The prompt-fission-neutron spectrum of ^{252}Cf is a recommended neutron-emission standard. However, it has not received experimental attention appropriate for a standard. The present investigations focussed on corrections and associated uncertainties for a large variety of effects which might have been overlooked in previous measurements. Considerations of the various issues in such measurements resulted in an experimental design quite different from previous work. The major part of the spectrum was measured with a Black Neutron Detector which has a well-known efficiency. The time-calibration pulser, a random pulser, the neutron-detector time-of-flight spectrum, the pulse-shape-discriminator gamma-ray time spectrum, and the detector response spectra were simultaneously recorded for the prompt fission neutrons and for transmission through carbon and shadow bars in a total-cross-section-type measurement. The data are presently being analyzed.

---

* Visiting scientist from Tohoku University, Sendai, Japan

C. CHARGED-PARTICLE PHYSICS

1. The $^7Li(d,p)^8Li$ Reaction Cross Section Near 0.78 MeV
(A. J. Elwyn, R. E. Holland, C. N. Davids, and W. Ray, Jr.)

The total cross section for the $^7Li(d,p)^8Li$ reaction has been obtained at four energies near 0.78-MeV from measurements, by time-of-flight techniques, of the differential cross sections for the outgoing protons at lab-angles between 20° and 155°. This cross section is used as normalization in the determination of the rate of the $^7Be(p,\gamma)$ reaction which, as a link in the proton-proton chain of nuclear reactions that take place in the sun, is of prime importance to the calculation of the solar-neutrino capture rate expected in the ^{37}Cl neutrino-capture experiments.

The result for the total cross section, 146 ± 13 mb, is about 20% lower than the weighted mean of all previous absolute measurements, which differ from each other by as much as 40%. It does, however, agree with a new measurement (described in the report immediately following) in which the ^8Be breakup alpha particles from the ^8Li beta-decay were detected. If the present $^7Li(d,p)$ cross section is used to scale previously measured $Be(p,\gamma)$ values, the predicted solar-neutrino capture rate is reduced by > 1 solar-neutrino unit from previously predicted rates.

2. The $^7Li(d,p)^8Li$ Reaction
(B. Filippone*, A. J. Elwyn, D. Koetke,** and W. Ray, Jr.)

A measurement of the absolute cross section for the $^7Li(d,p)^8Li$ reaction by detecting the delayed α particles from ^8Li decay has been completed. The value of this cross section at the peak of the 0.77 MeV resonance has been used as the normalizing reaction for most of the previous measurements of the $^7Be(p,\gamma)^8B$ reaction mentioned above.

The cross section at the 0.77-MeV resonance has been measured to be 148 ± 12 mb. This new value for the cross section lowers the predicted neutrino capture rate in the ^{37}Cl experiment by about 15% when used to normalize the $^7Be(p,\gamma)^8B$ reaction.

3. The $^7Be(p,\gamma)^8B$ Reaction
(B. Filippone,* A. J. Elwyn, D. Koetke,** and W. Ray, Jr.)

The development of a $^7Be(t_{1/2} = 53$ days) target is under way in order to measure the $^7Be(p,\gamma)^8B$ cross section at low energies. It is this reaction in the sun that leads directly to the production of high-energy neutrinos from ^8B decay which comprise ≈ 80% of the neutrino capture rate in the ^{37}Cl solar neutrino experiment.

A preliminary target (≈ 0.5 mCi), homogeneous to better than 10%, has been produced by a high voltage electroplating technique. The ^7Be is first produced from the $^7Li(p,n)^7Be$ reaction and then is chemically separated from the Li. Following the plating of the ^7Be onto a thin Pt backing it is ignited to the oxide to form the refractory BeO. A Pb collimated Ge(Li) detector allows a measurement of the uniformity of the target.

Work is continuing on making a much stronger target (≈ 50 mCi) to permit measurement of the $^7Be(p,\gamma)^8B$ cross section down to low energy.

---

* Thesis Student, University of Chicago, Chicago, IL.
** Valparaiso University, Valparaiso, IN.

4. Study of Non-Resonant Capture in the $^{27}Al(p,\gamma)$ and $^{19}F(p,\gamma)$ Reactions at Low Energy
(A. J. Elwyn, G. Hardie,* R. E. Segel,** M. Weischer,*** and W. Ray Jr.)

Using high beam currents ($\approx$ 100 μ-amps) and both Ge(Li) and NaI detectors, we are studying the non-resonant γ-ray yield in radiative-capture reactions on ^{27}Al and ^{19}F targets at incident energies near and below 1 MeV. In this region, non-resonant processes are expected to arise predominantly from a direct-capture mechanism where the incident projectile radiates a photon and enters a shell-model orbit of the target nucleus. Both reactions are of astrophysical interest in that measured cross sections should more clearly define the role of side branches in various nucleosynthesis processes.

For $^{27}Al(p,\gamma)$, we have identified γ-ray transitions consistent with the direct-capture process to both the ground and 1.78-MeV state in ^{28}Si. An excitation function for such transitions has been obtained between $\approx$ 0.8 and 1.8 MeV. Unfortunately, the existence of a large number of narrow resonances in this reaction makes the interpretation of the observed "non-resonant" yield somewhat uncertain. In the $^{19}F(p,\gamma)$ reaction, direct-capture transitions to the 1.634-MeV state in ^{20}Ne are observed between incident energies from 0.6 to 1.2 MeV. By improving our techniques, particularly in the reduction of pile-up due to the very intense yield of 6-7 MeV γ-rays from the $^{19}F(p,\gamma)$ reaction, we hope to investigate nonresonant processes at incident energies well below 0.5 MeV. These experiments will continue through the present year.

*Western Michigan University, Kalamazoo, MI.
**Northwestern University, Evanston, IL.
***Ohio State University, Columbus, OH.

D. EVALUATION

1. Covariance Matrices and Applications to the Field of Nuclear Data
(D. L. Smith)

A student's introduction to covariance error analysis and least-squares evaluation of data is provided. It is shown that the basic formulas used in error propagation can be derived from a consideration of the geometry of curvilinear coordinates. Procedures for deriving covariances for scaler and vector functions of several variables are presented. Proper methods for reporting experimental errors and for deriving covariance matrices from these errors are indicated. The generalized least-squares method for evaluating experimental data is described. Finally, the use of least-squares techniques in data fitting applications is discussed. Specific examples of the various procedures are presented to clarify the concepts. This practical guide is available as the report ANL/NDM-62.

E. FACILITIES AND INSTRUMENTATION

1. Fast-Neutron Generator Beam Handling System
(A. Smith and A. Engfer)

The improved isochronous beam-handling system, noted in the previous report, has been installed and satisfactorily tested. Marked improvements were achieved in the areas of time resolution, background suppression, and geometric control.

2. A new PIG injector system has been tested on a bench setup. The results are encouraging with 3-4 mA of analyzed hydrogen beam well focused through a gap lense consistent with the Fast Neutron Generator acceptance. Engineering improvements with the objective of increased reliability are now in progress in preparation for installation at the accelerator.

☆ U.S. GOVERNMENT PRINTING OFFICE: 714-037#49